DE GRUYTER OPEN

HUNGARIAN JOURNAL OF INDUSTRY AND CHEMISTRY
Vol. 46(2) pp. 1-100 (2018)
hjic.mk.uni-pannon.hu

HUNGARIAN JOURNAL OF INDUSTRY AND CHEMISTRY
HJIC

Contents

DE GRUYTER OPEN

HUNGARIAN JOURNAL OF INDUSTRY AND CHEMISTRY
Vol. 46(2) pp. 1-11 (2018)
hjic.mk.uni-pannon.hu
DOI: 10.1515/hjic-2018-0011

HUNGARIAN JOURNAL OF INDUSTRY AND CHEMISTRY
HJIC

TRIBOLOGICAL BEHAVIOUR OF POLYMERS IN TERMS OF PLASMA TREATMENT: A BRIEF REVIEW

HAYDER AL-MALIKI *[1] AND GÁBOR KALÁCSKA[1]

[1]Faculty of Mechanical Engineering, Mechanical Engineering PhD School, Szent István University, Páter Károly utca 1, H-2100 Gödöllő, HUNGARY

A review to enrich the literature concerning the effect of various plasmas on the tribological behaviour of polymers and monitor the developments of plasma for the modification of polymer surfaces over recent decades using up-to-date data. A comparative study of plasmas was conducted to identify the most useful and efficient ones which facilitate optimal improvements with regard to the characterizations of polymer surfaces and tribological properties. The studies included in this review strongly suggest that (besides Plasma-Immersion Ion Implantation, PIII) atmospheric plasmas (dielectric barrier discharges, DBD) are an effective technique in terms of modifying the characterizations of polymer surfaces thereby enhancing the tribological behaviour of polymers under different operating conditions that extends the operating life of elements within the machine.

Keywords: polymer, plasma treatment, surface characterization, tribology

1. Introduction

The term tribology originates from two Greek words, namely $\tau\rho\iota\beta\omega$ (tribo), a verb which means "I rub"; and the suffix *-logy* which is derived from $\lambda\omega\gamma\iota\alpha$ (logia) which can be translated as "study of" or "knowledge of". This word was introduced by the British scientists Bowden, Tabor [1] and Jost in 1964 [2]. Luke Mitchell, a professor of lubrication, observed the problems caused by increasing the level of friction exerted on machines [3]. Tribology is the science which studies the principles and applications of friction, wear and lubrication [4]. Friction and wear are widespread phenomena in our daily lives. Processes that result in friction occur when moving surfaces are in contact with each other [5]. Friction is a consequence of two main non-interacting components (adhesion and deformation) and can be considered as an approach for all materials including polymers. Polymers are nonpolar materials that exhibit unique tribological behaviour, and some of them possess good self-lubrication characteristics, examples of which are stated in [6, 7]. The rapid development of industry was accompanied by the urgent need to decrease the size of equipment which in turn leads to a higher degree of friction and enhanced rates of wear to be exerted on the elements of machines. This prompted the evolution of several surface-modification techniques, in particular for polymers, to diminish the disadvantages of friction and wear. The alteration of surface properties such as hydrophilicity, chemical composition and roughness lead to inevitable changes in tribological behaviour which provided an opportunity for researchers to govern such behaviour with regard to polymers. Therefore, specific techniques have been developed over the last few years to modify the surfaces of polymers to improve frictional behaviour and adhesive bonding performance. A lot of chemical and physical techniques have been developed to treat the surfaces of polymers. Chemical techniques are the processes which deal with wet or chemical reactions on surfaces, for instance, wet etching, grafting, acid-induced oxidation and plasma polymerization. Physical techniques deal with the modification of physical surfaces such as corona discharge, ion or electron beams, photon beams, plasma discharge and oxidizing flames [8].

Experimentally, the chemical treatments of polymer surfaces exhibit some disadvantages such as localized corrosion and environmental pollution. In contrast, physical treatments have been adapted recently to modify the surface of polymers [9]. One of the most effective techniques to modify the surfaces of polymers are plasmas which facilitate changes in the properties of polymer surfaces by several processes, for instance, cleaning, ablation, crosslinking and surface chemical functionalization [10].

Recently, plasma surface treatment was referred to as the most accepted method of modifying the surface of polymeric materials due to its remarkable stability concerning the enhancement of surface properties compared to conventional techniques, in particular, atmospheric plasma treatment which has the ability to operate under ambient atmospheric conditions (in terms of temperature

*Correspondence: haidrlatif@gmail.com

and humidity) and does not require a vacuum [9, 11]. The literature often suggests that plasma treatment may improve the hydrophilicity of polymers [12–16], which has also been demonstrated in our previous works [17–19]. Even though plasmas often increase the surface roughness of polymers [15, 20, 21], some studies have proven that a decrease in surface roughness might occur after shorter treatment times [16, 22].

The present study attempts to review the tribological aspects of polymeric materials treated by various plasmas and compared to their pristine surface behaviour by taking into consideration the influence of plasmas on the characteristics of polymer surfaces which vastly governs the tribological behaviour of polymers. Finally, plasma types that may currently be recommended to utilize and reinforce the tribological properties of polymers are highlighted.

2. Plasma Modification of Plastic Surfaces

Plasma can be defined as a chemically active media. The composition of plasmas varies depending on the way they are generated and their working power. Plasmas produce either low or very high temperatures and according to the heat they generate they can be termed as cold or thermal plasmas. Thermal plasmas, especially arc plasmas, were widely industrialized by the aeronautic sector in particular. Cold plasma technologies have evolved in the microelectronics industry, but they have a limited use due to their vacuum equipment. There have been many attempts to transpose plasmas to work under atmospheric pressure without the need for a vacuum. The research has led to various sources that are described in [23].

It is known that plasma is the fourth state of matter and it is more or less an ionized gas that constitutes about 99 % of the universe. Plasma consists of electrons, ions and neutrons; these constituents may exist in fundamental or excited states. From a laboratory point of view, plasma is electrically neutral. However, it contains some free charge carriers thus is electrically conductive [24, 25]. The degree of plasma ionization can range from small values, e.g. $10^{-4} - 10^{-6}$ for partially ionized gases to 100 % for fully ionized gases. In a laboratory, two types of plasma can be generated; the first are high-temperature plasmas which are also referred to as fusion plasmas, the second are low-temperature plasmas or gas discharges [26].

2.1 Classification of plasmas

Plasmas can be differentiated into several groups depending on the energy supply and amount of energy transferred to them since the properties of a plasma change depending on electronic density or temperature as presented in Fig. 1 [23]. There are two major plasma groups - the first are thermal equilibrium plasmas and the second are those not in thermal equilibrium. Plasmas that consist of

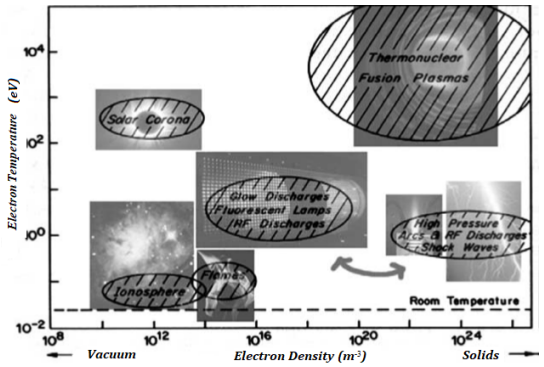

Figure 1: 2D classification of plasmas (electron temperature versus electron density) [28].

particles (electrons, ions and neutral species) of uniform temperature are known as thermal equilibrium plasmas, for instance, stars and fusion plasmas. Usually they are termed as "local thermodynamic equilibrium plasmas" which is abbreviated to LTE. High temperatures typically ranging from 4,000 K to 20,000 K are required to obtain thermal equilibrium plasmas. Otherwise, plasmas that are not in thermal equilibrium, abbreviated as non-LTEs, will be formed, for example, interstellar plasma matter [25]. LTE and non-LTE plasmas can be distinguished according to the gas pressure the plasma is subjected to. A high gas pressure is indicative of many collisions in the plasma and it could be argued that just a few collisions occur in the plasma when the gas pressure is low, for example, dielectric-barrier discharge and atmospheric pressure glow discharge plasmas. More details about types, sources and applications of plasmas can be found in [27].

2.2 Influence of plasmas on the surface characteristics of polymers

Different types of plasma treatments have exhibited potential changes in the physical and chemical surface characteristics of polymers. The variation in wettability is a fundamental parameter that controls adhesion, lubrication and/or interactions with molecules. The formation of polar groups at the surface following plasma treatments, such as carbonyl, carboxyl and hydroxyl groups, enhances the surface energy. The enhancement of wettability following plasma treatment can be a combined effect of surface functionalization and an increase in surface roughness. When surface grafting occurs relatively quickly, an increase in surface roughness has mainly been observed following longer treatment times [21]. Depending on the selection of adequate parameters, different types of plasma treatment are used for either enhancing as well as diminishing adhesion or surface hardness.

Experimentally, Tóth et al. [29] observed a significant improvement in the surface hardness of ultra-high molecular weight polyethylene (UHMWPE) following nitrogen plasma ion implantation (NPII). The hydrogen plasma

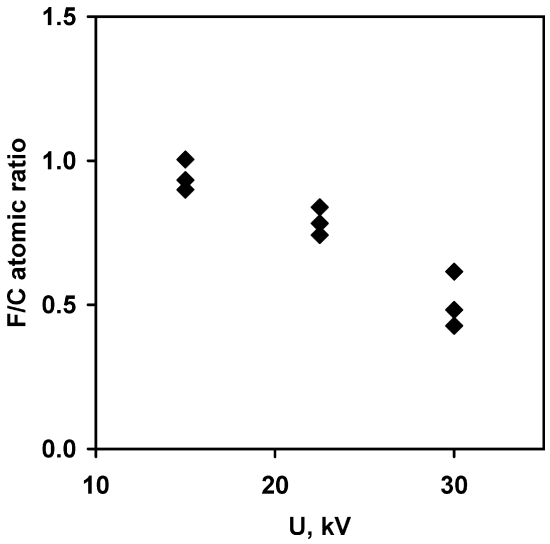

Figure 2: F/C atomic ratio vs. voltage.

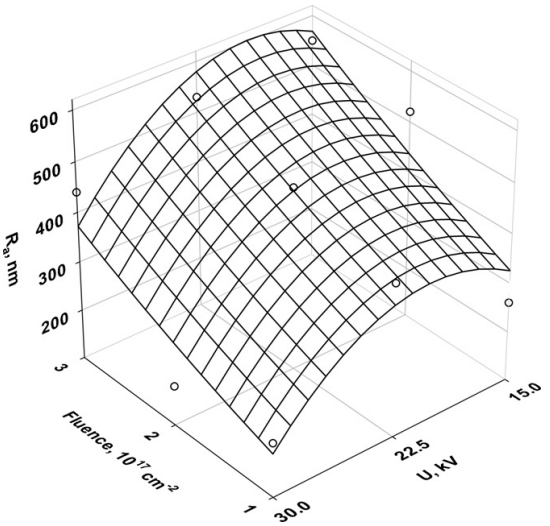

Figure 3: Mean surface roughness of PTFE vs. fluence and voltage.

immersion ion implantation (HPIII) treatment of the surface of UHMWPE induces amelioration in terms of the scratch resistance, temperature, mean surface roughness, oxygen content, and surface hardness, while the surface slope and elastic modulus often decreased, but it is possible to enhance these characteristics upon treatment. Low values of temperature and mean roughness favour the reduction of the surface slope [30]. In parallel, the nanomechanical, chemical and wear properties of the UHMWPE surface have been significantly enhanced following treatment with helium plasma immersion ion implantation (HePIII). Over the ranges of the parameters, the surface hardness increased by up to six times, whereas the loss in volume following multipass decreased by up to about 2.5 times [31].

In a related study, the influence of nitrogen plasma immersion ion implantation (NPIII) on the surface of UHMWPE was investigated as well. The results suggested a relative increase in surface hardness, macroscopic temperature and mean surface roughness, while the loss in volume decreased. However, the elastic modulus decreased or maybe even increased depending on the actual parameter set applied in the process. According to the parameter range studied, a reduction in wear rate is strongly dependent on thermal effects [32]. A statistical study by Tóth et al. [33] that revised the literature of engineering plastics treated by plasma-based ion implantation (PBII) and plasma-based ion implantation and deposition (PBIID) concluded that there is a rapidly trending in the number of related publications. As a consequence, the effect of nitrogen plasma-based ion implantation (NPBII) on poly(tetrafluoroethylene) (PTFE) was discovered by Kereszturi et al. [34]. The study observed that the F/C atomic ratio significantly decreased in an inverse relationship with the voltage as shown in Fig. 2. Meanwhile the surface roughness increased inversely with the voltage and correlated directly with fluence as shown in Fig. 3. Although a clear relationship between wear volume and the main process parameters was not observed, in general this was improved following treatment along with an increase in surface roughness and O/C atomic ratio. Furthermore, the water contact angle recorded increased under low voltages and high fluences.

Atmospheric dielectric barrier discharge (DBD) plasmas enhance the wettability and surface roughness of polypropylene (PP) proportionally to an increase in the duration of plasma exposure [35]. Also, the surface roughness of PP increases linearly with the exposure time of atmospheric DBD plasma due to degradation of the polymer surface and the formation of nodule-like features. These nodules are shaped by highly oxidized short fragments of polymer which are referred to as low-molecular-weight oxidized materials (LMWOMs) in the literature [15]. In a subsequent study, Kostov et al. [36] reported that modifications in terms of the surface of different engineering plastics, such as polyethylene terephthalate (PET), polyethylene (PE) and PP could be achieved by atmospheric pressure plasma jets (APPJ). The primary aim of this research was to identify the optimal treatment conditions as well as compare the effect of APPJs on another source of atmospheric pressure plasmas, e.g., DBD on the characteristics of polymer surfaces. As a consequence of APPJ treatment the surface roughness is increased as shown in Fig. 4. However, nodule-like structures were produced as well, but were much smaller compared to those constituted in the previous study when the polymer was treated by DBD. This was attributed to the higher degree of polymer degradation during DBD treatment. The adhesion strength of PP and perfluoroalkoxy alkanes (PFAs) has been significantly enhanced due to atmospheric plasma treatment under several gas flows. The characteristics of the surface introduced hydrophilic functional groups where the level

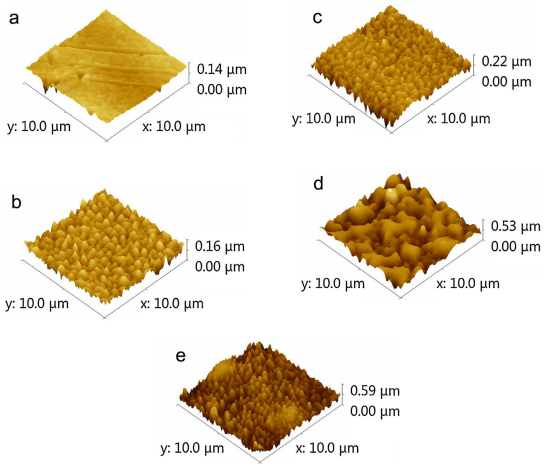

Figure 4: AFM images of PP (a) untreated; (b) 30 s treated; (c) 30 s treated and washed; (d) 60 s treated; (e) 60 s treated and washed. All treatments were conducted with sample reciprocations using a signal amplitude of 10 kV, frequency of 37 kHz and Ar flow of 1.3 l/min.

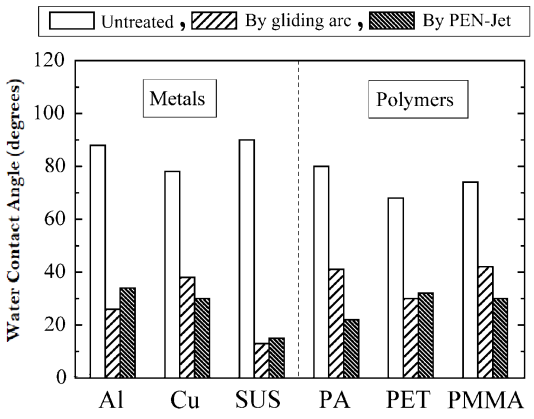

Figure 6: Water contact angles of various materials after treatment.

of improvement changed in proportion to the duration of the treatment as illustrated in Fig. 5 [37]. Although atmospheric pressure glow (APG) discharge plasma treatment is moderate in terms of energy characteristics, APG-derived fluoropolymers exhibit similar surface properties under conventional low-pressure plasmas [38]. Treating metals and polymers by a cold arc-plasma jet under atmospheric pressure leads to a superficial improvement in hydrophilicity and a decrease in the water contact angle of these materials as shown in Fig. 6 [39].

On the other hand, the literature shows that modifications to the surface of aromatic polymers by dielectric barrier discharge (DBD) can achieve a substantial degree of chemical functionalization on the polymer surface by applying relatively low or intermediate levels of power without suffering severe topographical damage [40]. The surface modification of a PET film by an atmospheric-pressure plasma in combination with different gas flows promptly improved its hydrophilicity and was followed by hydrophobic recovery after longer durations [41]. In parallel, significant changes in the morphology and reactivity of PET surfaces have been observed [42,43]. When

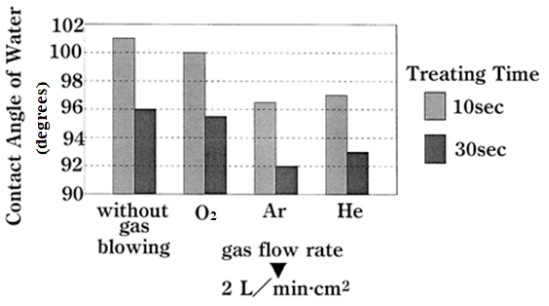

Figure 5: Effect of gas blowing on wettability of PFA film.

exposed to air the processing parameters, such as discharge power, processing speed, processing duration, and electrode configurations, affect the nature and scale of changes to the surface. In general, longer durations (low processing speed and a high number of cycles) and high levels of power induced greater changes in the surface wettability of the polymer [44].

Among the various environmental gases studied, air and oxygen yielded the highest levels of hydrophilicity, while argon and nitrogen resulted in lower degrees of hydrophilicity of the PET surface [45]. Cold atmospheric-pressure plasmas (surface dielectric barrier discharge - SDBD) improve the oxygen and nitrogen contents of PET [46]. In comparison to PET, the effects of plasma treatment on polyether ether ketone (PEEK) have been studied less frequently, but also lead to enhanced degrees of hydrophilicity and adhesion [47] due to the incorporation of functional groups and greater surface roughness following DBD [48]. The hydrophilicity, which is governed by the oxygenation of PEEK following DBD in the air, also recovered after several months through loss of the structurally related functional groups, but it remained more stable than other non-aromatic polymers [49]. Nylon 6 (PA6) exhibited a reduction in surface roughness, and an increase in the O/C and N/C ratios due to diffuse coplanar surface barrier discharge (DCSBD) plasma treatment in two different gas flows (nitrogen and oxygen). However, the oxygen DCSBD plasma was more efficient in terms of modifying the surface compared to the nitrogen equivalent [16]. Also, plasma treatment enhances the contact angle and alters the surface topography of Nylon 66 (PA66) [50]. Plasma pre-treatment of the surface of the biopolymer Poly L Lactic Acid (PLLA) leads to the formation of pits in the crystalline phase accompanied by a mild increase in surface roughness [51].

3. Tribology of Plasma-treated polymer surfaces

3.1 Friction of polymers

Many studies have dealt with the tribology of polymers [52, 53]. Hardness and the elastic modulus are governed by the penetration depth, maximum load and strain rate [54]. Microcuttings are a consequence of ploughing, and they may exacerbate the friction force under specific conditions. Friction that results from elastic hysteresis is known as the deformation component [55, 56]. “The mechanical component results from the resistance of the softer material to "ploughing" by asperities of the harder one” [57]. The adhesive bonds generated between the surfaces in the frictional contact are referred to as the adhesion component. The adhesion component is higher than the deformation (mechanical) equivalent [58]. The friction force is equal to the sum of the adhesion and deformation components as shown in Eq. 1 [59]. From this, the reason for polymer transferred layers forming on the metal counterface during frictional contact can be determined. The transferred films are an essential factor which must be taken into consideration whilst estimating the tribological behaviour of polymers [53]. The effect of load, sliding velocity and temperature on friction are also important parameters that could influence the tribological behaviour of the polymer:

$$F_{\mathrm{f}}{=}F_{\mathrm{a}}{+}F_{\mathrm{d}}\ [\mathrm{N}] \tag{1}$$

where F_{f} represents the friction force, F_{a} the adhesion component, and F_{d} the deformation component of friction. Under low loads, $F_{\mathrm{f}} \approx F_{\mathrm{a}}$ since F_{d} is far smaller than F_{a}.

3.2 Wear of polymers

Wear is the undesirable removal of layers from the surface of a material. Wear occurs when two materials come into contact as a result of movement. Mechanical stress, temperature and chemical reactions directly influence the characteristics of the surface layer. Polymers are sensitive to these factors due to their particular structure and mechanical behaviour. The interface temperature can be significantly higher than the temperature of the environment. The wear of some polymers, that were examined by Lancaster [60] whilst being slid against steel, was found to be influenced by temperature with regard to polymers that the pass is minimum at the characteristic temperature. The accurate classification with regard to the wear of a polymer is not a trivial matter due to the highly diverse nature of such mechanisms [53, 61, 62]. However, abrasion, adhesion and fatigue are the three most common types of polymer wear that occur during the sliding process.

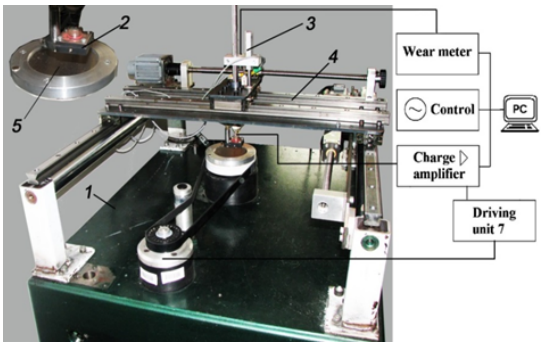

Figure 7: Pin-on-disc tribological test system : 1) base frame, 2) pin holder, 3) loading head, 4) positioning rail, 5) rotating steel disc.

3.3 Tribological tests of polymers

The tribological behaviour of a specific material is not inherent of its properties as far as strength, elastic modulus, etc., are concerned. The influence of friction and wear on the overall performance of a polymer is strongly dependent on the entire configuration of the test. To evaluate the polymer under operating conditions that occur in actual structures, test configurations have to simulate the main sliding mode as accurately as possible in terms of system pair materials, contact geometry, contact pressure, sliding motion, sliding velocity, environmental conditions, mechanical stiffness, etc. As a consequence, regular basis tribo-test systems are assembled from test apparatus that has yet to be standardized.

Several parameters should be taken into consideration to select the most favourable test system, i.e. the structure of the material (macro- or microstructure), contact conditions (whether the contacting bodies possess the same radii of curvature as in a pin-on-disc test or different radii of curvature as in the ball-on-disc test), and energy dissipation (sliding temperature) [63]. The real tribosystem of the elements of a polymer is considered to be the most dependable test, however, due to its expense and impractical nature the test cannot be conducted regularly.

The scale of tribological tests varies from ‘field tests’ that consist of ‘large-scale simulation tests’ on real components to ‘laboratory tests’ on artificial samples which are widespread in the field of the tribological research of polymers due to the small apparatus used and their relatively low cost and versatility with regard to the testing of various materials under different test conditions, e.g. pin-on-disc Fig. 7).

3.4 Tribological behaviour of the surface of polymers treated by plasmas

It is hard to accurately predict the effects of plasma surface treatment on the tribological behaviour of polymers, due to the multitude of mechanisms that govern such processes. It can be expected that functionalization,

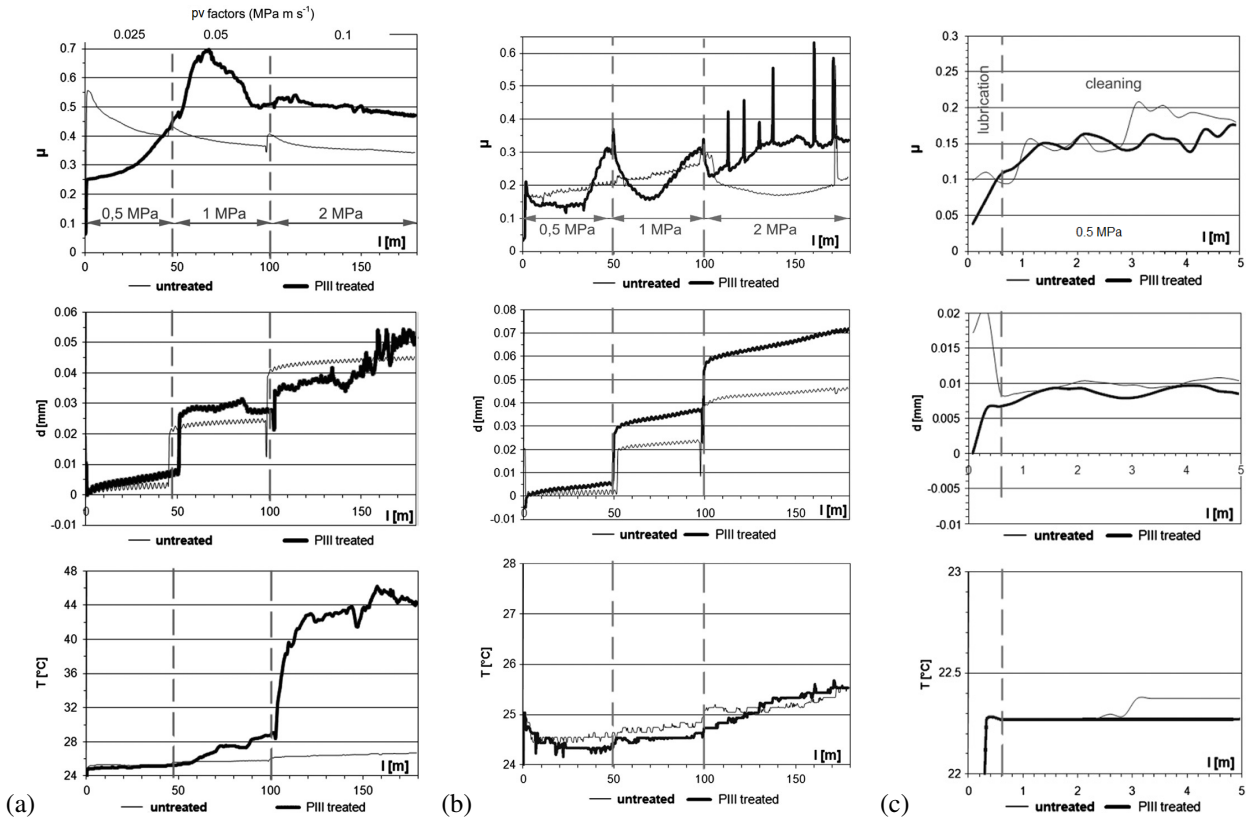

Figure 8: Tribological behaviour of pristine and NPIII-treated PA6; (a) dry conditions; (b) water lubrication conditions; and (c) run-out lubrication conditions.

crosslinking and chain scission will affect their chemical and mechanical surface properties after plasma treatment, which in turn will alter friction and wear characteristics. However, it cannot be confirmed whether such alterations lead to improved tribological properties or not, this can only be ascertained after the treated surface is tested.

The tribological behaviour of rubber treated by plasma has been thoroughly investigated, indicating improvements in terms of friction and wear resistance [13]. The pin-on-disc test yields the lower friction coefficient of PC and PP, whereas PE and PS exhibit larger coefficients of friction after atmospheric plasma treatment compared to their pristine surfaces. Bismarck et al. [64] attributed the significant decrease with regard to the friction coefficient of PC either to the most substantial reduction in contact angle or the changes in the chemical and simultaneously the physical properties of PC after treatment. On the other hand, the increase in the extent of crosslinking after atmospheric plasma treatment resulted in lower levels of friction and wear of PEEK composites [65], while argon plasma treatment led to a higher friction coefficient of PET [12].

The effects of Nitrogen plasma immersion ion implantation (NPIII) on PET indicated improvements with regard to scratch resistance [66]. Kalácska et al. [67] demonstrated that the benefits of sliding tribological properties are strongly dependent on the sliding conditions: a lower degree of friction and enhanced wear performance of PET treated by PIII only occurred in the presence of low *pv* factors under dry or water-lubricated sliding conditions. Five minutes of atmospheric plasma treatment is sufficient to reduce the coefficient of friction and enhance the wear properties of a UHMW-PE film under a constant *pv* factor [68]. In contrast, UHMW-PE treated by atmospheric pressure gas plasma does not exhibit a significant change in terms of wear properties after a treatment time of two minutes.

Since the level of wear reduced by half after longer treatment times, the duration a polymer is exposed to a plasma plays a major role with regard to the tribological properties of the treated surface, in particular for UHMW-PE [69]. UHMW-PE treated by a cold argon plasma using dielectric barrier discharge (DBD) supports such a finding since (under dry conditions) an increase in the friction coefficient with treatment time was observed whereas the wear volume reduced over the treatment time due to modifications of its surface. Under normal saline (N-saline) lubrication conditions, wear volume and friction were reduced over the treatment time which is indicative of an increase in surface wettability and, therefore, enhanced surface lubrication capability [70]. Sagbas [71] reported an increase in friction and improvement in the wear properties of conventional UHMW-PE after plasma treatment, whereas the friction coefficient was unaffected in terms of

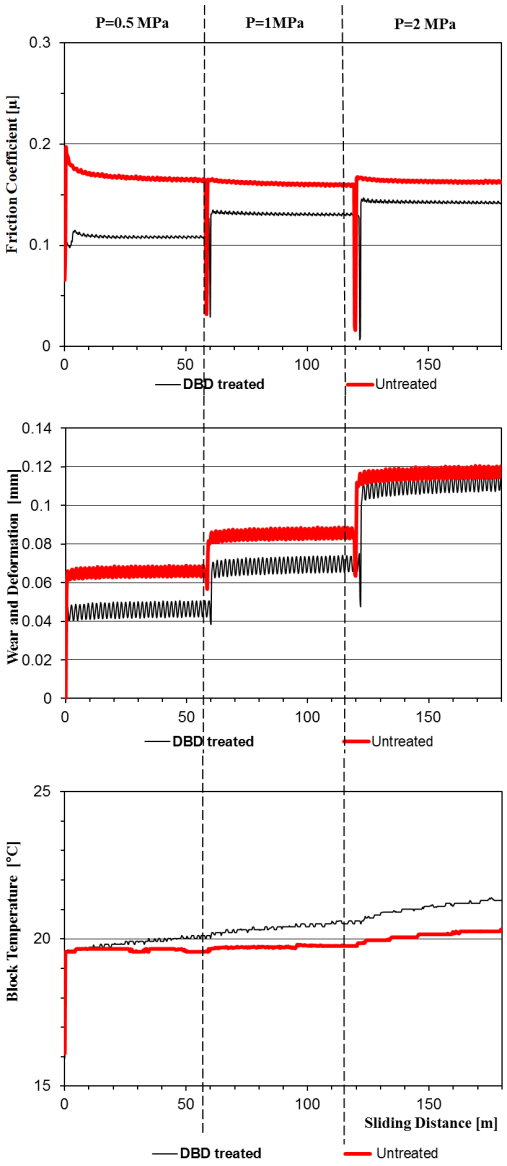

Figure 9: Tribological testing under dry sliding conditions at 0.5; 1; and 2 MPa; including online measurements of coefficients of friction, (specific wear and displacement Δh), and temperature.

vitamin-E-blended UHMW-PE under the same test conditions. However, the wear factor slightly decreased compared to the significant improvement with regard to the wear properties of conventional UHMW-PE as a consequence of the highly cross-linked nature of conventional UHMW-PE.

According to the brief review above with regard to the effect of some plasmas on different polymers, the ability of plasmas to alter the surface characterization and thereby the tribological behaviour of polymers is unquestionable. However, the tribological behaviour of the treated surface depends on several factors such as the type of plasma, treatment method, exposure time, operating mechanism and lubrication conditions amongst many other factors. Kalácska et al. [72] studied the tribological behaviour of PA6 treated by nitrogen plasma immersion ion implantation (NPIII) under different conditions (dry, water and oil lubrication) and various pressure velocity factors (*pv)*. The results show that the friction coefficient and specific wear of treated PA6 are lower than that of the untreated one under dry sliding conditions and low *pv* factors, while the friction coefficient, specific wear and contact temperature of treated PA6 are higher than the pristine equivalent under high *pv* factors (Fig. 8a).

On the other hand, the water lubricant reduces the adhesive component of friction after treatment, which was reflected in the fluctuation of the friction behaviour of the treated surface (Fig. 8b). However, under continuous oil lubrication, no difference could be detected between the treated and untreated parameters, therefore, the run-out type was preferred in terms of detecting such a difference. Test conditions in terms of run-out oil lubrication exhibit a lower friction coefficient for treated PA6 than the pristine equivalent in the presence of low *pv* factors as a consequence of an increase in the dispersive component (Fig. 8c).

In contrast, our last work [73] elaborated on the effect of atmospheric DBD plasma on the tribological behaviour of PET under various test conditions (3 “dry” normal load and “run-out lubrication” constant normal load conditions). The effect of DBD plasma treatment on the characterization of the surface was interpreted as an enhancement of the surface energy and reduction in the surface roughness due to the melting of surface asperities. However, increasing the surface wettability induces higher coefficients of friction according to Archard’s theory of friction [74]. The dry tribological test yielded unexpected behaviour where the coefficient of friction of the treated surface was lower than the pristine equivalent under different *pv* factors. Also, the specific wear and the vertical deformation were enhanced. However, the interface temperature of the treated surface was higher than the untreated one (Fig. 9). The reduction in the coefficient of friction can be theoretically attributed to the smaller contributions of a deformation component. In a related context, a “run-out” oil lubrication test yielded a lower coefficient of friction for the treated surface due to a rise in the surface energy after treatment, leading to a favourable enhancement with regard to the adsorption of the lubricant as shown in Fig. 10. By using the analysis and comparison of the previously reviewed studies, it can be said that atmospheric DBD plasma can be an effective technique nowadays for the treatment of polymer surfaces that aims to reduce friction and improve wear under dry and run-out lubrication conditions under various *pv* factors, especially under lower ones compared to other techniques, e.g. NPIII.

4. Conclusion

In conclusion, the reviewed research and results have apparently shown the capability of plasmas to modify the

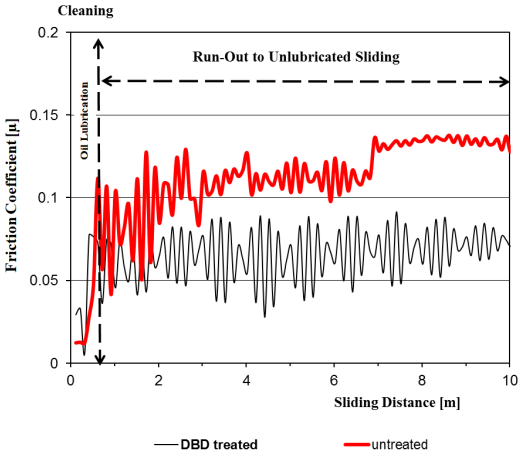

Figure 10: Tribological testing under lubricated sliding and "run-out" conditions at 0.5 MPa.

surfaces of polymers which results in a change in the tribological properties of surfaces. However, the effect of plasmas depends on several factors such as the sources of plasmas, vacuum, temperature, pressure, etc. The essential points concerning the tribological behaviour of polymers that are subjected to plasma treatment are summarized below:

- Plasmas can efficiently alter the characterization of polymer surfaces by utilizing different sources such as APPJ, PIII, APG, PBII and DBD and various vacuums which results in the enhancement of surface wettability and an increase in surface roughness with few exceptions. Atmospheric DBD plasma can achieve the optimum surface configuration in a shorter time.
- There is a paucity of studies which deal with the tribological behaviour of polymers in terms of plasma treatment. Most studies focused on the effect of plasmas on the tribology of engineering polymers especially PET, PA6, and in some cases PEEK. However, no studies appear to deal with Polyolefins, except some studies which investigate the tribology of UHMW-PE for medical applications in particular.
- UHMW-PE exhibits a higher coefficient of friction and improvements in specific wear after plasma treatment under dry conditions where cross-linking plays a prominent role in terms of controlling the wear rate upon plasma treatment. However, the lubricated tribological test of UHMW-PE resulted in a lower coefficient of friction due to an increase in wettability.
- The comparative investigation of engineering polymers treated by different plasmas under the same conditions (PA6 treated by NPIII and PET treated by atmospheric DBD) can explain the remarkable effect of atmospheric DBD plasma on the tribological behaviour of PET under dry conditions where the friction coefficient of PET remained lower than the pristine equivalent, whilst subjected to different *pv* factors. In contrast, PA6 can only sustain low *pv* factors if a low coefficient of friction is desired in the case of NPIII treatment.
- With regard to the aforementioned comparative investigation, atmospheric DBD plasma yielded a unique reduction in the friction coefficient of PET throughout the duration of the test under "run-out" oil lubrication conditions. On the other hand, a slight reduction in the friction coefficient was recorded when PA6 was treated by NPIII under the same test conditions.

REFERENCES

[1] Field, J.: David Tabor. 23 October 1913-1926 November 2005, *Biographical Memoirs of Fellows of the Royal Society,* 2008 DOI: 10.1098/rsbm.2007.0031

[2] Jost, P.: Interview with Luminary Professor H. Peter Jost - The Man Who Gave Birth to the Word "Tribology". (N. C. Jim Fitch, Interviewer), online at: Machinerylubrication.com, accessed on 2017-05-24

[3] Mitchell, L. (2012). The Fiction of Nonfriction, Ward, J. ed. *Popular Science*, 2012 **281**(5), 40

[4] Wikipedia: Tribology, online at: https://en.wikipedia.org/wiki/Tribology#cite_note-1, accessed on 2017-10-24

[5] Myshkin, N.K.; Petrokovets, M.I.; Kovalev, A.V.: Tribology of polymers: adhesion, friction, wear, and mass-transfer, *Tribology International*, 2005 **38**(11-12), 910-921 DOI: 10.1016/j.triboint.2005.07.016

[6] Briscoe, B.J.: Interfacial Friction of Polymer Composites: General Fundamental Principles, *Composite Materials Series*, 1986 **1**, 25-59 DOI: 10.1016/B978-0-444-42524-9.50006-5

[7] Singer, I.L.; Pollock, H. (Eds.): Fundamentals of friction: macroscopic and microscopic processes (Kluwer Academic Publisher, London) 1992 ISBN: 978-94-011-2811-7

[8] Akram, M.; Jansen, K.M.B.; Ernst, L.J.; Bhowmik, S.: Atmospheric plasma modification of polyimide sheet for joining to titanium with high temperature adhesive, *International Journal of Adhesion and Adhesives*, 2016 **65**, 63-69 DOI: 10.1016/j.ijadhadh.2015.11.005

[9] Petrie, E.M.: Handbook of Adhesives and Sealants, Second Edition (McGraw-Hill Companies, Inc., New York) 2007 ISBN: 9780071479165

[10] Noeske, M.; Degenhardt, J.; Strudthoff, S.; Lommatzsch, U.: Plasma jet treatment of five polymers at atmospheric pressure: surface modifications and the relevance for adhesion, *International Journal of Adhesion and Adhesives*, 2004 **24**(2), 171-177 DOI: 10.1016/j.ijadhadh.2003.09.006

[11] Rotheiser, J.: Joining of Plastics, 3rd Edition (Carl Hanser Verlag GmbH & Co. KG, Cincinnati) 1998 ISBN: 978-1-56990-445-9

[12] Leggett, G.J.; Beake, B.D.: Development of surface morphology, local friction, and adhesion in plasma treated poly (ethylene terephthalate) films, *Polymer Preprints(USA)*, 1998 **39**(2), 1228-1229

[13] Segu, D.Z.: NBR surface modification by Ar plasma and its tribological properties, *Industrial Lubrication and Tribology*, 2016 **68**(2), 227-232 DOI: 10.1108/ILT-05-2015-0062

[14] Kostov, K.G.; Hamia, Y.A.A.; Mota, R.P.; Dos Santos, A.L.R.; Nascente, P.A.P.: Treatment of polycarbonate by dielectric barrier discharge (DBD) at atmospheric pressure, *Journal of Physics: Conference Series*, 2014 **511**(1), 012075. IOP Publishing DOI: 10.1088/1742-6596/511/1/012075

[15] Kostov, K.G.; Nishime, T.M.C.; Hein, L.R.O.; Toth, A.: Study of polypropylene surface modification by air dielectric barrier discharge operated at two different frequencies, *Surface and Coatings Technology*, 2013 **234**, 60-66 DOI: 10.1016/j.surfcoat.2012.09.041

[16] Novák, I.; Popelka, A.; Valentín, M.; Chodák, I.; Špírková, M.; Tóth, A.; Kleinová, A.; Sedliačik, J.; Lehocký, M.; Marônek, M.: Surface behavior of polyamide 6 modified by barrier plasma in oxygen and nitrogen, *International Journal of Polymer Analysis and Characterization*, 2014 **19**(1), 31-38 DOI: 10.1080/1023666X.2014.850907

[17] Károly, Z.; Klébert, S.; Al-Maliki, H.; Pataki, T.: Comparison of NPIII and DBD Plasma Treatment in Terms of Wettability of PTFE and PA6, *Scientific Bulletin Series C: Fascicle Mechanics, Tribology, Machine Manufacturing Technology*, 2016 **30**, 47

[18] Al-Maliki, H.; Zoltán, Sz.; Róbert, K.; Kalácska, G.: Shear strength of polypropylene bonded joints using pristine and DBD plasma treated surfaces, *Mechanical Engineering Letters R&D, SZIE,* 2016 **14**, 71-77

[19] Al-Maliki, H.; Kalácska, G.: The effect of atmospheric DBD plasma on surface energy and shear strength of adhesively bonded polymer, *Hungarian Agricultural Engineering*, 2017 **31**, 52-58 DOI: 10.17676/HAE.2017.31.52

[20] Ionita, M.D.; Teodorescu, M.; Stancu, C.; Stancu, E.C.; Ionita, E.R.; Moldovan, A.; Acsente, T.; Bazavan, M.; Dinescu, G.: Surface modification of polymers at atmospheric pressure in expanding RF plasmas generated by planar dielectric barrier discharges, *Journal of Optoelectronics and Advanced Materials*, 2010 **12**(3), 777-782

[21] Nastuta, A.V.; Rusu, G.B.; Topala, I.; Chiper, A.S.; Popa, G.: Surface modifications of polymer induced by atmospheric DBD plasma in different configurations, *Journal of Optoelectronics and Advanced Materials*, 2008 **10**(8), 2038-2042

[22] Hergelová, B.; Homola, T.; Zahoranová, A.; Plecenik, T.; Kováëik, D.: Plasma surface modification of biocompatible polymers using atmospheric pressure dielectric barrier discharge, *WDS'12 Proceedings of Contributed Papers, Part II*, pp. 128-133, 2012 ISBN: 978-80-7378-225-2

[23] Tendero, C.; Tixier, C.; Tristant, P.; Desmaison, J.; Leprince, P.: Atmospheric pressure plasmas: A review, *Spectrochimica Acta Part B: Atomic Spectroscopy*, 2006 **61**(1), 2-30 DOI: 10.1016/j.sab.2005.10.003

[24] Chapman, B.: Glow Discharge Processes (Wiley, New York) 1980 ISBN: 978-04-7107-828-9

[25] Lieberman, M.A.; Lichtenberg, A.J.: Principles of plasma discharges and materials processing, *MRS Bulletin*, 1994 **30**, 899-901 DOI: https://doi.org/10.1557/mrs2005.242

[26] Conrads, H.; Schmidt, M.: Plasma generation and plasma sources, *Plasma Sources Science and Technology*, 2000 **9**(4), 441 IOP Publishing

[27] Kalácska, G.; Károly, Z.; Klébert, S.; András, E.: NPIII Treatment towards to Cold Atmospheric Plasma as Surface Modification Technics of Engineering Polymers, *Scientific Bulletin Series C: Fascicle Mechanics, Tribology, Machine Manufacturing Technology*, 2015 **29**, 51

[28] Boulos, M.I.; Fauchais, P.; Pfender, E.: Thermal plasmas: fundamentals and applications (Springer Science & Business Media, New York) 2013

[29] Tóth, A.; Bertóti, I.; Szilágyi, E.; Dong, H.; Bell, T.; Juhász, A.; Nagy, P.M.: Surface characterization of ultrahigh molecular weight polyethylene after nitrogen ion implantation, *Surface and Interface Analysis*, 2000 **30**(1), 434-438 DOI: 10.1002/1096-9918(200008)30:1<434::AID-SIA788>3.0.CO;2-W

[30] Tóth, A.; Mohai, M.; Ujvári, T.; Bertóti, I.: Hydrogen plasma immersion ion implantation of ultrahigh molecular weight polyethylene, *Surface and Interface Analysis*, 2006 **38**(4), 898-902 DOI: 10.1002/sia.2197

[31] Tóth, A.; Mohai, M.; Ujvári, T.; Bertóti, I.: Advanced surface modification of ultrahigh molecular weight poly (ethylene) by helium plasma immersion ion implantation, *Polymers for Advanced Technologies*, 2006 **17**(1112), 898-901 DOI: 10.1002/pat.788

[32] Tóth, A.; Bertóti, I.; Mohai, M.; Ujvári, T.: Surface modification of polyethylene by nitrogen PIII: Surface chemical and nanomechanical properties, *Materials Science Forum*, 2007 **537**, 255-262 DOI: 10.4028/www.scientific.net/MSF.537-538.255

[33] Tóth, A.; Kereszturi, K.; Mohai, M.; Bertóti, I.: Plasma based ion implantation of engineering polymers, *Surface and Coatings Technology*, 2010 **204**(18), 2898-2908 DOI: 10.1016/j.surfcoat.2009.12.004

[34] Kereszturi, K.; Tóth, A.; Mohai, M.; Bertóti, I.; Szépvölgyi, J.: Nitrogen plasma-based ion implantation of poly (tetrafluoroethylene): Effect of the main parameters on the surface properties, *Applied*

Surface Science, 2010 **256**(21), 6385-6389 DOI: 10.1016/j.apsusc.2010.04.021

[35] Nishime, T.M.C.; Tóth, A.; Hein, L.R.O.; Kostov, K.G.: Surface characteristics analysis of polypropylene treated by dielectric barrier discharge at atmospheric pressure, *Journal of Physics: Conference Series*, 2012 **370**(1), 012025 IOP Publishing DOI: 10.1088/1742-6596/370/1/012025

[36] Kostov, K.G.; Nishime, T.M.C.; Castro, A.H.R.; Tóth, A.; Hein, L.R.D.O.: Surface modification of polymeric materials by cold atmospheric plasma jet, *Applied Surface Science*, 2014 **314**, 367-375 DOI: 10.1016/j.apsusc.2014.07.009

[37] Tsuchiya, Y.; Akutu, K.; Iwata, A.: Surface modification of polymeric materials by atmospheric plasma treatment, *Progress in Organic Coatings*, 1998 **34**(1), 100-107 DOI: 10.1016/S0300-9440(97)00117-3

[38] Prat, R.; Koh, Y.J.; Babukutty, Y.; Kogoma, M.; Okazaki, S.; Kodama, M.: Polymer deposition using atmospheric pressure plasma glow (APG) discharge, *Polymer*, 2000 **41**(20), 7355-7360 DOI: 10.1016/S0032-3861(00)00103-8

[39] Toshifuji, J.; Katsumata, T.; Takikawa, H.; Sakakibara, T.; Shimizu, I.: Cold arc-plasma jet under atmospheric pressure for surface modification, *Surface and Coatings Technology*, 2003 **171**(1), 302-306 DOI: 10.1016/S0257-8972(03)00290-1

[40] Upadhyay, D.J.; Cui, N.Y.; Meenan, B.J.; Brown, N.M.D.: The effect of dielectric barrier discharge configuration on the surface modification of aromatic polymers, *Journal of Physics D: Applied Physics*, 2005 **38**(6), 922 IOP Publishing DOI: 10.1088/0022-3727/38/6/022

[41] Gotoh, K.; Kobayashi, Y.; Yasukawa, A.; Ishigami, Y.: Surface modification of PET films by atmospheric pressure plasma exposure with three reactive gas sources, *Colloid and Polymer Science*, 2012 **290**(11), 1005-1014 DOI: 10.1007/s00396-012-2600-7

[42] Esena, P.; Riccardi, C.; Zanini, S.; Tontini, M.; Poletti, G.; Orsini, F.: Surface modification of PET film by a DBD device at atmospheric pressure, *Surface and Coatings Technology*, 2005 **200**(1), 664-667 DOI: 10.1016/j.surfcoat.2005.02.188

[43] Rashed, U.M.; Ahmed, H.; Al-Halwagy, A.; Garamoon, A.A.: Surface characteristics and printing properties of PET fabric treated by atmospheric dielectric barrier discharge plasma, *The European Physical Journal-Applied Physics*, 2009 **45**(1), pp.11001-p1–11001-p5 DOI: 10.1051/epjap:2008197

[44] Liu, C.; Brown, N.M.; Meenan, B.J.: Uniformity analysis of dielectric barrier discharge (DBD) processed polyethylene terephthalate (PET) surface, *Applied Surface Science*, 2006 **252**(6), 2297-2310 DOI: 10.1016/j.apsusc.2005.04.016

[45] Onsuratoom, S.; Rujiravanit, R.; Sreethawong, T.; Tokura, S.; Chavadej, S.: Silver loading on DBD plasma-modified woven PET surface for antimicrobial property improvement, *Plasma Chemistry and Plasma Processing*, 2010 **30**(1), 191-206 DOI: 10.1007/s11090-009-9199-6

[46] Novák, I.; Popelka, A.; Luyt, A.S.; Chehimi, M.M.; Špírková, M.; Janigová, I.; Kleinováa, A.; Stopkaf, P.; Šloufe, M.; Vankog, V.; Chodá, I.; Valentin, M.: Adhesive properties of polyester treated by cold plasma in oxygen and nitrogen atmospheres, *Surface and Coatings Technology*, 2013 **235**, 407-416 DOI: 10.1016/j.surfcoat.2013.07.057

[47] Zhang, S.; Awaja, F.; James, N.; McKenzie, D.R.; Ruys, A.J.: A comparison of the strength of autohesion of plasma treated amorphous and semi-crystalline PEEK films, *Polymers for Advanced Technologies*, 2011 **22**(12), 2496-2502 DOI: 10.1002/pat.1791

[48] Luo, H.; Xiong, G.; Ren, K.; Raman, S.R.; Liu, Z.; Li, Q.; Ma, C.; Li, D.; Wan, Y.: Air DBD plasma treatment on three-dimensional braided carbon fiber-reinforced PEEK composites for enhancement of in vitro bioactivity, *Surface and Coatings Technology*, 2014 **242**, 1-7 DOI: 10.1016/j.surfcoat.2013.12.069

[49] Upadhyay, D.J.; Cui, N.Y.; Anderson, C.A.; Brown, N.M.D.: Surface recovery and degradation of air dielectric barrier discharge processed poly (methyl methacrylate) and poly (ether ether ketone) films, *Polymer Degradation and Stability*, 2005 **87**(1), 33-41 DOI: 10.1016/j.polymdegradstab.2004.07.006

[50] Labay, C.P.; Canal Arias, J.M.; Navarro Sentanyes, A.; Canal Barnils, C.: Comparison of the effects of corona and low pressure plasma on the release of caffeine from PA66 filaments, *51st Dornbirn Manmade Fibers Congress Lectures CD*, pp. 1-6, 2012

[51] Slepička, P.; Michaljaničová, I.; Švorčík, V.: Controlled biopolymer roughness induced by plasma and excimer laser treatment, *Express Polymer Letters*, 2013 **7**(11), 950-958 DOI: 10.3144/expresspolymlett.2013.92

[52] Kragelskii, I.V.: Friction and Wear (Pergamon Press, Elmsford) 1982 ISBN: 978-00-8027-591-8

[53] Kovalev, N.K.; Myshkin, A.V.: Adhesion and friction of polymers, in: *Polymer Tribology*, Eds.: Sujeet, K.S.; Briscoe, B.J. (Imperial College Press, Singapore) 2009 DOI: 10.1142/9781848162044_0001

[54] Kovalev, A.; Shulha, H.; Lemieux, M.; Myshkin, N.; Tsukruk, V.V.: Nanomechanical probing of layered nanoscale polymer films with atomic force microscopy, *Journal of Materials Research*, 2004 **19**(3), 716-728 DOI: 10.1557/jmr.2004.19.3.716

[55] Bowden, F.P.; Tabor, D.: Friction and lubrication of solids (Clarendon Press, Oxford) 1964 ISBN: 019851204X

[56] Moore, D.F.: The Friction and Lubrication of Elastomers (Pergamon Press, Oxford) 1972 ISBN: 978-00-8016-749-7

[57] Yamaguchi, Y.: Tribology of plastic materials (Elsevier, Tokyo) 1990 ISBN: 978-00-8087-580-4

[58] Bely, V.A.; Sviridenok, A.I.; Petrokovets, M.I.; Savkin, V.G.: Friction and Wear in Polymer-Based Materials (Pergamon Press, Oxford) 1982

[59] Kalácska, G.: An engineering approach to dry friction behaviour of numerous engineering plastics with respect to the mechanical properties, *Express Polymer Letters*, 2013 **7**(2), 199-210 DOI: 10.3144/expresspolymlett.2013.18

[60] Lancaster, J.K.: Relationships between the wear of polymers and their mechanical properties, *Proceedings of the Institution of Mechanical Engineers, Conference Proceedings*, 1968 **183**(16), 98-106

[61] Myshkin, N.K.; Kim, C.K.; Petrokovets, M.I.: Introduction to tribology (Chong Moon Gak, Seoul) 1997

[62] Blau, P.: Friction and wear transitions of materials (Noyes Publication, New York) 1989 ISBN: 978-08-1551-196-0

[63] Samyn, P.; Schoukens, G.; Quintelier, J.: Scaling Effects in Tribotesting of Polymers, in: *Polymer Tribology*, Eds.: Sujeet, K.S.; Briscoe, B.J. (Imperial College Press, Singapore) 2009 DOI: 10.1142/9781848162044_0003

[64] Bismarck, A.; Brostow, W.; Chiu, R.; Hagg Lobland, H.E.; Ho, K.K.: Effects of surface plasma treatment on tribology of thermoplastic polymers, *Polymer Engineering & Science*, 2008 **48**(10), 1971-1976 DOI: 10.1002/pen.21103

[65] Zhang, R.; Häger, A.M.; Friedrich, K.; Song, Q.; Dong, Q.: Study on tribological behaviour of plasma-treated PEEK and its composites, *Wear*, 1995 **181**, 613-623 DOI: 10.1016/0043-1648(95)90177-9

[66] Kereszturi, K.; Tóth, A.; Mohai, M.; Bertóti, I.: Surface chemical and nanomechanical alterations in plasma immersion ion implanted PET, *Surface and Interface Analysis*, 2008 **40**(34), 664-667 DOI: 10.1002/sia.2643

[67] Kalácska, G.; Zsidai, L.; Kereszturi, K.; Mohai, M.; Tóth, A.: Sliding tribological properties of untreated and PIII-treated PETP, *Applied Surface Science*, 2009 **255**(11), 5847-5850 DOI: 10.1016/j.apsusc.2009.01.017

[68] Samad, M.A.; Satyanarayana, N.; Sinha, S.K.: Tribology of UHMWPE film on air-plasma treated tool steel and the effect of PFPE overcoat, *Surface and Coatings Technology*, 2010 **204**(9), 1330-1338 DOI: 10.1016/j.surfcoat.2009.09.011

[69] Perni, S.; Kong, M.G.; Prokopovich, P.: Cold atmospheric pressure gas plasma enhances the wear performance of ultra-high molecular weight polyethylene, *Acta Biomaterialia*, 2012 **8**(3), 1357-1365 DOI: 10.1016/j.actbio.2011.12.007

[70] Naresh, K.N.; Yap, S.L.; Khan, M.Z.; Pattela, S.R.S.: Effect of Argon Plasma Treatment on Tribological Properties of UHMWPE/MWCNT Nanocomposites, *Polymers*, 2016 **8**(8), 295 DOI: 10.3390/polym8080295

[71] Sagbas, B.: Effect of argon plasma surface modification on tribological behavior of biopolymers, *Industrial Lubrication and Tribology*, 2016 **68**(4), 508-514 DOI: 10.1108/ILT-11-2015-0176

[72] Kalácska, G.; Zsidai, L.; Keresztes, R.; Tóth, A.; Mohai, M.; Szépvölgyi, J.: Effect of nitrogen plasma immersion ion implantation of polyamide-6 on its sliding properties against steel surface, *Wear*, 2012 **290**, 66-73 DOI: 10.1016/j.wear.2012.05.011

[73] AlMaliki, H.; Zsidai, L.; Samyn, P.; Szakál, Z.; Keresztes, R.; Kalácska, G.: Effects of atmospheric plasma treatment on adhesion and tribology of aromatic thermoplastic polymers, *Polymer Engineering & Science,*(Early View) DOI: 10.1002/pen.24689

[74] Archard, J.: Contact and rubbing of flat surfaces, *Journal of Applied Physics*, 1953 **24**(8), 981-988 DOI: 10.1063/1.1721448

DE GRUYTER OPEN

HUNGARIAN JOURNAL OF INDUSTRY AND CHEMISTRY
Vol. 46(2) pp. 13-17 (2018)
hjic.mk.uni-pannon.hu
DOI: 10.1515/hjic-2018-0012

HUNGARIAN JOURNAL OF INDUSTRY AND CHEMISTRY
HJIC

APPLICATION OF 2N DESIGN OF EXPERIMENT METHOD FOR THE EVALUATION OF THE EFFICIENCY AND CROSS-EFFECTS OF OILFIELD CHEMICALS

ZOLTÁN LUKÁCS *[1] AND TAMÁS KRISTÓF[1]

[1]Department of Physical Chemistry, Institute of Chemistry, University of Pannonia, Egyetem u. 10, Veszprém, H-8201, HUNGARY

It has been known for a long time that oilfield chemicals used for different purposes (corrosion and scale inhibitors, scavengers, biocides, etc.) can modify the efficiency of each other. These cross-effects can exhibit adverse or beneficial impacts and may modify the overall corrosiveness of the medium to a great extent. However, there is no standard procedure in order to evaluate the cross-effects, i.e. the extent to which the effect of one of the chemicals is modified by the addition of another. The 2N Design of Experiment (DoE) method provides a robust and simple statistical way to evaluate the change in efficiency of oilfield chemicals owing to the addition of other additives. The 2N DoE method can also be applied to other systems. In the present work the effects and cross-effects in systems consisting of a corrosion inhibitor, as well as an oxygen and a hydrogen sulphide scavenger are investigated and successfully demonstrated in a typical oilfield corrosion system with electrochemical corrosion monitoring methods.

Keywords: oilfield chemicals, corrosion inhibitor, Design of Experiment

1. Introduction

The chemical treatment of wet oils that are produced is a widely used method for mitigating unfavorable phenomena in the production, transportation and processing of crude oils: corrosion, scaling, emulsion forming, etc. On the way from the oil well to the refinery a variety of oilfield treatment chemicals are added to the oil: corrosion and scale inhibitors, biocides, hydrogen sulfide and oxygen scavengers (typically with wash waters), demulsifiers, anti-foam agents, etc. [1–4]. The effects of these chemicals are typically well defined in themselves, but the cross-effects, i.e. the influence on each other, are rarely discussed and even more rarely investigated, especially *in situ*. The reason for this is rather complex. From a practical perspective, there is no standard or well-established procedure for such testing. From a theoretical standpoint, the evaluation of such tests, if any, is rather problematic because if the effects of factors are strongly correlated (i.e. one or more "cross-effects" are significant in the system) then the evaluation of the effects by usual means (i.e. least square model fitting [5–7]) is subject to a significant error, if not impossible.

In order to formulate the problem, let us consider a dependent variable, y, e.g. the corrosion rate, and assume that it is a quantitative function of some other quantitative independent variables:

$$y = p_1 x_1 + p_2 x_2 + \cdots + p_n x_n. \tag{1}$$

This is an uncorrelated multilinear model, that is, the $(p_1, \cdots, p_n)$ parameter set, the set of the ***factor coefficients***, is invariant throughout the whole $(x_1, \cdot, x_n)$ model variable space. If the $(p_1, ..., p_n)$ parameter set is dependent on the location in the model variable space then the following correlated multilinear model can be applied:

$$\begin{aligned} y = \quad & p_1 x_1 + p_2 x_2 + \cdots + p_n x_n + \\ & + q_{1,2} x_1 x_2 + \cdots + q_{n-1,n} x_{n-1} x_n, \end{aligned} \tag{2}$$

where the $q_{1,2}, \cdots q_{n-1,n}$ coefficients represent the ***cross-effects coefficients*** (the effect of quadratic and higher order contributions is not discussed here). If the cross-effects are significant in a model, i.e. the coefficients of the cross-effects are comparable to the coefficients of the factors, then severe computational difficulties may occur, especially if a remarkable error (random or systematic) is superimposed on the measurement data. In such cases conventional parameter-fitting procedures generally fail to provide realistic and accurate model coefficients.

For the investigation of cross-effects, a viable technique is the so-called 2N Design of Experiment (DoE) method. As this method is not widely used in the field of corrosion science and technology, its basic concepts are outlined in brief here.

*Correspondence: lukacs600131@gmail.com

In the methodology of the Design of Experiment technique the independent variables are known as factors and the values of the factors are referred to as factor levels. The factor levels are fixed, discrete values (in contrast to the continuous range of the independent variables). The variance in the factor levels, if any, will be transformed into a variance of the dependent variable. The Design of Experiment methods are typically used in industrial quality assurance testing, where the fixed factor levels correspond to certain standardized levels of the factors that are assumed to influence a quality parameter (i.e. the dependent variable). In oilfield chemical performance tests a fixed value with regard to the factor of the "corrosion inhibitor" can be the concentration recommended by the supplier. Apart from the fixing of the factor levels, the general Design of Experiment schemes and the supporting mathematical apparatus basically do not differ from conventional multilinear parameter fitting. However, a special type of DoE, the 2N Design of Experiment method, possesses some noteworthy mathematical properties that make it especially applicable for studying cross-effects.

In the 2N DoE method every factor possesses exactly two factor levels and they are normalized to -1 and $+1$. In some cases, if all the factors are quantitative, a factor level of 0 exists in order to test the linearity of the model. With the normalization of the factor levels to -1 and $+1$, all the factors and cross-effects are orthogonal, i.e. independently calculable from each other. This is a great advantage, making the method applicable to study cross-effects.

On the other hand, the normalization of the factor levels to the arbitrary -1 and $+1$ levels is costly. The coefficients of the factors and cross-effects, determined after the calculations, do not have any direct physical meaning, they can only be interpreted in terms of a comparison with one another and to the variance of the measurement data. A comparison of the factors and cross-effects with one another can yield a series of more and less significant effects and a comparison to the variance can provide information on the statistical significance of the respective factor/cross-effect. Obviously, the value of the obtained factor and cross-effect coefficients is dependent on the chosen spread between the two factor levels, therefore, this choice must be made with careful consideration. For example, if effects and interactions of oilfield chemicals are investigated, then one of the factor levels would be proposed to be "no chemical added" (concentration = 0) and the other factor level would be termed as the chemical added to the fluid within the recommended range.

The purpose of this work was to demonstrate the applicability of the 2N DoE method for studying the factors and cross-effects of oilfield chemicals in a suitably chosen model system.

2. Experimental

The model system was chosen as a typical corrosion system, containing a carbon steel electrode in a well-buffered, slightly acidic electrolyte (0.1 M $NaHSO_4$ + 0.1 M Na_2SO_4), which maintains a nearly constant corrosiveness and reduces the accumulation of solid corrosion products on the surface of the electrode which also improves the reproducibility of the tests. As the aim was to simulate the effects and cross-effects of oilfield chemical treatment additives (corrosion inhibitor, as well as hydrogen sulfide and oxygen scavengers), 1 mM of Na_2S was added to the solution.

The carbon steel plates (three specimens) were applied for three parallel runs in each measurement set. The specimens were abraded with emery paper and then degreased in acetone for one hour. Before each run the species were etched in 5 % HCl, degreased in an alkaline degreasing solution and etched in 5 % HCl again (all dippings lasted for a duration of 5 minutes). 600 cm^3 of the solution was poured into a cylindrical test cell of 1000 cm^3 in volume and a carbon steel plate electrode with a surface area of 17 cm^2 was introduced into the cell, equipped with a silver/silver chloride (3.5 M) reference electrode and two mixed metal oxide-coated titanium tube counter electrodes both 3 mm in diameter and 50 mm in length. The solution was not de-aerated and the measurements were conducted at room temperature (25 $^\circ$C).

The corrosion rate was determined by impedance measurements carried out at 1 kHz and 0.1 Hz with a 20 mV p-p amplitude AC signal superimposed on the corrosion potential, which was established to a satisfactorily stationary level (max. 1 mV/min drift) of no more than 10 minutes. The polarization resistance of the electrode was determined by subtracting the high-frequency resistance (solution resistance) from the low-frequency resistance. The measurements were conducted by an Electroflex EF-430 potentiostat and a PicoScope 3403D oscilloscope. The results were cross-checked by a Metrohm potentiostat. In order to simulate the components of a typical oilfield chemical treatment procedure, a commercial corrosion inhibitor (BPR 81100, Baker Hughes, 100 ppm), zinc acetate as a model compound for a hydrogen sulfide scavenger at a concentration of 2 mM, and sodium metabisulfite ($Na_2S_2O_5$) also at a concentration of 2 mM were added. All chemicals were of p.a. quality. The 2N DoE scheme is shown in Table 1 below. All experimental sets were repeated 3 times with different electrodes.

3. Results and Discussion

The effect of three factors (a corrosion inhibitor, as well as hydrogen sulfide and oxygen scavengers) was studied on the polarization resistance (compensated for by the ohmic drop in the solution, see the previous Section) and the corrosion current. The relationship between the po-

Table 1: Levels of factors and cross-effects of factors in the DoE sets.

	Factors			Factor cross effects		
Set #	Corrosion inhibitor	Hydrogen sulfide scavenger	Oxygen scavenger	Corrosion inhibitor × Hydrogen sulfide scavenger	Corrosion inhibitor × Oxygen scavenger	Hydrogen sulfide scavenger × Oxygen scavenger
1	-1	-1	-1	1	1	1
2	-1	-1	1	1	-1	-1
3	-1	1	-1	-1	1	-1
4	-1	1	1	-1	-1	1
5	1	-1	-1	-1	-1	1
6	1	-1	1	-1	1	-1
7	1	1	-1	1	-1	-1
8	1	1	1	1	1	1

larization resistance and the corrosion current was calculated as:

$$j_0[A] = \frac{1}{2.303}\frac{\left(b_a^{-1}[V] + b_c^{-1}[V]\right)^{-1}}{R_p[\Omega]} = \frac{1}{2.303}\frac{0.04[V]}{R_p[\Omega]}, \tag{3}$$

with a typical value of $b_a = 0.06$ V/decade and $b_c = 0.12$ V/decade, furthermore, R_p is measured in Ohms and j_0 in Amperes. The units of measurement are shown in square brackets.

The Design of Experiment scheme is shown in Table 1 The scheme consists of $2^3 = 8$ sets. The levels of interactions (cross-effects) are simply the product of the levels of the respective factors.

The original assumption of the work was that the polarization resistance and/or the corrosion current of the test specimen depend on the factors according to the following model:

$$Y_S = \overline{Y} + \sum_f A_f E_f + \sum_i B_i E_i, \tag{4}$$

where Y_S stands for the value of the target function in the respective set (the polarization resistance or corrosion current), $\overline{Y}$ denotes the total average of the same, E_f and E_i represent the level of the respective factor/cross-effect in the respective set (-1 or $+1$), and A_f and B_i are the values of the respective effect/interaction coefficients. The overall standard deviation of the measurement data was determined via

$$\sigma(Y) = \sqrt{\frac{1}{S(J-1)}\sum_{s=1}^{S}\sum_{j=1}^{J}\left(Y_{s,j} - \overline{Y}_s\right)^2}, \tag{5}$$

where $S = 8$ is the number of sets, $J = 3$ stands for the number of runs per set, $Y_{s,j}$ denotes the measurement result (polarization resistance or the corrosion current) and $\overline{Y}_s$ represents the average of the latter for a certain set.

The results based on the model of Eq. 4 are included in Tables 2 and 3 for the polarization resistance and corrosion current, respectively.

By comparing the coefficients in the tables above it is striking at first sight that – apart from the coefficient of the corrosion inhibitor factor, which possesses the greatest absolute value in both tables – there is great variation in the relative significance of the corresponding values. It could be expected that if a factor/cross-effect is more significant in the model describing the variations of the

Table 2: Factors (in diagonal cells), cross-effect coefficients and the variance of the measurement data for the evaluation of polarization resistance values. Values larger than the standard deviation are set in bold.

Factors	Corrosion inhibitor	Hydrogen sulfide scavenger	Oxygen scavenger
Corrosion inhibitor	**3.359**	−1.086	**−3.319**
Hydrogen sulfide scavenger		0.022	−0.082
Oxygen scavenger			**−3.087**
Standard deviation of measurement data	**2.125**		

Table 3: Factors (in diagonal cells), cross-effect coefficients and the variance of the measurement data for the evaluation of corrosion current values. Values larger than the standard deviation are set in bold.

Factors	Corrosion inhibitor	Hydrogen sulfide scavenger	Oxygen scavenger
Corrosion inhibitor	$\mathbf{-9.06 \cdot 10^{-4}}$	$\mathbf{7.39 \cdot 10^{-4}}$	$\mathbf{8.71 \cdot 10^{-4}}$
Hydrogen sulfide scavenger		$\mathbf{-7.31 \cdot 10^{-4}}$	$\mathbf{7.45 \cdot 10^{-4}}$
Oxygen scavenger			-3.98×10^{-4}
Standard deviation of measurement data	$\mathbf{4.55 \cdot 10^{-4}}$		

Table 4: Factors (in diagonal cells), cross-effect coefficients and the variance of the measurement data for the evaluation of the logarithm of the polarization resistance values. Values larger than the standard deviation are set in bold.

Factors	Corrosion inhibitor	Hydrogen sulfide scavenger	Oxygen scavenger
Corrosion inhibitor	**0.275**	−0.143	**−0.266**
Hydrogen sulfide scavenger		0.110	−0.117
Oxygen scavenger			−0.110
Standard deviation of measurement data	**0.172**		

polarization resistance, then the same factor/cross-effect will exhibit approximately the same relative significance in the model of the corrosion current. However, in this case great differences exist in terms of the relative significance. The coefficient of the factor concerning the hydrogen sulfide scavenger and its cross-effect with the oxygen scavenger are both negligible in the model of the polarization resistance (Table 2) and much more significant (compared to the standard deviation of the measurement data in Table 3). This magnitude of the differences cannot simply be attributed to some changes with regard to the weighing of measurement data due to the reciprocal transformation from the polarization resistance to the corrosion current (cf. Eq. 3 and raises doubts suggesting that the model in Eq. 4 is invalid. Eq. 4 suggests that the contribution of the additives (corrosion inhibitor and the scavengers) to the dependent variable is a linear function of the concentration. However, if it is taken into consideration that the effects of the additives are basically kinetic, then it can be implied that instead of the linear Eq. 4 a logarithmic approximation might exist:

$$\ln Y_S = \ln \overline{Y} + \sum_f A_f \ln E_f + \sum_i B_i \ln E_i, \qquad (6)$$

which is in agreement with the general experience that the effects (activities) of components are proportional to the logarithm of concentration. By applying Eq. 6, the factors and cross-effect coefficients of the models for the polarization resistance and corrosion current will be identical apart from a multiplicator of (-1).

The model-fitting results of Eq. 6 are shown in Table 4 for the polarization resistance data. From the results it can be concluded that the corrosion inhibitor has the greatest effect on the system and it increases the polarization resistance significantly. The hydrogen sulfide scavenger also decreases the corrosion rate in itself, but its application along with the corrosion inhibitor is less favorable. The use of an oxygen scavenger is not at all advisable under these conditions.

4. Summary

The general aspects of the 2N Design of Experiment method and also a specific application for a chemical treatment model system were discussed. The effects and interactions of a corrosion inhibitor, as well as hydrogen sulfide and oxygen scavenger model compounds were studied. The linear model for these additives yielded controversial results, namely the fitting of the model on the polarization resistance data provided totally different results to those on the corrosion current data. By applying the logarithmic model, the results are consistent and their interpretation straightforward.

It has been proven that – by carefully selecting the appropriate mathematical model – the proposed method is applicable for the investigation of the effects and cross-effects of different oilfield treatment chemicals.

Acknowledgement

Present article was published in the frame of the project GINOP-2.3.2-15-2016-00053 (“Development of engine fuels with high hydrogen content in their molecular structures (contribution to sustainable mobility)”).

REFERENCES

[1] Rahmani, Kh.; Jadidian, R.; Haghtalabb, S.: Evaluation of inhibitors and biocides on the corrosion, scaling and biofouling control of carbon steel and copper–nickel alloys in a power plant cooling water system, *Desalination*, 2016 **393**(1), 174–185 DOI: 10.1016/j.desal.2015.07.026

[2] Barmatov, E.; Hughes, T.; Nagl, M.: Efficiency of film-forming corrosion inhibitors in strong hydrochloric acid under laminar and turbulent flow conditions, *Corr. Sci.*, 2015 **92**, 85–94 DOI: 10.1016/j.corsci.2014.11.038

[3] Papavinasam, S.: Corrosion Control in the Oil and Gas Industry, Chapter 7 – Mitigation – Internal Corrosion (Elsevier, Amsterdam) 2014 p. 361 ISBN: 978-0-12-397022-0

[4] Song, G.-L.: The grand challenges in electrochemical corrosion research, *Front. Mater.*, 2014 **1**(2), 1–3 DOI: 10.3389/fmats.2014.00002

[5] Giunta, A.A.; Wojtkiewicz Jr., S.F.; Eldred, M.S.: Overview of modern design of experiments methods for computational simulations, Proceedings of 41st Aerospace Sciences Meeting and Exhibit 2003; Reno, NV; USA. AIAA 2003-0649

[6] Garud, S.S.; Karimi, I.A.; Kraft, M.: Design of computer experiments: A review, *Comput. Chem. Eng.*, 2017 **106**, 71–95 DOI: 10.1016/j.compchemeng.2017.05.010

[7] Kemény, S.; Deák, A.: Kísérletek tervezése és kiértékelése [Design and Evaluation of Experiments, in Hungarian] (Műszaki Könyvkiadó, Budapest) 2002 ISBN: 978-963-2799-12

DE GRUYTER OPEN

HUNGARIAN JOURNAL OF INDUSTRY AND CHEMISTRY
Vol. 46(2) pp. 19-25 (2018)
hjic.mk.uni-pannon.hu
DOI: 10.1515/hjic-2018-0013

HUNGARIAN JOURNAL OF INDUSTRY AND CHEMISTRY
HJIC

STRONG REACHABILITY OF REACTIONS WITH REVERSIBLE STEPS

ESZTER VIRÁGH *[1] AND BÁLINT KISS[1]

[1]Department of Control Engineering and Information Technology, Budapest University of Technology and Economics, Magyar Tudósok krt. 2, Budapest, 1117, HUNGARY

The controllability of reactions is an important issue in the chemical industry. The control of reactions is of great practical interest in order to ensure the energy- and time-efficient production of compounds. This paper studies the dynamical models of some chemical reactions in order to verify their controllability with regard to a candidate input signal, namely the change in the ambient temperature of a reaction.

Keywords: reversible reaction, strong reachability, controllability, Lie algebra

1. Introduction

Chemical reactions are widely applied during the synthesis and transformation processes of organic compounds. The reaction mechanism and resulting products depend mainly on the concentrations of the species, the catalyst used, the ambient temperature, and the ambient pressure. If the values of these parameters are changed, one can obtain different products from the original ones but it is also possible to increase the productivity and energy-efficiency of the reaction. Hence the application of a proper feedback law to ensure the latter scenario may be envisaged.

A study of the local controllability by considering the reaction rate coefficient as an input has been presented in Ref. [1]. The authors of Ref. [2] have also considered the reaction rate coefficient as an input and extended the results by claiming that global controllability holds. The controllability of another control input, namely the dilution ratio, is studied in Ref. [3]. General conditions for strong reachability in the case of a temperature input were reported earlier in Ref. [4]. Moreover, the conditions of strong reachability for polymer electrolyte membrane fuel cells (PEMFC), controlled by concentrations, have also been analysed. The motivation to consider the concentrations and temperature (or their rate of change) as input signals is due to the fact that these quantities can be easily modified efficiently by industrial equipment that is currently in use, thus these results can be used as a basis to establish control laws to stabilize a desired reaction performance without major changes being made to the equipment used in production. The oxidation of acetone with hydroxylamine (the oximation reaction) was investigated by Raman spectroscopy [5]. Knowing the mechanism, the controllability is important for this reaction.

Throughout this paper, the candidate variable for control is the rate of change in the temperature $\dot{T}$, i.e. the first time derivative of the ambient temperature. From a practical point of view, this is a simplification since the variable which can be changed externally, denoted by u, is not $\dot{T}$ but an algebraic expression involving u and other variables of the system as well. For the dynamics considered in this paper it is always possible, however, to obtain the values of u as a function of $\dot{T}$ and other state variables.

The remaining part of this paper is organized as follows. Sec. 2 briefly revisits the concepts related to the strong reachability of nonlinear dynamical systems and conditions of strong reachability. The differential equations describing the dynamics of reactions are presented so that the rate of change in temperature is considered as the controlled input in Sec. 3. In Sec. 4 the strong reachability of the oximation reaction is studied. The systems in the case of acidic medium in Subsection 4.1 and in weakly basic medium in Subsection 4.2 are analyzed.

In Ref. [4] a sufficient condition for strong reachability was given for reactions with general dynamics. In Sec. 5, the conditions for strong reachability are given, if the reaction also contains reversible steps. In the last section the conclusions of the paper are drawn.

2. Study of strong reachability

Consider the following nonlinear dynamical system, given by the differential equation:

$$\dot{\xi} = f(\xi) + g(\xi)u, \quad \xi(0) = \xi^* \in \mathbb{R}^n, \tag{1}$$

where $f, g \in \mathbb{C}^\infty(\mathbb{R}^n, \mathbb{R}^n)$ are smooth vector fields and $u \in \mathbb{R}$ is the control-input variable. The vector fields

*Correspondence: viragh.eszter@gmail.hu

f and g are often referred to as drift and control vector fields, respectively. For the sake of completeness, let us revisit some definitions used in Refs. [4, 6].

Definition 1 (Reachability set)**.** *Consider the system given by Eq. 1. The set $\mathcal{R}(\xi^*, t) \subset \mathbb{R}^n$ is referred to as the reachability set from the point ξ^* at time t and it is the union of values at t of the solutions to Eq. 1 for some admissible input function u with the initial condition $\xi(0) = \xi^*$.*

Definition 2 (Strong reachability)**.** *The system Eq. 1 is referred to as strongly reachable from the point ξ^*, if the set $\mathcal{R}(\xi^*, t)$ has an interior point for all $t > 0$.*

Definition 3 (Lie bracket)**.** *Suppose that $f \in \mathbb{C}^\infty(\mathbb{R}^n, \mathbb{R}^n)$ and $g \in \mathbb{C}^\infty(\mathbb{R}^n, \mathbb{R}^n)$, then the Lie bracket of the vector fields f and g is*

$$[f, g] = Dg\ f - Df\ g. \tag{2}$$

The operator $\mathrm{ad}_g^n f : \mathbb{C}^\infty(\mathbb{R}^n, \mathbb{R}^n) \times \mathbb{C}^\infty(\mathbb{R}^n, \mathbb{R}^n) \to \mathbb{C}^\infty(\mathbb{R}^n, \mathbb{R}^n)$ is defined as:

$$\mathrm{ad}_g^0 f = f, \qquad \mathrm{ad}_g^n f = [g, \mathrm{ad}_g^{n-1} f]. \tag{3}$$

Definition 4 (Lie algebra)**.** *Consider the vector fields $f, g \in \mathbb{C}^\infty(\mathbb{R}^n, \mathbb{R}^n)$. The Lie algebra generated by f and g is denoted by $\Lambda = Lie(f, g)$ and is the smallest linear subspace of $\mathbb{C}^\infty(\mathbb{R}^n, \mathbb{R}^n)$ that satisfies the following conditions:*

1. *$f, g \in \Lambda$,*
2. *for any $a, b \in \Lambda$, $[a, b] \in \Lambda$.*

It should be noted that Λ also defines a distribution.

Definition 5 (Distribution)**.** *The distribution Δ is the operator which assigns a linear subspace of $\mathbb{R}^N$ to $\forall x \in \mathbb{R}^N$.*

Definition 6 (Controllability distribution)**.** *The controllability distribution Δ_c of Eq. 1 is the smallest distribution which satisfies the following conditions:*

1. *$g \in \Delta_c$,*
2. *Δ_c is invariant to the vector field f ($\forall \eta \in \Delta_c, [\eta, f] \in \Delta_c$),*
3. *Δ_c is involutive ($\forall \eta_1, \eta_2 \in \Delta_c, [\eta_1, \eta_2] \in \Delta_c$).*

The controllability distribution has a subspace spanned by vector fields g and $[f, g]$. The following theorem is a fundamental result used in Ref. [6].

Theorem 1 (Reachability rank condition)**.** *Consider the controllability distribution Δ_c of Eq. 1. The system Eq. 1 is strongly reachable at point $\xi^* \in \mathbb{R}^n$ if $\dim\{\Delta\}_c(\xi^*) = n$.*

3. Strong reachability of kinetic equations

The active control of chemical processes may be necessary to maximize the amount of target products and minimize the amount of by-products. To achieve such a control objective, a suitable input variable must be selected so that the resulting dynamical system is controllable from that input. To check if this requirement is satisfied, the tools introduced in the previous section will be applied to the equations describing the reaction dynamics.

Consider a system of R reaction steps and with M species ($R, M > 0$). By borrowing notational conventions from chemistry, each reaction step can be generally defined by

$$\sum_{m=1}^{M} \alpha(m,\ r)\mathrm{X}(m) \xrightarrow{k_r} \sum_{m=1}^{M} \beta(m,\ r)\mathrm{X}(m), \qquad r = 1, 2, \ldots, R, \tag{4}$$

where $\alpha(\cdot,\ r) = (\alpha(1,\ r), \alpha(2,\ r), \ldots, \alpha(m,\ r))^T$ denotes the reactant complex vector, $\beta(\cdot,\ r) = (\beta(1,\ r), \beta(2,\ r), \ldots, \beta(m,\ r))^T$ represents the product complex vector, $\mathrm{X}(m)$ is the mth species and k_r is the reaction rate coefficient of the rth reaction step. The species on the left-hand side of Eq. 4 are referred to as reactant species and reactant complexes refer to their formal linear combinations. Similarly, one may find the products and their linear combinations (product complexes) on the right-hand side of the reaction described in Eq. 4.

Let us also define the stoichiometric matrix, denoted by γ. The matrix γ consists of R columns and M rows, such that each column is obtained by

$$\gamma(\cdot,\ r) = \beta(\cdot,\ r) - \alpha(\cdot,\ r). \tag{5}$$

Eq. 4 defines the reaction but it does not specify its mass action kinetics. However, in order to study the controllability, the differential equations of the reaction dynamics need to be obtained in the form of differential equation Eq. 1. These equations are obtained from the heat balance [7–9] of reaction Eq. 4 as

$$\dot{x}_m = \sum_{r=1}^{R} \gamma(m,\ r) k_r x^{\alpha(\cdot,\ r)} \quad m = 1, 2, \ldots, M, \tag{6}$$

$$\dot{T} = \sum_{r=1}^{R} \frac{1}{\beta_{r,0}} k_r x^{\alpha(\cdot,\ r)} + u, \tag{7}$$

where x_m denotes the concentration of species m, T is the temperature, and $x^{\alpha(\cdot,\ r)} = \prod_{p=1}^{M} x_p^{\alpha(p,\ r)}$. Recall that the single input u appears in the expression of $\dot{T}$. The state vector ξ for the dynamics Eqs. 6–7 reads $\xi = (x_1, x_2, \ldots, x_m, T)^T$.

The reaction rate coefficient k_r can be given as

$$k_r = k_{r,0} e^{-\frac{E_r}{R_0 T}} \tag{8}$$

where $k_{r,0}, E_r, R_0 \in \mathbb{R}^+$.

To study reachability, one has to determine the number of linearly independent Lie brackets spanning the Lie algebra generated by the vector fields g and $\mathrm{ad}_g f$. Thanks to the special structure of the reaction dynamics, the linear independence can be examined by factorizing the matrix of Lie brackets and checking the rank of the factors. First, let us define the reaction dynamics matrix:

Definition 7 (Reaction dynamics matrix D_R)**.** *Introduce the notation*

$$k_j^{(i)} := \frac{\partial^i}{\partial T^i} k_j \qquad i, j \in \{1, 2, \ldots, R\} \tag{9}$$

The matrix of size $R \times R$ of the derivatives of the reaction rate coefficient defined as

$$D_R = \begin{pmatrix} k_1^{(1)} & k_1^{(2)} & \ldots & k_1^{(R)} \\ k_2^{(1)} & k_2^{(2)} & \ldots & k_2^{(R)} \\ \vdots & \vdots & \ddots & \vdots \\ k_R^{(1)} & k_R^{(2)} & \ldots & k_R^{(R)} \end{pmatrix} \tag{10}$$

is referred to as the reaction dynamics matrix.

The following Lemma and Theorem have been shown in Ref. [4]. They are also provided here for completeness.

Lemma 1. *Consider a reaction with R steps. Suppose that the activation energies $E_1, E_2, \ldots, E_R$ of the reaction steps are all different and strictly positive, then the reaction dynamics matrix D_R is of full rank for every $T > 0$.*

Theorem 1 cannot be applied directly to the reaction dynamics Eq. 6–7, because the right-hand sides (RHS) of some equations in Eq. 6 may be linearly dependent. Let δ denote the number of linearly dependent RHSs in Eq. 6. The system of chemical reactions is considered to be strongly reachable from a point $\xi^* \in \mathbb{R}^{M+1}$ if and only if the dimension of the controllability distribution is $M - \delta + 1$. The additional dimension is due to Eq. 7 with the temperature T as an additional variable.

Using Theorem 1, the controllability subspace for particular reactions can be deduced, so the conditions for strong reachability of the reactions can be determined.

Theorem 2. *Consider a reaction with M species and R reaction steps. Suppose that the activation energies $E_1, E_2, \ldots, E_R$ of the reaction steps are all different and strictly positive. Then the reaction dynamics with the temperature change ($\dot{T}$) as an input variable are strongly reachable if the concentrations of all reactant species are positive.*

Theorem 2 provides a condition for the strong reachability of reactions in a general form. However, for some reactions where the reaction dynamics have additional properties, weaker conditions may be sufficient to ensure strong reachability. In Sec. 4, the strong reachability conditions in the case of oximation reactions were investigated.

4. Controllability study of the oximation reaction

The oxidation of acetone with hydroxylamine was investigated by Raman spectroscopy in Ref. [5]. The reaction is strongly exothermic and the concentration of the intermediate highly depends on the pH and temperature. The process can be hazardous, however, it is not dangerous to run in a laboratory with low concentrations and in a controlled manner. Strong reachability is a necessary condition to be able to control the reaction.

4.1 Oximation reaction in acidic medium

In oximation reactions, the sequence (number and nature) of reaction steps depends on the pH. The equations of the reaction steps are different in acidic and weakly basic media.

In the case of acidic media the reaction takes place over two reaction steps as given by

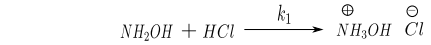

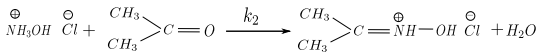

For the sake of notational simplicity, the symbols A, B, C, D, E, and F will denote the species such that the two reaction steps above read:

$$\mathrm{A} + \mathrm{B} \xrightarrow{k_1} \mathrm{C} \tag{11}$$

$$\mathrm{C} + \mathrm{D} \xrightarrow{k_2} \mathrm{E} + \mathrm{F}. \tag{12}$$

Let us denote the concentrations of the species by $a, b, c, d, e, f \geq 0$. It is assumed that the reaction rate coefficients $k_1, k_2 > 0$.

Theorem 2 implies that the reaction is strongly reachable, provided that the conditions are met. It follows from strong reachability that it is possible to arrive at any concentrations of $M - \delta$ species and at any temperatures by suitable manipulation of the input. Recall that there is no guarantee that such concentrations and temperatures also define a steady-state for the system.

Note that Theorem 2 only provides a sufficient condition for strong reachability. For chemical reactions, the positivity condition of activation energies is almost always satisfied. Considering the reaction steps of the oximation reaction in acidic media the two remaining conditions of strong reachability will be studied: (1) the positivity of the concentration of all reactant species; (2) the distinctness of activation energies.

Let us now suppose that the system in Eqs. 11–12 is strongly reachable. The stoichiometric matrix for the re-

action steps reads:

$$\gamma = \begin{pmatrix} -1 & 0 \\ -1 & 0 \\ 1 & -1 \\ 0 & -1 \\ 0 & 1 \\ 0 & 1 \end{pmatrix} \tag{13}$$

and it is easy to verify that $\delta = 2$ in this case. The differential equation of the reaction:

$$\begin{pmatrix} \dot{a} \\ \dot{b} \\ \dot{c} \\ \dot{d} \\ \dot{e} \\ \dot{f} \\ \dot{T} \end{pmatrix} = \begin{pmatrix} -k_1 ab \\ -k_1 ab \\ k_1 ab - k_2 cd \\ -k_2 cd \\ k_2 cd \\ k_2 cd \\ \frac{k_1}{\beta} ab + \frac{k_2}{\beta} cd \end{pmatrix} + \begin{pmatrix} 0 \\ 0 \\ 0 \\ 0 \\ 0 \\ 0 \\ 1 \end{pmatrix} u = \tag{14}$$
$$= f(\xi) + g(\xi)u$$

is in a form similar to Eq. 1, where $\xi = (a, b, c, d, e, f, T)^T$ and the vector field $g(\xi)$ is constant.

Since the rank of the stoichiometric matrix γ is 2 and the temperature is a scalar quantity, Theorem 1 implies that the system is strongly reachable if $\dim\{\Delta\}_c = 2 + 1 = 3$. Hence, to study strong reachability, the number of linearly independent vector fields spanning the Lie algebra generated by the vector fields $\mathrm{ad}_g f$ and g must be determined. The Lie brackets $\mathrm{ad}_g f$ and $\mathrm{ad}_g^2 f$ read:

$$\mathrm{ad}_g^{(i)} f = \begin{pmatrix} -k_1^{(i)} ab \\ -k_1^{(i)} ab \\ k_1^{(i)} ab - k_2^{(i)} cd \\ -k_2^{(i)} cd \\ k_2^{(i)} cd \\ k_2^{(i)} cd \\ \frac{k_1^{(i)}}{\beta} ab + \frac{k_2^{(i)}}{\beta} cd \end{pmatrix}, \tag{15}$$

where $i \in \{1,\ 2\}$.

To study the dimension of the controllability distribution Δ_c one has to determine the rank of the matrix whose columns are g, $\mathrm{ad}_g f$ and $\mathrm{ad}_g^2 f$ which reads:

$$\begin{pmatrix} \mathrm{ad}_g f & \mathrm{ad}_g^2 f & g \end{pmatrix} =$$
$$= \begin{pmatrix} -k_1^{(1)} ab & -k_1^{(2)} ab & 0 \\ -k_1^{(1)} ab & -k_1^{(2)} ab & 0 \\ k_1^{(1)} ab - k_2^{(1)} cd & k_1^{(2)} ab - k_2^{(2)} cd & 0 \\ -k_2^{(1)} cd & -k_2^{(2)} cd & 0 \\ k_2^{(1)} cd & k_2^{(2)} cd & 0 \\ k_2^{(1)} cd & k_2^{(2)} cd & 0 \\ \frac{k_1^{(1)}}{\beta} ab + \frac{k_2^{(1)}}{\beta} cd & \frac{k_1^{(2)}}{\beta} ab + \frac{k_2^{(2)}}{\beta} cd & 1 \end{pmatrix}. \tag{16}$$

The last row is linearly independent of all other rows in the matrix of Eq. 16, hence, by deleting the last row and column from the matix, the rank will be decreased by 1. The remaining matrix is denoted by Θ and defined as

$$\Theta = \begin{pmatrix} -k_1^{(1)} ab & -k_1^{(2)} ab \\ -k_1^{(1)} ab & -k_1^{(2)} ab \\ k_1^{(1)} ab - k_2^{(1)} cd & k_1^{(2)} ab - k_2^{(2)} cd \\ -k_2^{(1)} cd & -k_2^{(2)} cd \\ k_2^{(1)} cd & k_2^{(2)} cd \\ k_2^{(1)} cd & k_2^{(2)} cd \end{pmatrix}. \tag{17}$$

It is clear that the condition $\dim\{\Delta_c\} = 3$ holds true if and only if $\mathrm{rank}(\Theta) = 2$. It is easy to see that the matrix Θ can be factorized as

$$\Theta = \begin{pmatrix} -ab & 0 \\ -ab & 0 \\ ab & -cd \\ 0 & -cd \\ 0 & cd \\ 0 & cd \end{pmatrix} \begin{pmatrix} k_1^{(1)} & k_1^{(2)} \\ k_2^{(1)} & k_2^{(2)} \end{pmatrix} = A \cdot D_2. \tag{18}$$

The condition of $\mathrm{rank}(\Theta) = 2$ can hold true if and only if the matrices A and D_2 are of full rank according to the multiplication theorem of determinants. Matrix A is of full rank ($\mathrm{rank}(A) = 2$) if and only if $a \neq 0$, $b \neq 0$, $c \neq 0$ and $d \neq 0$. The reaction dynamics matrix D_2 is of full rank if and only if there is no constant $c \in \mathbb{R} \setminus \{0\}$ such that $k_1^{(2)} = ck_1^{(1)}$ and $k_2^{(2)} = ck_2^{(1)}$, hence

$$\frac{k_1^{(2)}}{k_1^{(1)}} = \frac{k_2^{(2)}}{k_2^{(1)}} (= c) \tag{19}$$

cannot be true. Recalling that the reaction rate coefficients are $k_r = k_{r,0} e^{-\frac{E_r}{R_0 T}}$ ($k_{r,0}$, E_r, and R_0 are positive constants), it is easy to determine the time derivatives:

$$k_r^{(1)} = \left(\frac{E_r}{R_0 T^2} \right) k_{r,0} e^{\frac{-E_r}{R_0 T}}, \tag{20}$$

$$k_r^{(2)} = k_{r,0} \left(\frac{E_r^2}{R_0^2\, T^4} - \frac{2E_r}{R_0\, T^3} \right) e^{\frac{-E_r}{R_0 T}}. \tag{21}$$

The ratios of the first- and second-order time derivatives are obtained as

$$\frac{k_r^{(2)}}{k_r^{(1)}} = \frac{k_{r,0} \left(\frac{E_r^2}{R_0^2\, T^4} - \frac{2E_r}{R_0\, T^3} \right) e^{\frac{-E_r}{R_0 T}}}{\left(\frac{E_r}{R_0 T^2} \right) k_{r,0} e^{\frac{-E_r}{R_0 T}}} = \frac{E_r - 2R_0 T}{R_0 T^2}. \tag{22}$$

Based on Eq. 22, the equality in Eq. 19 holds true if and only if $E_1 = E_2$.

As a result it has been proven that if the reaction dynamics are strongly reachable then the concentrations a, b, c and d are positive and $E_1 \neq E_2$. Thus the conditions of Theorem 2 are also necessary for strong reachability in the case of oximation reactions in acidic media.

4.2 Oximation reaction in weakly basic medium

In the case of weakly basic media the reaction occurs according to the reaction steps given by:

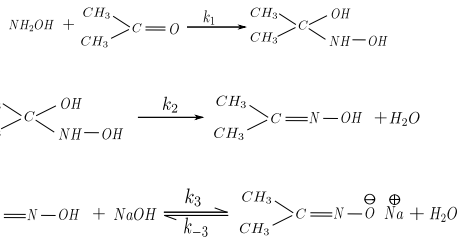

Since the specific chemical compositions of the species are irrelevant to the controllability analysis, the symbols A, B, C, D, E, F, and G will denote the species such that the above reaction steps read:

$$\mathrm{A} + \mathrm{B} \xrightarrow{k_1} \mathrm{C}, \tag{23}$$

$$\mathrm{C} \xrightarrow{k_2} \mathrm{D} + \mathrm{E}, \tag{24}$$

$$\mathrm{D} + \mathrm{F} \underset{k_{-3}}{\overset{k_3}{\rightleftharpoons}} \mathrm{G} + \mathrm{E}. \tag{25}$$

Let us denote the concentration of the species by a, b, c, d, e, f, $g \geq 0$. It is assumed that the reaction rate coefficients are strictly positive: k_1, k_2, k_3, $k_{-3} > 0$.

Recall that Theorem 2 only provides a sufficient condition for strong reachability. By considering oximation reactions in weakly basic media the remaining conditions of strong reachability will be studied.

Let us suppose now that the system of Eqs. 23–25 is strongly reachable. The stoichiometric matrix for the reaction steps reads:

$$\gamma = \begin{pmatrix} -1 & 0 & 0 & 0 \\ -1 & 0 & 0 & 0 \\ 1 & -1 & 0 & 0 \\ 0 & 1 & -1 & 1 \\ 0 & 1 & 1 & -1 \\ 0 & 0 & -1 & 1 \\ 0 & 0 & 1 & -1 \end{pmatrix}. \tag{26}$$

The differential equation of the reaction

$$\begin{pmatrix} \dot{a} \\ \dot{b} \\ \dot{c} \\ \dot{d} \\ \dot{e} \\ \dot{f} \\ \dot{g} \\ \dot{T} \end{pmatrix} = \begin{pmatrix} -k_1 ab \\ -k_1 ab \\ k_1 ab - k_2 c \\ k_2 c - k_3 df + k_{-3} ge \\ k_2 c + k_3 df - k_{-3} ge \\ -k_3 df + k_{-3} ge \\ k_3 df - k_{-3} ge \\ \frac{k_1}{\beta} ab + \frac{k_2}{\beta} c + \frac{k_3}{\beta} df + \frac{k_{-3}}{\beta} ge \end{pmatrix} + \begin{pmatrix} 0 \\ 0 \\ 0 \\ 0 \\ 0 \\ 0 \\ 0 \\ 1 \end{pmatrix} u = f(\xi) + g(\xi) u \tag{27}$$

is in a form similar to Eq. 1, where the vector field $g(\xi)$ is constant and $\xi = (a, b, c, d, e, f, g, T)^T$.

Since the rank of the stoichiometric matrix γ is 3 and the temperature is a scalar quantity, Theorem 1 implies that the system is strongly reachable if $\dim\{\Delta\}_c = 3 + 1 = 4$. Hence, the number of linearly independent vector fields spanning the Lie algebra generated by the vector fields $\mathrm{ad}_g f$ and g must be determined.

The Lie–brackets $\mathrm{ad}_g f$, $\mathrm{ad}_g^2 f$ and $\mathrm{ad}_g^3 f$ read:

$$\mathrm{ad}_g^i f = \begin{pmatrix} -k_1^{(i)} ab \\ -k_1^{(i)} ab \\ k_1^{(i)} ab - k_2^{(i)} c \\ k_2^{(i)} c - k_3^{(i)} df + k_{-3}^{(i)} ge \\ k_2^{(i)} c + k_3^{(i)} df - k_{-3}^{(i)} ge \\ -k_3^{(i)} df + k_{-3}^{(i)} ge \\ k_3^{(i)} df - k_{-3}^{(i)} ge \\ \frac{k_1^{(i)}}{\beta} ab + \frac{k_2^{(i)}}{\beta} c + \frac{k_3^{(i)}}{\beta} df + \frac{k_{-3}^{(i)}}{\beta} ge \end{pmatrix}, \tag{28}$$

where $i \in \{1, 2, 3\}$. To study the dimensions of the controllability distribution Δ_c one has to give the rank of the matrix whose columns are $\mathrm{ad}_g f$, $\mathrm{ad}_g^2 f$, $\mathrm{ad}_g^3 f$, and g:

$$\begin{pmatrix} \mathrm{ad}_g f & \mathrm{ad}_g^2 f & \mathrm{ad}_g^3 f & g \end{pmatrix}. \tag{29}$$

The last row is linearly independent of all other rows in matrix Eq. 30, hence, by deleting the last row and column from the matrix, the rank will be decreased by 1. The remaining matrix is denoted by Θ and defined as

$$\Theta = \left\{ \begin{pmatrix} -k_1^{(i)} ab \\ -k_1^{(i)} ab \\ k_1^{(i)} ab - k_2^{(i)} c \\ k_2^{(i)} c - k_3^{(i)} df + k_{-3}^{(i)} ge \\ k_2^{(i)} c + k_3^{(i)} df - k_{-3}^{(i)} ge \\ -k_3^{(i)} df + k_{-3}^{(i)} ge \\ k_3^{(i)} df - k_{-3}^{(i)} ge \end{pmatrix}_{i=1,2,3} \right\} \tag{30}$$

The condition $\dim\{\Delta\}_c = 4$ holds true if and only if $\mathrm{rank}(\Theta) = 3$. It is easy to see that the matrix Θ can be factorized as

$$\Theta = A \cdot D = \begin{pmatrix} -ab & 0 & 0 & 0 \\ -ab & 0 & 0 & 0 \\ ab & -c & 0 & 0 \\ 0 & c & -df & ge \\ 0 & c & df & -ge \\ 0 & 0 & -df & ge \\ 0 & 0 & df & -ge \end{pmatrix} \begin{pmatrix} k_1^{(1)} & k_1^{(2)} & k_1^{(3)} \\ k_2^{(1)} & k_2^{(2)} & k_2^{(3)} \\ k_3^{(1)} & k_3^{(2)} & k_3^{(3)} \\ k_{-3}^{(1)} & k_{-3}^{(2)} & k_{-3}^{(3)} \end{pmatrix} \tag{31}$$

The condition $\mathrm{rank}(\Theta) = 3$ can hold true only if $\mathrm{rank}(A) \geq 3$ and $\mathrm{rank}(D) \geq 3$. T he 3rd and 4th columns in matrix A are linearly dependent, thus $\mathrm{rank}(A) \leq 3$. The condition $\mathrm{rank}(A) = 3$ can hold true only if the concentrations a, b, and c as well as the

concentrations d and f, or the concentrations g and e are strictly positive. Matrix D is of full rank only if D consists of a 3×3 times full-rank matrix. Lemma 1 implies that the reaction dynamics matrix D_3 is of full rank if the activation energies are different. Hence, matrix D is of full rank, if 3 different activation energies exist.

The system was proven to be strongly reachable if 3 of the activation energies are all different and concentrations a, b, c and d, f, or g, e are positive. Thus a condition for strong reachability coule be given more precisely in the case of oximation reaction in weakly basic media.

5. Reversible reaction step

For reactions of general types, Theorem 2 provides a condition for strong reachability. However, it will be shown that if the reaction contains one or more reversible steps, weaker conditions are sufficient for strong reachability.

The concentrations are defined by $x_1, x_2, \ldots, x_M$, as in the previous sections. The notation $\mathcal{A}$ is introduced for the matrix describing the effect of concentrations:

$$\mathcal{A} := \gamma \operatorname{diag}(x^{\alpha(\cdot\,,1)}, x^{\alpha(\cdot,\,2)}, \ldots, x^{\alpha(\cdot,\,R)}), \tag{32}$$

where $x^{\alpha(\cdot,r)} = \prod_{m=1}^{M} x_m^{\alpha(m,\,r)}$ and γ is the stoichiometric matrix as introduced by Eq. 5. The vector $k = (k_1, k_2, \ldots, k_R)^T$ is composed of the reaction rate coefficients. The notation $\mathcal{D}$ is introduced for the following matrix composed of the derivatives of reaction rate coefficients:

$$\mathcal{D} := \left(k^{(1)}\ k^{(2)}\ \ldots\ k^{(\operatorname{rank}(\gamma))}\right). \tag{33}$$

Lemma 2. *The reaction dynamics in Eqs. 6–7 with the input variable $\dot{T}$ are strongly reachable, if* $\operatorname{rank}\gamma = \operatorname{rank}(\mathcal{AD})$*, where γ is the stoichiometric matrix and $\mathcal{A}$ and $\mathcal{D}$ are defined as above.*

Proof The differential equation of the reaction reads:

$$\begin{pmatrix} \dot{x} \\ \dot{T} \end{pmatrix} = \begin{pmatrix} v \\ \sum_{r=1}^{R} \frac{k_r}{\beta_{r,0}} x^{\alpha(\cdot,\,r)} \end{pmatrix} + \begin{pmatrix} 0 \\ 1 \end{pmatrix} u, \tag{34}$$

where $\dot{x} = (\dot{x}_1, \dot{x}_2, \ldots, \dot{x}_M)^T$, u is the control input and the vector field v stands for the vector composed of the right-hand sides of Eq. 6.

As in the previous sections, the study of strong reachability means verification of the dimension of the controllability distribution Δ_c. The dimension of the controlled input (the dimension of the change in temperature) is 1, thus, Theorem 1 implies that the system is strongly reachable if and only if $\dim\{\Delta\}_c = \operatorname{rank}(\gamma) + 1$.

The vector fields spanning the controllability distribution are g and $\operatorname{ad}_g^i f$ for $i > 0$. The Lie bracket $\operatorname{ad}_g^i f$ reads:

$$\operatorname{ad}_g^i f = \begin{pmatrix} v^{(i)} \\ \sum_{r=1}^{R} \frac{k_r^{(i)}}{\beta_{r,0}} x^{\alpha(\cdot,\,r)} \end{pmatrix} = \begin{pmatrix} \mathcal{A} \cdot k^{(i)} \\ \sum_{r=1}^{R} \frac{k_r^{(i)}}{\beta_{r,0}} x^{\alpha(\cdot,\,r)} \end{pmatrix} \tag{35}$$

for $i \in \{1, 2, \ldots, \operatorname{rank}\gamma\}$. The rank of the controllability distribution is hence the rank of the matrix

$$\begin{pmatrix} \operatorname{ad}_g f & \operatorname{ad}_g^2 f & \ldots & \operatorname{ad}_g^{\operatorname{rank}\gamma} f & g \end{pmatrix} = \begin{pmatrix} \mathcal{A} \cdot k^{(1)} & \ldots & \mathcal{A} \cdot k^{(\operatorname{rank}\gamma)} & 0 \\ \sum_{r=1}^{R} \frac{k_r^{(1)}}{\beta_{r,0}} x^{\alpha(\cdot,\,r)} & \ldots & \sum_{r=1}^{R} \frac{k^{(\operatorname{rank}\gamma)}}{\beta_{r,0}} x^{\alpha(\cdot,\,r)} & 1 \end{pmatrix} \tag{36}$$

The last row in Eq. 36 is linearly independent of the others, hence, the same reasoning as earlier is followed and the last row and columns are eliminated, thus, decreasing the rank by one. The resulting matrix is denoted by Θ and reads:

$$\Theta = \begin{pmatrix} \mathcal{A} \cdot k^{(1)} & \mathcal{A} \cdot k^{(2)} \ldots \mathcal{A} \cdot k^{(\operatorname{rank}\gamma)} \end{pmatrix} = \\ = \mathcal{AD}. \tag{37}$$

Since the dimension of the controllability distribution is $\operatorname{rank}(\Theta) + 1$, the reaction dynamics are strongly reachable if $\operatorname{rank}\gamma = \operatorname{rank}\Theta$ or if $\operatorname{rank}\gamma = \operatorname{rank}(\mathcal{AD})$.

Theorem 3. *Consider the reaction dynamics Eqs. 6–7 such that the activation energies E_1, E_2, …, E_R are positive and different in pairs. Suppose that the concentrations of reactant species are positive in the case of one-way reaction steps and at least one of the ways is positive in the case of reversible reaction steps. Then, the reaction dynamics controlled by $\dot{T}$ are strongly reachable.*

Proof If the system does not contain reversible reaction steps, Theorem 2 is obtained.

Without loss of generality, it can be supposed that the system contains one reversible reaction step. This step can be replaced by pairs of irreversible reaction steps, with reaction rate coefficients denoted by k_e and k_{-e}. The changes in the concentrations are equal in the reaction step with rate coefficient k_e and in the reaction step with rate coefficient k_{-e}, only the direction is different. Thus, the two columns in matrix γ for the reversible reaction steps are always linearly dependent. Lemma 2 implies that the system is strongly reachable if and only if $\operatorname{rank}\gamma = \operatorname{rank}(\mathcal{AD})$. If the activation energies are positive and all different, Lemma 1 implies that matrix $\mathcal{D}$ is of full rank. The matrix $\mathcal{A}$ is defined by Eq. 32, thus, the columns for k_e and k_{-e} are linearly dependent. The column for k_e contains the factor of the concentrations of the reactant species in the transformation step and k_{-e} contains the factor of the concentrations of the reactant species in the transformation step in the opposite direction with the arbitrary sign in the place of non-zero elements. By substituting one of the two vector fields with a zero vector field, the rank of matrix $\mathcal{A}$ remains unchanged. Thus, in the case of reversible reactions for strong reachability, it is sufficient if the reactant species have positive concentrations only in one of the directions, and the activation energies are positive and all different.

6. Conclusion

The reaction dynamics of strong reachability where the control variable is selected as the rate of change in the ambient temperature ($\dot{T}$) have been studied. First, the strong reachability was analyzed in the case of the oximation reaction. Since the processes depend on the pH, conditions that facilitate strong reachability in acidic as well as weakly basic media were studied. For our analysis, Theorem 2 was used. It provides sufficient conditions to facilitate strong reachability, however, these conditions are not always necessary. It was proven that the conditions in Theorem 2 are necessary to facilitate strong reachability of the oximation reaction in the case of acidic media. In weakly basic media, the system contained a reversible reaction step, thus, the conditions of Theorem 2 could be determined.

Strong reachability has also been studied for reaction dynamics of a general type that contain at least one reversible reaction step where the conditions of Theorem 2 could also be further refined. For reversible reaction steps it has been shown that positive reactant concentrations are unnecessary to facilitate strong reachability in both directions of the reversible steps, in one direction is sufficient.

Acknowledgement

The chemistry-related comments from Zsombor Kristóf Nagy and György Marosi at the BME Department of Organic Chemistry and Technology are gratefully acknowledged.

REFERENCES

[1] Farkas, G.: Local controllability of reactions, *J. Math. Chem.*, 1998 **24**, 1–14 DOI: 10.1023/A:1019150014783

[2] Drexler, D.A., Tóth, J.: Global controllability of chemical reactions, *J. Math. Chem.*, 2016 **54**, 1327–1350 DOI: 10.1007/s10910-016-0626-7

[3] Dochain, D., Chen, L.: Local observability and controllability of stirred tank reactors, *J. Math. Chem.*, 1992 **2**, 139–144 DOI: 10.1016/0959-1524(92)85003-F

[4] Drexler, D.A., Virágh, E., Tóth, J.: Controllability and reachability of reactions with temperature and inflow control, *Fuel*, 2017 **211**, 906–911 DOI: 10.1016/j.fuel.2017.09.095

[5] Csontos, I., Pataki, H., Farkas, A., Bata, H., Vajna, B., Nagy, Z.K., Keglevich, G., Marosi, G.J.: Feedback Control of Oximation Reaction by Inline Raman Spectroscopy, *Organic Process Research & Development*, 2014 **19**, 189–195 DOI: 10.1021/op500015d

[6] Isidori, A.: Nonlinear Control System (Springer Verlag, London), 1995 DOI: 10.1007/978-1-84628-615-5

[7] Érdi, P., Tóth, J.: Mathematical models of chemical reactions. Theory and applications of deterministic and stochastic models (Princeton University Press, Princeton, New Jersey), 1989 ISBN: 9780719022081

[8] Turányi, T., Tomlin, A.S.: Analysis of Kinetic Reaction Mechanisms (Springer Berlin Heidelberg), 2014 ISBN: 9783662445624

[9] Atkins, P.W.: Physical Chemistry (Oxford University Press), 2010 ISBN: 9780199543373

DE GRUYTER OPEN

HUNGARIAN JOURNAL OF INDUSTRY AND CHEMISTRY
Vol. 46(2) pp. 27–31 (2018)
hjic.mk.uni-pannon.hu
DOI: 10.1515/hjic-2018-0014

HUNGARIAN JOURNAL OF INDUSTRY AND CHEMISTRY
HJIC

PRODUCTION OF A BIOLUBRICANT BY ENZYMATIC ESTERIFICATION: POSSIBLE SYNERGISM BETWEEN IONIC LIQUID AND ENZYME

ZSÓFIA BEDŐ[1], KATALIN BÉLAFI-BAKÓ[1], NÁNDOR NEMESTÓTHY[1], AND LÁSZLÓ GUBICZA *[1]

[1]Research Institute of Bioengineering, Membrane Technology and Energetics, University of Pannonia, Egyetem u. 10, Veszprém, 8200, HUNGARY

The possible replacement of lubricants with fossil-fuel sources and the manufacture of biolubricants with more beneficial features were studied. Oleic acid and isoamyl alcohol were reacted with an enzyme in an ionic liquid. During the reaction conventional as well as microwave heating was applied. After the experimental determination of the optimal reaction parameters, it was unexpectedly found that a synergistic effect occurred by applying ionic-liquid and microwave-heat treatment simultaneously. The enzyme exhibited a much higher level of activity than the value expected based on the measurements carried out separately by using an ionic liquid instead of an organic solvent and microwave-heat treatment or a conventional method. In the experiments with recycled enzyme it was found that ionic liquid maintained the enzyme more effectively, as if it was immobilized by it: the enzyme managed to maintain its activity and recycling ability.

Keywords: synergistic effect, ionic liquid and microwave heating, biolubricant production, enzyme reuse

1. Introduction

Lubricants from mineral oils have a considerable detrimental effect on the environment due to the aromatic organic compounds within their chemical structures. Mineral oils that have leached into water or soil are toxic for living organisms, they substantially decrease the level of dissolved oxygen in the water. These lubricants can hardly be degraded biologically. During their manufacture several by-products form and further additives are needed for the lubricants. Hence the demand for biolubricants from plant oils has been growing recently, since they are natural, renewable, non-toxic as well as environmentally-friendly compounds, and often cheaper than synthetic oils. Therefore, they are suitable for eliminating the disadvantages of mineral oil, moreover, our dependence on mineral oils and other non-renewable sources might be decreased [1, 2].

The production of synthetic and semi-synthetic lubricants is necessary since now it is not possible to conduct all lubrication tasks by using lubricants derived exclusively from mineral oils. In several cases non-coking lubricants with extremely high degrees of viscosity are able to operate at low temperatures (below -50 °C). Biolubricants are used in numerous fields of application, but in all of them it is vital to prevent the contamination (only a negligible level is acceptable) of the product and environment. These provide an alternative to the mineral oil-based lubricants in industrial applications that are used in the automotive industry as hydraulic fluids during metal processing and oils for driving gears [3]. They are not considered as biological hazards in water systems when applied in watercrafts.

In biotechnological methods for the manufacture of biolubricants, raw materials with a high oleic acid content are generally used for the transesterification processes. Biolubricants are mainly produced from plant oils, e.g. sunflower oil, soybean oil and castor oil [4, 5]. The lifetime of these biolubricants that possess esters is usually longer than those obtained from mineral oils. On the other hand, their widespread industrial usage is hindered by the fact that certain equipment must be converted to run on biolubricants [6].

Various esters can be enzymatically produced from acids and alcohols of different chain lengths in non-conventional systems (organic solvents, ionic liquids, supercritical fluids, solvent-free media). Thus, the esterification of acids and alcohols of short chain lengths by lipase results in flavour esters [7, 8]. The esterification of fatty acids (acids with carbon numbers of between 12 and 18) and alcohols may yield both biolubricants and biofuels depending on alcohols' chain lengths [9, 10]. Biodiesel is obtained when alcohols of short chain lengths are used, while biolubricants can be manufactured by alcohols of long chain lengths.

The formation of a biolubricant from oleic acid and isoamyl alcohol in organic solvents has been studied previously [11–13]. The term 'biolubricant' may be used since both isoamyl alcohol and oleic acid are considered

*Correspondence: gubiczal@almos.uni-pannon.hu

to occur naturally and the reaction is carried out by a naturally-occurring catalyst, an enzyme. Koszorz et al. studied the same reaction and stated that the water formed as a by-product of the esterification reaction had a negative effect on the rate of reaction and activity of the enzyme. To enhance the effectiveness of the process, water had to be removed by an integrated system where the reaction was combined with a pervaporation unit [14].

Turkish researchers applied fusel oil – a by-product of bioethanol production – containing a significant amount of isoamyl alcohol that was used to synthesize a biolubricant with high yield [15].

In addition to organic solvents, good results were achieved recently using ionic liquids as solvents. In the field of heat treatment microwave irradiation has yielded excellent results in both organic synthetic and enzymatic reactions [16, 17]. In transesterification reactions even a synergy effect was observed between the enzyme and ionic liquid [18–20].

The aim of this paper was twofold: (i) to study the possibility of applying ionic liquids instead of organic solvents; (ii) to investigate the role of microwave irradiation to achieve the highest possible degree of conversion in the minimum amount of time.

2. Experimental

The reactions were conducted in an incubator shaker and microwave equipment using conventional heating and microwave irradiation, respectively. Similar compositions and reaction volumes were used in the measurements to be able to compare the experimental results.

2.1 Samples and Measurements

All chemicals were commercially available and used without further purification.

Novozym 435 (immobilised Candida antarctica lipase B, CALB), a triacylglycerol acylhydrolase (E.C. 3.1.1.3.) immobilized on an acrylic resin, was a gift from Novozymes (*Bagsvćrd*, Denmark). Its nominal catalytic activity and water content were 7000 propyl laurate units (PLU)/g and 1-2 %, respectively. Isoamyl alcohol (98 %) and oleic acid (99 %) were used as received from Sigma-Aldrich. The ionic liquid 1-butyl-3-methylimidazolium hexafluorophosphate ([bmim]PF_6) ($\geq$98.5 %) was purchased from Sigma-Aldrich while n-hexane and isooctane (99 %) were acquired from Reanal.

To follow the yield of the ester, a HP-5890A gas chromatograph (GC) was used. The device was equipped with a split/splitless injector, flame ionization detector (FID), and DB-FFAP column (length: 10 m, inner diameter: 0.53 mm, film thickness: 1.00 μm). The following heating programme was applied: 130 °C, 3 mins.; temperature ramp up: 10 °C min^{-1}; 240 °C, 5 mins. Isooctane was used as an internal standard. For the analysis, a 10 μL sample of the reaction mixture was extracted.

Reaction mixtures that contain ionic liquids cannot be injected into the GC, since they – as a viscous liquid – form a deposit on the inner side of the column that causes fouling. Moreover, they may be degraded due to the high temperature, thus, the precision of the measurements will be affected and undesirable peaks may appear in the chromatograms. During the measurements the components are usually separated from the ionic liquid by extraction and injected into the column.

In our measurements – to preserve the GC column – fiberglass and adsorbent material were placed inside the injector, which retained the ionic liquid after injection while the component to be analysed was transferred in a gas phase to the column as a result of the high temperature. In this way extraction of the product from the reaction mixture could be avoided, therefore, the errors that originate from the incomplete extraction (effectiveness) could be eliminated.

2.2 Experimental setups

Two different procedures were used for the production of biolubricants. Firstly, by using conventional heating the synthesis of biolubricants was conducted in Eppendorf tubes (1.5 mL) at 40 °C rotated at 200 rpm (IKA incubator shaker KS 4000i). In a typical experiment 5 cm^3 of reaction mixture (22.5 mmol of isoamyl alcohol and 3.75 mmol of oleic acid dissolved in n-hexane or [bmim]PF_6) was prepared in a volumetric flask, and the Eppendorf tubes were each filled with 1 cm^3 of the reaction mixture. The reaction started when 10 mg of the enzyme was added.

Tests under microwave conditions were performed in a commercial microwave synthesizer (Discover series, BenchMate model, CEM Corporation, USA). It was equipped with a magnetic stirrer and a fibre-optic sensor to monitor the temperature, which was set by varying the power of the microwave. For the esterification of biolubricant, 10 W of energy was used to maintain the temperature of the reaction between 40 and 60 °C. The volume and composition of the reaction mixture was identical to under conventional conditions.

Experiments to study the reusability of enzymes were conducted by separating the enzyme from the reaction mixture and starting a novel reaction with a reaction mixture of the same volume.

3. Results and Analysis

3.1 Experiments

Certain ionic liquids may catalyse esterification reactions. Even though in the case of [bmim]PF_6 this phenomenon does not occur according to earlier publications, measurements were conducted in reaction mixtures which did not contain enzymes to be able to exclude this effect. Our experiments confirmed previous results from the literature: [bmim]PF_6 did not catalyse the reactions.

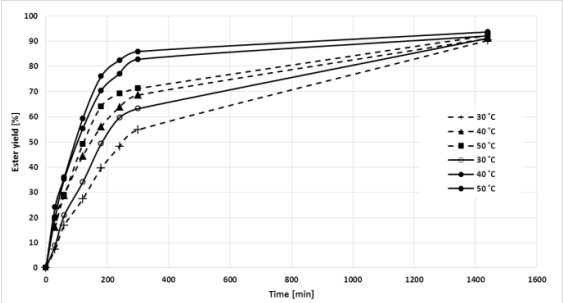

Figure 1: Biolubricant production in the organic solvent (dashed lines) and ionic liquid (solid lines) using conventional heating.

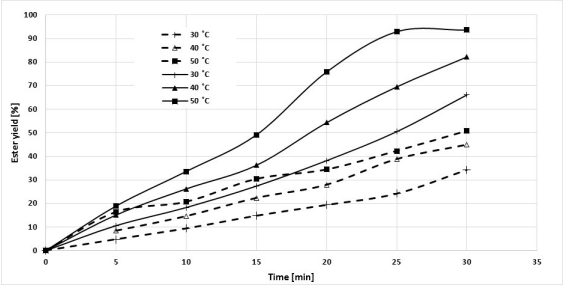

Figure 2: Biolubricant production in the organic solvent (dashed lines) and ionic liquid (solid lines) using microwave irradiation.

The experimental conditions were selected according to data from the literature in addition to our earlier observations, and they were checked by preliminary measurements. Thus, the molar ratio of isoamyl alcohol to oleic acid was adjusted to 6:1, with a shaking rate of 200 rpm. The measurements were conducted at a temperature of between 30 and 50 °C to follow the eventual changes at various temperatures. It would have been possible to carry out measurements at higher temperatures using the enzyme Novozym 435 or the ionic liquid [bmim]PF_6, furthermore, changes over longer reaction times could be more suitable to follow and evaluate.

3.2 Experiments using conventional heating

Firstly, measurements under the conditions described in section 2.2 were conducted using conventional heating (Fig. 1). As can be seen esters were produced in high yields during the reactions in the ionic liquid as well as expected, and the yield was always higher in the ionic liquid at the same temperature.

3.3 Experiments using microwave heating

The results of the measurements using microwave irradiation are presented in Fig. 2. As can be observed, a much shorter time was necessary to reach equilibrium, and the reaction rate was also faster in the ionic liquid.

3.4 Investigation of enzyme reuse

The reusability of the enzyme Novozym 435 was studied under similar conditions in an ionic liquid (i.e. using conventional and microwave heating). The results indicated that the activity of the enzyme declined more rapidly using conventional heating.

4. Discussion

The results of the experiments conducted in the organic solvent, n-hexane, and in the ionic liquid, [bmim]PF_6, under similar conditions provided a good basis to compare the effects of conventional and microwave heating during the production of biolubricants using enzymes since in both cases the same reaction volumes were used.

As can be seen in Fig. 1, the reaction rate was higher in the ionic liquid (IL) than in n-hexane (n-H), the organic solvent that was usually applied. The data in Table 1 can be further compared. By comparing the values of C, IL/C and n-H (the ratio of enzyme activities in the ionic liquid and n-hexane using conventional (C) heating), it can be seen that the activity of the enzyme increased by a factor of 1.2 (on average) at each temperature due to the presence of the ionic liquid.

In the organic solvent the activity of the enzyme was found to be 2.8 times greater as a result of the microwave irradiation at each temperature (data of MW, n-H/C, n-H) compared to the conventional heating. In similar experiments in ionic liquids even more significant increases in the activity of enzymes were observed: microwave irradiation (MW) resulted in a 5.8-fold rise (data of MW, IL/C, IL).

A possible explanation for the significant increase is that the ionic liquid and microwave irradiation have a positive synergistic effect on the activity of the enzyme. Previously it was observed that ionic liquids seem to protect the enzyme in a similar way to the immobilising sup-

Table 1: Comparison of the activity of the enzyme under various conditions.

T / °C	Activity / $\mu mol \cdot min^{-1} \cdot g^{-1}$						
	Conventional heating		Microwave heating		C, IL/C, n-H	MW, n-H/C, n-H	MW, IL/C, IL
	n-H	IL	n-H	IL			
30	162	194	475	1120	1.19	2.93	5.77
40	342	444	990	2510	1.29	2.89	5.65
50	575	660	1650	3840	1.15	2.86	5.82

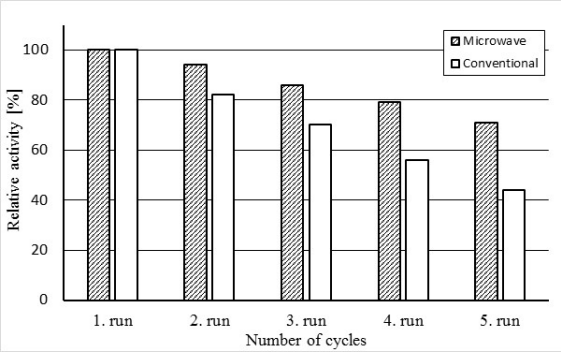

Figure 3: Reusability of the enzyme in the ionic liquid using microwave and conventional heating

port of the enzymes. In this work an immobilised enzyme was applied, thus, the synergistic effect simply strengthened the enzyme preparation or stabilised the active site of the enzyme. A similar effect has already been described in transesterification reactions in some papers in the literature [18, 20], but not with regard to esterification reactions.

The stabilisation effect of the ionic liquid was confirmed by the results presented in Fig. 3. By re-using the enzyme 5 times under conventional heating, the activity of the enzyme decreased much more rapidly than in the case of microwave heating. While in the first case 50 % of the original activity of the enzyme was maintained after the fifth application, using microwave irradiation this value was 70 %.

5. Conclusion

The experiments led to a definite answer to the original question, namely whether microwave irradiation may enhance the effectivity of the enzymatic production of a biolubricant from isoamyl alcohol and oleic acid. It was observed that microwave heating increased the rate of reaction. During the evaluation of the experiments an unexpected effect was discovered: a synergistic effect was observed between microwave irradiation and the ionic liquid. As a result, a significantly greater increase in the activity of the enzyme was achieved during the reaction in the ionic liquid using microwave irradiation than in the organic solvent or according to the value obtained in the ionic liquid using conventional heating.

Acknowledgement

REFERENCES

[1] Carrea, G.; Riva, S.: Organic synthesis with enzymes in non-aqueous media (WILEY-VCH Verlag GmbH & Co. KGaA, Weinheim, Germany) 2008 pp. 169–190 ISBN: 978-3-527-31846-9

[2] Salimon, J.; Salih, N.; Yousif, E.: Improvement of pour point and oxidative stability of synthetic ester basestocks for biolubricant applications, *Arab J. Chem.*, 2012 **5**, 193–200 DOI: 10.1016/j.arabjc.2010.09.001

[3] Akerman, C.O.; Hagström, A.E.V.; Mollaahmad, M.A.; Karlsson, S.; Hatti-Kaul, R.: Biolubricant synthesis using immobilised lipase: Process optimisation of trimethylolpropane oleate production, *Proc. Biochem.,* 2011 **46**, 2225–2231 DOI: 10.1016/j.procbio.2011.08.006

[4] Dossat, V.; Combes, D.; Marty, A.: Lipase-catalysed transesterification of high oleic sunflower oil, *Enzyme Microb. Tech.,* 2002 **30**, 90–94 DOI: S0141-0229(01)00453-7

[5] Hajar, M.; Vahabzadeh, F.: Modeling the kinetics of biolubricant production from castor oil using Novozym 435 in a fluidized-bed reactor, *Ind. Crop Prod.,* 2014 **59**, 252–259 DOI: org/10.1016/j.indcrop.2014.05.032

[6] Mobarak, H.M.; Mohamed, E.N.; Masjuki, H.H.; Kalam, M.A.; Al Mahmud, K.A.H.; Habibullah, M.; Ashraful, A.M.: The prospects of biolubricants as alternatives in automotive applications, *Renew. Sust. Ener. Rev.,* 2014 **33**, 34–43 DOI: org/10.1016/j.rser.2014.01.062

[7] Su, L.; Hong, R.; Guo, X.; Wu, J.; Xia, Y.: Short-chain aliphatic ester synthesis using Thermobifida fusca cutinase, *Food Chem.,* 2016 **206**, 131–136 DOI: 10.1016/j.foodchem.2016.03.051

[8] Cvjetko, M.; Vorkapic-Furac, J.; Znidarsic-Plazl, P.: Isoamyl acetate synthesis in imidazolium-based ionic liquids using packed bed enzyme microreactor, *Proc. Biochem.,* 2012 **47**, 1344–1350 DOI: 10.1016/j.procbio.2012.04.028

[9] Atadashi, I.M.; Aroua, M.K.; Aziz, A.R.A.; Sulaiman, N.M.N.: Production of biodiesel using high free fatty acid feedstocks, *Renew. Sust. Ener. Rev.,* 2012 **16**, 3275–3285 DOI: 10.1016/j.rser.2012.02.063

[10] Verma, P.; Sharma, M.P.: Review of process parameters for biodiesel production from different feedstocks, *Renew. Sust. Ener. Rev.,* 2016 **62**, 1063–1071 DOI: 10.1016/j.rser.2016.04.054

[11] Dörmő, N.; Bélafi-Bakó, K.; Bartha, L.; Ehrenstein, U.; Gubicza, L.: Manufacture of an environmental-safe biolubricant from fusel oil by enzymatic esterification in solvent-free system, *Biochem. Eng. J.,* 2004 **21**, 229–234 DOI: 10.1016/j.bej.2004.06.011

[12] Madarász, J.; Németh, D.; Bakos, J.; Gubicza, L.; Bakonyi, P.: Solvent-free enzymatic process for biolubricant production in continuous microfluidic reactor, *J. Clean Prod.,* 2015 **93**, 140–144 DOI: 10.1016/j.jclepro.2015.01.028

[13] Bányai, T.; Bélafi-Bakó, K.; Nemestóthy, N.; Gubicza, L.: Biolubricant production in ionic liquids by enzymatic esterification, *Hung. J. Ind. Chem.,* 2011 **39**(3), 395–399

[14] Koszorz, Z.; Nemestóthy, N.; Ziobrowski, Z.; Bélafi-Bakó, K.; Krupiczka, R.: Influence of pervaporation process parameters on enzymatic catalyst deactivation, *Desalination,* 2004 **162**, 307–313 DOI: 10.1016/S0011-9164(04)00064-5

[15] Güvenc, A.; Kapucu, N.; Kapucu, H.; Aydogan, Ö.; Mehmetoglu, Ü.: Enzymatic esterification of isoamyl alcohol obtained from fusel oil: Optimization by response surface methodology, *Enzyme Microb. Tech.,* 2007 **40**, 778–785 DOI: 10.1016/j.enzmictec.2006.06.010

[16] Vekariya, R.L.: A review of ionic liquids: Applications towards catalytic organic transformations, *J. Mol. Liq.,* 2017 **227**, 44–60 DOI: 10.1016/j.molliq.2016.11.123

[17] Major, B.; Nemestóthy, N.; Bélafi-Bakó, K.; Gubicza, L.: Enzymatic esterification of lactic acid under microwave conditions in ionic liquids, *Hung. J. Ind. Chem.,* 2008 **36,** 77–81

[18] Yadav, G.D.; Pawar, S.P.: Synergism between microwave irradiation and enzyme catalysis in transesterification of ethyl-3-phenylpropanoate with n-butanol, *Bioresource Technol.,* 2012 **109**, 1–6 DOI: 10.1016/j.biortech.2012.01.030

[19] Yu, D.; Wang, C.; Yin, Y.; Zhang, A.; Gao, G.; Fang, X.: A synergistic effect of microwave irradiation and ionic liquids on enzyme-catalyzed biodiesel production, *Green Chem.,* 2011 **13**, 1869–1875 DOI: 10.1039/c1gc15114b

[20] Kamble, M.P.; Chaudhari, S.A.; Singhal, R.S.; Yadav, G.D.: Synergism of microwave irradiation and enzyme catalysis in kinetic resolution of (R,S)-1-phenylethanol by cutinase from novel isolate Fusarium ICT SAC1, *Biochem. Eng. J.,* 2017 **117**, 121–128 DOI: 10.1016/j.bej.2016.09.007

DE GRUYTER OPEN

HUNGARIAN JOURNAL OF INDUSTRY AND CHEMISTRY
Vol. 46(2) pp. 33–36 (2018)
hjic.mk.uni-pannon.hu
DOI: 10.1515/hjic-2018-0015

HUNGARIAN JOURNAL OF INDUSTRY AND CHEMISTRY
HJIC

COMPARISON BETWEEN STATIC AND DYNAMIC ANALYSES OF THE SOLID FAT CONTENT OF COCONUT OIL

VINOD DHAYGUDE *[1], ANITA SOÓS[1], ILDIKÓ ZEKE[2], AND LÁSZLÓ SOMOGYI[1]

[1]Department of Grain and Industrial Plant Technology, Szent István University, Villányi út 29–43, Budapest, 1118, HUNGARY
[2]Department of Refrigeration and Livestock Products Technology, Szent István University, Ménesi út 43-45, Budapest, 1118, HUNGARY

The objective of this work was to compare the physical and thermal characteristics of two coconut oils and their blends which were observed by the results of differential scanning calorimetry (DSC) and pulsed nuclear magnetic resonance (pNMR). Fat blends composed of different ratios (fully hydrogenated coconut oil / non-hydrogenated coconut oil: 25/75, 50/50 and 75/25) were prepared and examined for solid fat content. The solid fat content of samples was determined as a function of temperature by pNMR. The DSC technique determines the solid fat index by measuring the heat of fusion successively at different temperatures. DSC calculates the actual content of solids in fat samples and how it changes throughout the duration of heating or cooling. A characteristic curve is constructed by the correlation of enthalpies. Based on our results, it is clear that both DSC and pNMR techniques provide very practical and useful information on the solid fat content of fats. DSC is dynamic and pNMR is static. A difference in the values of the solid fat indexes of samples was observed which may be due to a fundamental difference between the two techniques. These data can be used by food manufacturers to optimize processing conditions for modified coconut oil and food products fortified with coconut oil.

Keywords: solid fat content, solid fat index, pNMR, DSC, and Coconut oil

1. Introduction

Nowadays, a proper understanding of the crystallization and melting properties of coconut oil systems is essential to increase the number of applications in the food industry. Coconut oil is considered as a multi-component mixture of various triglycerides which determines the physical properties that affect the structure, stability, flavor as well as sensory and visual characteristics of foods [1]. Modification of the properties of solid fat has received much attention in research recently because of its importance during the processing and production of new food products. The crystallization and melting properties of modified fat used as a shortening in bakery products are critical [2]. The crystal networks present in modified fat strongly enhance its texture, stability and acceptance of fatty-food products.

An essential aspect of the industrial manufacture of edible oils and fats is the ability to measure the physical and thermal properties of the materials such as melting and crystallisation profiles, solid fat content (SFC), solid fat index (SFI) and enthalpy. Nuclear magnetic resonance (NMR) spectroscopy and differential scanning calorimetry (DSC) are easier to implement and faster techniques than dilatometry which is time-consuming and inaccurate [3]. NMR has been widely used for the analysis of food materials such as dairy products, fats and oils, in addition to wine and beverages. Over the past two decades, DSC has been increasingly utilised for the thermodynamic characterisation of edible oils and fats as well as the SFI determination of food fats.

Considering the significant scientific and practical importance of the physical properties of coconut oil from a few studies, the solid fat content determined by NMR and DSC methods was investigated and the obtained results compared. Ultimately, this research study is beneficial to the food industry which continues to reformulate many products.

2. Experimental

2.1 Materials

In this research study, Barco coconut oil was used as a source of non-hydrogenated coconut oil (NHCO) which was kindly provided by Mayer's Kft. in Budapest. The fully hydrogenated coconut oil (FHCO) was obtained from local industry in Hungary. Blends of NHCO and FHCO were mixed in 25:75, 50:50 and 75:25 (w/w) proportions. The blends were melted and maintained at 80 °C for 30 mins to erase crystal memory. Subsequently,

*Correspondence: vinod.dhaygude05@gmail.com

Table 1: Fatty acid composition (%) of NHCO, FHCO and their blends.

Fatty acid (%)	FHCO	FHCO:NHCO			NHCO
		75:25	50:5	25:75	
C6:0	0.1	0.225	0.35	0.475	0.6
C8:0	1.9	3.175	4.45	5.725	7
C10:0	2.7	3.4	4.1	4.8	5.5
C12:0	53.3	51.425	49.55	47.675	45.8
C12:1	0.1	0.075	0.05	0.025	–
C14:0	21.3	20.675	20.05	19.425	18.8
C16:0	10	10.025	10.05	10.075	10.1
C18:0	10	8.25	6.5	4.75	3
C18:1 trans	0.03	0.0575	0.085	0.1125	0.14
C18:1 cis	0.3	2.0	3.7	5.4	7.1
C18:2 trans	–	0.02	0.05	0.08	0.11
C18:2 cis	0.1	0.5	0.9	1.3	1.7
C20	0.1	0.1	0.1	0.1	0.1
Other	0.02	0.03	0.05	0.065	0.08

all blends and pure samples of fat were stored in a refrigerator at 10 °C until use.

2.2 Methodologies

Static analysis The static analysis of the solid fat content was conducted by pulsed nuclear magnetic resonance (pNMR) apparatus (Bruker Minispec 300, Bruker GmbH, Germany) according to the official method Cd 16b-93 of the American Oil Chemists' Society (AOCS) [4]. The solid fat content was measured at 5 °C, 10 °C, 15 °C, 20 °C, 25 °C and 30 °C. Three parallel measurements were conducted and average values reported (Fig. 1). Additionally, these SFC values were converted into percentages where the initial value was considered to be 100 %. These percentage SFCs were compared with the SFIs.

Dynamic Analysis Dynamic analyses of the samples were studied by DFC according to AOCS official method Cj 1–94 [4]. Samples of nearly 20 mg were loaded onto the middle of the aluminum pans using a small spatula and hermetically sealed by an empty pan that served as a reference. Samples were cooled to 0 °C at a rate of 1 °C min^{-1} and maintained at this temperature for 10 mins. The heating of blends and pure samples of oil was performed until a temperature of 80 °C was achieved at the same rate as for the cooling. The samples were maintained at 80 °C for 30 mins. The cooling process started after this period and the rate of cooling was 1 °C min^{-1} until the temperature reached −20 °C. Before being heated again to ambient temperature, the samples were maintained at this temperature for 10 mins. After that, heating commenced once more at a rate of 5 °C min^{-1} up to 20 °C at which point calorimetric measurements ended. Three parallel measurements were taken and the average thermogram was reported.

The SFI of fat is expressed as a function of temperature. The numbers of solids in the samples of oil in relation to the temperature were estimated on the basis of the calorimetric results. Areas of the thermograms were calculated and correlated with the percentage of solids in the samples.

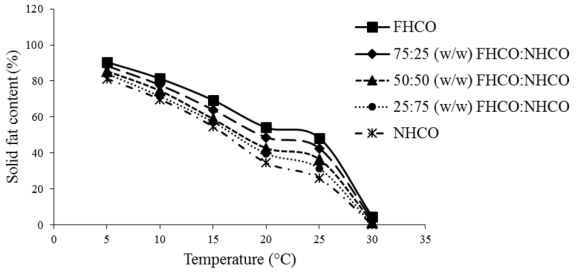

Figure 1: Solid fat content profiles of two coconut oils and their blends.

3. Results and Discussion

3.1 Fatty acid composition

Samples were characterized by their fatty acid composition (see Table 1). The dominant fatty acids in the sample of coconut oil were lauric acid (C12:0) 45.8-53.3 % and myristic acid (C18:0) 18.8-21.3 %. The NHCO exhibited a higher percentage of medium-chain fatty acids and a lower percentage of unsaturated fatty acids. The FHCO was rich in polyunsaturated fatty acids (PUFA) and monounsaturated fatty acids (MUFA).

3.2 Solid fat content according to NMR

The composition of fatty acids and triacylglycerols (TAG) would contribute to the percentage of solid fat particles in liquid oil at various temperatures. The SFC profiles of the original fats and their blends at temperatures ranging from 5 °C to 30 °C are presented in Fig. 1.

The SFC profile of NHCO exhibited low values of 81.06 %, 69.70 %, 54.61 %, 34.54 %, 25.86 % and 0.17 % over the temperature range of 5 °C – 30 °C because of the concentration of fatty acids. In the case of FHCO, the solid fat content was high at 90.49 %, 81.28 %, 69.29 %, 54.15 %, 48.30 % and 4.46 % over the same temperature range. The SFC profiles of blends changed following the addition of FHCO to NHCO. An increase in the maximum values of SFC was also observed by Ribeiro et al. following the addition of fully hydrogenated soybean oil to soybean oil [5]. This can be explained by the changes in the composition of triacylglycerols of the blends. At 5 °C, the blends exhibited SFCs ranging from 84.94 % to 90.02 %, which decreased non-linearly until melting completely at 30 °C. During the blending, the concentration of TAGs with high melting points increased and subsequently the SFC values of blends were modified. In all blends, the SFC values at 30 °C were almost identical to the SFC of the FHCO.

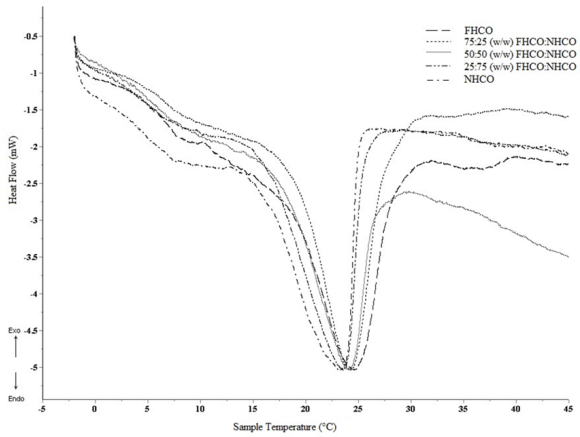

Figure 2: Melting profiles of two coconut oils and their blends.

Table 2: Thermal properties of NHCO, FHCO and their blends.

Sample	Max. temperature (°C)	Peak Enthalpy (J/g)
FHCO	24.61	80.24
75:25(w/w)FHCO:NHCO	24.30	76.21
50:50(w/w)FHCO:NHCO	23.96	63.44
25:75(w/w)FHCO:NHCO	23.52	55.84
NHCO	23.27	46.38

3.3 Melting characteristics

The melting profiles of NHCO in the presence of fully hydrogenated coconut are depicted in Fig. 2. The melting behavior of the original oils and blends was characterized by only one endothermic peak. A similar thermal behavior of coconut oil and hydrogenated coconut oil was observed by one major peak in various studies [6, 7]. Components with the lowest melting points tend to melt first and represent the most unsaturated triglycerides, while components with higher melting points that represent the most saturated triglycerides melt later. Similarly, results showed that NHCO started melting first compared to other samples because of its higher content of unsaturated triglycerides. The addition of FHCO to NHCO did not alter the melting behavior but as the content of FHCO was increased, the peaks according to the melting profiles of blends shifted towards the high-melting temperatures (Fig. 2).

This melting profiles provided an indication of the amount of crystallized fat and the occurrence of polymorphic transitions.

The thermal characteristics of the original oils and their blends are shown in Table 2. No significant differences were observed between the values of onset temperature (T_{on}) and peak temperature (T_p) in addition to the enthalpies of NHCO and FHCO. T_{on} ranged from 15.60 °C to 20.50 °C while T_p ranged from 23.27 °C to 24.61 °C. Melting enthalpies of NHCO following the addition of FHCO increased from 46.38 J/g to 80.24 J/g (see Table 2).

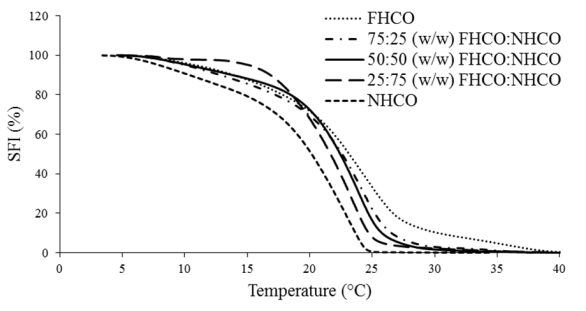

Figure 3: Solid fat index profiles of two coconut oils and their blends.

3.4 Solid fat index (SFI)

The solid-liquid ratio in fats expressed as solid fat content is determined from the melting curves that result from DSC by partial integration. The heat flow into or out of samples of fat was measured as they were heated and cooled isothermally. The estimation of the SFIs of samples is dependent upon the onset and final temperatures of melting. The SFI profiles of all samples calculated by melting thermographs are shown in Fig. 3. Non-hydrogenated coconut oil exhibited a characteristic steep slope and a rapid decrease in the percentage of solids at 20 °C. This ratio of solids to liquids decreases differently in these blends of fat as the temperature rises and is at its minimum for all blends at around 30 °C (see Fig. 3).

4. Discussion

The results obtained from two methods exhibited a wide range of solid fat content values of the same samples. The values of SFC calculated from pNMR results were lower than values of SFI according to DSC where DSC is a dynamic method and NMR is a static method. The values of the percentages of SFC for each blend at 15 °C calculated by DSC were 87.55 %, 88.38 % and 95.95 % (see Fig. 3) but 68.05 %, 68.83 % and 72.35 % when calculated by pNMR, respectively (see Fig. 4). DSC samples exhibited a sharp decline in their SFI or ratio of solids to liquids when heated from 15°C to 25°C, however, the SFC of samples according to NMR exhibited a gradual slope.

DSC measurements of physical behavior were observed under controlled heating conditions. The results of DSC describe the whole melting process whilst being heated. The NMR results indicate the statistical values of solid fat content. The difference between the two measurements was possibly due to the time-dependent process concerning the development of crystal structure where SFI describes the status of the fat system and SFC

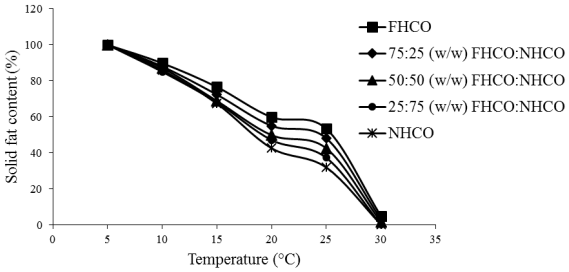

Figure 4: Solid fat content (%) of two coconut oils and their blends.

the solid status after stabilization. In addition NMR identified state vise crystals at respective temperatures. The difference in values may be due to the method of tempering, the rate of heating or cooling, and the degree of accuracy.

5. Conclusion

The results revealed that by combining FHCO with NHCO the melting behavior of blends of coconut oils was modified, leading to significant increments in the melting point and in the maximum solid fat content. These two methods yielded more descriptive and clear information about melting behaviour by determining amounts of solids in the samples of coconut oil in relation to the temperature. Static and dynamic analytical methods showed a difference in the solid-to-liquid ratio of samples which may be due to fundamental differences. The blending of FHCOs with vegetable oils can produce valuable blends of fat of good consistency and with reduced or even in the absence of trans-isomers of unsaturated fatty acids suitable for margarine.

Acknowledgement

This research was supported by the Doctoral School of Food Sciences at Szent István University.

REFERENCES

[1] Dayrit, F. M.: The properties of lauric acid and their significance in coconut oil. *J. Am. Oil Chem. Soc.*, 2015 **92**, 1–15 DOI: 10.1007/s11746-014-2562-7

[2] O'brien, R. D.: Fat and oils formulating and processing for applications Boca Raton, FL CRC/Taylor & Francis, 2009, USA ISBN: 9781420061666

[3] Walker, R. C.; Bosin, W. A.: Comparison of SFI, DSC and NMR methods for determining solid-liquid ratios in fats. *J. Am. Oil Chem. Soc.*, 1971 **48**, 50–53. DOI: 10.1007/BF02635684

[4] AOCS: Official Method Cd 16b-93 Solid fat content (SFC) by low-resolution nuclear magnetic resonance; in: Firestone, D. (ed.) Official methods and recommended practices of the AOCS. The American Oil Chemists Society, 2005 , Champaign, USA. ISBN: 9780935315974

[5] Ribeiro, A.; Grimaldi, R.; Gioielli, L. A.; Gonçalves, L.: Zero trans fats from soybean oil and fully hydrogenated soybean oil: Physicochemical properties and food applications. *Food Research International*, 2009 **42**, 401–410 DOI: 10.1016/j.foodres.2009.01.012

[6] Tan, C. P.; Che Man, Y. B.: Differential scanning calorimetric analysis of palm oil, palm oil based products and coconut oil: Effects of scanning rate variation. *Food Chemistry*, 2002 **76**, 89–102 DOI: 10.1016/S0308-8146(01)00241-2

[7] Shen, Z.; Birkett, A.; Augustin, M. A.; Dungey, S.; Versteeg, C.: Melting behavior of blends of milk fat with hydrogenated coconut and cottonseed oils. *J. Am. Oil Chem. Soc.*, 2001 **78**, 387–394 DOI: 10.1007/s11746-001-0273-4

DE GRUYTER OPEN

HUNGARIAN JOURNAL OF INDUSTRY AND CHEMISTRY
Vol. 46(2) pp. 37–42 (2018)
hjic.mk.uni-pannon.hu
DOI: 10.1515/hjic-2018-0016

HUNGARIAN JOURNAL OF INDUSTRY AND CHEMISTRY
HJIC

MONITORING OF CHEMICAL CHANGES IN RED LENTIL SEEDS DURING THE GERMINATION PROCESS

ILDIKÓ SZEDLJAK *[1], ANIKÓ KOVÁCS[1], GABRIELLA KUN-FARKAS[2], BOTOND BERNHARDT[3], SZABINA KRÁLIK[1], AND KATALIN SZÁNTAI-KŐHEGYI[1]

[1]Department of Grain and Industrial Plant Processing, Szent István University, Villányi út 29-43, Budapest, 1118, HUNGARY
[2]Department of Brewing and Distilling, Faculty of Food Science, Szent István University, Villányi út 29-43, Budapest, 1118, HUNGARY
[3]Department of Soil Chemistry and Turnover, Institute for Soil Sciences and Agricultural Chemistry, Centre for Agricultural Research, Hungarian Academy of Sciences, Herman Ottó út 15, Budapest, 1022, HUNGARY

Red lentils are a very important raw material in the food industry due to their high protein content and high level of health-promoting components. The nutritive value of red lentils is the most important attribute from a research point of view; it can be increased by germination, soaking as well as physical and biochemical processes. The antinutritive materials are reduced or denatured by the germination process and indigestible components become available to the human body. Heat treatment was applied to achieve different temperatures and increase the microbiological stability of germinating samples. The effect of heat treatment on the amounts of certain components and the activity of oxidative enzymes was tested during our experiments; the nutritional characteristics (water-soluble total polyphenol content (WSTPC), water-soluble protein content (WSPC), water-soluble antioxidant capacity, in addition to peroxidase and polyphenol oxidase enzyme activities) of different treatments in red lentil samples were monitored. The WSTPC in our samples ranged from 0.726 mg Gallic Acid Equivalent GAE/g DW (DW being dry weight) to 1.089 mg GAE/g DW, and the WSPC varied from 19.078 g / 100g DW to 29.692 g / 100 g DW. Results showed that germination led to an increase in the WSTPC and WSPC. The peroxidase enzyme activity also exhibited an increase during germination which could result in deepening of the colour of the finished products. Germination resulted in the water-soluble antioxidant capacity of red lentil samples decreasing.

Keywords: red lentil, germination, antioxidant activity, protein, enzyme

1. Introduction

Lentils (*Lens culinaris* M.) are bushy annual plants of the legume family. Lentils are grown for the high protein content and high nutritive value of their lens-shaped seeds. Lentils are primarily a cool-season crop; they are moderately resistant to high temperatures and droughts. Lentils are characterized by their high levels of plant protein, complex carbohydrates (resistant starch, slowly digestible starch and oligosaccharides), fibres (soluble and insoluble) as well as very low sodium and fat content. Additionally, lentils are rich in B-vitamins, e.g. folate, thiamin and niacin, and key minerals, namely iron, potassium, magnesium and zinc, make them a highly nutritious food.

The most common types of lentils are red, green and black of which red and green are the most commonly traded. The cultivation and consumption of red lentils are considerable in Asian countries. On the other hand, consumer demand for red lentils in the Western Hemisphere is not high [1].

Red lentils are a valuable source of macronutrients (proteins, fats, carbohydrates) and other important components (phytochemicals: phytic acid, phenolic acids, flavonols, flavanols and condensed tannins). Lentils have demonstrated many health benefits, e.g. lowering the glycemic index and their gluten-free status for people with metabolic disorders. The consumption of lentils can also lead to weight loss, which is recommended for all overweight and obese individuals [2, 3].

The germinated seeds and their compounds are possible components of functional foods. Functional foods play an important role in health promotion and disease prevention. Different scientific papers suggest that lentils provide protection against chronic diseases through a multitude of biological activities including anticancer, antioxidant and angiotensin-converting enzyme inhibition. Lentils also reduce blood lipid levels and the risk of developing cardiovascular diseases [4, 5].

*Correspondence: ildiko.szedljak@gmail.com

The nutritive value of lentil seeds can be improved by the germination process. Germination is a complex metabolic process during which the lipids, carbohydrates and storage proteins within seeds are broken down in order to obtain the necessary energy and amino acids. These changes influence the bioavailability of essential nutrients [6]. The presence of antinutritional factors might be reduced by germination. Red lentils have been gaining increasing attention due to their health benefits as part of the human diet and they are considered to be an excellent source of dietary antioxidants largely because of their high level of bioactive phytochemicals [1,7]

In Hungary, small-scale (20 seeds) red lentil germination experiments have already been conducted during which the effect of germination on the lectin content was studied [8]. The main purpose of our research was to examine the suitability of the germinated red-lentil grist as a raw material of dry pasta.

Red lentils were selected for our experiments due to their aforementioned favourable nutritional characteristics. In addition, its flour can be suitable in the development of gluten-free pasta products in the form of enrichment and gluten-free raw materials. The formation of more digestible water-soluble components was conduced by seed germination, but at the same time a loss may be observed due to the heat treatments (drying pasta) used in the manufacture of the products. The same loss may occur during the boiling process. Therefore, it is important to check for all kinds of changes that occur during heat treatment. The control of the activity of enzymes which generate oxidation processes is also essential during germination as is technological / kitchen-technological processing from the point of view of the expected quality of the finished products.

Developing food diversity by incorporating red lentil seeds and its flour into western diets is highly recommended.

2. Experimental

The aim of our study was to examine the chemical changes in red lentil seeds during the germination process. The effect of different heat treatments on the amount of certain components and the activity of oxidative enzymes were monitored. Moreover, a connection between the parameters and the extent to which these variables interact was sought.

2.1 Samples and Measurements

Samples 10 kg of raw organic whole red lentil was purchased from BiOrganik Online Kft. 3 kg of which was added to the germination device. 500 g of both soaked and sprouting seeds were sampled and heat-treated at three different temperatures. The heat-treated seeds were milled using a hammer grinder and then homogenized. The aqueous extracts were made from the control samples and the heat-treated grists.

Steeping, Germination and Heat Treatment Steeping and germination were performed in a Schmidt-Seeger, KMA-A1-2008 micromalting plant. The micromalting plant was controlled by a personal computer with a special controlled by a personal computer with special software. During germination the temperature of the air was regulated and wetted with special jets.

During the steeping process compressed air was dispersed in the steeping water. Alternate wet and dry periods were implemented during steeping, because during the latter the oxygen uptake of grains is more effective. Wet steeping lasted for 3 hours at 20 °C with aerations of 6.67 minutes in duration every 8 minutes. This was followed by a 2 hour-long dry period at 22 °C with humidification. The second 2-hour-long wet period was performed at 20 °C. Steeping was stopped when an adequate moisture content was achieved. Germination lasted for 96 hours at 22 °C with humidification. During the first 48 hours, the germinating seeds were rotated 30 times every two hours, then every three hours. Germinating seeds were not sprayed during the process.

Germinating red lentil samples were taken daily at the same time. Heat treatment was applied at different temperatures (60 °C, 80 °C, 100 °C) in order to increase the microbiological stability of germinating samples. The effect of heat treatment on the amount of certain components and the activity of oxidative enzymes was tested during our experiments.

Chemical Analysis The samples were homogenized and 0.10 ml of distilled water was added to each sample. The centrifugation process was conducted after extraction for 10 minutes at 4 °C and 10,000 rpm. The water-soluble polyphenolic content was measured by colorimetric analysis using Folin & Ciocalteu's phenol reagent [9] and the results were expressed in Gallic Acid Equivalent (GAE) (mg GAE/g DW – DW being dry weight). The WSPC was measured by a method discovered by Layne [10].

The water-soluble antioxidant activity was determined using a Ferric Reducing Antioxidant Power (FRAP) Assay Kit [11]. The polyphenol oxidase (PPO) enzyme activity was measured by using a synthetic substrate, pyrocatechol. The oxidized form of the substrate can be synthesized photometrically at 420 nm by a spectrophotometer [12]. The peroxidase (POD) enzyme activity of the extracts was determined using o-Dianisidine as a hydrogen donor in sodium acetate (pH 5.1) [13]. The reagents for the chemical measurements were provided by Sigma-Aldrich Kft.

Statistical Methods All of the measurements were replicated five times. The Kruskal-Wallis test was applied to calculate the exact p-value ($\alpha = 0.05$) and Dunn's post hoc pair-wise test was chosen with an adjustment by Bonferroni. The relationship between the parameters was determined by Spearman's rank correlation coeffi-

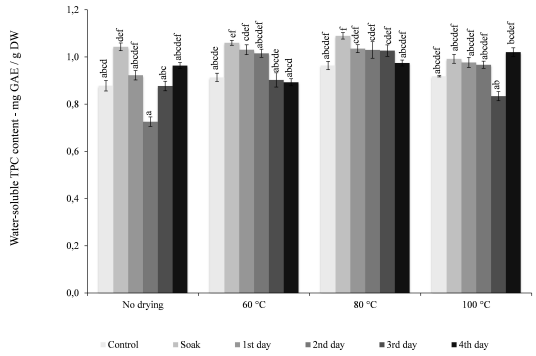

Figure 1: Water-soluble total polyphenol content in red lentil samples. Different letters indicate significant differences between treatments ($p \leq 0.05$).

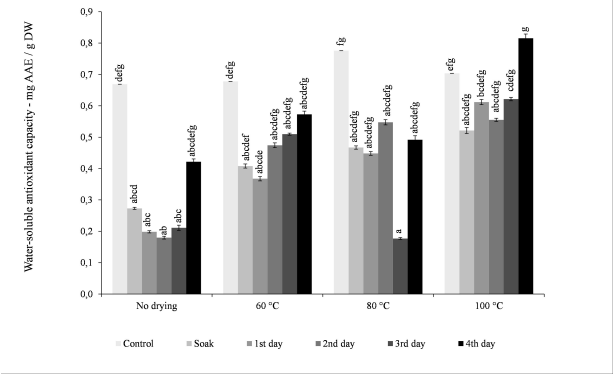

Figure 2: Water-soluble antioxidant capacity of red lentil samples. Different letters indicate significant differences between treatments ($p \leq 0.05$).

cient (non-parametric equivalent of Pearson's correlation coefficient) (α = 0.05) using the XLSTAT-Sensory solution software, version 2013.1.01 (Addinsoft, 28 West 27th Street, Suite 503, New York, NY 10001, USA).

During the correlation test the correlation between the variables regardless of their units was examined.

3. Results and Evaluation

3.1 Water-soluble total polyphenol content (WSTPC)

Zhang et al. [14] measured the total polyphenol content (soluble and insoluble in water) using Folin Ciocalteu's reagent in raw red-lentil extracts (5.04 $\pm$ 0.36 mg GAE/g DW – 7.02 $\pm$ 0.48 mg GAE/g DW). According to their data all extracts of lentils cultivated in Canada were significantly different from each other. In contrast to this TPC values changed over a very narrow range (from 5.9 $\pm$ 0.1 mg GAE/g DW to 5.93 mg GAE/g DW) in the samples of red-lentil flour tested [15–17]. The results of TPC are shown in Fig. 1. The WSTPC in our samples ranged from 0.726 mg GAE/g DW to 1.089 mg GAE/g DW. Our WSTPC values were 5 to 10 times smaller than in the aforementioned experiments.

By comparing the control and soaked samples, it can be observed that the WSTPC increased during the soaking process. These values were higher than the measured data from germinated samples (Fig. 1).

According to our experiments heat treatment at high temperatures (80 °C and 100 °C) equalized the WSTPC values in red lentil samples. Furthermore, germination and heat treatments did not effect the WSTPC of the seeds.

3.2 Water-soluble antioxidant capacity

The results of water-soluble antioxidant capacity were measured using a FRAP Assay Kit. The values ranged between 0.177 mg Ascorbic Acid Equivalent (AAE)/g DW and 0.815 mg AAE/g DW. As a result of the germinating process, the antioxidant capacity of the samples was significantly reduced compared to that of the control sample. However, treatment at a high temperature (100 °C) led to a further increase in the amount of new water-soluble components with antioxidant capacity. Samples that were not dried during the first 3 days were significantly different from the control samples in all of the categories. Moreover, they differed from the sample dried at 100 °C on the 4th day (Fig. 2).

The highest water-soluble antioxidant capacities were measured in the control samples, except for the control sample treated at 100 °C. By comparing control samples to germinated samples, it is evident that the germinating process did not result in an increase in the water-soluble antioxidant capacity. Our results showed that whilst being soaked the water-soluble antioxidant capacity started to decrease.

The water-soluble antioxidant capacity in the heat-treated sample on the 3rd day of germination at 80 °C decreased drastically compared to the control sample. The same change occurred with the samples that were not dried. Nevertheless, the significant decrease had already occurred on the 1st day of germination.

No correlation was found between the WSTPC and water-soluble antioxidant capacity.

3.3 Water-soluble protein content (WSPC)

WSPCs, given in Fig. 3, ranged from 19.078 g / 100 g DW (dry weight) to 29.692 g / 100 g DW.

By comparing the control and soaked samples, it is evident that the WSPC increased during the soaking process. In the case of samples that were not dried in addition to those treated at 80 °C and 100 °C, no significant differences were observed between treatments except for samples treated at 60 °C where those soaked and on their 2nd day of germination had significantly higher values compared to the control sample. The highest WSPC was

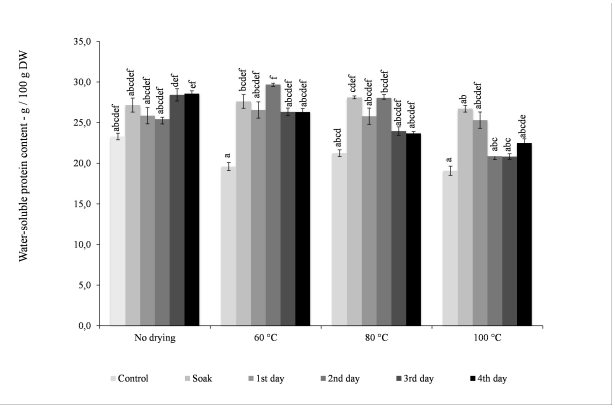

Figure 3: Water-soluble protein content in red lentil samples. Different letters indicate significant differences between treatments ($p \leq 0.05$).

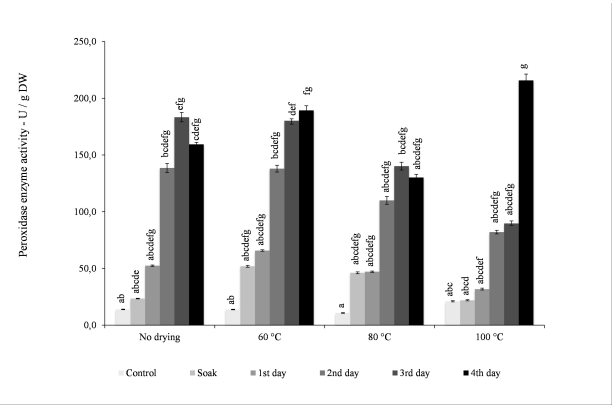

Figure 4: Peroxidase enzyme activity of red lentil samples. Different letters indicate significant differences between treatments ($p \leq 0.05$).

measured on the 2nd day of germination at 60 °C, which was significantly higher than all the heat-treated control samples as well as samples treated at 100 °C except for the value on the 1st day of germination.

As the germination process advanced – especially on the 3rd and 4th days – the WSPC of samples heat-treated at 80 °C and 100 °C started to decrease compared to the same phenophases of those that were not dried or heat-treated at 60 °C. This may be explained by the fact that plant proteins are more easily degraded at higher temperatures over prolonged periods of time. A negative correlation was observed between the WSPC and water-soluble antioxidant capacity.

The total protein content was determined using the Dumas method as described by Hefnawy [18]. In this study the total protein content was 26.6 ± 0.50 g / 100 g DW and the effect of the heat treatment was insignificant.

3.4 Peroxidase (POD) Enzyme Activity

The changes in POD enzyme activity of red-lentil samples are shown in Fig. 4. The POD adversely affects the nutritive value, taste, texture and colour of food products. These enzymes are referred to as heat-tolerant enzymes and can regain their activity following heat treatment and storage (Fig. 4).

POD enzyme activity ranged from 10.815 U/g DW to 215.785 U/g DW with statistically significant differences. The highest value (215.785 U/g DW) was found in the sample dried at 100 °C on the 4th day.

The samples that were not dried or heat-treated were identical to each other on the same level (control, soaked, 1st-4th day). POD activity progressively increased during the germination process in almost all cases. The POD activity of the sample dried at 100 °C was 20-fold higher than that of the control sample. The POD activity of different tempered lentil samples was also measured by Pathiratne et al. [19] and their maximum value was 186.4 U/g protein. However, in another study by Świeca et al. [20], the POD activity of germinated lentil samples was much higher than the aforementioned ones, 10.3 ± 0.24 kU/mg protein.

Elevated temperatures of heat treatment resulted in an increase in the POD activity during the germination process.

3.5 Polyphenol oxidase (PPO) enzyme activity

PPOs and PODs are the most studied enzymes in fruit and vegetables. Świeca et al. [20] studied the PPO enzyme activity in sprouts of lentils according to the method described by Galeazzi et al. [21] and measured 2.24 ± 0.05 kU/mg protein. They reported that enzymatic markers of the stress metabolism of plants, e.g. PPO activities, did not differ significantly between sprouts. In our study a catechol substrate was also used but no PPO enzyme activity was detected in the samples.

4. Conclusion

Of all the parameters studied, the WSPC of red lentils strongly correlated with the values of water-soluble antioxidant capacity measured using the FRAP Assay Kit (data not shown). The correlation is inversely proportional, hence, the greater the WSPC, the lower the water-soluble antioxidant capacity. Seed germination is one of the most important stages in the life cycle of plants and germinated seeds may be a useful source of healthy food. Germinated seeds are very complex living matrices and it is very difficult to understand the biochemical changes that occur during sprouting. Further studies on the germination process of red lentils are needed to help understand and identify the important parameters that are able to describe such changes.

Functional foods play an important role in terms of consumer acceptance [22], thus, a more suitable approach

may well be sensory evaluation in the case of our red-lentil samples. The latest development methodologies should be used, namely preference mapping methods, Just-About-Right (JAR) scaling and eye-tracking methods [23–25].

REFERENCES

[1] Zhang, B.; Deng, Z.; Tang, Y.; Chen, P.; Liu, R.; Ramdath, D. D.; Liu, Q.; Hernandez, M.; Tsao, R.: Fatty acid, carotenoid and tocopherol compositions of 20 Canadian lentil cultivars and synergistic contribution to antioxidant activities. *Food Chem.*, 2014 **161**, 296–304. DOI: 10.1016/j.foodchem.2014.04.014

[2] Papanikolaou, Y.; Fulgoni, V. L.: Bean consumption is associated with greater nutrient intake, reduced systolic blood pressure, lower body weight, and a smaller waist circumference in adults: results from the National Health and Nutrition Examination Survey 1999–2002. *J. Am. Coll. Nutr.*, 2008 **27**(5), 569–576. DOI: 10.1080/07315724.2008.10719740

[3] Sravanthi, B.; Jayas, D. S.; Alagusundaram, K.; Chelladurai, V.; White, N. D. G.: Effect of storage conditions on red lentils. *J. Stored Prod. Res.* 2013 **53**, 48–53. DOI: 10.1016/j.jspr.2013.01.004

[4] Duane, W. C.: Effects of legume consumption on serum cholesterol, biliary lipids, and sterol metabolism in humans. *J. Lipid Res.*, 1997 **38**(6), 1120–1128.

[5] Shepherd, J.; Cobbe, S. M.; Ford, I.; Isles, C. G.; Lorimer, A. R.; MacFarlane, P. W.; McKillop, J. H.; Packard, C. J.: Prevention of coronary heart disease with pravastatin in men with hypercholesterolemia. *N. Engl. J. Med.*, 1995 **333**(20), 1301–1308. DOI: 10.1056/NEJM199511163332001

[6] Urbano, G.; Lopez-Jurado, M.; Hernandez, J.; Fernandez, M.; Moreu, M. C.; Frias, J.; Diaz-Pollan, C.; Prodanov, M.; Vidal-Valverde, C.: Nutritional assessment of raw, heated and germinated lentils. *J. Agric. Food Chem.*, 1995 **43**(7), 1871–1877. DOI: 10.1021/jf00055a022

[7] Zou, Y.; Chang, S. K. C.; Gu, Y.; Qian, S. Y.: Antioxidant activity and phenolic compositions of lentil (*Lens culinaris* var. Morton) extract and its fractions. *J. Agric. Food Chem.*, 2011 **59**(6), 2268–2276. DOI: 10.1021/jf104640k

[8] Cuadrado, C.; Gelencsér, É.; Perdoza, M. M.; Ayet, G.; Muzquiz, M.; Puszati, A.; Hajós, Gy.; Burbano, C.: Influence of germination on lectin in Lens culinaris seeds. *Acta Aliment.*, 2000 **29**(3), 231–240. DOI: 10.1556/AAlim.29.2000.3.3

[9] Singleton, V. L.; Rossi, J. A.: Colorimetry of total phenolics with phosphomolybdic-phosphotungstic acid reagents. *Am. J. Enol. Viticult.*, 1965 **16**(3), 144–158.

[10] Layne, E.: Spectrophotometric and turbidimetric methods for measuring proteins. Chapter in *Methods Enzymol.*, 1957, pages 447–454. DOI: 10.1016/S0076-6879(57)03413-8

[11] Benzie, I. F. F.; Strain, J. J.: The ferric reducing ability of plasma (FRAP) as a measure of "antioxidant power": the FRAP assay. *Anal. Biochem.,* 1996 **239**(1), 70–76. DOI: 10.1006/abio.1996.0292

[12] Watson, R. A.; Flurkey, W. H.: Use of contact prints for recording polyphenoloxidase isoenzymes separated by electrophoresis. *J. Sci. Food Agric.*, 1986 **37**(8), 791–796. DOI: 10.1002/jsfa2740370812

[13] Björkstén, F.: Participation of horseradish oxyperoxidase (compound III) in interenzymic reaction steps. *Biochem. Biophys. Acta*, 1968 **151**(1), 309–311. DOI: 10.1016/0005-2744(68)90196-4

[14] Zhang, B.; Deng, Z.; Tang, Y.; Chen, P.; Liu, R.; Ramdath, D. D.; Liu, Q.; Hernandez, M.; Tsao, R.: Fatty acid, carotenoid and tocopherol compositions of 20 Canadian lentil cultivars and synergistic contribution to antioxidant activities. *Food Chem.*, 2014 **161**, 296–304. DOI: 10.1016/j.foodchem.2014.04.014

[15] Xu, B. J.; Yua, S. H.; Chang, S. K. C.:Comparative analyses of phenolic composition, antioxidant capacity, and color of cool season legumes and other selected food legumes. *J. Food Sci.* 2007 **72**(2), 167–177. DOI: 10.1111/j.1750-3841.2006.00261.x

[16] Boye, J. I.; Aksay, S.; Roufik, S.; Ribéreau, S.; Mondor, M.; Farnworth, E.; Rajamohamed, S. H.: Comparison of the functional properties of pea, chickpea and lentil protein concentrates processed using ultrafiltration and isoelectric precipitation techniques. *Food Res. Int.*, 2010 **43**(2), 537–554. DOI: 10.1016/j.foodres.2009.07.021

[17] Shaheen, N.; Goto, M.; Watanabe, J.; Takano-Ishikawa, Y.: Antioxidant capacity and total phenol content of commonly consumed indigenous foods of Asian tropical regions. *J. Food Sci. Eng.*, 2012 **2**(4), 187–195. DOI: 10.17265/2159-5828/2012.04.001

[18] Hefnawy, T. H.: Effect of processing methods on nutritional composition and anti-nutritional factors in lentils (*Lens culinaris*). *Ann. Agric. Sci.*, 2011 **56**(2), 57–61. DOI: 10.1016/j.aoas.2011.07.001

[19] Pathiratne, S. M.; Shand, P. J.; Pickard, M.; Wanasundara, J. P. D.: Generating functional property variation in lentil (*Lens culinaris*) flour by seed micronization: Effects of seed moisture level and surface temperature. *Food Res. Int.*, 2015 **76**(1), 122–131. DOI: 10.1016/j.foodres.2015.03.026

[20] Świeca, M.; Sęczyk, Ł.; Gawlik-Dziki, U.: Elicitation and precursor feeding as tools for the improvement of the phenolic content and antioxidant activity of lentil sprouts. *Food Chem.*, 2014 **161**, 288–295. DOI: 10.1016/j.foodchem.2014.04.012

[21] Galeazzi, M. A. M.; Sgarbieri, V. C.; Constantinides, S. M.: Isolation, purification and physiochemical characterization of polyphenoloxidases (PPO) from dwarf variety of banana (*Musa Cavendishii*, L.). *J. Food Sci.*, 1981 **46**(1), 150–155. DOI: 10.1111/j.1365-2621.1981.tb14551.x

[22] Bagdi, A.; Tóth, B.; Lőrincz, R.; Szendi, Sz.; Gere, A.; Kókai, Z.; Sipos, L.; Tömösközi, S: Effect of aleurone-rich flour on composition, baking, textural, and sensory properties of bread. *LWT - Food Sci. Tech.,* 2016 **65**, 762–769. DOI: 10.1016/j.lwt.2015.08.073

[23] Gere, A.; Kovács, S.; Pásztor-Huszár, K.; Kókai, Z.; Sipos, L.: Comparison of preference mapping methods: a case study on flavoured kefirs. *J. Chemom.,* 2014 **28**(4), 293–300. DOI: 10.1002/cem.2594

[24] Gere, A.; Sipos, L.; Héberger, K.: Generalized pairwise correlation and method comparison: Impact assessment for JAR attributes on overall liking. *Food Qual. Prefer.*, 2015 **43**, 88–96. DOI: 10.1016/j.foodqual.2015.02.017

[25] Gere, A.; Danner, L.; De Antoni, N.; Kovács, S.; Dürrschmid, K.; Sipos, L.: Visual attention accompanying food decision process: An alternative approach to choose the best models. *Food Qual. Prefer.*, 2016 **51**, 1–7. DOI: 10.1016/j.foodqual.2016.01.009

DE GRUYTER OPEN

HUNGARIAN JOURNAL OF INDUSTRY AND CHEMISTRY
Vol. 46(2) pp. 43–46 (2018)
hjic.mk.uni-pannon.hu
DOI: 10.1515/hjic-2018-0017

HUNGARIAN JOURNAL OF INDUSTRY AND CHEMISTRY
HJIC

RECOVERY OF ITACONIC ACID BY ELECTRODIALYSIS

VERONIKA VARGA[1], KATALIN BÉLAFI-BAKÓ[1], DÁVID VOZIK[1], AND NÁNDOR NEMESTÓTHY *[1]

[1]Research Institute of Bioengineering, Membrane Technology and Energetics, University of Pannonia, Egyetem u. 10, Veszprém, 8200, HUNGARY

Itaconic acid is an organic acid produced mainly for non-food purposes. It can be manufactured by biotechnological synthesis using various strains which results in the salt form of the acid. In this work, the separation of sodium itaconate by electrodialysis was studied. Homopolar cation- and anion-selective membranes were applied and the module was operated under a constant voltage. The transport of the acid was followed by on-line ultraviolet and visible absorption spectroscopy, where the detector was installed in the system. The experiments with models of aqueous solutions confirmed that the technique is suitable for the effective recovery of itaconic acid.

Keywords: ultraviolet and visible absorption spectroscopy, on-line detection, monopolar membranes

1. Introduction

Itaconic acid was discovered by Baup in 1837 as the coproduct resulting from the degradation of citric acid [1]. Itaconic acid (2-methylene,1,4-butanedioic acid) is an unsaturated dicarboxylic acid, a rather reactive compound due to its conjugated double bond and two carboxyl groups. Therefore, it can easily participate in polymerisation reactions.

Itaconic acid – unlike citric acid – is applied exclusively for non-food purposes [2]. It is used mainly in the production of synthetic fibres and ion-exchange resins as well as in the pulp and paper industry.

Itaconic acid can be synthesized biotechnologically. Kinoshita was first to describe the process in 1932 when it was isolated from the broth of *Aspergillus itaconicus* [3]. Later a similar strain, *Aspergillus terreus*, was found to produce itaconic acid. Other microbes suitable for the fermentation of itaconic acid are listed in Table 1.

The main problem with downstream processing is that several similar organic acids are present in the broth, thus, recovery of itaconic acid is difficult. Separation of itaconic acid can be conducted by filtration with the aid of activated carbon and crystallisation (consecutive steps) or adsorption by strong anion-exchange resins, like Purolite A-500 P or PFA-300 [10]. The efficiency of the separation depends mainly on the temperature, pH and concentration.

An application of electrodialysis (ED) as a membrane process is the separation of organic acids [11–14]. Malic acid and galacturonic acid amongst others can be separated by ED using monopolar and bipolar membranes by implementing batch and continuous modes of operation.

Table 1: Biotechnological synthesis of itaconic acid

Strain	Reference
Aspergillus itaconicus	Kinoshita et al. (1932) [3]
Ustilago maydis	Steiger et al. (2013) [4]
Pseudozyma antarctica	Levinson et al. (2006) [5]
Yarrowia lipolytica	Kuenz et al. (2018) [6]
Synechocystis cyanobacteria	Heidorn et al. (2011) [7] Chin et al. (2015) [8]
Aspergillus terreus	Karaffa et al. (2015) [9]

The majority of these acids are produced as a salt, thus, the aim of the separation by ED is to transport the organic acid through the anion-selective membrane, while the cation should pass through the cation-selective membrane. The other neutral components remain in the feed solution. Usually the mobility of the acid is sufficient for effective transport, hence both the acid and cation can be recovered by ED.

The aim of this paper was to study the possibility of applying ED for the recovery of sodium itaconate.

2. Experimental

Itaconic acid, sodium sulphate, sulphuric acid, sodium hydroxide and all the other chemicals used were of an-

*Correspondence: nemesn@almos.uni-pannon.hu

Table 2: Features of the membranes

Feature	Fumasep FAA	Fumasep FKS
selectivity	>92 %	>96 %
electrical resistance	<2 Ωcm^2	<8 Ωcm^2
pH stability	in acidic media	5-13
thickness	0.13-0.15 mm	0.11-0.13 mm
ion-exchange capacity	>1.2 meq/g	>1.0 meq/g
conductivity	>8 mS/cm	>5 mS/cm

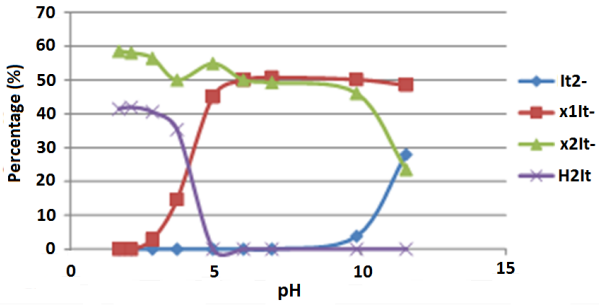

Figure 1: Percentages of the four distinct forms of itaconic acid.

alytical grade and purchased from Sigma-Aldrich. The anion- and cation-selective membranes were Fumasep FAA and FKS membranes, respectively. The main features of the membranes are summarized in Table 2. The membranes were activated by sodium chloride and sulphuric acid before usage.

For analytical purposes a Young Lin Instrument Co., Ltd. (YL9100-type) high-performance liquid chromatography (HPLC) system (including a YL9109 vacuum degasser, YL9110 quaternary pump and YL9150 automatic sample dispenser) was used to determine the concentration of itaconic acid with a Hamilton HPLC column (15 cm in length, 4.6 mm inner diameter, 5 μm particle size) and a YL9120 UV/Vis detector.

The Luff-Schoorl method was used to determine the glucose concentration which is based on the reduction of cupric (Cu(II)) cations in a boiling alkaline solution of cuprous (Cu(I)) oxide [15]. The surplus of Cu(II) was measured by iodometry using a titration with sodium thiosulfate.

The conductivity of the solutions was measured by a Radelkis OK-102/1 conductivity meter equipped with a Radelkis OK-9023 bell electrode using a cell constant of 0.7 cm^{-1}. Data concerning the voltage and current were measured by a National Instruments USB-600866009 device. All the experimental data were collected online using LabVIEW software.

An electrodialysis module was constructed from 2 anion- and 2 cation-selective membranes using spacers between them. The electrode solution was an aqueous solution of sodium sulphate.

Electrodialysis measurements were conducted using diluted (aqueous) model solutions of sodium itaconate and sodium itaconate mixed with glucose. The module was operated under a constant voltage.

3. Results

In this project, the final aim was to connect the ED device to the fermentation of itaconic acid in order to set up an integrated system. For this purpose, firstly the operation of ED was investigated by using model solutions of sodium itaconate and a simple ED device with monopolar ion-exchange membranes. The transport of the itaconic acid through the anion-selective membranes was the focus of the study

To follow the process, it was important to determine the exact concentration of itaconic acid. If the acid is the only compound in the solution, measuring the conductivity is a simple method for detection. However, if any other charged compound is present, it will disturb such measurements. In this case, HPLC is suggested for the analysis [9].

Itaconic acid is a dicarboxylic acid (consisting of three different ionic forms) and its dissociated forms and ionic strengths vary according to the pH. Thus, four distinct peaks over different retention times can be detected in HPLC chromatograms. The percentages of the four distinct forms as a function of pH were determined and are presented in Fig. 1.

Since it is quite difficult to measure the actual concentration of itaconic acid, another method was chosen. Itaconic acid has a UV absorption maximum at 243 nm which can be used for detection. This method seemed sufficiently sensitive for our purposes.

In our work, a loop was constructed from the solution (recirculated in the ED module) to the UV detector. Thus, online detection was applied to follow the concentration

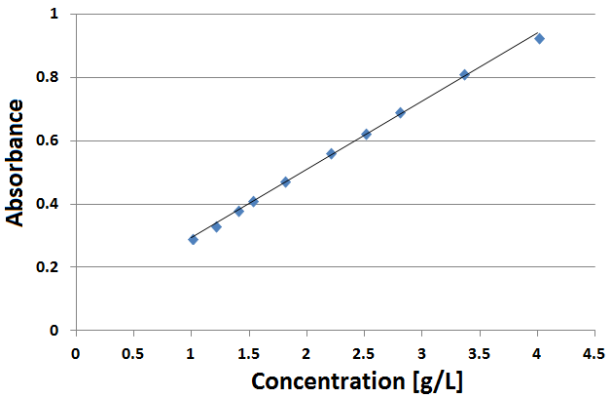

Figure 2: Calibration curve for the determination of itaconic acid concentration by UV detection

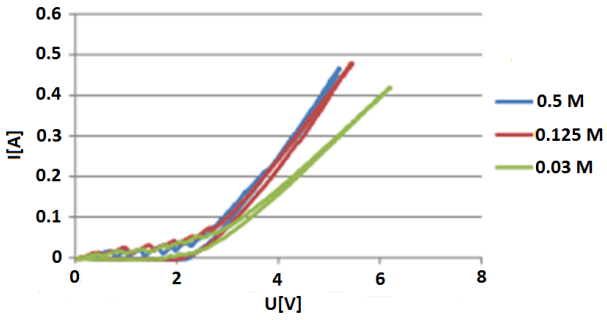

Figure 3: Polarization curves

of itaconic acid as a function of operating time. Firstly, a calibration curve was recorded (Fig. 2) over the concentration range of itaconic acid that was planned to be used. The data measured by the online UV system were checked by HPLC.

To test the ED module, polarization curves were taken using a potentiostat by applying a range of voltages from 0 to 10 V (Fig. 3). The current data were recorded as a function of the voltage data. The measurements were repeated in various electrode solutions.

It seems that beyond a sodium sulphate concentration of 0.125 M, the ED operated properly.

Experiments were conducted in the ED module by using aqueous model solutions of itaconic acid (with an initial concentration of 3-3 g/l). The electrode solution was a 0.16 M Na_2SO_4 solution. The experiments were conducted under a constant voltage (10 V) and the current intensity varied between 0.11 and 0.15 A.

Subsequently, the conductivity in the diluate solution was measured. The concentration of the acid decreased gradually to half its initial value after an operating time of 70 mins as can be seen in Fig. 4. This means that itaconic acid was able to pass through the anion-selective membrane, while sodium ions were able to diffuse across the cation-selective membrane. Therefore, the measurements confirmed that the mobility of this acid is sufficient to separate it by ED.

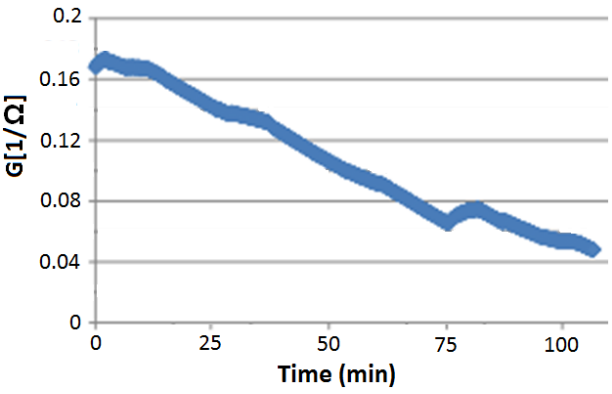

Figure 4: Conductivity data of the diluate of ED

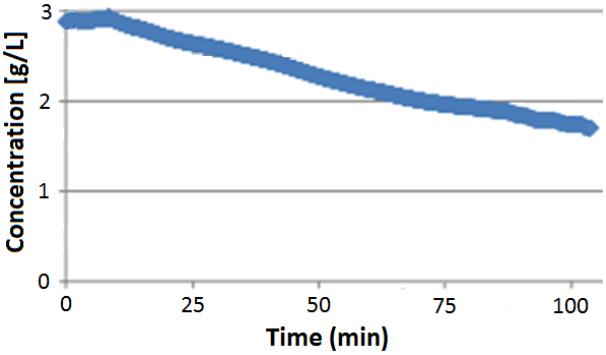

Figure 5: Concentration of itaconic acid in the diluate solution

In the next series of experiments, glucose was added to the acid (4 g/L) to investigate whether the ED module was able to separate the two compounds. The concentration of itaconic acid in the diluate was followed online by the UV detector installed in the loop. The concentration of the glucose was determined by the Luff-Schoorl method.

The concentration of the acid decreased from 3.0 to 1.5 g/L during the experiment (Fig. 5), while the glucose concentration was monitored in all three streams. In the diluate (originally feed) solution, a slight decrease in glucose concentration was observed (to 3.52 g/L), its concentration was negligible (0.20 g/L) in the electrode solution, while in the concentrate solution 0.59 g/L glucose was measured probably due to its diffusion from the feed solution.

4. Conclusion

The measurements provided a definite answer to the original question, namely whether ED is a suitable technique for the recovery of itaconic acid. The results of the experiments using model solutions (sodium itaconate on its own as well as a mixture of sodium itaconate and glucose) confirmed that ED is an effective method for the separation of itaconic acid. Based on these results, further experiments are being planned using more complex model solutions, similar to the composition of the fermentation broth. Subsequently, it is our intention to connect the ED module to the fermentation process.

Acknowledgements

This research was supported by the National Research, Development and Innovation Fund project OTKA K 119940 entitled “Study on the electrochemical effects of bioproduct separation by electrodialysis” and by the financial support of Széchenyi 2020 within project EFOP-3.6.1-16-2016-00015.

REFERENCES

[1] Baup, S.: Über eine neue Pyrogen- Citronensäure, und über Benennung der Pyrogen Säure überhaupt, *Ann. Chim. Phys.,* 1837 **9**, 29–38 DOI: 10.1002/jlac.18360190107

[2] Delidovich, I.; Hausoul, P. J.; Deng, L.; Pfutzenreuter, R.; Rose, M.; Palkovits, R.: Alternative monomers based on lignocellulose and their use for polymer production, *Chem. Rev.*, 2016 **116**(3), 1540–1599 DOI: 10.1021/acs.chemrev.5b00354

[3] Kinoshita, K.: Über die Produktion von Itaconsäure und Mannit durch einen neuen Schimmelpilz, Aspergillus itaconicus, *Acta Phytochimica*, 1932 **5**, 271–287

[4] Steiger, M.; Blumhoff, G.; Marzena, L.; Mattanovich, D.; Sauer, M.: Biochemistry of microbial itaconic acid production, *Front. Microbiol.,* 2013 **4**(23), 1–5 DOI: 10.3389/fmicb.2013.00023

[5] Levinson, W. E.; Kurtzman, C. P.; Kuo, T. M.: Production of itaconic acid by *Pseudozyma antarctica* NRRL Y-7808 under nitrogen-limited growth conditions, *Enzyme Microb. Technol.,* 2006 **39** (4), 824–827 DOI: 10.1016/j.enzmictec.2006.01.005

[6] Kuenz, A.; Krull, S.: Biotechnological production of itaconic acid—things you have to know, *Appl. Microbiol. Biotechnol.,* 2018 **102**(9), 3901–3914 DOI: 10.1007/s00253-018-8895-7

[7] Heidorn, T.; Camsund, D.; Huang, H.; Lindberg, P.; Oliveria, P.; Stensjo, K.; Lindblad, P.: Synthetic Biology in Cyanobacteria: Engineering and Analyzing Novel Functions, *Methods Enzymol.*, 2011 **497**, 539–579 DOI: 10.1016/B978-0-12-385075-1.00024-X

[8] Chin, T.; Sano, M.; Takahashi, T.; Ohara, H.; Aso, Y.: Photosynthetic production of itaconic acid in *Synechocystis* sp. PCC6803, *J. Biotechnol.,* 2015 **195,** 43–45 DOI: 10.1016/j.jbiotec.2014.12.016

[9] Karaffa, L.; Diaz, R.; Papp, B.; Fekete, E.; Sandor, E.; Kubicek, C. P.: A deficiency of manganese ions in the presence of high sugar concentrations is the critical parameter for achieving high yields of itaconic acid by *Aspergillus terreus*, *Appl. Microbiol. Biotechnol.*, 2015 **99**(19), 7937–7944 DOI: 10.1007/s00253-015-6735-6

[10] Magalhães, A. I.; de Carvalho, J. C.; Ramírez, E. N. M.; Medina, J. D. C.; Soccol, C. R.: Separation of Itaconic Acid from Aqueous Solution onto Ion-Exchange Resins, *J. Chem. Eng. Data,* 2016 **61** (1), 430–437 DOI: 10.1021/acs.jced.5b00620

[11] Lameloise, M. L.; Matinier, H.; Fargues, C.: Concentration and purification of malate ion from a beverage industry waste water using electrodialysis with homopolar membranes, *J. Membr. Sci.,* 2009 **343**(1-2), 73–81 DOI: 10.1016/j.memsci.2009.07.013

[12] Molnár, E.; Nemestóthy, N.; Bélafi-Bakó, K.: Galacturonic acid recovery from pectin rich agrowastes by electrodialysis with bipolar membranes, *Hung. J. Ind. Chem.*, 2008 **36**, 95–99 DOI: 10.1515/186

[13] Stodollick, J.; Femmer, R.; Gloede, M.; Melin, T.; Wessling, M.: Electrodialysis of itaconic acid: A short-cut model quantifying the electrical resistance in the overlimiting current density region, *J. Membr. Sci.,* 2014 **453**, 275–281 DOI: 10.1016/j.memsci.2013.11.008

[14] Bélafi-Bakó, K.; Molnár, E.; Csanádi, Z.; Nemestóthy, N.: Comparative study on electrodialysis systems for galacturonic acid recovery, *Hung. J. Ind. Chem.*, 2012 **40**, 65–67 DOI: 10.1515/343

[15] Koutinas, A.; Bélafi-Bakó, K.; Kabiri-Badr, A.; Tóth, A.; Gubicza, L.; Webb, C.: Enzymatic hydrolysis of polysaccharides: Hydrolysis of starch by an enzyme complex from fermentation by *Aspergillus awamori*, *Food Bioprod. Process.,* 2001 **79**, 41–45 DOI: 10.1205/09603080151123353

DE GRUYTER OPEN

HUNGARIAN JOURNAL OF INDUSTRY AND CHEMISTRY
Vol. 46(2) pp. 47–54 (2018)
hjic.mk.uni-pannon.hu
DOI: 10.1515/hjic-2018-0018

HUNGARIAN JOURNAL OF INDUSTRY AND CHEMISTRY
HJIC

THE INITIAL MAGNETIC SUSCEPTIBILITY OF DENSE AGGREGATED DIPOLAR FLUIDS

SÁNDOR NAGY *[1]

[1]Institute of Mechatronics Engineering and Research, University of Pannonia, Gasparich M. u. 18/A, Zalaegerszeg, H-8900, HUNGARY

To correlate the dipole moment and density dependence of the initial magnetic susceptibility on the basis of the former related theories and the probability analysis of chain formation, physically based analytical correlation equation was derived. After the local magnetic field strength and the chaining probability between two particle have been determined the chain and particle distributions came from the geometric distribution. The initial magnetic susceptibility was resulted from the summation of Langevin initial susceptibility of k-length chains. Two particles were considered in a chain if the interaction energy between them was below a certain limit. By varying slightly this energy limit around 70–75 % good agreement has been obtained between the simulation and theoretical data. Monte Carlo simulations were used to calculate the initial magnetic susceptibility of dipolar hard sphere system at different dipole moments and densities.

Keywords: dipolar fluids, initial susceptibility, Monte Carlo simulation

1. Introduction

The investigation of dipolar fluids has been induced by the evolution of magnetorheology and electrorheology over the last two decades. The viscosity of electrorheological (ER) fluids increases dramatically due to an external electric field. ER fluids can be obtained by dispersing solid particles with dielectric permittivity ϵ_{p} in a fluid with dielectric permittivity ϵ_{f}, where $\epsilon_{\mathrm{p}} > \epsilon_{\mathrm{f}}$. The dispersed particles are of between 0.1 mm and 100 mm in diameter. The polarized particles are organized into pairs and chains. The magnetic analogy of the phenomenon described above is the magnetorheological (MR) effect. If the magnetic permeabilities of the liquid and dispersed particles differ, then in an external magnetic field the particles are also arranged in chains. The dispersing medium can be water, oil, an organic solvent, etc. while the dispersed particles can be some kind of iron oxide or ferrit. In this paper, the magnetic terminology and centimetre-gram-second (CGS) system of units are used. In the figures, the reduced quantities are applied.

Electro- and magnetorheological fluids typically exhibit a reduced density of up to $\rho^* = 0.4$ (where $\rho^* = \rho\sigma^3$; ρ and σ are the concentration and diameter of the suspended particles, respectively). The magnetic properties, e.g. magnetization curve and initial magnetic susceptibility, are well described by the various theories within this range of reduced density. The magnetization $\mathbf{M}$ can be obtained by summation of the dipole moments in the unit volume:

$$\mathbf{M} = \frac{1}{V}\sum_i \mathbf{m}_i. \tag{1}$$

In the absence of any external magnetic field the fluid is isotropic and according to Eq. 1 the magnetization is zero. When any external magnetic field is present, the field-oriented components of dipole moments should be summarized as

$$\mathbf{M} = \rho m \langle \cos\Theta \rangle \frac{\mathbf{H}_0}{H_0}, \tag{2}$$

where $H_0 = |\mathbf{H}_0|$ and $\langle \cos\Theta \rangle$ is the ensemble average of the cosine of the angle between $\mathbf{m}_i$ and $\mathbf{H}_0$, and $m = |\mathbf{m}_i|$. Since the directions of $\mathbf{H}_0$ and $\mathbf{M}$ are identical, vector notation can be omitted. The initial magnetic susceptibility is equal to the initial gradient of the magnetization curve

$$\chi_0 = \left.\frac{\partial M}{\partial H_0}\right|_{H_0=0}. \tag{3}$$

In practice, ER and MR fluids can be used for the transmission of torque or force, in vibration dampers and braking systems, etc. The magnetic properties generally are calculated from Monte Carlo simulations because it is not necessary to know the velocity and acceleration of the particles nor the forces between them.

The expressions of the related models are listed in Table 1. (One line belongs to one theory and the first line is the head of the table, e.g. Table 1: 2.4 refers to the 4th cell in the 2nd line within the 1st table.) Three different

*Correspondence: sata123.sandor@gmail.com

Table 1: The expressions of the effective magnetic field, the magnetization and the initial magnetic susceptibility of the related theories.

Model	H_e – Effective magnetic field	M – Magnetization	χ_0 – Initial magnetic susceptibility
1 "Langevin" [1]	H_0	$\rho m L\left(\frac{mH_0}{k_\mathrm{B}T}\right)$	$\frac{\rho m^2}{3k_\mathrm{B}T}=\chi_\mathrm{L}$
2 "Weiss" [2]	$H_0+\frac{4\pi}{3}M(H_\mathrm{e})$	$\rho m L\left(\frac{mH_\mathrm{e}}{k_\mathrm{B}T}\right)$	$\frac{\chi_\mathrm{L}}{1-\frac{4\pi}{3}\chi_\mathrm{L}}$
3 "Pshenichnikov" [3]	$H_0+\frac{4\pi}{3}M(H_0)$	$\rho m L\left(\frac{mH_\mathrm{e}}{k_\mathrm{B}T}\right)$	$\chi_\mathrm{L}\left(1+\frac{4\pi}{3}\chi_\mathrm{L}\right)$
4 "Ivanov" [4]	$H_0+\frac{4\pi}{3}M(H_0)\left(1+\frac{4\pi}{48}\frac{\partial M}{\partial H_0}\right)$	$\rho m L\left(\frac{mH_\mathrm{e}}{k_\mathrm{B}T}\right)$	$\chi_\mathrm{L}\left(1+\frac{4\pi}{3}\chi_\mathrm{L}+\frac{(4\pi)^2}{144}\chi_L^2\right)$
5 "Tani" and "Szalai" [5, 6]	$M(H_0)=\rho m L+\frac{4\pi}{3}\rho^2\beta m^3 LL'+\frac{1}{10}\rho^2\beta^2 m^5\zeta' I_{dd\Delta}$ $-\frac{16\pi^2}{27}\rho^3\beta^2 m^5 LL'+\frac{1}{3}\rho^3\beta^2 m^5 LL' I_{dd\Delta}$		$\chi_\mathrm{L}\left(1+\frac{4\pi}{3}\chi_\mathrm{L}+\frac{(4\pi)^2}{144}\chi_L^2 f(\rho)\right)$

magnetic fields will be used. The applied external magnetic field is denoted by H_0 and the sum of the external and generated magnetic fields by H_e. H_e is always parallel to H_0. The third one is the local magnetic field H_l which is of chain-parallel orientation and its formation is due to dipole-dipole interactions between the particles.

The well-known Langevin function is applied from the initial theory [1] in the magnetization formula (Table 1: 1.3), where $L(\alpha)=\coth\alpha\ -1/\alpha$. The magnetic dipole moment of the particles is denoted by m and the applied external magnetic field by H_0, while the Boltzmann constant is represented by k_B. The expression of magnetic susceptibility can be written as in Table 1: 1.4. This is known as Langevin susceptibility which is indicated by χ_L as well. In this approach the effective magnetic field H_e exerted on the given particle is equal to the external magnetic field (Table 1: 1.2).

According to the more accurate model by Weiss [2] the effective magnetic field is equal to the sum of the external magnetic field and the magnetic field induced by the magnetization (Table 1: 2.2). The formula of the magnetization (Table 1: 2.3) is similar to the previous one but H_0 is substituted by H_e. Due to the iterative nature of the magnetization expression the initial magnetic susceptibility (Table 1: 2.4) exhibits divergence at $\chi_\mathrm{L}=3/4\pi$, therefore, overestimates the real values. Above this initial magnetic susceptibility limit, when $\chi_\mathrm{L}\geq 3/4\pi$, the zero-field magnetization is not equal to zero: $M(H_0)\not\to+0$, if $H_0\to+0$. Moreover, in weak external magnetic fields, one H_0 value belongs to three equilibrium magnetization values.

The effective magnetic field has been substituted for the external magnetic field in the expression of the effective magnetic field (Table 1: 3.2) in the theory by Pshenichnikov et al. [3]. The magnetization formula (Table 1: 3.3) is the same as in Weiss' theory. The initial magnetic susceptibility (Table 1: 3.4) is in good agreement with the simulations but underestimates them at higher densities or higher dipole moments.

That is why it seems to be a good method to extend the expression of the effective magnetic field (Table 1: 4.2) by Ivanov et al. [4]. The magnetization formula is once again identical (Table 1: 4.3) but a new term is introduced in the initial magnetic susceptibility (Table 1: 4.4). Although at higher densities it yields higher values than in Pshenichnikov's model, it underestimates the simulation data as well. The factor of the third term is $(4\pi)^2/144=1.0966$ and perhaps it could be higher, but in this case at low densities the initial magnetic susceptibility overestimates the simulations.

The perturbation theory by Tani et al. [5] is worth mentioning because a density-dependent correction was used to complete the third term of the susceptibility (Table 1: 5.4), where $f(\rho)=9I_{\mathrm{dd}\Delta}/\pi^2-16$, and

$$I_{\mathrm{dd}\Delta}=\frac{17\pi^2}{9}\left[\frac{1-0.93952\rho^*+0.36714(\rho^*)^2}{1-0.92398\rho^*+0.23323(\rho^*)^2}\right].$$

The formula of the magnetization curve for this perturbation theory was calculated by Szalai et al. The expressions that are not mentioned in Table 1: 5.2 can be found in Ref. [6]. The values of the susceptibility more closely resemble the simulation data but still underestimate those.

It is worth mentioning the study by Huke and Lücke [7] who introduced the so-called "dipolar coupling constant" into the second term of the initial magnetic susceptibility, but the third term was ignored in expressions in Table 1: 4.4 and 5.4. Thereby their theory at higher densities underestimates and at lower densities overestimates the simulation data. Furthermore, the theory of mean-spherical approximation (MSA) [8–10] should also

be mentioned which provides a formula for initial magnetic susceptibility and magnetization as well, but the validity of these are within the range of up to $m^* < \sqrt{1.5}$.

With regard to the distribution of chain aggregates in ferrofluids [11, 12], it has been found that in the absence of any external magnetic field, the chain size distribution is proportional to $p^k \exp(-\epsilon)$, where the chain length is denoted by k and the dimensionless energy parameter ϵ is a function of the maximum dipole interaction energy but independent from the density, therefore, it is a constant here and the probability of bond formation between two adjacent particles in a chain is p. Subsequently, the chain size distribution decreases according to an exponential function because $p^k = \exp(-k/k_0)$, where $k_0 = -1/\ln p$. Based on some publications [13, 14], in the case of high dipole moments this exponential expression turns into a power law: $g(k) \propto k^{-\iota}$, with exponent $\iota \approx 2.0 - 2.5$.

Our investigation was performed in a dipolar hard-sphere (DHS) monodisperse system with a permanent magnetic dipole moment and of fixed density. It is supposed that the chains are perfectly straight and parallel to the local magnetic field. Furthermore, the average distance between two neighbouring particles in a chain is the same as the distance between two neighbouring parallel chains. The particles interact with each other only by the evolved mean magnetic field and the applied external magnetic field is superimposed on this, thus, the chains influence each other only by this mean magnetic field.

2. Theory

2.1 *The appearance of probability analysis in the initial magnetic susceptibility*

The distribution of chains was calculated with the aid of probability analysis in a zero applied magnetic field. As was mentioned in the "Introduction", Weiss' theory states that the effective (now "local") magnetic field converges to zero when $\chi_\mathrm{L} < 3/4\pi$ and non-zero values when $\chi_\mathrm{L} \geq 3/4\pi$. The central and surrounding particles are under the influence of this local magnetic field. The chain is oriented in the same direction as the local magnetic field. Let us denote the probability of chain formation between two particles whose direction relative to each other is parallel to the local magnetic field by p.

Now using this approach the exact distribution of chain length can be calculated because the probability that the chain length ought to be equal to k follows the geometric distribution with parameter q:

$$g_k = qp^{k-1}, \tag{4}$$

where $q = 1-p$ and the "chain distribution" is denoted by g_k. According to its definition the geometric distribution shows the probability that a kth particle is connected to a chain of length $k-1$ thus forming a chain of length k. A geometric sequence is described in Eq. 4, where the common ratio is denoted by p and the first term by q. The sum of the terms of a geometric sequence is $S_\infty = \frac{ft}{1-cr}$, thus, $\sum_{k=1}^{\infty} g_k = \frac{q}{1-p} = \frac{q}{q} = 1$.

It is also important to calculate the so-called "particle distribution" that implies the number of those particles which are members of the chains of length k:

$$h_k = q^2 k p^{k-1}. \tag{5}$$

The detailed deduction of h_k and the sum of h_k terms are described in Appendix A.

The expected value of the geometric distribution with parameter q is $1/q$, thus, here the average chain length is $1/q$.

The number of chains is equal to the number of particles divided by the average chain length: $\frac{n}{1/q} = nq$, where the number of particles is denoted by n.

Until now only the local magnetic field which arises from the strength of interaction energies between neighbouring particles and induces spontaneous magnetization in a random direction has been discussed, thus, the total magnetization of the system of volume V is equal to zero.

When an infinitesimal external magnetic field $\mathbf{H}_0$ is switched on, non-zero total magnetization is formed. Since $\mathbf{H}_0$ is parallel to $\mathbf{M}$, scalar notations are used in the following. As was observed from Pshenichnikov's model the effective magnetic field is the sum of the external H_0 and secondary $(4\pi/3)M(H_0)$ magnetic fields. The question arises why it is legitimate to use the expression of effective magnetic field from "Pshenichnikov" (Table 1: 3.2) instead of from "Weiss" (Table 1: 2.2). The answer is because H_0 modifies infinitesimally the orientation of the chains but does not align them with its own direction, thus, the average angle between the local and external or even the effective magnetic fields is not equal to zero.

When calculating the initial magnetic susceptibility, a chain of length k is considered as a particle with a dipole moment km, thus, in terms of magnetization the argument of the Langevin function is $\frac{kmH_\mathrm{e}}{k_\mathrm{B}T}$. The Langevin function is weighted by the distribution h_k, and finally the gradient of magnetization in an infinitesimal external magnetic field is calculated as

$$\chi_0 = \left.\frac{\partial}{\partial H_0}\right|_{H_0=0} \rho m \sum_{k=1}^{\infty} h_k L\left(\frac{kmH_\mathrm{e}}{k_\mathrm{B}T}\right). \tag{6}$$

An infinitesimally weak external magnetic field can be written as

$$\chi_0 = \frac{1+p}{1-p}\chi_\mathrm{L}\left(1 + \frac{4\pi}{3}\chi_\mathrm{L}\right), \tag{7}$$

where the following infinite expression is used ($|p| < 1$):

$$\sum_{k=1}^{\infty} p^{k-1}k^2 = \frac{1+p}{(1-p)^3}. \tag{8}$$

The detailed derivation of the initial magnetic susceptibility (Eq. 7) is given in Appendix B.

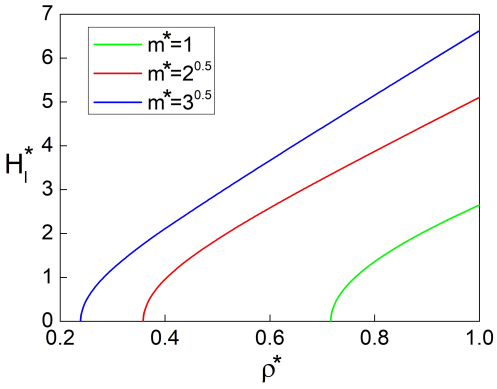

Figure 1: The rates of the local magnetic field as a function of the density from Eq. 9 at three different dipole moments in the absence of any external magnetic field.

2.2 The numerical calculation of the probability of chain formation "p"

The main challenge of our approach is the determination of p. The particles form chains because of the local magnetic field even in the absence of any applied external magnetic field. According to Weiss' model when $\chi_{\mathrm{L}} \geq 3/4\pi$ this local magnetic field predicts an infinite initial magnetic susceptibility. The problem with this model is that it assumes that the orientation of the local magnetic field is parallel with the external magnetic field. Nevertheless, Weiss' model is applicable to predict the extent of the local magnetic field by the expression (when $H_0 = 0$):

$$H_{\mathrm{l}} = \frac{4\pi}{3}\rho m L\left(\frac{mH_{\mathrm{l}}}{k_{\mathrm{B}}T}\right). \tag{9}$$

H_{l}^* as a function of the reduced density ρ^* at three different dipole moments is presented in Fig. 1. The definitions of the reduced quantities are $H^* = H\sqrt{\sigma^3/k_{\mathrm{B}}T}$; $M^* = M\sqrt{\sigma^3/k_{\mathrm{B}}T}$; $m^* = m/\sqrt{\sigma^3 k_{\mathrm{B}}T}$.

All particles are considered to be influenced by this local magnetic field H_{l}, in the absence of any external magnetic field H_0 when calculating the initial magnetic susceptibility. As was mentioned before, the most accepted criterion for chaining is to determine an energy level and if the dipolar energy between two given particles is under this level, the particles are in a bound relationship. Generally [15–17], this energy level is 70-75 % of the minimum of the dipolar energy, i.e. $U_{\mathrm{lim}}^* = -0.7 * 2(m^*)^2$.

Here the well-known dipolar energy is defined as the interaction between point dipoles:

$$U_{ij}^{\mathrm{dd}} = -\frac{m^2}{r_{ij}^3}\left[3\left(\widehat{\mathbf{m}}_i \cdot \widehat{\mathbf{r}}_{ij}\right)\left(\widehat{\mathbf{m}}_j \cdot \widehat{\mathbf{r}}_{ij}\right) - \left(\widehat{\mathbf{m}}_i \cdot \widehat{\mathbf{m}}_j\right)\right], \tag{10}$$

where the particles have dipole moments of strength m as well as an orientation given by unit vectors $\widehat{\mathbf{m}}_i$ and $\widehat{\mathbf{m}}_j$. Furthermore, the distance between the centers of the particles is denoted by r_{ij} and $\widehat{\mathbf{r}}_{ij} = \mathbf{r}_{ij}/r_{ij}$.

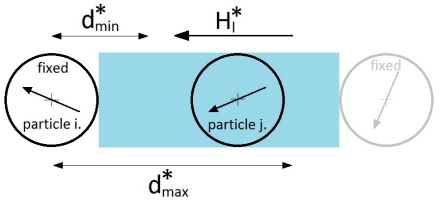

Figure 2: The feasible location of a particle between two fixed particles.

As is shown in Fig. 2, according to our model particle j can move along the direction of the chain between the two fixed adjacent particles, namely i and the grey one, in the tube with a light blue background. Logically, the minimum distance between two particles in a hard sphere system is σ, on a reduced scale $d_{\mathrm{min}}^* = 1$, while for the maximum distance $d_{\mathrm{max}}^* = 2\langle r^*\rangle - 1$, where the reduced average distance between two adjacent particles is denoted by $\langle r^*\rangle$.

Obviously the maximum distance between two neighbouring particles could be greater than d_{max}^* but at higher densities in particular the surrounding particles obstruct the movement of the central particle. Assuming that the distance distribution is isotropic, it is given by $\langle r^*\rangle = \sqrt[3]{1/\rho^*}$.

Taken all round to calculate p the probability of those states of particle pairs should be totalled when the dipolar interaction energy is less than or equal to the aforementioned energy limit U_{lim} and the interval of integration in distance is $[d_{\mathrm{min}}^*,\ d_{\mathrm{max}}^*]$, that is

$$p = \int_{U^{\mathrm{dd}} \leq U_{\mathrm{lim}}} P(\theta_i)d\theta_i P(\theta_j)d\theta_j P(\phi_i)d\phi_i P(\phi_j)d\phi_j, \tag{11}$$

where $0 \leq \theta < \pi$ and $0 \leq \phi < 2\pi$ are the usual spherical angles of the dipoles and the probabilities when magnetic field H (here $H = H_{\mathrm{l}}$) is applied in general are

$$P(\theta)d\theta = \frac{\exp\left(\frac{mH}{k_{\mathrm{B}}T}\cos\theta\right)\sin\theta d\theta}{\int_0^{\pi}\exp\left(\frac{mH}{k_{\mathrm{B}}T}\cos\theta\right)\sin\theta d\theta} \tag{12}$$

and $P(\phi)\,d\phi = d\phi/2\pi$.

The calculation of p was performed by numerical integration. Particles i and j (Fig. 2) are under the influence of the local magnetic field independently from each other. For both particles, all possible values of θ, ϕ, and r are swept and taken into account if the dipolar interaction energy between particles i and j is less than or equal to U_{lim}. This is expressed by Eq. 11.

For instance, when $\rho^* = 0.8$ and $m^{*^2} = 3.0$ then $H_l^* = 5.154$ and $d_{\mathrm{max}}^* = 1.154435$. The probability of chaining between particles i and j as a function of distance is shown in Fig. 3. The requested probability p is

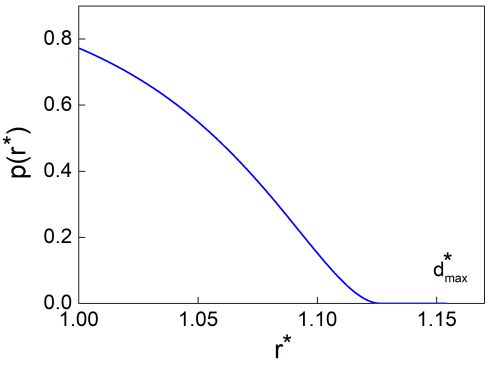

Figure 3: An example calculation of p. The parameters are $rho^* = 0.8$, $(m^*)^2 = 3.0$, $H_l^* = 5.154$, $d^*_{\max} = 1.154435$, and $U^*_{\lim} = 0.7U^*_{\min}$. The requested probability p is the average of this curve in the interval $[d^*_{\min},\ d^*_{\max}]$.

the average of this curve from 1 to $d^*_{\max}$, i.e. $p = 0.3454$, if $U^*_{\lim} = 0.7U^*_{\min}$.

3. Simulation results and discussion

To determine the initial magnetic susceptibility, Monte Carlo simulations of DHS fluids were performed using a canonical *NVT* ensemble. Boltzmann sampling [18], periodic boundary conditions and the minimum-image convention were applied. In order to take into account the long-range character of the dipolar interaction, the reaction field method under boundary conditions of conduction was used. After 100,000 equilibration cycles, between 1 and 10 million production cycles were conducted involving $N = 512$ particles. In the absence of an external magnetic field, the initial magnetic susceptibility was obtained from the following fluctuation formula:

$$\chi_0 = \frac{1}{3k_{\mathrm{B}}TV}\left(\left\langle \mathbf{M}^2\right\rangle_0 - \left\langle \mathbf{M}\right\rangle_0^2\right), \qquad (13)$$

where $\mathbf{M} = \sum_{i=1}^{N} \mathbf{m}_i$.

The exact results of the probability of chain formation from Eq. 11 applied to the local magnetic field, given by Eq. 9, are shown in Table 2. The data associated with the aforementioned dipole moments were rounded to three non-zero decimals. According to Fig. 1 at low densities the values of the local magnetic field are zero, nevertheless, the rates of the probability of chaining are not equal to zero. The value of the energy limit was fitted to the best agreement between the simulation data and our theory lines.

Our theoretical findings (green lines, Eq. 7) in terms of the initial magnetic susceptibility according to our Monte Carlo simulation data (blue dots) and the values of Ivanov's theory (grey lines, Table 1: 4.4) are compared in Figs. 4-6. The variability is not indicated where its magnitude is comparable to the size of the dot. The values of dipole moments in the order $m^* = 1$, $m^* = \sqrt{2}$ and $m^* = \sqrt{3}$ are shown in Figs. 4-6.

Table 2: The probability of chaining at three different dipole moments. The applied energy limit at $m^* = 1$ and $m^* = \sqrt{2}$ is $U_{\lim} = 0.77U_{\min}$ and $U_{\lim} = 0.71U_{\min}$ at $m^* = \sqrt{3}$.

	p		
ρ^*	$m^* = 1$	$m^* = \sqrt{2}$	$m^* = \sqrt{3}$
0.1	0.000260	0.000263	0.000580
0.2	0.000426	0.000429	0.000943
0.3	0.000615	0.000617	0.00794
0.4	0.000852	0.00292	0.0250
0.5	0.00117	0.0110	0.0521
0.6	0.00164	0.0253	0.0953
0.7	0.00241	0.0515	0.170
0.8	0.0135	0.107	0.320
0.85	0.0269	0.164	0.471
0.9	0.0539	0.273	0.649
0.95	0.101	0.416	0.775

In the case of $m^* = 1$ (Fig. 4), the energy limit is $U_{\lim} = 0.77U_{\min}$. A significant difference was only observed between Ivanov's theory and the simulation data beyond a reduced density of 0.8 and the simulation dots were tracked by our present theory. The maximum relative deviation from the simulation data is $|\chi_{0\ \mathrm{sim}} - \chi_{0\ \mathrm{th}}|\,/\chi_{0\ \mathrm{sim}} = 4.175\%$.

When $m^* = \sqrt{2}$, the appropriate energy criterion is $U_{\lim} = 0.77U_{\min}$ as well. Up to a reduced density of 0.6 the former theory and simulation are in good agreement (Fig. 5), but in the present theory more than double the surplus is shown in the region of high density compared to Table 1: 4.4. The maximum relative deviation from the simulation data is 8.024 %.

Here it is quite conceivable that the simple series expansion of initial magnetic susceptibility as the summation of positive integer powers of Langevin susceptibility is unsatisfactory. By increasing the third coefficient in

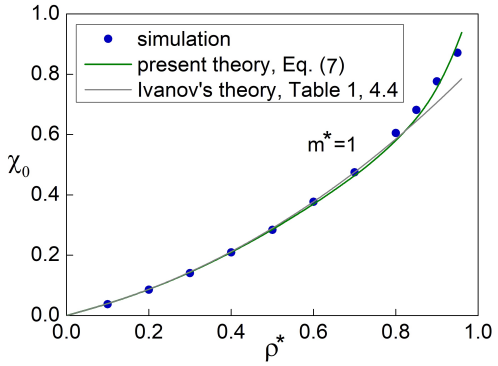

Figure 4: Initial magnetic susceptibility of DHS fluid as a function of reduced density with dipole moment $m^* = 1$. Monte Carlo simulation results are denoted by symbols and the solid lines correspond to the present (Eq. 7) and Ivanov's (Table 1: 4.4) theories.

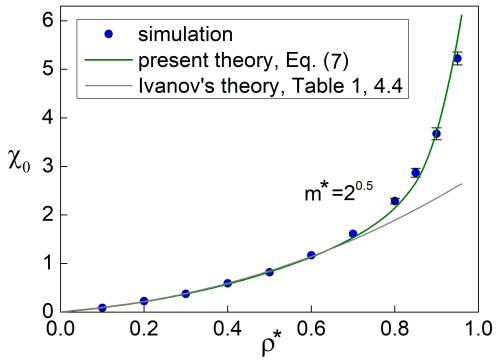

Figure 5: Initial magnetic susceptibility of DHS fluid as a function of reduced density with dipole moment $m^* = \sqrt{2}$. Monte Carlo simulation results are denoted by symbols and the solid lines correspond to the present (Eq. 7) and Ivanov's (Table 1: 4.4) theories.

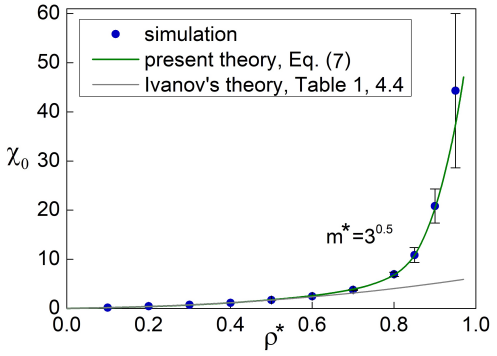

Figure 6: Initial magnetic susceptibility of DHS fluid as a function of reduced density with dipole moment $m^* = \sqrt{3}$. Monte Carlo simulation results are denoted by symbols and the solid lines correspond to the present (Eq. 7) and Ivanov's (Table 1: 4.4) theories.

Table 1: 4.4, the initial magnetic susceptibility at lower densities is also increased.

When $m^* = \sqrt{3}$ the difference is even more spectacular between the theories (Fig. 6). At high densities the uncertainty of initial magnetic susceptibility is quite large with regard to the simulation data. The best fit curve belongs to an energy limit of 71 %, which is very close to the value from references [15–17] of 70 %. The maximum relative deviation from the simulation data is 15.850 %.

When $m^* = 1$ and $\rho^* = 0.95$, with an energy limit of 70 %, the theoretical value of initial magnetic susceptibility is $\chi_0 = 1.042$, and if the energy limit is 75 %, $\chi_0 = 0.937$. Both values are higher than the corresponding simulation data, thus, the energy limit has to be raised to 77 %. The situation is similar when $m^* = \sqrt{2}$ and $\rho^* = 0.95$, namely $\chi_0 = 8.701$ when the energy limit is 70 % and $\chi_0 = 6.363$ when it is 75 %.

Probably at lower dipole moments and higher densities the two adjacent particles cannot be considered as a chain even though the interaction energy exceeds an energy limit of 70 % or 75 % for example because the average kinetic energy is closer to this interaction energy than is the case when $m^* = \sqrt{3}$. Therefore, the duration of chain formation is short to draw the particles together.

4. Conclusion

The initial magnetic susceptibility of dipolar hard sphere fluids was described by the help of the probability variable p supplemented by Pshenichnikov's well-known theory. The validity of the present theory is up to $\rho^* = 0.95$ and at least $m^* = \sqrt{3}$. In addition to the theoretical work, Monte Carlo simulations were run to confirm our investigation. At higher densities, especially with higher dipole moments, the former related theories significantly underestimate the simulation data but good results are also provided by the presented theory within this range. By considering the green curves and blue dots in Figs. 4-6, it is obvious that the simple quadratic or tertiary polynomial approach is outdated, therefore, the Taylor series expansion of $(1+p)/(1-p)$ contains powers even as high as infinity.

5. Appendix

5.1 Appendix A

The particle distribution can be obtained by dividing the number of particles in chains of length k by the total number of particles:

$$h_k = \frac{kg_k}{\sum kg_k} = \frac{kqp^{k-1}}{\sum kqp^{k-1}} = \frac{kp^{k-1}}{\sum kp^{k-1}} = \frac{kp^{k-1}}{1+2p+3p^2+\cdots} =$$
$$= \frac{kp^{k-1}}{(1+p+p^2+\cdots)+(p+p^2+p^3+\cdots)+(p^2+p^3+p^4+\ldots)+\cdots} =$$
$$= \frac{kp^{k-1}}{(1+p+p^2+\cdots)+(p+p^2+p^3+\cdots)+(p^2+p^3+p^4+\cdots)+\cdots} =$$
$$= \frac{kp^{k-1}}{\frac{1}{1-p}+\frac{p}{1-p}+\frac{p^2}{1-p}+\cdots} = \frac{qkp^{k-1}}{1+p+p^2+\cdots} = \frac{qkp^{k-1}}{\frac{1}{1-p}} = q^2kp^{k-1}. \quad (14)$$

The sum of h_k terms must be equal to one:

$$\sum_{k=1}^{\infty} h_k = \sum_{k=1}^{\infty} q^2 k p^{k-1} = q^2 \left(1 + 2p + 3p^2 + \dots\right) = q^2 \left[\left(1 + p + p^2 + \cdots\right) + \left(p + p^2 + p^3 \cdots\right) + \cdots\right] =$$

$$= q^2 \left[\frac{1}{1-p} + \frac{p}{1-p} + \frac{p^2}{1-p} + \cdots\right] = q\left[1 + p + p^2 + \dots\right] = q\frac{1}{1-p} = 1. \tag{15}$$

5.2 Appendix B

$$\chi_0 = \left.\frac{\partial}{\partial H_0}\right|_{H_0=0} \rho m \sum_{k=1}^{\infty} h_k L\left(\frac{kmH_e}{k_\mathrm{B}T}\right) = \left.\frac{\partial}{\partial H_0}\right|_{H_0=0} \rho m \sum_{k=1}^{\infty} q^2 k p^{k-1} L\left(\frac{km\left(H_0 + \frac{4\pi}{3}\rho m L\left(\frac{mH_0}{k_\mathrm{B}T}\right)\right)}{k_\mathrm{B}T}\right) =$$

$$= q^2 \rho m \left.\frac{\partial}{\partial H_0}\right|_{H_0=0} \sum_{k=1}^{\infty} k p^{k-1} L\left(\frac{kmH_0}{k_\mathrm{B}T} + \frac{\frac{4\pi}{3} k\rho m^2 L\left(\frac{mH_0}{k_\mathrm{B}T}\right)}{k_\mathrm{B}T}\right) =$$

$$= q^2 \rho m \sum_{k=1}^{\infty} k p^{k-1} \frac{1}{3}\left(\frac{km}{k_\mathrm{B}T} + \frac{\frac{4\pi}{3} k\rho m^2 \frac{1}{3}\frac{m}{k_\mathrm{B}T}}{k_\mathrm{B}T}\right) = q^2 \sum_{k=1}^{\infty} k^2 p^{k-1}\left(\frac{1}{3}\frac{\rho m^2}{k_\mathrm{B}T} + \frac{1}{9}\frac{4\pi}{3}\frac{\rho^2 m^4}{k_\mathrm{B}^2 T^2}\right) =$$

$$q^2\left(\chi_\mathrm{L} + \frac{4\pi}{3}\chi_\mathrm{L}^2\right)\sum_{k=1}^{\infty} k^2 p^{k-1} = \frac{1+p}{1-p}\chi_\mathrm{L}\left(1 + \frac{4\pi}{3}\chi_\mathrm{L}\right). \tag{16}$$

REFERENCES

[1] Langevin, P.: Sur la théorie du magnétisme, *Journal de Physique Théorique et Appliquée,* 1905 **4**(1), 678–693 DOI: 10.1051/jphystap:019050040067800

[2] Weiss, P.: L'hypothése du champ moléculaire et la propriété ferromagnétique, *Journal de Physique Théorique et Appliquée,* 1907 **6**(1), 661–690 DOI: 10.1051/jphystap:019070060066100

[3] Pshenichnikov, A. F.; Mekhonoshin, V. V.: Equilibrium magnetization and microstructure of the system of superparamagnetic interacting particles: numerical simulation, *Journal of Magnetism and Magnetic Materials,* 2000 **213**(3), 357–369 DOI: 10.1016/S0304-8853(99)00829-X

[4] Ivanov, A. O.; Kuznetsova, O. B.: Magnetic properties of dense ferrofluids: An influence of interparticle correlations, *Phys. Rev. E,* 2001 **64**(4), 041405 DOI: 10.1103/PhysRevE.64.041405

[5] Tani, A.; Henderson, D.; Barker, J. A.; Hecht, C. E.: Application of perturbation theory to the calculation of the dielectric constant of a dipolar hard sphere fluid, *Mol. Phys.*, 1983 **48**(4), 863–869 DOI: 10.1080/00268978300100621

[6] Szalai, I.; Nagy, S.; Dietrich, S.: Linear and nonlinear magnetic properties of ferrofluids, *Phys. Rev. E,* 2015 **92**(4), 042314 DOI: 10.1103/PhysRevE.92.042314

[7] Huke, B.; Lücke, M.: Magnetization of ferrofluids with dipolar interactions: A Born-Mayer expansion, *Phys. Rev. E,* 2000 **62**(5), 6875–6890 DOI: 10.1103/PhysRevE.62.6875

[8] Wertheim, M. S.: Exact solution of the mean spherical model for fluids of hard spheres with permanent electric dipole moments, *J. Chem. Phys.,* 1971 **55**(9), 4291–4298 DOI: 10.1063/1.1676751

[9] Hansen, J.-P.; McDonald, I. R.: Theory of Simple Liquids (Elsevier, New York) 2005 ISBN: 9780123705358

[10] Szalai, I.; Dietrich, S.: Magnetization and susceptibility of ferrofluids, *J. Phys.: Cond. Matt.,* 2008 **20**(20), 204122 DOI: 10.1088/0953-8984/20/20/204122

[11] Zubarev, A. Y.; Iskakova, L. Y.: Theory of physical properties of magnetic liquids with chain aggregates, *J. Exp. Theor. Phys.,* 1995 **80**(5), 857–866

[12] Zubarev, A. Y.; Iskakova, L. Y.: Effect of chain-like aggregates on dynamical properties of magnetic liquids, *Phys. Rev. E,* 2000 **61**(5), 5415–5421 DOI: 10.1103/PhysRevE.61.5415

[13] Stauffer, D.; Aharony, A.: Introduction to percolation theory (CRC Press, London) 1994 ISBN: 9780748402533

[14] Del Gado, E.; Kob, W.: A microscopic model for colloidal gels with directional effective interactions: network induced glassy dynamics, *Soft Matter,* 2010 **6**(7), 1547–1558 DOI: 10.1039/B916813C

[15] Weiss, J. J.; Levesque, D.: Chain formation in low density dipolar hard spheres: A Monte Carlo study, *Phys. Rev. Lett.,* 1993 **71**(17), 2729–2732 DOI: 10.1103/PhysRevLett.71.2729

[16] Levesque, D.; Weis, J. J.: Orientational and structural order in strongly interacting dipolar hard spheres, *Phys. Rev. E,* 1994 **49**(6), 5131–5140 DOI: 10.1103/PhysRevE.49.5131

[17] Stevens, M. J.; Grest, G. S.: Structure of soft-sphere dipolar fluids, *Phys. Rev. E,* 1995 **51**(6), 5962–5975 DOI: 10.1103/PhysRevE.51.5962

[18] Allen, M. P.; Tildesley D. J.: Computer Simulation of Liquids (Clarendon Press, Oxford) 1987 ISBN: 978-0198556459

DE GRUYTER OPEN

HUNGARIAN JOURNAL OF INDUSTRY AND CHEMISTRY
Vol. 46(2) pp. 55–62 (2018)
hjic.mk.uni-pannon.hu
DOI: 10.1515/hjic-2018-0019

HUNGARIAN JOURNAL OF INDUSTRY AND CHEMISTRY
HJIC

WORKER MOVEMENT DIAGRAM BASED STOCHASTIC MODEL OF OPEN PACED CONVEYORS

TAMÁS RUPPERT[1] AND JÁNOS ABONYI *[1]

[1]MTA-PE Lendület Complex Systems Monitoring Research Group, Department of Process Engineering, University of Pannonia, Egyetem u. 10, Veszprém, H-8200, HUNGARY

Human resources are still utilized in many manufacturing systems, so the development of these processes should also focus on the performance of the operators. The optimization of production systems requires accurate and reliable models. Due to the complexity and uncertainty of the human behavior, the modeling of the operators is a challenging task. Our goal is to develop a worker movement diagram based model that considers the stochastic nature of paced open conveyors. The problem is challenging as the simulator has to handle the open nature of the workstations, which means that the operators can work ahead or try to work off their backlog, and due to the increased flexibility of the moving patterns the possible crossings which could lead to the stopping of the conveyor should also be modeled. The risk of such micro-stoppings is calculated by Monte-Carlo simulation. The applicability of the simulator is demonstrated by a well-documented benchmark problem of a wire-harness production process.

Keywords: Industry 4.0, Operator 4.0, Monte-Carlo simulation, Process development, Line balancing, Wire-harness assembly

1. Introduction

Conveyor lines are more productive than regular assembly lines [1]; therefore there are more prevalent in the automotive industry [2]. The movement of these conveyors mostly has paced and cyclic characteristic where at the beginning of the cycle, every station moves to the next position [3]. It can happen that the operator cannot finish his/her work before the product leaves the workstation. There are two alternative approaches for completing the unfinished work. We speak about close station production when the operator must stop the conveyor even in case of a minor delay [4]. Such processes are typical in Japan. In U.S.-type production systems, the operator does not have to finish his or her job, he or she can move with the product to the next station to work off the backlog. In these open stations the operators can work ahead or can be delayed [5], and the production stops only when the delay exceeds a critical limit. These open workstations reduce capacity loss by decreasing the risk of stopping the conveyor, but the modeling and optimization of these processes is much more challenging as the model has to handle idle and delay times [6]. Worker movement diagrams are widely used to model the work of operators at conveyor belts [7]. Such models can be used to reduce the risk of conveyor stoppage [8] and optimize production sequence [9], since the optimal distribution of the products can also reduce the probability of critical backlogs [10].

*Correspondence: researcher@abonyilab.com

Worker movement diagrams focus only one station. In open paced conveyors the operators effect on each other; therefore the model should handle the interactions between the workstations, especially for the prediction of the conveyor stoppage.

Our goal is to develop a worker movement diagram based model for open paced conveyors, which model considers the stochastic nature of production and recognizes the meeting point of operators and analyzes the idle times due to working in the same zones and risk of stopping the production in case of unmanageable backlogs. We introduce stochastic variables into the movement diagram representation based model and apply Monte-Carlo simulation to evaluate the risk of conveyor stoppage and give robust estimates of the effects of different parameter settings. The simulator is developed in Python environment. The applicability of the proposed model and simulator is demonstrated by a well-documented benchmark problem of a wire-harness production process.

Section 2 describes the worker movement diagram and the sections defined based on the relative position of the operators and the conveyor. The model of the paced conveyor is based on equations that represent the movement of the operators in these sections. Based on these equations we calculate when the conveyor should be stopped. Section 3 describes the applicability of the developed simulator in a wire harness production system.

2. Model of the paced conveyor

2.1 Problem definition

The most widespread paced open station conveyors are used to produce wire harnesses in the automobile industry. The optimization and cost estimation of these processes are an economically significant problem [11]. These modular assembly lines consist of manual workstations (tables) shown in Fig. 1. Human operators work at the tables that are moving similarly as a conveyor belt (see Fig. 2). These tables move with a fixed speed which is determined based on the tact time, t_c. After the cycle, every table moves to the next station. The modeling the relative position of the operators and the tables can be represented by worker movement diagrams that will be presented in the next section.

2.2 Movement diagram of an open station

The paced conveyor has $k, k = 1, \ldots, K$ is number of workstations that moves in every $n = 1, \ldots, N$ cycle. The speed of the conveyor is v_c, and the walking speed of operator is v_w. The t_c is the tact time determines the assembly speed:

$$v_n^k = \frac{L}{t^k_{\pi(n-k)}} \tag{1}$$

where L represents the length o the workstation, the $t^k_{\pi(n-k)}$ the assembly time which is dependent on the produced product. The sequence of the products is represented by a π vector of the labels of the types, so $\pi(k) = p_j$ states that type product p_j started to be produced during the k-th production cycle. The modeling of the paced conveyor is complex task as the conveyor moves only for a $t_{cm} < t_c$ period of the time, which defines several sections of the tack time according to the speed and position of the table and the operators.

As it is depicted in Figs. 3 and 4, the worker movement diagram is divided for six sections ($s = 1, \ldots, 6$) .

1. The operator moves to the starting point of the table

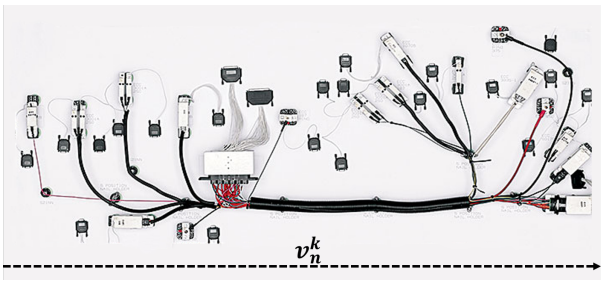

Figure 1: An example assembly table in wire harness manufacturing. The dashed line with an arrow represents the worker motion at the table. The operator works on the table from left to right. The assembly speed is v_n^k.

Figure 2: The most widely used open station paced conveyors are used in wire harness assembly, where the operators are working at tables that moving in every cycle of the production [12].

2. The operator works before the new cycle
3. The operator and the table move together
4. The operator works and the table stays
5. The operator and the table move together after the end of tact time
6. The operator works and the table stays after the end of tact time

In the first section, $s = 1$, the operator walks to the left side of the table, $F(1)^k_n$. After reaching this position the operator starts the assembly process and moves with the conveyor till the conveyor moves to its next workspace. After this $F(3)^k_n$ position the operator works at the standing table with a v_n^k speed. When the job is finished, the operator reaches the end of the table, $F(4)^k_n = kL$, as it is shown at Fig. 5). The second, fifth and sixth sections happen when operator deviates from this normal case (work ahead or delayed).

In the following, we present a model that describes how the positions of the table and the operators are changing in time. In the model $F(s)^k_n$ denotes the position of kth operator at nth cycle step in sth section of diagram, where the positions are measured from the starting point of the first table.

Section 1. - The operator moves to the starting point of the table

At the beginning of the cycle, the operator moves the starting point of the next table which is $2L$ far from its actual position. The $F(1)^k_n$ position when the kth operator reaches the staring point of table should be calculated as

$$F(1)^k_n = F(6)^k_{n-1} - T(1)^k_n v_w \tag{2}$$

$$T(1)^k_n = \mathrm{NWT} + \mathrm{DWT} + \mathrm{CDWT} + \mathrm{IWT} \tag{3}$$

where $F(6)^k_{n-1}$ is the kth operator finishing position in the previous cycle step $(n-1)$, while the $T(1)^k_n$ required

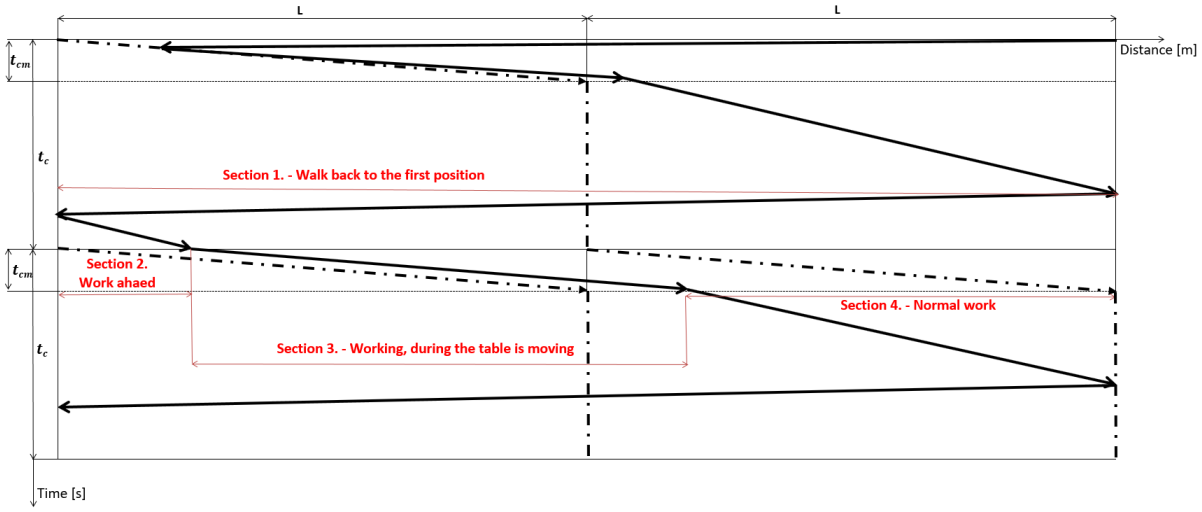

Figure 3: Worker movement diagram of the sections when the operator works ahead. Lines with arrow represent the motion of the operator, while dashed lines represent movement of the table.

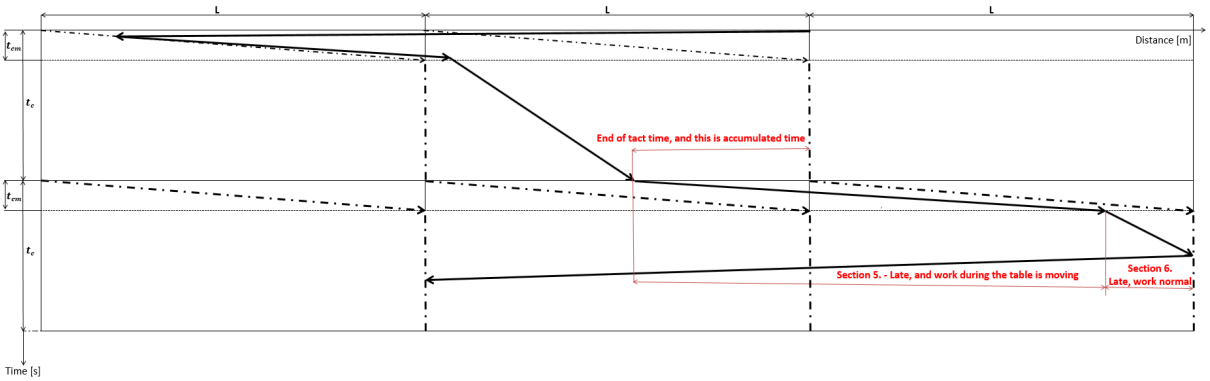

Figure 4: Worker movement diagram of the sections when the operator has a backlog. Lines with arrow represent the motion of the operator, while dashed lines represent movement of the table.

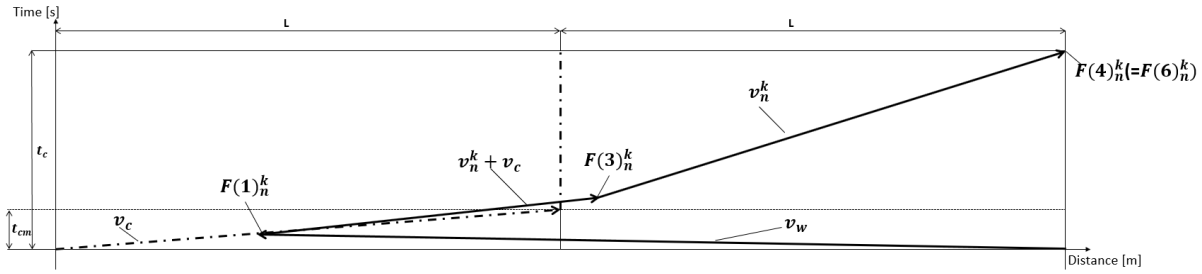

Figure 5: Worker movement diagram of one station. The first meeting point with the table and the operator is $F(1)_n^k$. $F(3)_n^k$ and $F(4)_n^k$ are the positions at the end of the second and third sections. When there is no delay or the operator does not work ahead $F(4)_n^k = F(6)_n^k$, where $F(6)_n^k$ is the finishing position.

time can be decomposed into four components, which will be modeled in the following subsections:

- NWT - Normal Walking Time
- DWT - Delayed Walking Time
- CDWT - Critically Delayed Walking Time
- IWT - Idle Walking Time

NWT**: Normal Walking Time**

In the normal case, the operator and the conveyor move together at the beginning of the cycle with v_c+v_w relative speed. The effect of the a^k_{n-1} idle time and the l^k_{n-1} late time of the previous cycle is represented by the $\mathrm{NWT_a}$ and $\mathrm{NWT_b}$ variables that are used to calculate the NWT walking time:

$$\mathrm{NWT} = \max[\min(\mathrm{NWT_a}; \mathrm{NWT_b}); 0] \tag{4}$$

$$\mathrm{NWT_a} = \max\left(\frac{2L - a^k_{n-1}v_w}{v_c + v_w}; 0\right) \tag{5}$$

$$\mathrm{NWT_b} = \min\left(t_{cm} - l^k_{n-1}, \frac{2L}{v_c + v_w}\right), \tag{6}$$

where $a^k_{n-1}v_w$ represents the walking distance of operator at the end of the previous cycle. When $t_{cm} - l^k_{n-1}$ is less than zero, then operator does not have to walk, because he or she still works on the last $(n-1)$ product (In this case we should calculate DWT).

DWT**: Delayed Walking Time**

When the assembly time in the previous cycle exceeds t_c, DWT is equal to the time which necessary for the reaching the table after t_c.

$$\mathrm{DWT} = \text{IF } [t_{cm} - l^k_{n-1} > 0 \text{ OR } l^k_{n-1} = 0]; \text{ THEN } \mathrm{DWT_h}; \text{ ELSE } 0 \tag{7}$$

$$\mathrm{DWT_h} = \max\left[\frac{2L}{v_c + v_w} - \max\left(t_{cm} - l^k_{n-1}; 0\right); 0\right] v_{cw} \tag{8}$$

where $v_{cw} = \frac{v_c+v_w}{v_w}$ is the walking speed of operator, when the conveyor is moving.

CDWT**: Critically Delayed Walking Time**

When l^k_{n-1} is more than t_{cm}, the operator moves to the beginning of the table when the conveyor is standing.

$$\mathrm{CDWT} = \text{IF } [t_{cm} - l^k_{n-1} <= 0 \text{ OR } l^k_{n-1} = 0]; \text{ THEN } \frac{2L}{v_w}; \text{ ELSE } 0 \tag{9}$$

IWT**: Idle Walking Time**

When the conveyor does not move and a^k_{n-1} is bigger than the necessary walking time, $\frac{2L}{v_w}$, then

$$\mathrm{IWT} = \min\left(a^k_{n-1}, \frac{2L}{v_w}\right) \tag{10}$$

Section 2. - The operator works before the new cycle

The $F(2)^k_n$ staring position and $T(2)^k_n$ duration of the The second section is calculated as:

$$F(2)^k_n = F(1)^k_n + T(2)^k_n v^k_n \tag{11}$$

$$T(2)^k_n = \max\left(a^k_{n-1} - \frac{2L}{v_w}; 0\right) \tag{12}$$

where v^k_n is the average speed of the assembly.

Section 3. - The operator and table move together

In this section, operator and the conveyor are moving together for a time period shorter than $t_c m$, so they will meet at:

$$F(3)^k_n = F(2)^k_n + T(3)^k_n(v_c + v^k_n) \tag{13}$$

$$T(3)^k_n = \min\left(\max\left[(n-1)t_c + t_{cm} - T^k; 0\right]; t_{cm}\right) \tag{14}$$

where $(n-1)t_c + t_{cm}$ describes the time instant the section will finish. In normal situation $T(3)^k_n$ equals to t_{cm}, while in extreme case the operator has as significant idle time as he or she finishes his or her job before the end of this section.

Section 4. - The operator works and table stays

In this section the operator works with v^k_n linear speed until the conveyor does not move, so this section finishes at:

$$F(4)^k_n = F(3)^k_n + T(4)^k_n v^k_n \tag{15}$$

$$T(4)^k_n = \min\{\max[nt_c - T; 0]; \frac{L}{v^k_n} - T(2)^k_n - T(3)^k_n\}, \tag{16}$$

where $\frac{L}{v^k_n} - T(2)^k_n - T(3)^k_n$ defines the remaining assembly time before the end of the tact time.

The idle and delay times

At the end of the cycles the a^k_n idle or l^k_n delay time is calculated as:

$$l^k_n = \max\left(\tfrac{L}{v^k_n} + T(1)^k_n - a^k_{n-1} + l^k_{n-1} - t_c; 0\right) \tag{17}$$

$$a^k_n = \max\left(t_c - \tfrac{L}{v^k_n} - T(1)^k_n + a^k_{n-1} - l^k_{n-1}; 0\right) \tag{18}$$

The prediction of conveyor stoppage is the most important ability of the model which will be calculated based on the delay time as it will be presented in the following subsection.

Section 5. - The operator and the table move together after the end of tact time

This section can be considered as the modification of the third section with the delay of the operator. As we already know l_n^k and the operator can work in this section maximum till t_{cm}, the calculation is straightforward:

$$F(5)_n^k = F(4)_n^k + T(5)_n^k(v_c + v_n^k) \quad (19)$$
$$T(5)_n^k = \min\left(l_n^k, t_{cm}\right) \quad (20)$$

Section 6. - The operator works and the conveyor stays after the end of tact time

As the duration of this section is limited as $t_c - t_{cm}$, the variables that define the end of the section are calculated as:

$$F(6)_n^k = F(5)_n^k + T(6)_n^k v_n^k \quad (21)$$
$$T(6)_n^k = \min\left[\max\left(l_n^k - t_{cm}; 0\right); t_c - t_{cm}\right] \quad (22)$$

Calculation of the stoppage and the idle time

The open station type operation of the paced conveyor has increased flexibility as the conveyor has to be stopped only when the delay of the kth operator is as significant as it disturbs the work of the neighboring $k-1$th operator. We define this situation as:

$$T^k + T(1)_n^k <= T^{k-1} + T(1)_{n-1}^{k-1} + \frac{t_c}{4} \quad (23)$$

In this case the idle I_n^k time has to be modified by $T(1)_n^k$ and reset the value of a_n^k to zero.

$$I_n^k = (n-1)t_c - T(1)_n^k \quad (24)$$

When the $l_n^k - T(6)_n^k$ is smaller than t_{cm}, the operator stops the conveyor. The l_n^k is reset and the stoppage time is:

$$S_n^k = \max(l_n^k - T(6)_n^k - t_{cm}; 0) \quad (25)$$

2.3 KPIs and the developed simulator

The developed simulator handles the stochastic and open nature of the conveyor, simulates all workstations, the interactions between the operators and predicts stoppage. The worker movement diagram representation helps in the stoppages prediction (see Fig. 6).

Production planners can use the developed simulator to try sequencing strategies and analyze a new production lines capability. The following key performance indicators (KPIs) calculated based on Monte-Carlo simulation gives a realistic picture about the production.

- The balance of conveyor line is depended on the maximum of the late times of operators, $\mathbf{l}^k = [l_1^k, l_2^k, \ldots, l_n^k]$:

$$B = \frac{\sum_{k=1}^{K} \max(\mathbf{l}^k)}{K} \frac{1}{t_c} \quad (26)$$

- The efficiency of production is calculated based on to the sum of the $\frac{L}{v_n^k}$ assembly times divided by the maximum of the $\mathbf{T}(6)^k = T(6)_1^k, T(6)_2^k, \ldots, T(6)_n^k)$ finishing times and the sum of stoppage times multiplied by the number of workstations.

$$P = \frac{\sum_{k=1}^{K} \frac{L}{v_n^k}}{\{\max[\mathbf{T}(6)^k] + \sum_{n=1}^{N}\sum_{k=1}^{K} S_n^k\}K} \quad (27)$$

- The sum of the S stoppage times (Eq. 25).
- The mean of the assembly times.

The simulator and the movement diagram are developed in Python environment. d The developed simulator and the related dataset is freely and fully available on the website of authors: www.abonyilab.com.

3. Application to wire harness production

To demonstrate the applicability of the simulator three typical types of production sequencing strategies were analyzed. In the first case, the sequence follows the random customer demand which case often happens in Just In Time (JIT) production. Batch production is a more efficient sequencing strategy. In this case, batches of lower and higher complexity products are following each other. One of the best solutions is the $\pi = m_1, m_2, m_1, \ldots$ high/low sequencing strategy because it utilizes the open station nature of the conveyor.

The studied conveyor contains $K = 5$ workstations. The number of manufactured products is $N = 100$, and two different group of products ($M = 2$) are produced. The assembly times are represented by a normal distribution, which is $t_1 = \mathcal{N}(250, 30)$ for the lower complexity product and $t_2 = \mathcal{N}(310, 30)$ for the higher complexity product. The tact time of the conveyor is constant and set to $t_c = 280s$ which is the average assembly time of the products.

Fig. 7 shows the results of 1,000 simulations of the three sequence types. This scatter matrix plot shows the main KPIs, the balance, the number of the manufactured products, the number of stoppages, and the average assembly times. The green dots represent the High/Low, the blues the batched, and the red the random sequences.

As shown in Fig. 7, the difference between the random (blue) and high/low (green) sequences is significant on all KPIs. The batched sequence (red) has similar performance to the high/low sequence, but many times this batch production is not manageable because of the high variance of the products and the short delivery times.

4. Conclusions

As human resources are still necessary for many manufacturing systems, the development of production process should also focus on the performance of operators.

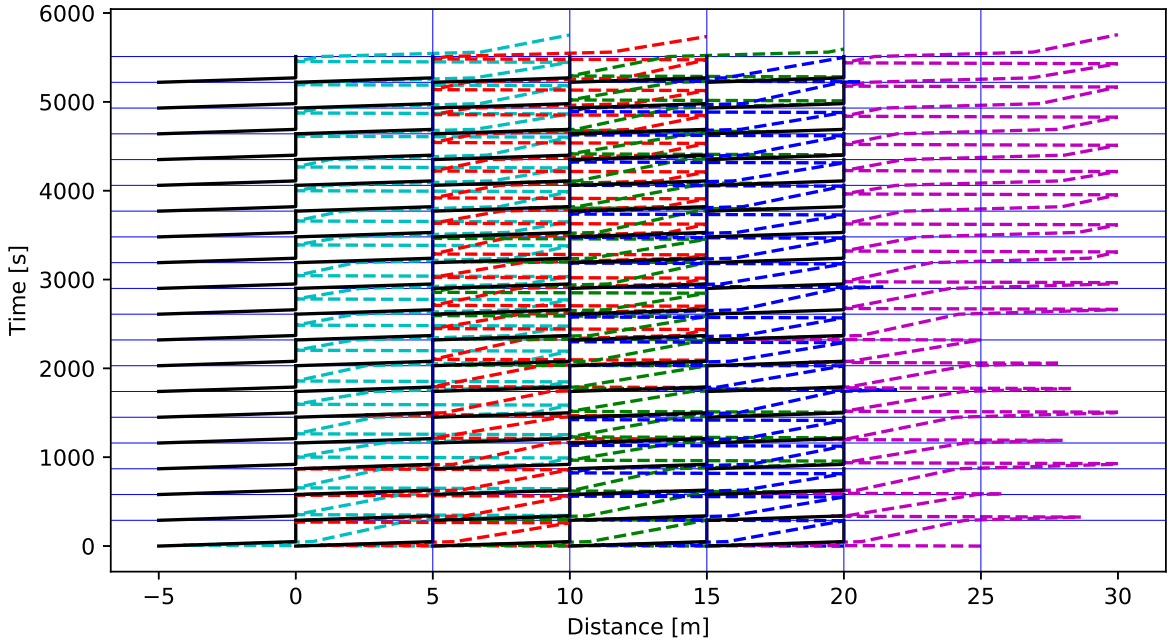

Figure 6: The developed worker movement diagram of five stations and 18 cycle steps. The distance begins at -5 m to represent the previous workstation.

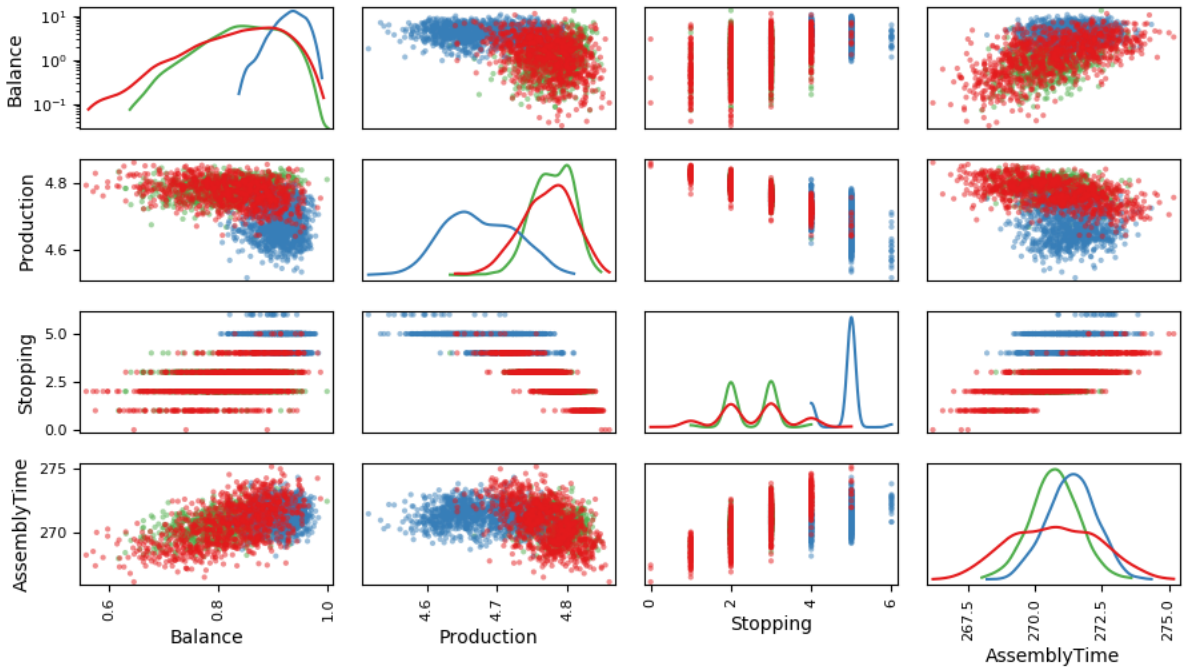

Figure 7: The result of a Monte-Caro simulation of three different sequencing strategies. The scatter plot shows all of KPIs. The high/low sequence is denoted by green, the batch by red, and the random by blue dots. The difference between the random and high/low sequences is significant on all KPIs.

According to the digital twin concept, this development should be based on the model of the production system, which necessaries the development of simulators that can handle uncertainties related to the human nature of the operators. The developed worker movement diagram based model handles the paced and open workstations of the conveyors and the stochastic nature of production. The worker movement representation helps in the analysis of the operators which is needed to predict production stoppages. The introduction of stochastic variables and the Monte-Carlo simulation-based evaluation of the key performance indicators provide a realistic picture about the production. The applicability of the simulator in the analysis of the effect of production sequencing is demonstrated by a well-documented benchmark problem of a wire-harness production process. The developed simulator is not specialized to the studied wire harness production; it can be used to model all of the types of paced conveyors even open or closed workstations.

Acknowledgement

This research was supported by the National Research, Development and Innovation Office NKFIH, through the project OTKA-116674 (Process mining and deep learning in the natural sciences and process development) and the EFOP-3.6.1- 16-2016- 00015 Smart Specialization Strategy (S3) Comprehensive Institutional Development Program.

Notations

KPI	Key Performance Indicator
NWT	Normal Walking Time
DWT	Delayed Walking Time
CDWT	Critically Delayed Walking Time
IWT	Idle Walking Time
k	index of workstation $k = 1, \ldots, K$
K	number of workstations
n	index of cycle step $n = 1, \ldots, N$
N	number of cycle steps
s	index of section s=1, $\ldots$, 6
v_n^k	assembly speed of th operator $[\frac{\mathrm{m}}{\mathrm{s}}]$
v_w	walking speed of the operator $[\frac{\mathrm{m}}{\mathrm{s}}]$
v_c	speed of the conveyor $[\frac{\mathrm{m}}{\mathrm{s}}]$
v_{cw}	walking speed of the operator when the conveyor is moving $[\frac{\mathrm{m}}{\mathrm{s}}]$
t_c	tact time [s]
t_{cm}	conveyor movement time [s]
$t^k_{(\pi(n)}$	assembly time of actual the product at kth operator [s]
$T(s)_n^k$	duration of the actual s section in nth cycle step a kth workstation [s]
$\mathbf{T}(6)^k$	finishing times of the kth operator [s]
a_n^k	work ahead time in nth cycle step at kth operator [s]
l_n^k	late time in nth cycle step at kth operator [s]
$\mathbf{l}_k$	late times of kth operator [s]
T	actual simulated time [s]
I_n^k	final idle time in nth cycle step at kth workstation [s]
S_n^k	stoppage time in nth cycle step at kth workstation [m]
$F(s)_n^k$	position of operator at the actual s section in nth cycle step a kth workstation [m]
$Table_n^k$	table position in nth cycle step at kth operator [m]
$\pi(n)$	sequence of products [$-$]
L	length of the workstation [m]
T_n^k	position of the tables [m]

REFERENCES

[1] Estrada, F., Villalobos, J.R., Roderick, L., Estrada, F., Villalobos, J.R., Roderick, L.: Evaluation of Just-In-Time alternatives in the electric wire-harness industry, *Taylor and Francis*, 1997 **35**(7), 1993–2008, DOI: 10.1080/002075497195038

[2] Lodewijks, G.: Two Decades Dynamics of Belt Conveyor Systems *Bulk Solids Handling*, 2002 **22**(2), 1–2

[3] Xiaobo, Z., Zhou, Z., Asres, A.: Note on Toyota's goal of sequencing mixed models on an assembly line, *Computers and Industrial Engineering*, 1999 **36**(1), DOI: 10.1016/S0360-8352(98)00113-2, 57–65

[4] Sarker, B.R., Pan, H.: Designing a Mixed-Model, Open-Station Assembly Line Using Mixed-Integer Programming, *The Journal of the Operational Research Society Palgrave Macmillan Journals*, 2001 **52**(52), 545–558 DOI: 10.1057/palgrave.jors.2601118

[5] Bukchin, J., Tzur, M.: Design of flexible assembly line to minimize equipment cost, *IIE Transactions (Institute of Industrial Engineers)*, 2000 **32**(7), 585–598 DOI: 10.1080/07408170008967418

[6] Bautista, J., Cano, J.: Minimizing work overload in mixed-model assembly lines, *International Journal of Production Economics*, 2008 **112**(1), 177–191 DOI: 10.1016/j.ijpe.2006.08.019

[7] Xiaobo, Z., Ohno, K.: Algorithms for sequencing mixed models on an assembly line in a JIT production system, *Computers ind. Engng*, 1997 **32**(1), 47–56 DOI: 10.1016/s0360-8352(96)00193-3

[8] Xiaobo, Z., Ohno, K.: Properties of a sequencing problem for a mixed model assembly line with conveyor stoppages, *European Journal of Operational Research*, 2000 **124**(3), 560–570 DOI: 10.1016/S0377-2217(99)00198-8

[9] Fattahi, P., Salehi, M.: Sequencing the mixed-model assembly line to minimize the total utility and idle costs with variable launching interval, *International Journal of Advanced Manufacturing Technology*, 2009 **45**(9-10), 987 DOI: 10.1007/s00170-009-2020-0

[10] Tsai, L.H.: Mixed-Model Sequencing to Minimize Utility Work and the Risk of Conveyor Stoppage Mixed-model Sequencing to Minimize Utility Work and the Risk of Conveyor Stoppage, *Source: Management Science*, 1995 **41**(3), 485–495 DOI: 10.1287/mnsc.41.3.485

[11] Ong, N.S., Boothroyd, G.: Assembly times for electrical connections and wire harnesses, *The International Journal of Advanced Manufacturing Technology*, 1991 **6**(2), 155–179 DOI: 10.1007/BF02601438

[12] Assembly Line Conveyor Systems, 2015, https://www.pacline.com/photos/photos-by-solution/assembly-line-conveyors/

DE GRUYTER OPEN

HUNGARIAN JOURNAL OF INDUSTRY AND CHEMISTRY
Vol. 46(2) pp. 63–66 (2018)
hjic.mk.uni-pannon.hu
DOI: 10.1515/hjic-2018-0020

HUNGARIAN JOURNAL OF INDUSTRY AND CHEMISTRY
HJIC

INVESTIGATIONS INTO FLOUR MIXES OF *TRITICUM MONOCOCCUM* AND *TRITICUM SPELTA*

KATALIN KÓCZÁN-MANNINGER *[1] AND KATALIN BADAK-KERTI[1]

[1]Department of Grain and Industrial Plant Processing, Szent István University, Villányi út 29-43, Budapest, 1118, HUNGARY

Bread samples were made using flour mixes of *Triticum monococcum (Tr. monococcum)* and *Triticum spelta (Tr. spelta)*. They were tested for their rheological behaviour over the first 3 days of storage at room temperature, and for their characteristics based on a Hungarian Standard. Parameters were set such as the volume of the baked product, baking loss, crumb characteristics and elasticity of crumbs. The behaviour of flour from einkorn wheat is different to that of *Tr. spelta*. The properties of the tested flour mixes measured by a farinograph show that *Tr. spelta* produces an acceptable dough, on the other hand, the dough of *Tr. monococcum* develops quickly but is very unstable so weakens within minutes of being kneaded. This also suggests that doughs composed of einkorn wheat flour require a different type of kneading than those of *Tr. spelta* (or *Tr. aestivum*, also referred to as common wheat) flours. Breads composed of *Tr. spelta* were comparable with those made with *Tr. aestivum*, the crumb elasticity was above 90 % on the day of baking, which indicates high quality. The *Tr. monococcum* breads, however, were of low grade: the volume of the breads decreased by increasing the ratio of *Tr. monococcum* to *Tr. spelta* and the elasticity reduced to unacceptable levels (less than 60 %). It should be mentioned that the grading was based on breads made purely from *Tr. aestivum* flours.

Keywords: spelt, einkorn, bread, texture analysis

1. Introduction

As a result of the increasing number of cases of celiac disease and allergies, as well as the growing popularity of conscious nutrition, interest in older varieties of wheat is once again on the rise. In general, consumers think that these species of wheat are potentially less immunogenic than their modern equivalents. The manufacturing properties of doughs produced from ancient varieties of wheat are much weaker than those of common wheat. In order to obtain good quality bakery products, it may be necessary to use mixtures of flours from different varieties.

In our research, the properties of the flour of einkorn and spelt wheats in addition to breads that consist of different proportions of these flours were prepared and investigated. During measurements, attempts were made to determine whether these wheat species – which are in theory suitable for baking bread – could improve the baking performance or whether a significant difference exists between the characteristics of the finished products of various compositions.

Crossing more modern varieties results in higher yields, greater resistance, more uniform ripening times and higher gluten contents. Although these breeding procedures facilitated processing, the genetic diversity and nutritional value decreased significantly which virtually resulted in the total displacement of indigenous species [1, 2]. One reason for this is that *Tr. monococcum* was consumed primarily as a mush or simply cooked; these methods did not require proofing, which was originally used in ancient Egypt during bread baking [3]. Bread made from spelt flour is also of lower quality than that of common wheat, both in terms of specific volume and crumb structure [4].

According to previous research, spelt wheat flour produces less stable and elastic but stickier dough than plain flour. Due to its sticky and soft nature after kneading, it is difficult to handle [5, 6]. Breads made from einkorn flour exhibit a wide range of possible specific volumes, ranging from very low to high. Although only a few subtypes are suitable for making breads, most versions are suitable for preparing pasta or biscuits [7], or utilisation for special purposes like fermentation processes [8].

The first phase of the investigations concerned the quality of the gluten, followed by the preparation and testing of loaves of bread. The main question concerned how the blends of flours of these species of wheat influence the quality of the final products.

*Correspondence: koczan.gyorgyne@etk.szie.hu

2. Experimental

2.1 Samples and Measurements

Triticum monococcum (einkorn) and *Triticum spelta* wheat flours were manufactured by Szabó Hengermalom Kft. using conventional technology and contained no additives or bread improvers. For the measurements fine flours were used, i.e. small grain particles with low bran content, to ensure they contained only a negligible amount of outer shell.

The determination of wet gluten content was performed according to a standard using the Glutomatic System. After gluten washing, a gluten index was also calculated using a gluten centrifuge.

The moisture content was determined by a Sartorius moisture analyser. The uniformly dispersed sample of 2.5 g was dried at 105 °C to a constant weight (which has not changed for 20 seconds more than 1 mg). The change in mass could be deduced from the moisture content of the whole test substance.

The determination of water absorption was conducted by a Brabender farinograph in accordance with a Hungarian standard (MSZ 6369-6:2013) in duplicates, followed by further experimentation using a baking test (MSZ 6369-8:1988).

The volume of the bread samples was measured by placing a loaf in a container of known volume and pouring in a known quantity of mustard seeds around the loaf until the container was full. By measuring the amount of seeds remaining once the container was full, the volume of the loaf could be calculated.

The quality of the bread texture was evaluated by a TA.XTplus texture analyser (Stable Micro Systems, Surrey, UK), following a modified American Association of Cereal Chemists (AACC) International approved method (74-09) and expressed as crumb firmness (force, 1/g) and relative elasticity (%). A 40 % compression of a 25 mm-thick sample was achieved, following a resting time of 30 seconds (at the same compression depth) and then the measuring head was slowly lifted and the springiness of the sample calculated. Thus, it was a "measure of force in compression" test using an AACC 36mm-diameter cylinder probe with radius (P/36R). The analyser was set at a 'return to start' cycle with a pre-test speed of 1 mm s^{-1}, a test speed of 0.5mm s^{-1}, a post-test speed of 10 mm s^{-1} and a pre-defined percentage (40 %) of the original sample height. The relative elasticity was calculated from the difference between the original height and the height to which the sample recovered (after pressing and releasing the pressure).

Measurements were conducted in triplicates. Statistical evaluations were carried out using ANOVA (analysis of variance) tests in Excel.

Bread samples were stored at room temperature in plastic bags. Texture measurements were taken on the day of baking after the bread had been cooled to room temperature (Day 0) and on the following 2 days, namely Days 1 and 2.

Table 1: Composition of the samples (%)

	100A	80A	60A	40A	20A	100T
Tr. monoc. (A) %	100	80	60	40	20	0
Tr. spelta (T) %	0	20	40	60	80	100
Water %	57	62	64	65.4	65.8	71
Yeast %	4	4	4	4	4	4
Salt %	1.2	1.2	1.2	1.2	1.2	1.2

The ingredients consisted of 250 g of flour, 10 g of yeast and 3 g of salt, the only variable parameter was the amount of water used to make the dough. Initially, the dough consisted of approximately 60 % (150 ml) water based on the weight of the flour, and the amount of water was increased to form a homogeneous dough. The final compositions are shown in Table 1.

3. Results and Discussion

3.1 Experiments

In the case of the einkorn flour, gluten washing was ineffective as it could not be washed out. After the mixing phase, a yellowish substance remained on the bottom of the washer. In the case of spelt flour, gluten tests could be conducted without any problems.

The wet gluten content of the *Tr. spelta* flour was 46.73 %. According to the Hungarian regulations bread wheat flours must have a minimum wet gluten content of 28 % and for wheat flours used to improve the baking quality a minimum of 34 %. Bakers consider a gluten content in excess of 30 % to be good. The wet gluten content of the spelt flour examined is well above this value, but other factors are also taken into account to determine the quality of flour.

The gluten index, a measure of gluten quality, of spelt flour was 45.73 %. A value of between 60 and 90 % is considered to be ideal, below 60 % weak and in excess of 90 % too strong. Thus, the gluten quality of the spelt flour was clearly weak.

The gluten quality calculated from the results of the farinograph tests for spelt flour was 98 % which is acceptable but does not fully reflect the quality of the flour. Although the kneading and stability times of the doughs fell within the range of expected values, the planimetric area was greater due to the degree of softening. Thus, the quality score obtained by Hankóczy's evaluation method was smaller. The farinogram of spelt flour more closely resembles a flour of medium quality (Fig. 1).

This is especially true for the *Tr. monococcum* flour. It reaches its maximum consistency very quickly; the top of the curve barely exceeds the consistency line (500 BU – Brabender Units). The degree of softening is enormous, as is reflected well by the large planimetric area. The qualitative value assigned to the curve is very low (Fig. 2).

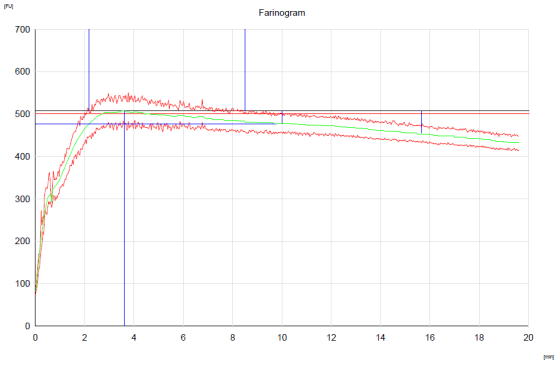

Figure 1: Farinogram of *Triticum spelta* flour.

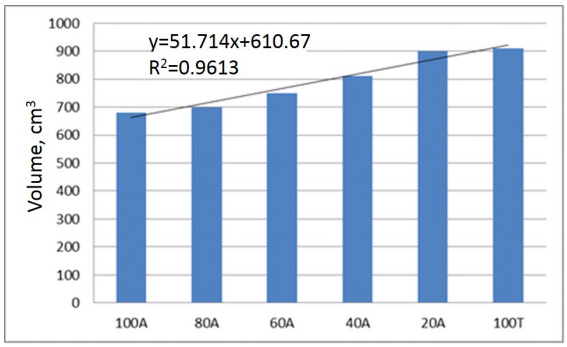

Figure 3: Volume of bread samples (A – einkorn flour, T – spelt flour; the numbers are the percentages of einkorn flour in the flour blend)

A direct correlation was identified between the volume of the bread samples and the amount of spelt flour in the flour blend (Fig. 3). This is in accordance with the gluten quality of the flour blends, as is seen from the results of the farinograph measurements.

The crumb hardness of the bread samples is shown in Fig. 4. As the samples started to age the compression force increased. By examining the initial and final forces (measures of crumb hardness), it can be stated that sample 60A showed the best results. In this case, the force increased by 29 % between Day 0 and Day 2. For samples containing less einkorn flour the crumbs seemed to be softer and the relative increase in hardness during storage less (when values on Day 2 were compared to those on Day 0). Even though sample 80A was initially even softer than 60A, by the end of Day 2 it needed 1.7 times the force to compress it. An explanation of this phenomenon can also be given with regard to the different compositions of the starch molecules in einkorn flour compared to those in spelt flour. The staling of bread is related to the crystallization processes of starch molecules.

Significant differences between samples consisting of 100 % spelt flour and those of 20 % einkorn flour mixed with 80 % spelt flour were shown by the results. The increase in crumb hardness during storage resulted in significant differences in all samples of identical compositions.

The elasticity of the bread crumbs increased as the amount of spelt flour increased in the flour blend (Fig. 5). This tendency persisted during storage as well. The slight increase in the elasticity of the bread composed of 100 % *Triticum monococcum* flour was probably due to improper handling of the samples, i.e. improper cooling before being packed, although it is questionable whether any moisture originating from the headspace of the packaging could cause such a change.

Taking into account that the results obtained could be derived from measurement and/or calculation errors, it may be worthwhile to consider the role of the chemical structure of einkorn flour during the baking process, and its effect on the elasticity during further targeted experiments.

By using a rating system for the *Tr. aestivum* flours, the bread samples can be classified. Although the same judgment about the "marketability" of the bread samples cannot be made for breads based on these special types of flour, trends can clearly be observed. By adding more einkorn flour to the flour blends, the "quality" of the crumb structure decreased.

Most of the samples did not achieve an elasticity of 80 % meaning that they did not return to 80 % of their original height after compression. With these values, most of the breads fall into the non-marketable category. Elastic-

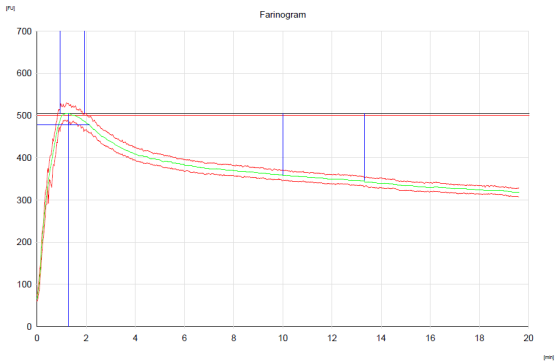

Figure 2: Farinogram of *Triticum monococcum* flour

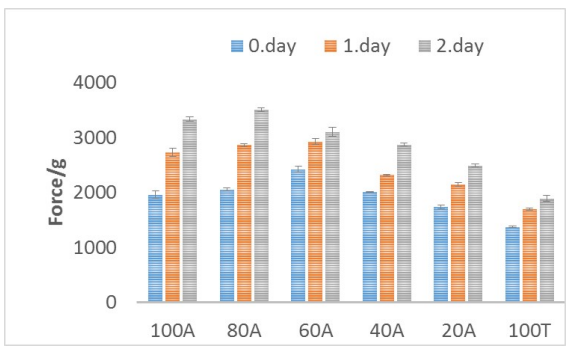

Figure 4: Crumb hardness (Force, 1/g) as a function of different flour compositions over 3 days

Figure 5: Change in the elasticity of the bread samples during storage at room temperature

ities of between 90 and 95 % are indicative of good quality breads. Such values were only achieved when 100 % *Triticum spelta* flour was used. After 2 days of storage at room temperature, the crumbs of 100 % spelt flour bread degraded to an average quality.

4. Conclusion

The purpose of our investigations was to examine the quality of flours from varieties of ancient wheats.

Gluten could not be washed out of einkorn samples and the wet gluten content of *Tr. spelta* was also very low. Farinograph measurements revealed that when only einkorn flour is used, the dough forms very fast but is very soft and almost completely unstable.

By mixing einkorn and spelt flours bread can be made, however, an acceptable ratio would not exceed 20 % of einkorn to 80 % of *Tr. spelta* flour. With this flour blend, the resulting bread volume is comparable to the accepted low values of bread composed of 100 % spelt flour. The hardness and elasticity of the bread crumbs already changed significantly at the lowest mixing ratios.

Further studies on the sensory characteristics of these breads and consumer tests are needed before deciding on the use of flour blends of *Triticum monococcum* and *Triticum spelta* in the absence of any addition of *Triticum aestivum* flour.

REFERENCES

[1] Draskovics, M. R.: Seed plants (*Spermatophyta*) In: Turcsányi, G. (ed.) Agricultural botany, Mezőgazdasági Szaktudási Kiadó, Budapest, Hungary, 2000 pp 363-365 ISBN: 9633563593

[2] Dinu, M.; Whittaker, A.; Paglia, G.; Benedettelli, S.; Sofi, F.: Ancient wheat species and human health: biochemical and clinical implications. *J. Nutr. Biochem.,* 2018 **52**, 1-9 DOI: 10.1016/j.jnutbio.2017.09.001

[3] Brandolini, A.; Hidalgo, A.: Chapter 8: Einkorn (*Triticum monococcum*) Flour and Bread in Flour and Breads and their Fortification In: Preedy V. R.; Watson R. R.; Patel V. B.: Health and Disease Prevention, Academic Press/Elsevier, UK, 2011 pp 79-88 ISBN: 978-0-12-380886-8

[4] Abdel-Aal, E-S. M.; Hucl, P.; Sosulski, W.; Bhirud, P. R.: Kernel, milling and baking properties of spring-type spelt and einkorn wheats. *J. Cereal Sci.,* 1997 **26,** 363-370 DOI: 10.1006/jcrs.1997.0139

[5] Callejo, M. J.; Vargas-Kostiuk, M. E., Rodríguez-Quijano, M.: Selection, training and validation process of a sensory panel for bread analysis: Influence of cultivar on the quality of breads made from common wheat and spelt wheat. *J. Cereal Sci.*, 2015 **61**, 55-62 DOI: 10.1016/ j.jcs.2014.09.008

[6] Frakolaki, G.; Giannou, V.; Topakas, E.; Tzia, C.: Chemical characterization and breadmaking potential of spelt versus wheat flour. *J. Cereal Sci.*, 2017 **79**, 50-56 DOI: 10.1016/j.jcs.2014.09.008

[7] Hidalgo, A., Brandolini, A.: Lipoxygenase activity in wholemeal flours from *Triticum monococcum*, *Triticum turgidum* and *Triticum aestivum*. *Food Chem.,* 2012 **131**, 1499-1503 DOI: 10.1016/j.foodchem.2011.09.132

[8] Hetényi, K.; Németh, Á.; Sevella, A.: Examination of medium supplementation for lactic acid fermentation. *Hung. J. Ind. Chem.*, 2008 **36**(1-2) 49-53

DE GRUYTER OPEN

HUNGARIAN JOURNAL OF INDUSTRY AND CHEMISTRY
Vol. 46(2) pp. 67–71 (2018)
hjic.mk.uni-pannon.hu
DOI: 10.1515/hjic-2018-0021

HUNGARIAN JOURNAL OF INDUSTRY AND CHEMISTRY
HJIC

FORMATION OF GLYCIDYL ESTERS DURING THE DEODORIZATION OF VEGETABLE OILS

ERZSÉBET BOGNÁR *[1], GABRIELLA HELLNER[2], ANDREA RADNÓTI[2], LÁSZLÓ SOMOGYI[1], AND ZSOLT KEMÉNY[2]

[1]Department of Grain and Industrial Plant Processing, Szent István University, Villányi út 29-43, Budapest, 1118, HUNGARY
[2]BEMEA Katalin Kővári R&D Centre, Illatos út 38, Budapest, 1097, HUNGARY

Glycidyl esters are foodborne contaminants formed during the production of fats and oils, especially during the deodorization of palm oil. The hydrolyzed free form of glycidol has been categorized as probably carcinogenic to humans by the World Health Organization's International Agency for Research on Cancer. The aim of this research was to study the formation of glycidyl esters during the lab-scale deodorization of the three most widely produced seed oils in the world (sunflower, rapeseed and soybean). The effects of two independent factors – temperature and residence time – were analyzed by a 3^2 full factorial experimental design and evaluated by response surface methodology. In accordance with findings in the literature, the greatest amount of glycidyl esters was formed in the soybean oil matrix. For all three oils, the effects of both residence time and temperature were significant, while the latter was more so. To reduce the formation of glycidyl esters, milder deodorization is required, which is limited because of the purposes sought by the thermal operation and removal of volatile minor components and contaminants.

Keywords: glycidyl esters, deodorization, seed oils

1. Introduction

Glycidyl esters (GEs) are foodborne contaminants formed in fat-containing food and food ingredients during high-temperature thermal treatment. According to previous studies, glycidol is produced during digestion from the enzymatic hydrolysis of GEs [1,2]. The IARC (International Agency for Research on Cancer) has listed glycidol as a Group 2A or genotoxic carcinogen [3]. This year, the European Commission adopted the Commission Regulation (EU) 2018/290 that stipulates the maximum level of glycidyl fatty acid esters permitted in vegetable oils and fats, infant formula, follow-on formula and foods for special medical purposes intended for infants and young children. The maximum concentration of glycidyl fatty acid esters is 1 mg/kg in vegetable oils and fats placed on the market for end consumers or for use as an ingredient in food, and 0.5 mg/kg for vegetable oils and fats destined for the production of baby food and processed cereal-based food for infants and young children [4].

GEs are formed in vegetable oils during the refining process in the deodorization step, which is conducted at high temperatures (200-275 °C) under vacuum (of less than 10 mbar residual pressure) [5, 6]. Deodorization is the last step of refining of conventional edible oils and is intended to remove undesirable substances in order to improve the taste, odor, color and oxidative stability of such oils [7]. According to data from the literature, high levels of GEs are primarily measured in refined palm oil and its fractions. Destaillats et al. [8] showed in their study that GEs are formed from di- and monoacylglycerols (DAGs and MAGs), but not from triacylglycerols (TAGs). Accordingly, high levels of GE can be traced back to high levels of DAGs in crude palm oil [8]. The formation of GE starts at about 200 °C [8].

Analytical methods for the determination of GEs can be divided into two main groups: direct and indirect methods [9]. Individual GEs are determined by direct quantitation methods which are mainly based on liquid chromatography-mass spectrometry (LC-MS), requiring a significant number of reference compounds and internal standards [10, 11]. Indirect determination is based on the conversion of GEs into glycidol which is then isolated, derivatized, chromatographically separated and quantified. The result is expressed as the amount of glycidol that can be released from GEs. These methods require only a small number of internal standards [9].

In our study, the quantity of GEs in seed oil during lab-scale deodorization was determined in order to examine the effects of two independent factors – temperature and residence time – on the formation of GEs.

*Correspondence: zsofi.bognar@outlook.hu

2. Experimental

2.1 Samples and Measurements

Bleached sunflower, rapeseed and soybean oils were supplied by Bunge Limited (Bunge Zrt. Hungary and Bunge Ibérica, S.A.U.). Diethyl ether, ethyl acetate, *n*-hexane and high-performance liquid chromatography (HPLC)-grade water were obtained from VWR International Kft. (Debrecen, Hungary). Toluene, isohexane, sodium bromide and phenylboronic acid were obtained from Merck Kft. (Budapest, Hungary). Methanol, sodium hydroxide and anhydrous sodium sulfate were purchased from Reanal Laborvegyszer Kft. (Budapest, Hungary). The internal standards glycidyl palmitate-d_5 and 3-chloro-1,2-propanediol-d_5 (3-MCPD-d_5) were obtained from LabStandards (Budapest, Hungary). All reagents and chemicals were of analytical grade.

Lab-scale deodorization trials were conducted in 150 g batches at temperatures between 220 and 260 °C. The bleached oils (sunflower, rapeseed or soybean) were heated to the target temperature (220, 230, 240, 250 or 260 °C) within 10–15 minutes. The process lasted 3 hours at a pressure of 3–4 mbar using nitrogen as a stripping gas. Without breaking the vacuum, sampling was conducted after 0, 15, 30, 45, 60, 90, 120 and 150 minutes had elapsed.

The quantities of glycidyl esters were determined using the American Oil Chemists' Society (AOCS) Official Method Cd 29b-13, which is based on alkaline-catalyzed ester cleavage and transformation of the released glycidol into monobromopropanediol (MBPD) and derived free diols using phenylboronic acid (PBA). These derivatives are measured by the Gas Chromatography/Mass Spectrometry (GC/MS) coupled system (Agilent 6890 coupled with 5973) in the selected ion monitoring (SIM) mode. Quantitative determination was based on the deuterated internal standard using characteristic ions for derivatised glycidol-d_5 at m/z 150 and 245, and derivatised glycidol at m/z 147 and 240.

2.2 Experimental design and statistical analysis

The temperature and residence time were studied using response surface methodology (RSM). The results of the 3^2 full factorial experimental design (see Table 1) were evaluated by analysis of variance (ANOVA) models using Statistica 13. The center point of the 3^2 full factorial design (mid temperature 240 °C) and mid time 90 minutes) was repeated three times.

Only the significant effects (of main effects and interactions) were taken into account in the response surface methodology. The generalized polynomial model for describing the response of independent variables is given in

$$\begin{aligned} y &= \beta_0 + \beta_1 X_1 + \beta_2 X_1^2 + \beta_3 X_2 + \\ &+ \beta_4 X_2^2 + \beta_5 X_1 X_2 + \beta_6 X_1 X_2^2 + \\ &+ \beta_7 X_1^2 X_2 + \beta_8 X_1^2 X_2^2 \end{aligned} \quad (1)$$

Table 1: 3^2 full factorial experimental design

Independent variables		Levels		
		-1	0	+1
X1	Temperature (°C)	220	240	260
X2	Residence time (min)	0	90	180
Dependent Variables (Yi) Glycidyl esters (mg/kg)				

3. Results and Evaluation

3.1 Experiments

The results of the lab-scale investigation of GE formation are shown in Fig. 1. In our experimental design, the greatest amount of GEs formed in soybean oil, in which the concentration of GEs reached 5.5 mg/kg at 260 °C after 180 minutes (Fig. 1A). In the sunflower and rapeseed oils, the maximum concentrations of GEs reached were 1.6 and 1.5 mg/kg, respectively (Figs. 1B and 1C). The GE content of sunflower and rapeseed oils was kept under 1 mg/kg after 120 minutes of deodorization at a temperature of 250 °C or less, but for soybean oil this level was obtained at or below 230 °C. This demonstrates that the amounts of precursors in the oils strongly influence the formation of GE, and consequently the optimal deodorization temperature. The threshold concentration of

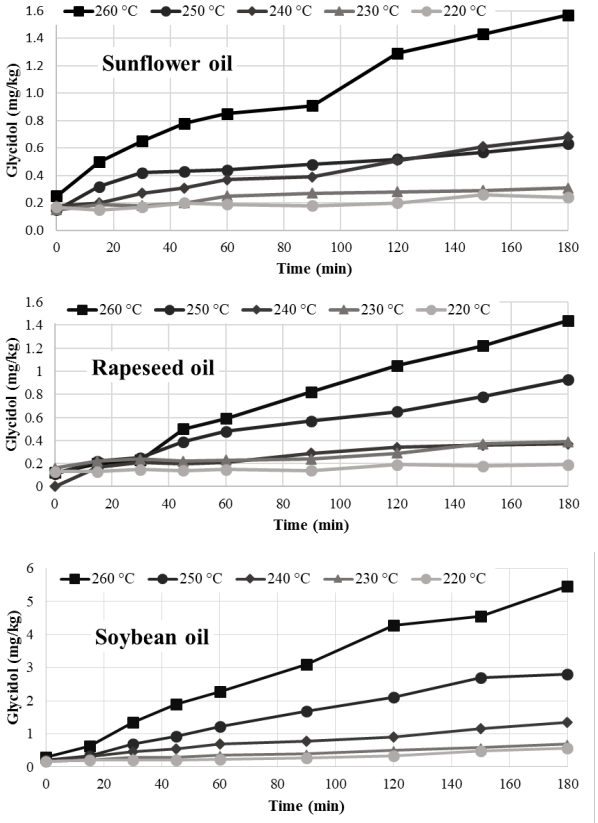

Figure 1: GEs of seed oils during deodorization: A) sunflower oil, B) rapeseed oil, C) soybean oil

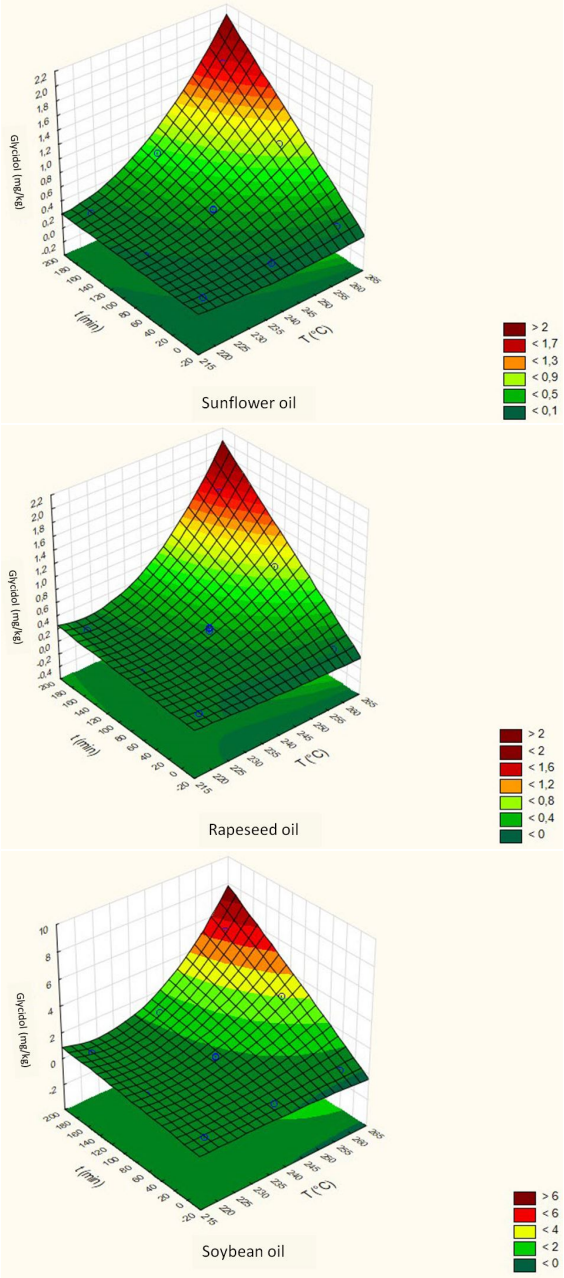

Figure 2: Fitted surfaces for seed oils: A) sunflower oil, B) rapeseed oil, C) soybean oil

0.5 mg/kg permitted for infant food was complied with at 240, 230 and 220 °C for rapeseed, sunflower and soybean oils, respectively (after 120 minutes of deodorization). In the applied experimental setup, up to 0.3 mg/kg of GE formed after 10–15 minutes of heating. At lower deodorization temperatures, the effect of time becomes practically insignificant, especially at 220 and 230 °C.

3.2 Statistical analysis

The application of RSM allowed the main effects and interactions to be determined simultaneously. ANOVA shows the significant effects, which can be used for building the response surface model. The fitted surfaces for sunflower, rapeseed and soybean oils are presented in Figs. 2A-C, respectively. The shapes of the surfaces are very similar, the only difference is in their heights. The interactions between the independent variables can be observed from the fitted surfaces, because at lower temperatures the concentrations of GEs gradually increased over time, while at higher temperatures a more rapid increase occurred.

Table 2: Regression coefficients for intercept (I), linear and quadratic factors, as well as interactions between factors in the fitted models of seed oils

	Sunflower oil	Rapeseed oil	Soybean oil
I	7.95	7.12	10.32
T	-6.72×10^{-2}	-5.9×10^{-2}	-9.02×10^{-2}
T^2	1.45×10^{-4}	1.23×10^{-4}	2×10^{-4}
t	1.17×10^{-1}	2.16×10^{-1}	1.14
t^2	n.s.	n.s.	n.s.
Tt	-1.13×10^{-3}	-1.96×10^{-3}	-1.01×10^{-2}
T^2t	3×10^{-5}	4×10^{-5}	2.2×10^{-5}
Tt^2	n.s.	n.s.	-2.38×10^{-8}

n.s.: effect not significant

For all three seed oils the temperature had the largest effect. The interaction between the independent variables and the effect of time were the second and third most significant, but the quadratic components and their interactions with the other factors were noticeable in most cases, as well. The regression coefficients are shown in Table 2 coefficients in the case of sunflower and rapeseed oils are very similar so the RSM diagrams of these oils fall within the same range of values (Figs. 2A and 2B).

4. Discussion

According to the data from the literature, the oil that has been studied the most in this respect is palm oil along with its fractions [8, 12]. Cheng et al. [13] summarized the data from previous studies and according to this review the highest concentrations of GEs in seed oil were found in soybean oil when compared to rapeseed and sunflower oils. This is in agreement with our observations. The higher concentrations of GEs that formed during deodorization were due to the higher levels of DAGs and MAGs in the raw material.

It was found that the critical temperature range is between 220 and 240 °C, above which more than 0.5 mg/kg of GEs may form, depending on the quality of the raw material. This conclusion is similar to the results of previous investigations. Craft et al. [12] concluded that between 230 and 240 °C, the formation of GE is extensive, consequently this value should be considered as an upper limit for the deodorization process. De Kock et al. [14] suggested conducting deodorization for a longer period

of time at temperatures below 240 °C, which might also minimize the formation of trans fatty acids.

5. Conclusion

The present investigation suggests that the formation of GEs in seed oils during deodorization is not negligible. The rate of formation can be traced back to the level of DAGs and MAGs [15] in the raw material. A simultaneous increase in temperature and time could result in extremely high levels of GEs in oils. On an industrial scale, the formation of GEs can be controlled in the oils examined, meaning that the upper limit of GEs (1 mg/kg) in vegetable oils and fats placed on the market for general consumption can be achieved through preventive measures. The stricter limit imposed on oils destined for the production of food for infants and young children presents greater challenges, and thus requires a combination of high quality raw materials as well as a controlled refining process.

Acknowledgement

Funding for this research was provided by the Doctoral School of Food Sciences at Szent István University (Budapest) and by the BEMEA Katalin Kővári R&D Centre. The Project is supported by the European Union and co-financed by the European Social Fund (grant agreement no. EFOP-3.6.3-VEKOP-16-2017-00005).

Symbols

β_{0-8}	Regression coefficients for intercept, linear and quadratic factors and interactions between factors
$X_1,\ X_2$	Independent factors
T	Deodorization temperature
t	Deodorization time

REFERENCES

[1] Appel, K.E.; Abraham, K.; Berge-Preiss, E.; Hansen, T.; Apel, E.; Schuchardt, S.; Vogt, C.; Bakhiya, N.; Creutzenberg, O.; Lampen, A.: Relative oral bioavailability of glycidol from glycidyl fatty acid esters in rats, *Arch. Toxicol.,* 2013 **87**(9), 1649–1659 DOI: 10.1007/s00204-013-1061-1

[2] Frank, N.; Dubois, M.; Scholz, G.; Seefelder, W.; Chuat, J.-Y.; Schilter, B.: Application of gastrointestinal modelling to the study of the digestion and transformation of dietary glycidyl esters, *Food Addit. Contam. Part A*, 2013 **30**(1), 69–79 DOI: 10.1016/j.foodchem.2010.08.036

[3] IARC (International Agency for Research on Cancer): Glycidol, *In*: IARC Monographs Volume 77. On the evaluation of carcinogenic risks to humans (WHO Press, Lyon, France) 2000 pp. 469–486 ISBN: 9283212770

[4] Official Journal of the European Union: COMMISSION REGULATION (EU) 2018/290 of 26 February 2018 amending Regulation (EC) No 1881/2006 as regards maximum levels of glycidyl fatty acid esters in vegetable oils and fats, infant formula, follow-on formula and foods for special medical purposes intended for infants and young children 2018

[5] Carlson, F.K.: Deodorization. *In*: Hui, Y. H. (ed.) Bailey's industrial oil and fat products. Edible oil and fat products: Processing technology. 5th Edition. Volume 4. (John Wiley & Sons Inc., New York, USA) 1996 pp. 411–449 ISBN: 9780471594284

[6] O'Brien, R.D.: Fats and oils formulating and processing for applications. Third Edition. (CRC Press Taylor & Francis Group, Boca Raton, Florida, USA) 2009 pp. 153–164 ISBN: 9781420061666

[7] Sipos, E.F.; Szuhaj, B.F.: Edible oil Processing. *In*: Hui, Y.H. (ed.) Bailey's industrial oil and fat products. Edible oil and fat products: Oils and oilseeds. 5th Edition. Volume 2. (John Wiley & Sons Inc., New York, USA) 1996 pp. 497–602 ISBN: 9780471594260

[8] Destaillats, F.; Craft, B.D.; Dubois, M.; Nagy, K.: Glycidyl esters in refined palm (Elaeis guineensis) oil and related fractions. Part I: Formation mechanism, *Food Chem.,* 2012 **131**(4), 1391–1398 DOI: 10.1016/j.foodchem.2011.10.006

[9] Ermacora, A.; Hrncirik, K.: Indirect detection techniques for MCPD esters and glycidyl esters. *In*: MacMahon, S. (ed.) Processing contaminants in edible oils MCPD and glycidyl esters (AOCS Press, Urbana, USA) 2014 pp. 57–90 ISBN: 9780988856509

[10] Thürer, A.; Granvogl, M.: Direct detection techniques for glycidyl esters. *In*: MacMahon, S. (ed.) Processing contaminants in edible oils MCPD and glycidyl esters (AOCS Press, Urbana, USA) 2014 pp. 91–120 ISBN: 9780988856509

[11] Blumhorst, M.R.; Venkitasubramanian, P.; Collison, M.W.: Direct determination of glycidyl esters of fatty acids in vegetable oils by LC–MS, *J. Am. Oil Chem. Soc.,* 2011 **88**(9), 1275–1283 DOI: 10.1007/s11746-011-1873-1

[12] Craft, B.D.; Nagy, K.; Seefelder, W.; Dubois, M.; Destaillats, F.: Glycidyl esters in refined palm (Elaeis guineensis) oil and related fractions. Part II: Practical recommendations for effective mitigation, *Food Chem.*, 2012 **132**(1), 73–79 DOI: 10.1016/j.foodchem.2011.10.034

[13] Cheng, W.W.; Liu, G.Q.; Wang, L.Q.; Liu, Z.S.: Glycidyl Fatty Acid Esters in Refined Edible Oils: A review on formation, occurrence, analysis, and elimination methods, *Compr. Rev. Food Sci. F.*, 2017 **16**(2), 263–281 DOI: 10.1111/1541-4337.12251

[14] De Kock, J.; Papastergiadis, A.; De Greyt, W.: Technological solutions and developments in edible oil processing to minimize contaminants in various oils and fats. *5th Leipzig Symposium 'Processing and*

Analytics: How does co-operation work in Practice?' (9-10 March 2016, Leipzig, Germany) 2016

[15] Csányi, E., Bélafi-Bakó, K.: Semi-continuous fatty acid production by lipase, *Hung. J. Ind. Chem.*, 1999 **27**(4), 293–295

DE GRUYTER OPEN

HUNGARIAN JOURNAL OF INDUSTRY AND CHEMISTRY
Vol. 46(2) pp. 73–77 (2018)
hjic.mk.uni-pannon.hu
DOI: 10.1515/hjic-2018-0022

HUNGARIAN JOURNAL OF INDUSTRY AND CHEMISTRY
HJIC

EFFECT OF ALGAE TREATMENT ON *STEVIA REBAUDIANA* GROWTH

RÉKA CZINKÓCZKY[1] AND ÁRON NÉMETH *[1]

[1]Department of Applied Biotechnology and Food Science, Budapest University of Technology and Economics, Műegyetem rkp. 3, Budapest, 1111, HUNGARY

Stevia rebaudiana Bertoni is a small, perennial and herbaceous shrub which originated in Paraguay (South America). *Stevia rebaudiana* is not native to Hungary but its cultivation and consumption may have many benefits, e.g. to reduce blood pressure and as a non-caloric sweetener. *Steviol glycosides*, mostly *stevioside* and *rebaudioside A*, located in the leaves are about 200–300 times sweeter than sucrose. *S. rebaudina* cultivation in Hungary would offer many opportunities in healthcare and the sweet industry. With the aim of achieving good green biomass yields, the effect of MACC4 autotrophic and heterotrophic algae strains was investigated by testing them as both leaf and soil fertilizers in the soil of *Stevia rebaudiana* seedlings and in its aqueous rooting experiments. In one of the later set up, the formation of roots was improved by combining the application of red light and algae treatment.

Keywords: *Stevia rebaudiana*, *Steviol glycosides*, algae treatment, *Chlorella vulgaris*

1. Introduction

Stevia rebaudiana Bertoni (Fig. 1) is a perennial shrub and a member of the *Asteraceae* family. Stevia originated in Brazil and Paraguay (South America). This plant is widely used by the Guaraní Indians of South America to sweeten tea [1, 2]. *S. rebaudiana* was botanically classified in 1899 by Moisés Santiago Bertoni, who described it in more detail. Initially called *Eupatorium rebaudianum*, its name changed to *S. rebaudiana* (Bertoni) in 1905.

The sweet principle was first isolated in 1909 and only in 1931 was the extract purified to produce stevioside, its chemical structure was established in 1952 as a diterpene glycoside. Stevioside (Fig. 2) is described as a glycoside comprised of three glucose molecules attached to an aglycone referred to as steviol moiety [3, 4]. *S. rebaudiana* also has other names like Sweet leaf, Sweet Herb of Paraguay, Sweet Honey Leaf and candyleaf. The sweetening components of the plant, i.e. steviol glycosides, were described in 1931 [5]. *S. rebaudiana* and its extracts have been used for a long time in Asia, South America and several countries in Europe. *S. rebaudiana* leaves and highly refined extracts are used as low-calorie sweeteners in Korea, Japan and Brazil [6]. Stevioside, one of the steviol glycosides, has been reported to lower the postprandial blood glucose concentration of Type II diabetics and the blood pressure of mildly hypertensive patients [7]. *S. rebaudiana* is used by diabetics as a diet therapy, and its extracts exhibit pharmacological effects such as anti-insulin resistance, the promotion of insulin secretion, as well as antihypertensive and anti-obesity properties [8]. Nowadays, the utilization of alternative sweeteners has become a viable option for producing low- or zero-calorie foods due to the development of the healthy food industry which intends to reduce the sucrose content of food products by the total or partial replacement of sucrose with alternative sweeteners.

Figure 1: Stevia rebaudiana

Steviol glycosides are mainly produced in the leaves of the plant. The major components are steviol, stevioside and rebaudioside A. The typical proportions of the major components of the leaves are stevioside (5–10 % of the

*Correspondence: naron@f-labor.mkt.bme.hu

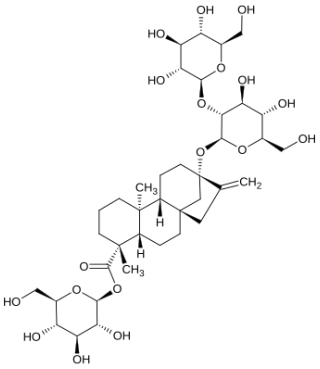

Figure 2: Structure of stevioside

total dry weight of the leaves), Reb A (2–4 %), Reb C (1–2 %) and dulcoside A (0.4–0.7 %) [9].

The leaves of*S. rebaudiana* are sessile, 3-4 cm in length, elongate-lanceolate or spatulate in shape with blunt-tipped laminae in addition to serrated margins from the middle to the tip and on the entire underside. The upper surface of the leaves is slightly glandular-pubescent. The stem is weak-pubescent at its base and woody. The rhizome has slightly branching roots. Flowers are composite surrounded by an involucre of epicalyx. The capitula are in loose, irregular, sympodial cymes. The flowers (Fig. 3) are white and pentamerous [5].

This plant can grow up to 1 m tall if it is exposed to sufficient light and receives enough nutrients as well as water. Therefore, it is worth considering the examination of crop production due to its wide range of applications.

Chlorella vulgaris is a eukaryotic unicellular green algae which is one of the fastest growing microalgae. This algae can be used in biodiesel processing following cell cultivation. The economic feasibility of algal biodiesel production highly depends on the biomass productivity and lipid yield [10]. Green algae (like *Chlorella vulgaris*) may produce phytohormones which can influence the growth of plants. Odgerel et al. used *Chlorella vulgaris* as a biofertilizer on barley and wheat. Faheed et al. used *C. vulgaris* as a biofertilizer on lettuce plants. These results showed that algae treatment yields longer roots and shoots of wheat compared to control [11, 12].

The aim of our work was to test *Chlorella vulgaris*

Figure 3: Stevia rebaudiana flowers

Figure 4: Plant cells

MACC4 autotrophic and heterotrophic cultures of microalgae to enhance the roots, biomass and stems of *S. rebaudiana*.

2. Materials and methods

In our work, the effects of hormones produced by algae on *S. rebaudiana* were tested. Phytohormones may improve its development. The plants were in a phytotron (25±1 °C) where they received 16 hours of light per day. Each plant was placed in a 4.5 cm × 5.0 cm planting cell (Fig. 4).

In Table 1, the blue background denotes the root-growing experiments where seedlings were placed into water as a control and into an aqueous algal suspension for trials. Furthermore, the green background indicates the modeling of experiments in land: while seedlings in samples of commercial potting soil were sprinkled with water as a control and an algal suspension as to test changes in biomass, the growth of roots and stems was recorded in terms of weight and length, respectively. Cells were replicated three times for each setting.

As algal suspensions, *Chlorella vulgaris* MACC4 heterotrophic and autotrophic cultivated strains were used. The cell suspension was diluted by up to 300 times with water to achieve a concentration of 5×10^7 colony-forming units (CFU)/ml. From this solution, 2 ml was sprinkled onto each cell every 2 to 3 days.

The duration of the experiments was about five weeks. At the end of the fifth week (Fig. 5), the mass of the total green biomass and the length of the stem and roots in both water and soil were measured. For the results a statistical evaluation was conducted with Minitab 17 statistical software. The statistical analysis consisted of a two-sample

Table 1: Planting cells (H: heterotrophic, A: autotrophic, C: control, Green: seedlings in soil, Blue: seedlings in water, White: empty cells)

1. H	5. C	9. -	13. H	17. C	21. A
2. H	6. C	10. -	14. H	18. C	22. A
3. H	7. C	11. -	15. H	19. C	23. A
4. A	8. A	12. A	16. -	20. -	24. -

Figure 5: S. rebaudiana plants at the end of the experiment

t-test where the algae-treatment samples were compared against the controls and each other.

3. Results and discussion

The two-sample t-test in terms of the growth in biomass observed in the seedlings planted in soil is presented in Fig. 6. The p-value shows whether or not the treatment had an effect on biomass growth.

The comparison between heterotrophic algae treatment and the control samples is presented in Fig. 6A. The p-value was 0.653, i.e. no significant difference exists between the two groups of results that were examined. A comparison between the heterotrophic and autrotrophic algae cultures is presented in Fig. 6B. The p-value was 0.511, i.e. no significant difference exists between them. A contrast is made between the autotrophic algae treatment and the control samples in Fig. 6C. The p-value was 0.316, i.e. no significant difference exists between these groups either. From the results it can be seen that algae treatment does not have a positive effect on the growth of the green biomass of *S. rebaudiana* with regard to model experiments in soil.

The two-sample t-tests in terms of stem growth are presented in Fig. 7. A comparison between the heterotrophic algae treatment and the control samples is presented in Fig. 7A. The p-value was 0.642, i.e. no significant difference exists between them. The results of heterotrophic versus autotrophic algae treatment cultures are shown in Fig. 7B. The p-value was 0.055, i.e. once more no significant difference exists between them. A contrast between autotrophic algae treatment and control samples is presented in Fig. 7C. The p-value was 0.147, i.e. yet again no significant difference exists between both groups. From these results it can be concluded that no significant improvements were observed in terms of the yield of plant biomass of algae treatments applied to seedlings planted in soil. However, the autotrophic al-

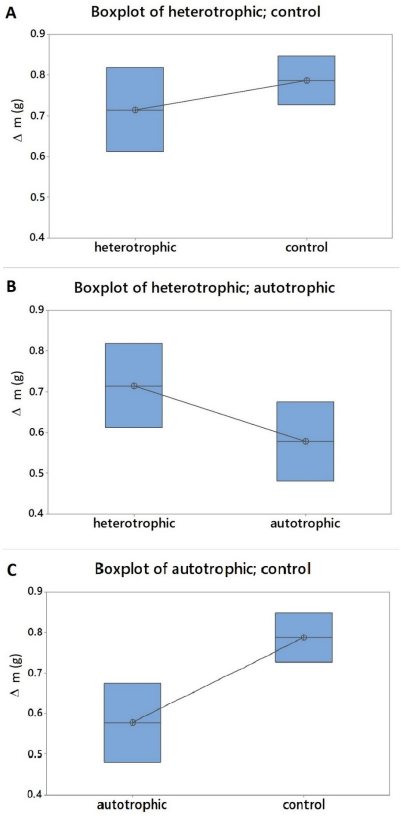

Figure 6: Box plots of two-sample t-tests: biomass growth in soil (A: heterotrophic algae vs. control, B: heterotrophic vs. autotrophic algae, C: autotrophic algae vs. control).

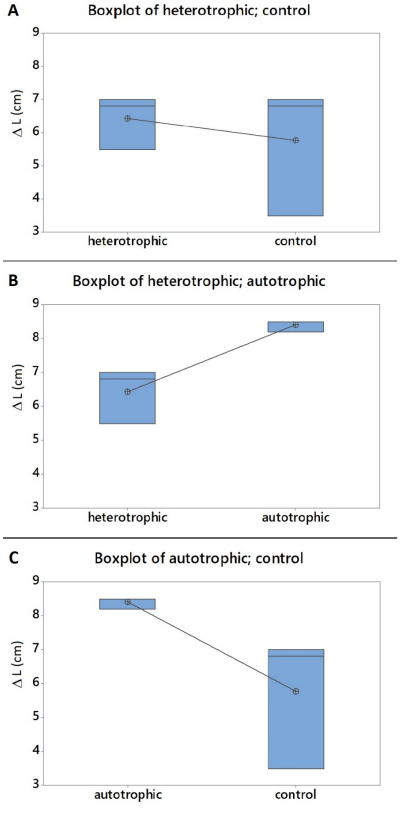

Figure 7: Box plots of two-sample t-tests in terms of stem growth in soil: (A: heterotrophic algae vs. control, B: heterotrophic vs. autotrophic algae, C: autotrophic algae vs. control)

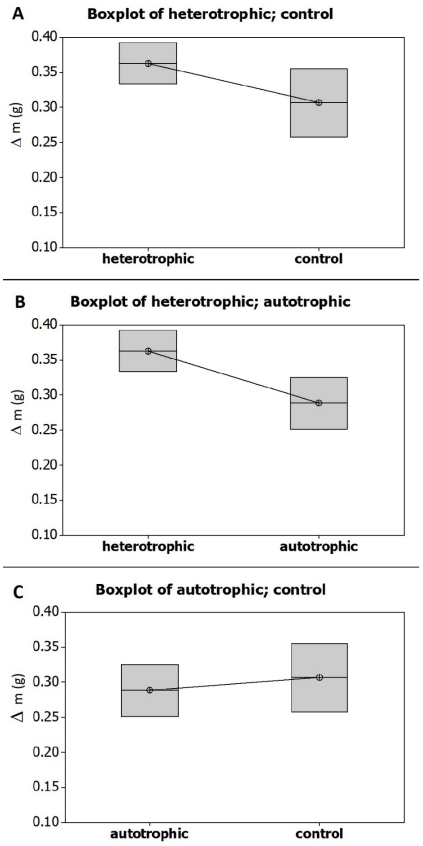

Figure 8: Box plots of two-sample t-tests in terms of root growth in land (A: heterotrophic algae vs. control, B: heterotrophic vs. autotrophic algae, C: autotrophic algae vs. control)

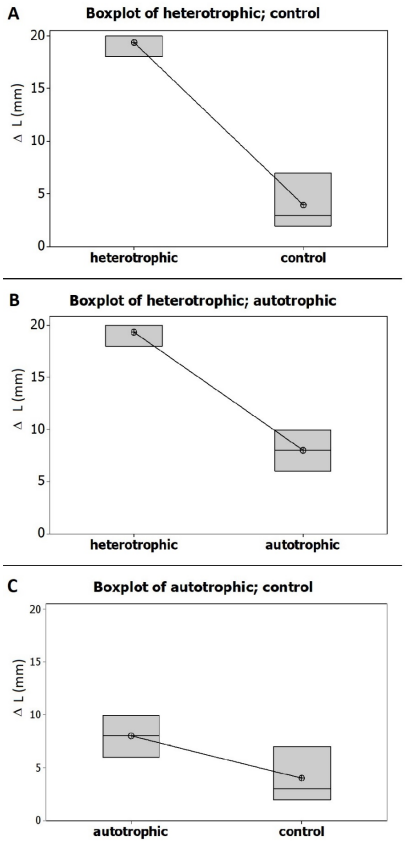

Figure 9: Box plots of two-sample t-tests in terms of root growth in water (A: heterotrophic algae vs. control, B: heterotrophic vs. autotrophic algae, C: autotrophic algae vs. control)

gae treatment seemed to be the most significant which suggests a weak positive effect in terms of the plant development of *S. rebaudiana* in soil may occur.

The two-sample t-tests in terms of the root growth observed in soil are presented in Fig.8. A comparison between heterotrophic algae treatment and the control samples is presented in Fig. 8A. The p-value was 0.503, i.e. no significant difference exists between them. A contrast between the heterotrophic and autotrophic algae treatments is shown in Fig. 8B. The p-value was 0.357, i.e. no significant difference exists between them either. The difference between autotrophic algae treatment and the control samples is presented in Fig. 8C. The p-value was 0.811, i.e. once again no significant difference exists between the examined two groups of results. These results suggest (without significance) that heterotrophic algae cultures maybe preferred for the root development of *S. rebaudiana* seedlings in soil.

The two-sample t-tests in terms of the root growth in water are presented in Fig. 9. A comparison between heterotrophic algae treatment and the control samples is shown in Fig. 9A. The p-value was 0.012, i.e. a significant difference exists between them and heterotrophic treatment is beneficial. A contrast between heterotrophic and autotrophic algae treatments is presented in Fig. 9B. The p-value was 0.003, i.e. a significant difference exists between them and heterotrophic algae treatment is also beneficial. The difference between autotrophic algae treatment and the control samples is shown in Fig. 9C. The p-value was 0.128, i.e. no significant difference exists between them. From these results it can be concluded that while heterotrophic algae treatment was found to be significantly advantageous for the root development of *S. rebaudiana* in water, the effect of autotrophic cultures did not significantly differ from that of the control samples.

In soil a lateral-like root was formed, while in water the formation of a thicker root was observed. Just like when the root fibers were grown in land, not all the soil could be washed out without damaging the root. Therefore, a comparison between the biomass yield in water and soil was not conducted.

4. Conclusion

The following conclusions can be drawn from the experiments with regard to the growth of *S. rebaudiana*. Neither heterotrophic nor autotrophic algae treatments had any positive effect on the biomass growth in soil. By examining the stem growth, the autotrophic culture seemed

to have a slightly positive effect but was not significant. In terms of root growth in soil, none of the treatments had any significant effect, but heterotrophic cultures seemed to have a slightly positive effect. Root growth in water supplemented regularly with heterotrophic algae cultures had a significant positive effect in comparison to the other treatments. Probably the positive effect of algae treatment in the case of the experiments on *S. rebaudiana* seedlings in water can be attributed to the fact that the applied algae provided complex nutrients unlike the pure tap water, while in the case of the experiments on seedlings in soil the additional nutrients provided by the algae treatment was practically negligible in comparison to those offered by the soil.

Therefore, further studies will be done to separate the effect of algae as a provider of nutrients and as a source of plant hormones.

Further studies would be necessary to prove whether changes in algae cell concentrations have an effect on the growth of *Stevia rebaudiana* or not, i.e. in soil, experiments on biomass growth should be applied differently in diluted algae suspensions with and without any additional nitrogen sources. Moreover, different types of light, e.g. red, blue and white, will be tested. These additional plant studies will be implemented using larger numbers of samples.

REFERENCES

[1] Geuns, J. M. C.: Stevioside. *Phytochemistry*, 2003 **64**(5), 913–921 DOI: 10.1016/S0031-9422(03)00426-6

[2] Kaur, G.; Pandhair, V.; Cheema, G. S.: Extraction and characterization of steviol glycosides from *Stevia rebaudiana bertoni* leaves. *J. Med. Plants. Stud.*, 2014 **2**(5), 41–45 ISSN: 2320-3862

[3] Lemus-Mondaca, R.; Vega-Gálvez, A.; Zura-Bravo, L.; Kong, A. H.: *Stevia rebaudiana Bertoni*, source of a high-potency natural sweetener: A comprehensive review on the biochemical, nutritional and functional aspects. *Food Chem.*, 2012 **132**(3) 1121–1132 DOI: 10.1016/j.foodchem.2011.11.140

[4] Barriocanal, L. A.; Palacios, M.; Benitez, G.; Benitez, S.; Jimenez, J. T.; Jimenez, N.; Rojas, V.: Apparent lack of pharmacological effect of steviol glycosides used as sweeteners in humans. A pilot study of repeated exposures in some normotensive and hypotensive individuals and in Type 1 and Type 2 diabetics. *Regul. Toxicol. Pharmacol.*, 2008 **51**(1), 37–41 DOI: 10.1016/j.yrtph.2008.02.006

[5] Madan, S.; Ahmad, S.; Singh, G. N.; Kohli, K.; Kumar, Y.; Singh, R.; Garg, M.: Stevia rebaudiana (Bert.) Bertoni – A Review. *Indian J. Nat. Prod. Resour.*, 2010 **1**(3), 267–286 ISBN: 3216321509, ISSN: 09760504

[6] Kinghorn, A. D. (ed.): Stevia - The genus Stevia in: Hardman, R. (ed.) Medicinal and aromatic plants – Industrial profiles series Vol. 19, CRC Press, Taylor & Francis, London UK, 2003. ISBN: 0-203-16594-2

[7] Gregersen, S.; Jeppesen, P. B.; Holst, J. J.; Hermansen, K.: Antihyperglycemic effects of stevioside in type 2 diabetic subjects. *Metabolism*, 2004 **53**(1), 73–76 DOI: 10.1016/j.metabol.2003.07.013

[8] Dyrskog, S. E. U.; Jeppesen, P. B.; Colombo, M.; Abudula, R.; Hermansen, K: Preventive effects of a soy-based diet supplemented with stevioside on the development of the metabolic syndrome and type 2 diabetes in Zucker diabetic fatty rats. *Metabolism*, 2005 **54**(9), 1181–1188 DOI: 10.1016/j.metabol.2005.03.026

[9] Puri, M.; Sharma, D.; Tiwari, A. K.: Downstream processing of stevioside and its potential applications. *Biotechnol. Adv.*, 2011 **29**(6), 781–791 DOI: 10.1016/j.biotechadv.2011.06.006

[10] Kim, J.; Lee, J-Y.: Growth kinetic study of *Chlorella vulgaris* (August 2016), pp. 2–7. 2009. ISBN: 9781615679140

[11] Odgerel, B.; Tserendulam, D.: Effect of Chlorella as a biofertilizer on germination of wheat and barley grains *Proc. Mong. Acad. Sci.*, 2017 **56**(4) 26 DOI: 10.5564/pmas.v56i4.839

[12] Faheed, F. A.: Effect of Chlorella vulgaris as biofertilizer on growth parameters and metabolic aspects of lettuce plant. *J. Agri. Soc. Sci.*, 2008 **4**(4) 165-169 ISSN: 1813-2235

DE GRUYTER OPEN

HUNGARIAN JOURNAL OF INDUSTRY AND CHEMISTRY
Vol. 46(2) pp. 79–84 (2018)
hjic.mk.uni-pannon.hu
DOI: 10.1515/hjic-2018-0023

HUNGARIAN JOURNAL OF INDUSTRY AND CHEMISTRY
HJIC

COMPARISON OF PARTICLE SIZE DISTRIBUTION MODELS FOR POLYMER SWELLING

ÁDÁM WIRNHARDT *[1] AND TAMÁS VARGA[1]

[1]Department of Process Engineering, University of Pannonia, Egyetem u. 10, Veszprém H-8200, HUNGARY

In polymer technologies, various particle shapes and size distributions can be found. One of these are heterodisperse polymer beads. The capabilities of polymer swelling can be used in industries, e.g in the production of ion-exchange resins, to intensify specific technological steps such as sulphonation in the manufacturing process of ion-exchange resins. According to the literature different approaches can be used to create models for describing the behavior of disperse systems, of which the simplest models are the particle size distribution models for a given state of the solid phase. The aim of our examination was to compare and evaluate these simple models in terms of modeling polymer swelling. Hence, most of these models examine how each of the investigated models can be applied to approximately describe growth in a heterodisperse polymer system and how the identified model parameters in each time step could be interpreted. All the models were fitted to generate particle size distributions based on a swelling rate constant. The swelling of a styrene divinylbenzene-based copolymer was chosen as the basis of our examination. A model is proposed that is capable of describing the changes in the size of beads over time in this system.

Keywords: polymer swelling, particle size distribution, heterodisperse polymer beads, modeling, ion-exchange resin

1. Introduction

Polymer beads are used as raw materials in a wide range of technologies, e.g. in the production of ion-exchange resins. Before the chemical modification of polymer beads, they are often swollen with different types of swelling agents such as dichloroethane, dichloromethane, toluene, etc.

Monodisperse and heterodisperse types of beads are known in polymer technologies. The process of the swelling of monodisperse beads is easily measurable and easily predictable. The production of monodisperse polymers is a more expensive process than the production of heterodisperse beads, which makes heterodisperse polymer beads a more popular form.

Heterodisperse polymer beads exhibit a closely normal distribution in terms of particle size. The prediction of the swelling of these particle systems is more difficult because the different beads can swell at significantly different rates due to the change in the specific area of each bead.

The swelling of the polymer network system has already been a subject of interest. Painter and Shenoy[1] considered the chemical properties of polymers. Schott [2] described the kinetics of polymer swelling. First order and second order kinetics were founded by him. A swelling model was formulated by Sweijen et al. [3] according to the diffusion properties of components in the polymer matrix. These models are capable of describing the swelling of polymer networks, but because of its complexity they are hard to apply in any kind of optimization process. Hence, the simplest particle size distribution (PSD) model, which can describe the swelling of polymers over time using the least number of parameters, can be of interest from a process intensification point of view.

Bayat et al. collected PSD models from the last seventy years [4, 5]. Thirty-five models were listed. These models describe the cumulative mass fraction of polymers as a function of the diameter of polymer beads. The models contain one, two, three or four unknown parameters, which can be identified with a specific polymer fraction. A hyperbolic tangent distribution [6, 7] PSD model composed of four parameters was added to this list by us.

This study is the first step in the process of developing this model which focuses on the investigation of the swelling phenomena of the styrene divinylbenzene copolymer system. Therefore, our focus is on identifying a simple PSD model which is capable of describing the swelling of heterodisperse polymer beads. Hence, all the previously mentioned PSD models are investigated and compared. Our aim was not only to identify a PSD model which is capable of describing the distribution of the investigated polymer system but to find a PSD model which

*Correspondence: wirnhardt.adam@fmt.uni-pannon.hu

exhibits a correlation between changes made to parameters and particle size.

2. Experimental

For the modelling of heterodisperse polymer systems physical experiments with regard to swelling should be performed to obtain the data necessary to validate the model. In our case, with the lack of experiments, the data were generated from a model implemented and solved in MATLAB. A code was made in MATLAB for the generation of these distributions. In the developed model, the swelling of polymer beads with a given theoretical rate of growth was calculated. The volume of each bead increased at the same rate. Hence, the diameter of the beads does not influence the rate of growth and the tension caused by the swelling process of the polymer beads is neglected in this investigation. The following simplifications were implemented in the model:

1. The shape of the polymer beads is a perfect sphere.
2. The particles swell until they reach a steady state.
3. The swelling rate of particles is constant until a steady state is achieved.
4. The number of particles is constant.
5. The initial PSD of the beads is close to normal.

To generate the distributions after different durations of swelling an initial unswollen distribution is required. The initial distribution was calculated by MATLAB from a picture of heterodispersed particles. The Varion KS preform styrene divinylbenzene copolymer was used for the zero-time distribution. The polymer beads were identified by a circle detection algorithm and the size distribution of the detected particles was calculated using a reference particle.

From the initial state, the size of the polymer particles starts to increase by applying a swelling agent to the system. The size of the particles increases until a steady state is achieved. The steady state in this case means that the size of the particles grows until a state when the amount of infiltration of the swelling agent is equal to the outcome amount. The size of the particles can increase until a maximum is reached because of the internal tension of the polymer. The data are generated using the parameters of the steady state. These parameters are the swelling rate (p [-]) and time required (t [sec]).

PSDs were generated at different times during the swelling process. The next step was to examine the PSD models to determine if they were able to describe the distribution in every instant.

2.1 PSD models

In this study only PSD models that are capable of describing cumulative mass fraction distribution were investigated. Altogether five models with one parameter, twelve with two, two with three and four with four were examined. They are collected in Table 1.

The cumulative mass fraction of particles is denoted by $P(d)$, the maxima and minima of the particle size range are represented by $d_{\max}$ and $d_{\min}$, respectively, and the particle diameter [mm] is denoted by d. The models were fitted to all the distributions collected over time using extreme value problem solver algorithms in MATLAB.

2.2 Theoretical methodologies

Two types of extreme value problem-solving methods were applied to fit the PSD models. One is a local extreme value problem solver known as the Nelder-Mead simplex algorithm and its function "fminsearch" to implement it in MATLAB. The other one is a global extreme value problem solver called "NOMAD" [8]. They are both components of the MATLAB toolkit.

MATLAB 2011b was applied in all modelling steps. The minimum difference was sought between the generated distribution data and calculated distributions based on each model. The parameters of PSD models were the results of this search. In every case, the goodness of fit was measured. For each model, every sample time was considered and the difference examined using the mean absolute difference. The average of the mean absolute difference of the percentage difference was calculated for every function. The extreme value problem solver attempted to find the minimum of the following equation

$$E_t = \frac{\left|P\left(d\right)'_t - P(d)_t\right|}{n_d} \tag{1}$$

where the mean absolute difference between the generated and calculated distribution is E_t at instant t. The calculated distribution is denoted by $P\left(d\right)'_t$ and the generated distribution by $P(d)_t$ at instant t. The number of items of data is represented by n_d.

2.3 Model selection

A selection could be made according to the average percentage differences. The selection was carried out with a criterion. This criterion was an average percentage difference of five percent because under this value the difference is not considerable but over it an unacceptable fit is shown. Three different models, namely the Rosin-Rammler, the Exponential-power_Pasikatan and the Logarithm-Zhuang models fitted to the generated data are shown in Fig. 1. The goodness of fit for these three models is 1 %, 5 % and 11 %, respectively. As can be seen the differences of 1 % and 5 % are negligible, and are only noticeable at diameters in excess of 0.7 mm. However, a considerable difference can be observed between the models with fits of 5 % and 11 %. It can be seen that a goodness of fit of under 5 % is appropriate.

Table 1: The investigated PSD models

	Name	**Model**
	1 parameter (k_1)	
1	Gaudy-Meloy	$P(d) = 1 - (1 - d/d_{\max})^{k_1}$
2	Nesbitt-Breytenbach	$P(d) = 10[(1/(k_1+1)](d/2)^{k_1+1}$ $+[0.1 - 1/(k_1+1)](d/2)^{1/[1/(k_1+1)-0.1]}$
3	Rosin-Rammler	$P(d) = 1 - \exp(-k_1 d)$
4	Jaky	$P(d) = \exp\left\{-\left(1/k_1^2\right)\left[\ln(d/d_{\max})\right]^2\right\}$
5	Schumann	$P(d) = (d/d_{\max})^{k_1}$
	2 parameters (k_1, k_2)	
6	Power low- Paskikatan	$P(d) = [k_1/(1-k_2)]d^{1-k_2}$
7	van Genuchten	$P(d) = \left[1 + (k_1/d)^{k_2}\right]^{1/k_2-1}$
8	Rosin-Rammler	$P(d) = 1 - \exp\left(-k_1 d^{k_2}\right)$
9	Fractal	$P(d) = \exp\{\ln(k_2))+$ $\left[\left(3k_1^2 - 13k_1 + 14\right) / \left(k_1^2 - 5k_1 + 4\right) + 1\right]\log(d)\}$
10	Power low - Gimenez	$P(d) = k_1 d^{k_2}$
11	BEST	$P(d) = \left[1 + (k_1/d)^{k_2}\right]^{2/k_2-1}$
12	Bennet	$P(d) = k_1 k_2 d^{k_1-1}\exp\left(-k_2 d^{k_1}\right)$
13	Exponential power- Pasikatan	$P(d) = \exp\left(-k_1 d^{k_2}\right)$
14	Logarithm-Zhuang	$P(d) = k_1 \ln(d) + k_2$
15	Log-exp-Kolev	$P(d) = k_1 \exp\left[k_2 \log(d)\right]$
16	Weibull-2par	$P(d) = 1 - \exp\left[-(d/k_1)^{k_2}\right]$
17	Lognormal- Zobeek	$P(d) = 1/\left\{k_1(2\pi)^{1/2}\exp\left[-(\log(d) - k_2)^2/(2k_1^2)\right]\right\}$
	3 parameters (k_1, k_2, k_3)	
18	S-Curve: Vipulanandan Ozgurel	$P(d) = 100\exp\left\{-k_1\left[k_2\ln(d/0.001)^{d/k_3}\right]\right\}$
19	Weibull-3par	$P(d) = k_1 - \exp\left[-(d/k_2)^{k_3}\right]$
	4 parameters (k_1, k_2, k_3, k_4)	
20	Gompertz	$P(d) = k_1 + k_2\exp\{-\exp\left[-k_3(d-k_4)\right]\}$
21	Weibull-4par	$P(d) = k_3 + (1-k_3)\left[1 - \exp\left(-k_1 k_4^{k_2}\right)\right]$ where $k_4 = (d - d_{\min})/(d_{\max} - d_{\min})$
22	Fredlund	$P(d) = \left\{1/\left[\ln\left(\exp(1) + (k_1/k_2)^{k_2}\right)\right]^{k_3}\right\}$ $\left\{1 - \left[\ln(1 + k_4/d)/\ln(1 + k_4/0.001)\right]^7\right\}$
23	Tanh	if $0<k_2+k_3 d$ then $P(d) = \left\{\tanh\left[(k_2 + k_3 d)^{k_4}\right]\right\}^{k_1}$ otherwise $P(d) = 0$

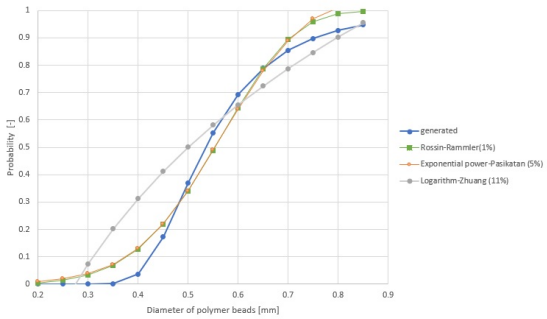

Figure 1: The cumulative distribution of the Rosin-Rammler (1 %), Exponential-power Pasikatan (5 %) and Logarithm-Zhuang (11 %) models as well as the generated data.

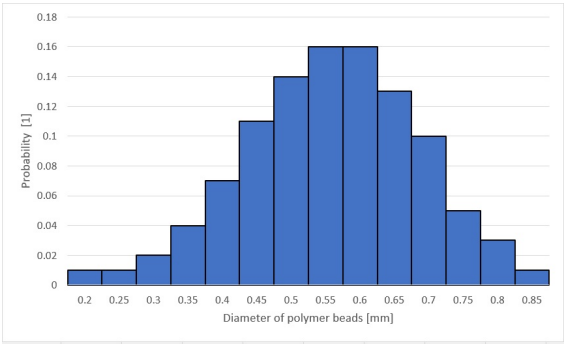

Figure 2: The probability distribution with regard to the size of the polymer beads before swelling within the diameter range of 0.2 to 0.9 mm.

2.4 Parameter correlation

The next step in the modelling process was the investigation into how the model parameters of each simple PSD model can be fitted into a monotonous series over time. Based on this experiment, these simple models can be applied to describe the swelling of specific material systems over time.

By depicting the parameters of the distribution functions as a function of time, a statement can be made for the models if they were capable of this task. Assuming that the correlation is linear for every model parameter, in each PSD model it can be calculated as follows:

$$k_x = A_x + B_x t \tag{2}$$

where the parameter of the PSD model is denoted by k_x, the parameters of the k parameter are A and B, and the time passed is t.

It is obvious that there are twice as many unknown model parameters than in the previous step, i.e. every model parameter in each model is defined by Eq. 2, however, only one set of parameters is required to describe the swelling process over time. In this examination, the mean absolute difference was also needed to fit the functions to different time instants. In this case the extreme value problem solver determined the minimum for the average of the mean absolute difference:

$$\overline{E} = \frac{\sum_{t=1}^{n_t} E_t}{n_t} \tag{3}$$

where the average of the mean absolute difference is denoted by $\overline{E}$ and the number of time instants by n_t.

3. Results and analysis

The zero distribution was evaluated by MATLAB based on a picture taken from a sample of polymer beads. The sample consisted of approximately five hundred beads within the diameter range of 0.2 to 0.9 mm. The probability distribution with regard to the size of the polymer beads is shown in Fig. 2.

The parameters for the generated data were $p = 2$ and $t = 1500$ s which means the polymer beads doubled their size in 1500 s and the steady-state size of the beads is this rate of growth. PSD was calculated twenty-five times between 0 and 1500 s. Three of the twenty-five distributions are shown in Fig. 3.

All 23 models were fitted to all the distributions generated at every instant. Altogether twenty-three times twenty-five curve fittings were performed. The parameters were calculated for all the fitted models. For every fitted value a mean absolute difference (E_t) was determined, the average of which are shown in Table 2

According to the values in Table 1 a selection of PSD models could be made. Those models show good agreement with the generated PSD, which yields an average mean absolute difference of less than five percent. A difference can be observed between the two methods to find extreme values. The global finder "NOMAD" has found a better fit for the two-parameter model known as BEST. In most cases the two search methods give the same results using the same model parameters. In some models, the global optimizer has found a better solution than was expected.

Eleven of the twenty-three models were found to be able to describe the distribution at all time instants. From

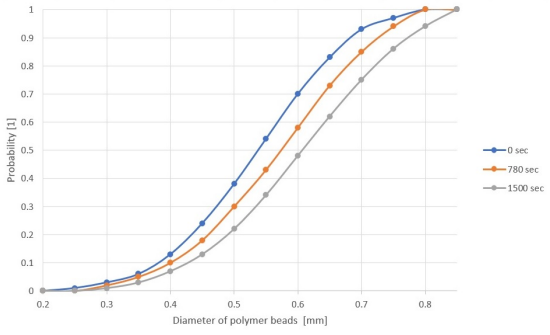

Figure 3: Cumulative distribution functions at three different time instants during the swelling of the polymer beads.

Table 2: The goodness of fit for the different models.

PSD Model ID	SIMPLEX fitting $\overline{E}$ [%]	NOMAD fitting $\overline{E}$ [%]
1	15	15
2	39	39
3	24	24
4	**2**	**2**
5	10	10
6	12	8
7	**3**	3
8	**1**	**1**
9	19	13
10	8	9
11	39	**2**
12	**5**	**5**
13	**5**	**5**
14	12	12
15	8	8
16	**1**	**1**
17	30	30
18	35	13
19	**0**	**0**
20	**2**	**1**
21	**1**	**1**
22	37	34
23	**1**	**1**

these, the best model was the Weibull-3par which is shown in Fig. 4. This result does not mean that the model is able to describe polymer growth. A correlation should be present in terms of changing the parameters.

By examining the correlation of model parameters in these eleven models, one model called Jaky exhibited a correlation as shown in Fig. 5 The other models did not show any kind of correlation over time.

The Jaky model consists of one parameter and it seems to describe properly the growth of heterodisperse polymer systems. The other models did not show any correlation in terms of the changing of the parameter over time. In most cases one parameter was present which did

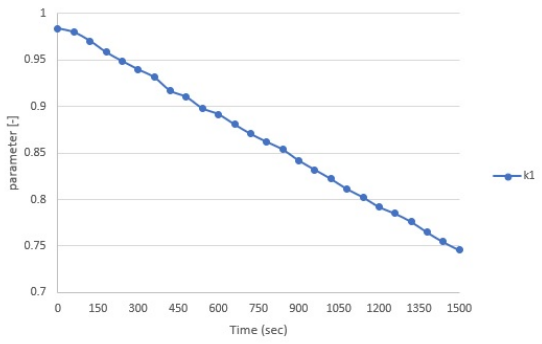

Figure 4: The change in the parameter of the Weibull-3par model after various durations of swelling.

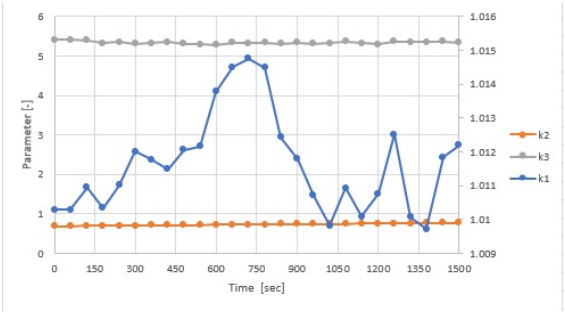

Figure 5: The change in the parameter of the Jaky model after various durations of swelling.

not show any regularity as is shown in Fig. 4.

The following examination sought to set a correlation between the change in the parameter and time due to the swelling of beads. With linear criteria (see Eq. 2) the goodness of fit will definitely deteriorate. The presumption was to find a model which exhibits a goodness of fit of under five percent after setting the criterion.

The results collected in Table 3 show that two of the eleven selected models produced a goodness of fit of under 5 %, the others were all in excess of 30 %. Therefore, the Jaky model consisting of one parameter and the Rosin-Rammler model of two exhibit a linear correlation for their parameters over time. The other nine models did not exhibit a linear correlation in their parameters over time. It would be worthwhile trying other non-linear functions to describe the parameters.

4. Conclusion

In polymer technologies, one of the steps is the swelling of the polymer beads. Several studies were conducted that deal with the swelling of polymer networks. Our aim was to examine the swelling of the polymer beads from a different point of view to find out if a simple PSD model exists which may be able to describe changes in size of this system.

Table 3: The goodness of fit of the linear correlation of parameters over time.

PSD Model ID	SIMPLEX fitting $\overline{E}$ [%]	NOMAD fitting $\overline{E}$ [%]
4	2	2
7	33	14
8	1	1
11	–	44
12	44	44
13	53	44
16	44	44
19	35	35
20	35	35
21	30	52
23	44	44

PSD models were examined according to their ability to describe the swelling of polymer beads. The results show that two models were present which could be used to describe and predict the behavior with regard to changes in size of the heterodisperse polymer bead systems.

In this examination, the copolymer styrene divinylbenzene was used. Two extreme value problem solvers were used to identify and confirm PSD models that are able to describe changes in size of the copolymer system.

Two models, namely the one-parameter Jaky model and the two-parameter Rosin-Rammler model, were able to describe the growth in size over time with an error of less than 2 %. The parameters of these models could be interpreted by a linear correlation over time according to the generated data that was produced in this study. Based on these working models a prediction can be made with regard to changes in size of a heterodisperse copolymer system over time.

Symbols

E_t	Mean absolute difference
$\overline{E}$	Average of mean absolute difference
$P\left(d\right)_t'$	Calculated distribution
$P(d)_t$	Generated distribution
n_d	Number of data
n_t	Number of time instants
k_x	Parameters of models

Acknowledgment

This research was supported by the Széchenyi 2020 project GINOP 2.2.1-15-2017-00059.

REFERENCES

[1] Painter, P.C.; Shenoy, S.L.: A simple model for the swelling of polymer networks, *J. Chem. Phys.*, 1993 **99**(2), 1409-1418 DOI: 10.1063/1.465385

[2] Schott, H.: Swelling kinetics of polymers, *J. Macromol. Sci., Part B: Physics*, 1992 **31**(1), 1-9 DOI: 10.1080/00222349208215453

[3] Sweijen, T.; van Duijn, C.J.; Hassanizadeh, S.M.: A model for diffusion of water into a swelling particle with a free boundary: Application to a super absorbent polymer particle, *Chem. Eng. Sci.*, 2017 **172**, 407-413 DOI: 10.1016/j.ces.2017.06.045

[4] Bayat, H.; Rastgou, M.; Nemes, A.; Mansourizadeh, M.; Zamani, P.: Mathematical models for soil particle-size distribution and their overall and fraction-wise fitting to measurements, *Eur. J. Soil Sci.*, 2017 **68**(3), 345-364 DOI: 10.1111/ejss.12423

[5] Bayat, H.; Rastgo, M.; Zadeh, M.M.; Vereecken, H.: Particle size distribution models, their characteristics and fitting capability, *J. Hydrology*, 2015 **529**, 872-889 DOI: 10.1016/j.jhydrol.2015.08.067

[6] Blickle, T.; Lakatos, B.G.; Ulbert, Zs.; Mihálykó, Cs.: The hyperbolic tangent distribution and its applications-I. mathematical foundations, *Hung. J. Ind. Chem.*, 1998 **26**, 89-96

[7] Blickle, T.; Lakatos, B.G.; Mihálykó, Cs.; Ulbert, Zs.: The hyperbolic tangent distribution family, *Powder Technology*, 1998 **97**, 100-108

[8] Le Digabel, S.: Algorithm 909: NOMAD: Nonlinear Optimization with the MADS Algorithm, *ACM Trans. Math. Softw.*, 2011 **37**(4), 1–15 DOI: 10.1145/1916461.1916468

DE GRUYTER OPEN

HUNGARIAN JOURNAL OF INDUSTRY AND CHEMISTRY
Vol. 46(2) pp. 85–90 (2018)
hjic.mk.uni-pannon.hu
DOI: 10.1515/hjic-2018-0024

HUNGARIAN JOURNAL OF INDUSTRY AND CHEMISTRY
HJIC

EFFECTS OF DIFFERENT HEAT TREATMENTS ON THE CHEMICAL AND MICROBIOLOGICAL CHARACTERISTICS OF EGG-FREE AND QUAIL EGG DRIED PASTA

ILDIKÓ SZEDLJAK *[1], VIKTÓRIA TÓTH[1], JUDIT TORMÁSI[1], ANIKÓ KOVÁCS[1], LÁSZLÓ SOMOGYI[1], LÁSZLÓ SIPOS[2], AND GABRIELLA KISKÓ[3]

[1]Department of Grain and Industrial Plant Processing, Faculty of Food Science, Szent István University, Villányi út 23, Budapest, 1113, HUNGARY
[2]Department of Logistics and Sensory Analysis, Faculty of Food Science, Szent István University, Villányi út 23, Budapest, 1113, HUNGARY
[3]Department of Microbiology and Biotechnology, Faculty of Food Science, Szent István University, Villányi út 23, Budapest, 1113, HUNGARY

In Hungary, dried pasta products are very popular amongst all groups of society. In recent years the demand for not only dried pasta made from hen eggs (*Gallus gallus domesticus*) but from alternative types of ingredients has increased. However, according to the literature the chemical and microbiological characteristics of this type of pasta have yet to be studied in depth. The effects of the use of quail eggs and heat treatments at different temperatures were studied by chemical and microbiological measurements. The activity of oxidative enzymes and nutritional characteristics (water-soluble total polyphenol content, water-soluble antioxidant capacity, peroxidase enzymatic activity, water-soluble protein content and yellow pigment content) was tested during our experiments. The data were evaluated by relevant statistical methods. Significant differences were found both between heat treatments and between the egg content of the dried pasta samples. The peroxidase enzymatic activity and yellow pigment content increased with temperature. However, the usage of quail eggs provides a higher water-soluble protein content and water-soluble antioxidant capacity. The presence of microorganisms is decreased by increasing the drying temperature. The number of all the examined microorganisms was within limits.

Keywords: dried pasta, quail egg, heat treatment, chemical and microbiological characteristics

1. Introduction

Present-day problems of globalization have led to a need for more diverse, long-lasting and convenient food products of high nutritional value. Mindful consumers look for products that have positive physiological effects and have been subject to a minimal degree of processing.

In Hungary, dried pasta products are popular amongst all groups of society. Their position in the global market is safe because these products possess all of the aforementioned qualities and fall within an affordable price range too. The amount of dried pasta products consumed in recent years has elevated [1], therefore, the food industry continuously tries to lower production costs as well as improve profits and their nutritional value [2].

One of the important ingredients of pasta are eggs. For the industrial processing of dried pasta only two kinds of eggs are usable; hen and quail eggs.

The most commonly used type of eggs are hen eggs (*Gallus gallus domesticus*). Pasta products made from this type of eggs have been well studied. However, recently a need has emerged for more unconventional dried pastas made from alternative ingredients [3].

Quail egg pasta (*Coturnix coturnix*) is one of these innovations. Quail eggs as an ingredient are of a relatively high nutritional value. When compared to hen eggs they possess more protein but less carbohydrate and fat [4].

Chemical changes during processing define the quality of the end product. The most determinative factors are the temperature of the drying process and its changes during the process [5]. Significant changes in chemical behavior occur even at lower temperatures. Enzyme-activated changes like protein denaturation and pigment oxidation take place below 60 °C. At temperatures higher than 80 °C the oxidative enzymes deactivate and the Maillard reaction occurs, simultaneously the lysine concentration of the pasta decreases [6]. Therefore, choosing the most suitable drying temperature is an important step when it comes to the quality of the heat-treated products, especially in the case of dried pastas.

When designing and processing products with long

*Correspondence: ildiko.szedljak@gmail.com

storage and shelf lives, another important concern is the microbiological safety of the product. With the diminished water activity of these kinds of foods, the activity of microorganisms also decreases. The main parameter in this case is the number of microorganisms when processing commences. During drying the microbes deactivate and their numbers decrease [7].

Chemical and microbiological properties depend on the nutritional characteristics and drying properties of the pasta. Since the chemical and microbiological characteristics of quail egg pasta, according to the literature, have yet to be studied in depth, our goal was to expand this knowledge. Studying the properties of this product is beneficial to both advancing the technology and food safety.

2. Experimental

The aim of our study was to examine and compare the chemical and microbiological characteristics of the egg-free and quail egg dried pasta that had been subjected to different heat treatments. Changes caused by the presence of quail eggs were sought. Differences made by varying the temperature of heat treatments were examined. Moreover, a connection between the microbiome and heat treatments was characterized.

Materials The wheat flour, *Triticum aestivum L.*, used and the quail eggs were bought from commercial sources. The reagents for the chemical and microbiological measurements were provided by Reanal Laborvegyszer Kereskedelmi Kft. The bacterial substrates were produced by Merck Kft.

Samples The tests were conducted on the samples of egg-free and "four hen egg pasta" doughs using sufficient quantities of quail eggs.

All the pastas were made from *Triticum aestivum L.* flour, water and quail eggs for the egg pasta. To improve the heat distribution the pastas were shaped into the form of linguine. The pasta doughs were treated at three different temperatures (40 °C, 60 °C and 80 °C) for twenty-five minutes in an Armfield-type fluid bed dryer.

The samples were subjected to chemical and microbiological measurements. In preparation for the chemical tests the samples were first grated then 100 mg/ml extracts were taken using distilled water. Every analytical method was conducted on five parallel samples.

Chemical Analysis The moisture content was determined by an MA50 Sartorius Moisture Analyzer. The water activity was measured by a Novasina MS1 water activity meter. For the measurement of color the Konica Minolta CR-310 Chroma Meter with a tristimulant objective in a laboratory coordinate system was used. To measure the pH, the SG23 Mettler-Toledo SevenGo Duo pH/conductivity meter was used. The acid values of the extracted samples were titrated with 0.1 M NaOH solution in the presence of the indicator phenolphthalein. The determination of pH and acid value was conducted based on Hungarian standards [8].

The water-soluble total polyphenol content was measured by Folin-Ciocalteu reagent [9] and expressed in gallic acid equvalent (GAE). Water-soluble antioxidant capacity was measured using a FRAP (ferric reducing antioxidant power) Assay Kit [10]. The peroxidase enzymatic activity was given by using ODA (o-dianisidine) as a hydrogen donor [11] and the data converted into ascorbic acid equivalent (AAE). For measuring the water-soluble protein content, a method by Layne [12] was used. The yellow pigment content of the samples was determined according to Hungarian standards extracted by butanol [13].

Microbiological Analysis Microbiological measurements were conducted given the relevant standards [14–16]. Three parallel measurements were made from each sample. All samples were tested for coliform bacteria, *Staphylococcus aureus* and molds. In addition, the presence of *Salmonella* using a European standard [17] was tested for.

Statistical Evaluation All the measurements were replicated five times using XLSTAT software [18]. Given the parallel samples, non-parametric probes were used. The Kruskal-Wallis test was applied to calculate the p-value ($\alpha = 0.05$) and Dunn's post hoc pair-wise test was used with Bonferroni correction on significant results. The correlation between parameters was determined by Spearman's rank correlation coefficient (non-parametric equivalent of Pearson's correlation) ($\alpha = 0.05$).

3. Results and Analysis

3.1 Chemical Analysis

Moisture content The moisture content of the dried pasta samples decreased as the temperature of heat treatment increased. The moisture content of all the dried pasta products was below the maximum set by Hungarian standards [19] of 13 %. When treated at the same temperature the quail egg pastas always contained less moisture than the egg-free samples. However, significant differences were not determined.

Water activity This parameter is important for determining the initial microbial count and activity of samples during storage. The water activity of the samples decreased as the temperature of the heat treatment increased. In the quail egg pastas, the numbers were higher ($\mathrm{aw}(80°\mathrm{C}) = 0.6254 \pm 0.0313$) compared to commercially available pastas ($\mathrm{aw} < 0.6$). Thus, at this level of water activity the xerotolerant and xerofil microbes could survive and reproduce. A significant difference was not determined.

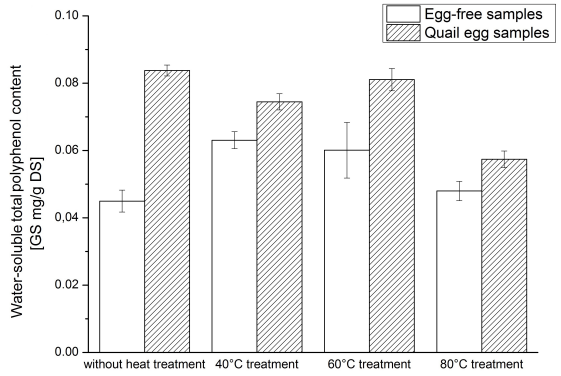

Figure 1: Water-soluble total polyphenol content of the samples in mg/g gallic acid equivalent.

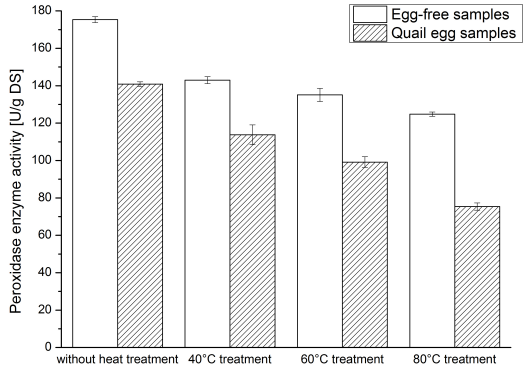

Figure 2: Peroxidase enzyme activity of the samples in U/g DS.

pH The pH also plays a key role in the reproduction and survival of microorganisms as well as in the activity of peroxidase. The pH of the quail egg samples was always lower than the egg-free samples. A significant difference was only measured in the quail egg (3.572 ± 0.128) and egg-free (5.898 ± 0.019) samples treated at 40 °C. Since the molds are capable of reproducing at a lower pH (pH = 2–4) [20], this value of the quail egg pasta poses a threat from a microbiological point of view.

Acid value (AV) This parameter was always lower in the quail egg samples. In the samples dried at 60 °C, significant differences were observed. All the acid values of measured samples were between 3.15 and 3.66 °SH, which falls within the Codex Alimentarius Hungaricus' guidelines [19] (in dried pastas AV = maximum of 5 °SH).

Water-soluble total polyphenol content For evaluating the water-soluble total polyphenol content (TPC) of the samples, the data was calibrated with the gallic acid equivalent as shown in Fig. 1, which gives the polyphenolic components in mg of gallic acid equivalent found in 1 gram of dried pasta.

The presence of the quail eggs resulted in higher water-soluble total polyphenol contents in each case. Significant differences based on the coupled comparison's p-values were only observed between the samples that were not heat treated.

Based on the results of the Kruskal-Wallis test a significant difference is observed between the TPC values of quail egg pastas. Among the quail egg samples, based on the comparison of pairwise p-values, a difference is found for at least two samples. This can be detected between the samples that were not heat treated and those treated at 80 °C as well as between samples treated at 60 °C and at 80 °C.

Based on these results, it can be stated that the TPC may be influenced by heat treatment.

Peroxidase enzymatic activity The peroxidase enzymatic activity was calculated on the basis of data from the literature and its value was given in terms of dry matter content (Björkstén, 1968). The graph in Fig. 2 clearly shows the effect of heat treatment. The enzymatic activity decreases as the temperature of the heat treatment increases and is always lower in the quail egg samples. The cause of this difference could be the different pH of the two types of pastas.

In both cases a significant difference is observed between the samples treated at 60 °C and those not subjected to heat treatment. In the results of the egg-free pastas, the decline is less than in the quail egg samples.

Water-soluble protein content The water-soluble protein content was always higher in the quail egg samples. Significant differences were observed between both the separate and cumulative evaluations. A significant difference was measured in the p-values in terms of the comparison of egg content when heat treated at 40 °C. In addition differences were observed between the egg-free samples that were not subjected to heat treatment and those heat treated at 80 °C, as well as between the quail egg samples that were not heat treated and those treated at 40 °C and 80 °C.

From these results it can be stated that the examined treatments influence the water-soluble protein content of the samples.

Water-soluble antioxidant capacity The measurements of the water-soluble antioxidant capacity were converted into ascorbic acid equivalent. The antioxidant capacity of the pastas rose as the temperature of the heat treatments increased, in terms of the egg-free samples, the maximum was observed at 60 °C. The statistical evaluation revealed significant differences in every case. The increase in the antioxidant capacity as the temperature of heat treatment rises is common in the literature [21, 22].

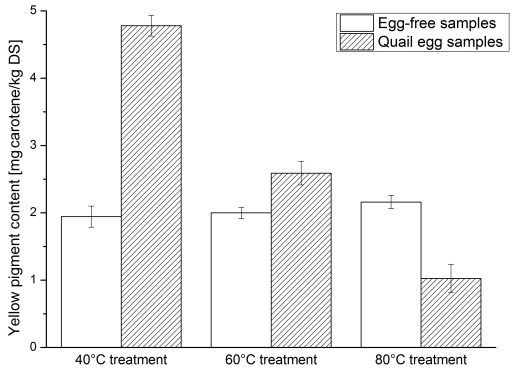

Figure 3: Yellow pigment content of samples given in mg carotene/kg DS.

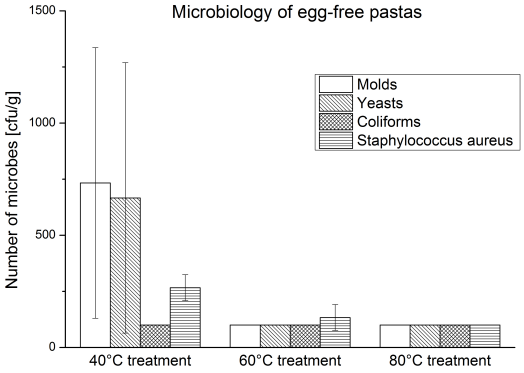

Figure 5: The results of the microbiological analysis of egg-free pastas.

Yellow pigment content and color measurement The yellow pigment content was only measured on samples of dried pasta. Both the egg-free and quail egg pastas exhibited significant differences between samples treated at 40 °C and 80 °C. As seen in Fig. 3 in the case of the quail egg samples, a significant decline in the yellow pigment content was observed as the temperature of heat treatment increased. Even so, the noticeable drop in the yellow pigment content of quail egg samples was still higher than in the case of the egg-free samples (except for the decline at 80 °C).

For the assessment of color the "LAB" color chart was used. The L^* value denotes the lightness and positive rate of the b^* value which represents the intensity of the color yellow. Neither of these two values changed significantly in the presence of the quail eggs. However, the heat treatment resulted in significant changes in both color rates. A significant change in the lightness has already been observed in all the samples treated at 40 °C. As shown in Fig. 4 the b^* value increased as the temperature of heat treatment rose, therefore, the pastas became yellower as the temperature increased. In both types of pastas, significant differences were observed between the samples that were not subjected to heat treatment and those treated at higher temperatures (60 °C and 80 °C).

The results of the yellow pigment content and color measurements are controversial in terms of the quail egg samples. The b^* value – which shows the intensity of the color yellow – increases while the yellow pigment content decreases. The seemingly ambiguous data might be caused by chemical and microbiological changes not examined by us.

The yellow pigment content continuously decreases during the drying process, therefore, choosing the most suitable drying temperature is critical. From these results, to retain the maximum amount of yellow pigments in the finished products, heat treatment at 60 °C is recommended.

3.2 Microbiological measurements

The microbiological contamination of egg-free samples remained below the limit (Figs. 5 and 6).

However, in the case of the quail egg pasta, the coliform bacteria appeared in the samples treated at 40 °C. The presence of the coliforms is not surprising since they

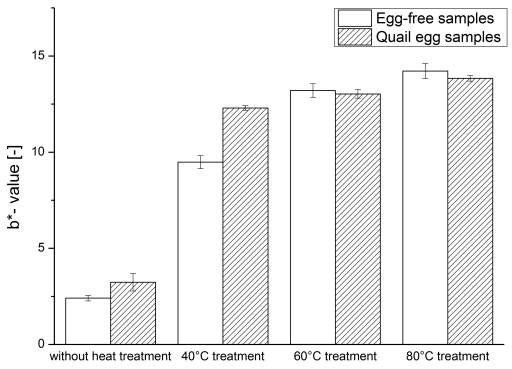

Figure 4: Yellow color intensity of samples from the CIELAB color space.

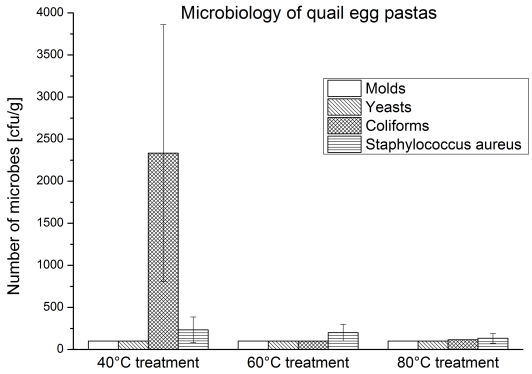

Figure 6: The results of the microbiological analysis of quail egg pastas.

Table 1: Spearman correlation matrix of the six studied parameters, "r" values ($r = 0$ no linear correlation, $r = -1$ perfect negative correlation, $r = 1$ perfect positive correlation).

Variables	POX	TPC	L^*	b^*	Antioxidant capacity	Yellow pigment content
Peroxidase enzymatic activity	**0**	0.2283	**0.0000**	**0.0159**	0.7815	0.8270
Total polyphenol content	0.2283	**0**	0.0502	**0.0009**	**0.0001**	**0.0024**
L^*	**<0.0001**	0.0502	**0**	0.5675	0.6137	0.4238
b^*	**0.0159**	**0.0009**	0.5675	**0**	**0.0016**	0.1523
Antioxidant capacity	0.7815	**0.0001**	0.6137	**0.0016**	**0**	0.1723
Yellow pigment content	0.8270	**0.0024**	0.4238	0.1523	0.1723	**0**

Values in bold are different from 0 with a significance level $\alpha = 0.05$

Table 2: Spearman coefficient determination matrix of the six studied parameters, "p" values

Variables	POX	TPC	L^*	b^*	Antioxidant capacity	Yellow pigment content
Peroxidase enzymatic activity	**1**	0.0512	0.4894	0.1930	0.0028	0.0017
Total polyphenol content	0.0512	**1**	0.1307	0.3397	0.4304	0.2910
L*	0.4894	0.1307	**1**	0.0117	0.0092	0.0228
b*	0.1930	0.3397	0.0117	**1**	0.3118	0.0717
Antioxidant capacity	0.0028	0.4304	0.0092	0.3118	**1**	0.0653
Yellow pigment content	0.0017	0.2910	0.0228	0.0717	0.0653	**1**

are found in the feces of warm-blooded animals (Bíró, 2014). As a result of the heat treatment the number of microbes decreased in both types of pasta. Based on these results it can be clearly seen that heat treatment increases the quality of both types of pasta from a microbiological standpoint. The higher the temperature of the heat treatment, the more microbiologically advantageous it is.

3.3 Statistical evaluation

In addition to the examination of significant differences between our data, correlation studies were conducted on six selected variables of the evaluated factors: peroxidase enzymatic activity (POX), water-soluble total polyphenol content (TPC), L^* and b^* values, yellow pigment content and water-soluble antioxidant capacity. Since five parallel measurements were taken, Spearman correlations were determined [23], which is the nonparametric equivalent of the Pearson's correlation.

Based on the obtained "r" and "p" values (Tables 1 and 2), two positive and three negative correlations were identified. The positive correlations were between the water-soluble total polyphenol content and yellow pigment content as well as between the water-soluble antioxidant capacity and b^* values. The negative correlations were identified between the peroxidase enzymatic activity and L^* value as well as b^* values, the water-soluble total polyphenol content and b^* values, in addition to the water-soluble total polyphenol content and water-soluble antioxidant capacity.

4. Conclusion

The aim of this study was to expand the literature on the chemical and microbiological characteristics of quail-egg dried pastas.

With regard to the nutritional value of the pastas almost all of the examined characteristics declined as the temperature of the heat treatment increased except for the water-soluble antioxidant capacity. From our study it was found that the heat treatments at 80 °C were the most effective. Based on these results, heat treatments at high temperatures (80 °C) are recommended especially from a microbiological point of view. The samples should also be maintained at this temperature for at least twenty-five minutes. Such treatment would ensure the production of higher quality and safer products.

While the industrial use of quail eggs causes technological and economic problems, this study could be a starting point for further research in this field.

REFERENCES

[1] International Pasta Organization – Survey. The world pasta industry in 2012; 2013.

http://www.internationalpasta.org

[2] Kumar S. B., Prabhasankar P., Low glycemic index ingredients and modified starches in wheat based food processing: A review, *Trends Food Science Technology* 2014 **35**(1), 32–41 DOI: 10.1016/j.tifs.2013.10.007

[3] Csapó J., Vargáné V. É., Élelmiszerkémia (*Food Chemistry)*, (University of Kaposvár, Kaposvár) 2011 http://www.tankonyvtar.hu/hu/tartalom/tamop425/0059_elelmiszerkemia/adatok.html

[4] Miguel M., Manso M. A., Lopez-Fandino R., Ramos M., Comparative study of egg white proteins from different species by chromatographic and electrophoretic methods, *European Food Research and Technology* 2005 **221**(3), 542–546 DOI: 10.1007/s00217-005-1182-8

[5] Anese M., Nicoli M. C., Massini R., Lerici C. R., Effects of drying processing on the Maillard reaction in pasta, *Food Research International* 1999 **32**(3), 193–199 DOI: 10.1016/S0963-9969(99)00076-9

[6] Dexter J. E., Tkachuk R., Matsuo R. R., Amino Acid Composition of Spaghetti: Effect of Drying Conditions on Total and Available Lysine, *Journal of Food Science* 1984 **49**(1), 225–228 DOI: 10.1111/j.1365-2621.1984.tb13713.x

[7] Lang E., Zoz F., Iaconelli C., Recovery Estimation of Dried Foodborne Pathogens Is Directly Related to Rehydration Kinetics, *PLoS ONE* 2016 **11**(8), e0160844 DOI: 10.1371/journal.pone.0160844

[8] MSZ 6369-1:1985 Flour test methods. Sensory analysis. Scoring and qualification

[9] Singleton V. L., Rossi J. A. Jr., Colorimetry of total phenolics with phosphomolybdic-phosphotungstic acid reagents, *American Journal of Enology and Viticulture* 1965 **16**(3), 144–158 DOI: 10.12691/ijebb-2-1-5

[10] Benzie I. F., Strain J. J., The ferric reducing ability of plasma (FRAP) as a measure of "antioxidant power": The FRAP assay, *Analytical Biochemistry* 1996 **239**(1), 70–76 DOI: 10.1006/abio.1996.0292

[11] Björkstén F., Participation of horseradish oxyperoxidase (compound 3) in interenzymic reaction steps, *Biochimica et Biophysica Acta* 1968 **154**(1), 309–311 DOI: 10.1016/0005-2744(68)90196-4

[12] Layne E., Spectrophotometric and Turbidimetric Methods for Measuring Proteins (Colowick P. S. and Kaplan N. O., Eds., Methods in Enzymology, Academic Press, Inc., New York) 1957, 447–454 OCLC number: 757246524

[13] MSZ 20500-2:1985 Pastry products. Test methods. Chemical analysis

[14] MSZ ISO 7954:1999 Microbiology - General guidance for enumeration of yeasts and moulds - Colony count technique at 25 °C

[15] ISO 4832:2006 Microbiology of food and animal feeding stuffs - Horizontal method for the enumeration of coliforms - Colony-count technique

[16] MSZ EN ISO 6888-1:2008 Microbiology of food and animal feeding stuffs. Horizontal method for the enumeration of coagulase-positive staphylococci (Staphylococcus aureus and other species). Part 1: Technique using Baird-Parker agar medium (ISO 6888-1:1999)

[17] MSZ EN ISO 6579:2006 Microbiology of food and animal feeding stuffs. Horizontal method for the detection of Salmonella spp. (ISO 6579:2002)

[18] XLSTAT software, Addinsoft 28 West 27th Street, Suite 503, New York, NY 10001 USA

[19] Codex Alimentarius Hungaricus 2-321 Dried pasta products

[20] Bíró G., Élelmiszer-higiénia (*Food Hygiene)* (Agroinform Kiadó, Educatio) 2014 https://www.tankonyvtar.hu/hu/tartalom/tamop425/2011_0001_533_ElelmiszerHigienia/index.html

[21] Muyonga J. H., Andabati B., Ssepuuya G., Effect of heat processing on selected grain amaranth physicochemical properties, *Food Science and Nutrition* 2014 **2**(1), 9–16 DOI: 10.1002/fsn3.75

[22] Phisut N., Jiraporn B., Characteristics and antioxidant activity of Maillard reaction products derived from chitoan-sugar solution, *International Food Research Journal* 2013 **20**(3), 1077–1085

[23] Sajtos L., Mitev A., SPSS kutatási és adatelemzési kézikönyv (*SPSS research and data analysis manual*) 2007 (Budapest, Alinea Kiadó, 203–245) ISBN: 978-963-9659-08-7

DE GRUYTER OPEN

HUNGARIAN JOURNAL OF INDUSTRY AND CHEMISTRY
Vol. 46(2) pp. 91–100 (2018)
hjic.mk.uni-pannon.hu
DOI: 10.1515/hjic-2018-0025

HUNGARIAN JOURNAL OF INDUSTRY AND CHEMISTRY
HJIC

OPTIMAL DESIGN AND OPERATION OF BUFFER TANKS UNDER STOCHASTIC CONDITIONS

BÁLINT LEVENTE TARCSAY[1], ÉVA MIHÁLYKÓ-ORBÁN[1], AND CSABA MIHÁLYKÓ *[1]

[1]Department of Mathematics and Computing, University of Pannonia, Egyetem u. 10, Veszprém, H-8200, HUNGARY

Safety regulations demand the elimination of random mistakes and the reliable operation of production units. However, the control and maintenance of batch and semi-continuous processes haalways been difficult. In this paper, a way of preventing malfunctions in batch and semi-continuous processes is presented by using appropriately designed buffer tanks. A stochastic model was investigated in which batch and continuous subsystems were linked by an intermediate storage tank. The main concern was the reliability of the system. Reliable operation was defined as neither the exhaustion of raw materials nor the excessive accumulation of them. The counting processes that describe the random batch-input and random batch-output processes are supposed to be independent homogeneous Poisson processes with different rates. By introducing a function that describes the material in storage, reliable operation is defined as when this function satisfies two inequalities for a time interval of any duration. By applying probabilistic methods, an integral equation is set up for the the reliability. Nevertheless, its analytical solution cannot be determined, hence the values according to a Monte Carlo simulation are approximated. By applying this method, a link could be identified between the necessary initial buffer and tank capacities that belong to a reliability level. Economic investigations were conducted to help determine the optimal initial buffer and tank capacities that satisfy the appointed reliability level.

Keywords: intermediate storage, stochastic modelling, batch system control, Monte Carlo simulation, economic optimization

1. Introduction

During the operations of chemical processes, one often encounters uncertainties. These events can stem from equipment failures, mistakes made by staff managing the process, or bad managerial decisions. These mistakes can often lead to malfunctions which cannot be tolerated in processes using dangerous or very expensive materials. A serious malfunction can cause damage to equipment, force the process to stop, or, in the worst-case scenario, endanger the lives of operators. All of these can cause serious financial damage to a company. Since these malfunctions carry considerable risks, some procedures are designed to be able to withstand and mitigate the effects of random events. A good control system with trained operators can be the key to neutralizing malfunctions. However, in batch and semi-continuous processes the implementation of control systems has always been difficult. One of the best ways to manage these processes is the ISA-88 standard. ISA-88 provides a consistent set of rules as well as terminology for batch control in addition to defining the physical model, procedures and recipes. However, the implementation of a control system which is up to standard is expensive given the costs of equipment, salaries of operators, etc. In the light of these factors, an attempt was made to devise a method for the design and operation of intermediate storages to mitigate the effects of malfunctions and reduce overall costs of equipment and operators in a plant.

Intermediate storages, also known as buffer tanks, are important units in the chemical industry. Throughout the paper the investigated units will be referred to as buffer tanks, intermediate storages or simply as tanks and storages. With these storages the production process can be made safer by creating an emergency reserve to provide raw materials for the operation of other units. The design of buffer tanks is not trivial even when uncertainties are disregarded which are present during the production process [1]. However, to ensure the reliable operation of a device, which is even subject to uncertainties, a more complex approach is required. Therefore, it could prove beneficial to use stochastic models for the design of units since with these models all random variables which define the operation process can be taken into account. Operating and design parameters of the buffer tank must be chosen so that the amount of material stored is always sufficient to satisfy the demands of customers while also providing

*Correspondence: mihalyko@almos.uni-pannon.hu

a reserve of the raw material in question in the event that other units malfunction. Nowadays, models used to determine these parameters under different operating conditions are a significant focus of research [2–5].

These models are closely related to those applied in insurance mathematics to calculate the amount of capital and insurance prices required to operate an insurance company so that the firm can cover the damages of its clients while still turning a profit. Many of the techniques used in that field can be applied following minor adjustments in these cases as well [5, 6].

During the study of chemical processes, infinite intervals of time are often presumed, meanwhile, the probabilities of the material in the tank overflowing or being exhausted are investigated separately. If the process is investigated over an infinite time interval, then the function that defines the reliability of the system can be expressed as a solution of Volterra- or Fredholm-type integral equations. Despite being difficult to solve, it must be noted that they are easier to handle than those that define reliability over a finite time interval. The main reason for this, in the case of finite intervals, is that not only the first occurrence but also the time remaining during the time interval contribute to the reliability of the system. In the case of infinite time intervals, this quantity is constant, namely infinity. If only the probability of the raw material in the tank being exhausted is studied as a function of the initial buffer capacity or the probability of it overflowing as a function of the tank capacity, then only the probability of malfunction as a function of one variable need be investigated [5, 6]. Solving equations with one variable is simpler than solving integral equations that describe the process as a function of two variables, namely initial buffer and tank capacities, supplemented with the time interval. The economical optimization of similar processes has already been conducted in some simpler cases [7].

In this publication, the focus of interest was on investigating the process over a fixed finite time interval where the reliability of the system was treated as a function of two variables. A chemical process was examined where a raw material was loaded into a buffer tank from a batch reactor. Some of this raw material was drained from the tank at randomly chosen intervals for customers as required. Moreover, the raw material could be constantly extracted which fed the unit after the tank had been used to separate components of the raw material and accumulate the key component. This differs from popular models which investigate such processes that by and large only deal with a batch feed and continuous extraction of the raw material.

To investigate the model, a function was defined to express the reliability of the process as a function of the initial buffer and tank capacities. The integral equation satisfied by the function, however, could not be solved analytically, therefore, a Monte Carlo simulation was used to approximate the reliability of the process numerically. Based on the investigations using one variable, a function was applied to the numerical results whose parameters were identified using the least squares method. By applying this function, the initial buffer and tank capacities required could be calculated to ensure the reliable operation of the unit over the examined finite time interval. However, the required degree of reliability could be achieved by an infinite number of parameter combinations. From among these combinations that ensure a safe operation, the optimal parameter pair was determined using economical optimization by considering the incomes and expenditure of the process.

To investigate a process like this based on actual data from a plant, a thorough knowledge of the distribution functions of every random variable present is required. To acquire such data, information about equipment failures or mistakes made by the operators is required which is documented in every chemical plant. Should the demand for the raw material vary, data with regard to economic trends from previous years can be used. If the amount of data is sufficiently large, then various methods can be used to compare the sample with a reference probability distribution. In this way a known cumulative distribution function can be used to approximate the empirical distribution function of the sample.

In this publication, instead of using authentic data, assumptions about the distribution of the random variables were made, however, the techniques shown in this paper can be applied to different distributions as well and by using our methods an answer to design and operation problems using authentic data can be found.

2. The investigated model

The change in mass of a raw material in a buffer tank was studied. The intermediate storage acts as a link between a batch system which feeds the tank and a batch in addition to a semi-continuous processes which both drain material from the tank (Fig. 1). The process was studied over the finite time interval of $[0, T_{\max}]$.

Over the course of the chemical process, the product is synthesised periodically in a batch reactor (1). Then the product, which is a mixture of byproducts, and the key component are fed into the buffer tank (2). The buffer tank, also known as the intermediate storage (2), is linked to a continuously operational unit, e.g. a fractionating column (3), which is responsible for purifying the product by separating the byproducts from the key component. However, as with most processes that produce multiple components, consumer demand is not exclusively focused on the key component but on the raw mixture of products as well. The goal of the plant is to design and operate the intermediate storage in a way which supplies the necessary amount of raw materials for the continuous subsystem whilst satisfying the demands of the clientele. The frequency and volume of consumer demand for the

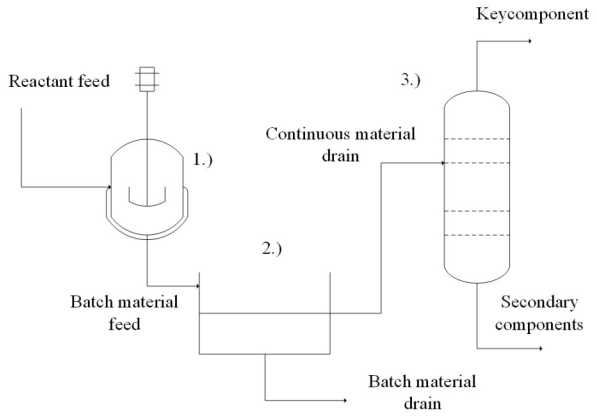

Figure 1: Illustration of the examined process (1. batch reactor, 2. buffer tank, 3. fractionating column).

raw products as well as those of equipment failures and mistakes made by operators within the batch subsystem occur randomly. Due to equipment failures or mistakes made by operators, the batch feeds that originate from the reactor (1) can vary in terms of both mass and time of arrival. The varying amounts and schedule of both feeds and drainings can cause two types of malfunctions to occur, the materials in the tank can either overflow or be completely exhausted which will hinder the rate of production in the continuous subsystem and render it impossible to meet consumer demands.

In the following, the mathematical assumptions of this problem is discussed. Let z_0 denote the initial buffer capacity of the intermediate storage, $z_{\max}$ represent the capacity of the tank, and the duration of the time intervals between the consecutive batch feeds be t_i^{b}, $i = 1, 2, \cdots$ It is assumed that these intervals are independent random variables of the exponential distribution with parameter λ_{l}. In the same way, let the duration of the time intervals between consecutive drainings from the intermediate storage be t_i^{l}, $i = 1, 2, \cdots$ which like the feeds are independent random variables of the exponential distribution with parameter λ_{l}. The number of feeds over time interval T denoted by $N_{\mathrm{b}}(T)$, and the number of periodic drainings by $N_{\mathrm{l}}(T)$, which, because of our assumptions, are random variables of Poisson distribution with parameter $\lambda_{\mathrm{b}} - T$ or $\lambda_{\mathrm{l}} T$, respectively. The amount of raw material fed into the intermediate storage during batch i is denoted by y_i^{b}, similarly the ith draining from the intermediate storage is represented by y_i^{l}. The character c represents the rate at which the raw product was drained from the intermediate storage by the continuous subsystem. The amounts of both the fed and drained batches are assumed to be random variables of identical distribution. The functions $g_{\mathrm{b}}(y)$and $g_{\mathrm{l}}(y)$ are their respective probability density functions. It is supposed that the amounts of materials in addition to the durations of feeds and drainings are independent of each other. Assuming the material in the intermediate storage was neither exhausted nor overflew throughout the operating time T then equation

$$0 < z_0 + \sum_{i=1}^{N_{\mathrm{b}}(T)} y_i^{\mathrm{b}} - \sum_{i=1}^{N_{\mathrm{l}}(T)} y_i^{\mathrm{l}} - cT \leq z_{\max} \qquad (1)$$

must be satisfied by the amount of material currently in the buffer tank. Since these inequalities contain random variables, they can only be fulfilled with a certain probability. The mass of material in the intermediate storage can be expressed by equation

$$z(T) = z_0 + \sum_{i=1}^{N_{\mathrm{b}}(T)} y_i^{\mathrm{b}} - \sum_{i=1}^{N_{\mathrm{l}}(T)} y_i^{\mathrm{l}} - cT, \qquad (2)$$

the reliability of the system, i.e. the probability that the material neither overflows nor is exhausted throughout the time interval $[0, T_{\max}]$, can be defined as shown in equation

$$\Psi(z_0, z_{\max}, T_{\max}) = P\left(0 < z(T) \leq z_{\max}\right) \quad \text{for all } 0 \leq T \leq T_{\max}. \qquad (3)$$

Conversely, $1 - \Psi\left(z_0, z_{\max}, T_{\max}\right)$ is the probability of a malfunction occurring, also referred to as a failure. Both are defined as functions of the initial buffer and tank capacities as well as the operating time.

The expectation of $z(T)$, i.e. $E(z(T))$, can be expressed by

$$E\left(z\left(T\right)\right) = E\left(y_i^{\mathrm{b}}\right)\lambda_{\mathrm{b}} T - E\left(y_i^{\mathrm{l}}\right)\lambda_l T - cT + z_0 \qquad (4)$$

If $0 > E\left(z\left(T\right)\right) - z_0$, then the process has decreasing tendency in average. If $0 < E\left(z\left(T\right)\right) - z_0$, then an overflow can be expected over a large time interval. If $0 = E\left(z\left(T\right)\right) - z_0$, then the process is in equilibrium.

To evaluate the process, the time the failure first occurred is required during the interval $[0, T_{\max}]$, when the amount of material exceeded the capacity of the tank or was equal to zero. The time of failure is defined as the following function:

$$TF\left(z_0, z_{\max}, T_{\max}\right) = \begin{cases} \inf\left\{T : 0 \leq T \leq T_{\max} : z(T) \leq 0 \text{ or } z_{\max} < z(T)\right\}, \text{if such a } T \text{ value exists} \\ \infty, \text{if for all } 0 \leq T \leq T_{\max} \quad 0 < z(T) \leq z_{\max} \end{cases} \qquad (5)$$

This time point is a random variable too, its expectation, $E(TF\,(z_0, z_{\max}, T_{\max}) \cdot 1_{TF(z_0,z_{\max},T_{\max})<\infty})$, will be denoted by $E(TF)$ and its standard deviation by $D(TF)$. They are finite, as $0 \leq TF\,(z_0, z_{\max}, T_{\max}) \cdot 1_{TF(z_0,z_{\max},T_{\max})<\infty} \leq T_{\max}$ is adhered to.

By applying the renewal theory [8], it can be proven that Ψ satisfies the integral equations

$$\Psi\,(z_0, z_{\max}, T_{\max}) = \frac{\lambda_{\mathrm{l}}}{\lambda_{\mathrm{l}}+\lambda_{\mathrm{b}}} \left(\int_0^{\min\left(\frac{z_0}{c}, T_{\max}\right)} \int_0^{z_0-ct_1} \Psi\,(z_0 - ct_1 - y_1, z_{\max}, T_{\max} - t_1) \cdot \lambda_l e^{-\lambda_l t_1} g_{\mathrm{l}}(y_1) dy_1 dt_1 + e^{-\lambda_{\mathrm{l}} T_{\max}} \right) +$$
$$+ \frac{\lambda_{\mathrm{b}}}{\lambda_{\mathrm{l}}+\lambda_{\mathrm{b}}} \left(\int_0^{\min\left(\frac{z_0}{c}, T_{\max}\right)} \int_0^{z_{\max}-(z_0-ct_2)} \Psi\,(z_0 - ct_1 + y_2, z_{\max}, T_{\max} - t_2) \cdot \lambda_{\mathrm{b}} e^{-\lambda_{\mathrm{b}} t_2} g_{\mathrm{b}}(y_2) dy_2 dt_2 + e^{-\lambda_{\mathrm{b}} T_{\max}} \right), \tag{6}$$

if $cT_{\max} \leq z_0$ and

$$\Psi\,(z_0, z_{\max}, T_{\max}) = \frac{\lambda_{\mathrm{l}}}{\lambda_{\mathrm{l}}+\lambda_{\mathrm{b}}} \left(\int_0^{\min\left(\frac{z_0}{c}, T_{\max}\right)} \int_0^{z_0-ct_1} \Psi\,(z_0 - ct_1 - y_1, z_{\max}, T_{\max} - t_1) \cdot \lambda_l e^{-\lambda_{\mathrm{l}} t_1} g_{\mathrm{l}}\,(y_1)\, dy_1 dt_1 \right) +$$
$$+ \frac{\lambda_{\mathrm{b}}}{\lambda_{\mathrm{l}}+\lambda_{\mathrm{b}}} \left(\int_0^{\min\left(\frac{z_0}{c}, T_{\max}\right)} \int_0^{z_{\max}-(z_0-ct_2)} \Psi\,(z_0 - ct_2 + y_2, z_{\max}, T_{\max} - t_2) \cdot \lambda_b e^{-\lambda_{\mathrm{b}} t_2} g_{\mathrm{b}}(y_2) dy_2 dt_2 \right) \tag{7}$$

if $z_0 < cT_{\max}$.

To design a buffer tank which is capable of operating with a desired degree of reliability of $1 - \alpha$ where α denotes the probability of malfunction during the time interval $[0, T_{\max}]$, solutions to equation

$$\Psi\,(z_0, z_{\max}, T_{\max}) = 1 - \alpha \tag{8}$$

must be found.

3. Parameter dependence of the reliability of the process and the expectation of failure time

Since the integral equation proved to be exceedingly difficult to handle analytically, a Monte Carlo simulation to approximate the probability values for different parameters was used. Monte Carlo simulations are more widely accepted tools in dealing with stochastic models [9, 10].

For the simulation environment, MATLAB R2015a [11] was used. Realization of the process when the parameters $T_{\max} = 50$ h, $\lambda_{\mathrm{l}} = 0.3\ \mathrm{h}^{-1}$, $\lambda_{\mathrm{b}} = 0.4\ \mathrm{h}^{-1}$ and $c = 5\ \mathrm{kgh}^{-1}$ were chosen is demonstrated in Fig. 2. The mean of the input suddenly increased in the function $z(t)$, the withdrawals from the batch caused sudden decreases and continuous withdrawal resulted in a reduction in linear parts.

The amounts drained and fed were defined as random variables from the Gaussian distribution. The initial buffer capacity was 50 kg and continuous withdrawal resulted in a linear decrease in the amount of material. At $T = 1$ h, the tank was filled. The amount of material in the tank increased by 3 kg, then the continuous withdrawal resumed. A little bit later a sudden withdrawal occurred. Similar events were repeated at random time points with random quantities. At $T = 7.8$ h a large withdrawal took place and the material became exhausted, therefore, $z(t)$ became negative. The time of failure, in this case the time a shortage was observed, was $TF = 7.8$ h.

Although the process was investigated over an interval of time, it is sufficient to compute the values of $z(t)$ only at those points where sudden changes occurred and at the endpoint of the interval. An overflow could only occur if an input was present. Both continuous and batch withdrawals can cause shortages. If the amount of material at the time points of batch inputs and outputs is com-

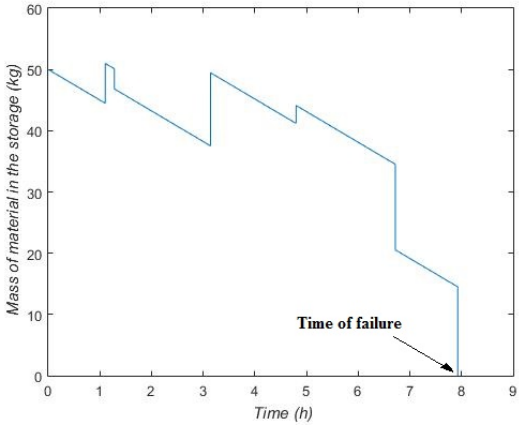

Figure 2: The change in the mass of material in the buffer tank.

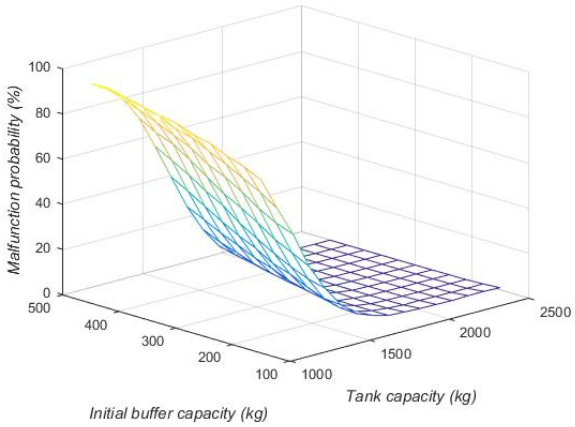

Figure 3: The probability of a failure as a function of the initial buffer and tank capacities.

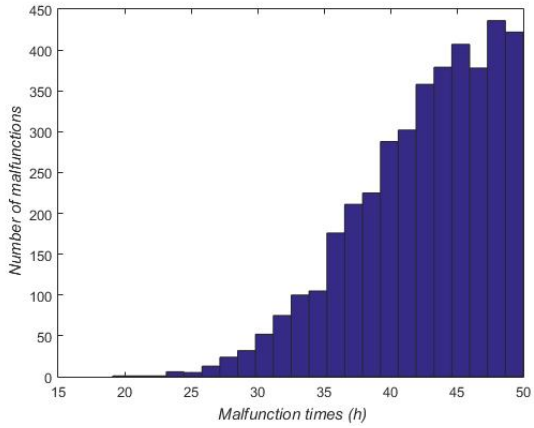

Figure 5: A histogram of the malfunction times.

puted, it can be determined whether or not the continuous withdrawal caused the shortage during the time interval bounded by the last two batch events. If it did, the time point of the shortage can also be computed by solving a linear equation.

By applying a Monte Carlo simulation, the probabilities were approximated by relative frequencies and the expected failure times were estimated by the average times. $10,000$ simulations were conducted which yielded an accuracy 0.01.

For example, $T_{\max} = 50$ h was fixed and the parameters of the process were $\lambda_{\mathrm{l}} = 8\ \mathrm{h}^{-1}$, $\lambda_{\mathrm{b}} = 12\ \mathrm{h}^{-1}$ and $c = 12\ \mathrm{kg\,h}^{-1}$. The amounts drained and fed were defined as random variables from the Gaussian distribution with a mean of 8 kg and a standard deviation of 2 kg. With the aforementioned parameters, the probability of malfunction was calculated and the following results obtained for the process under the indicated conditions (Fig. 3).

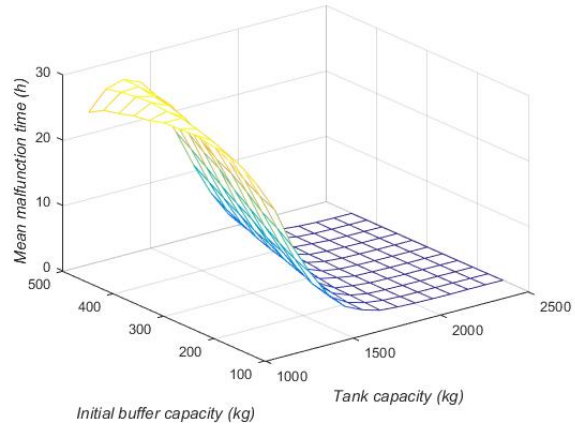

Figure 4: The expected malfunction times as a function of initial buffer and tank capacities.

In Fig. 3 it can be seen that when the tank capacity was fixed, the probability of failure increased as a function of the initial amount of material. This can be explained by the fact that although the likelihood of a shortage decreased, the amount of material in the tank tended to increase, therefore, the free volume of the tank decreased, hence the increase in the probability of overflow. On the other hand, when the initial buffer capacity was fixed, the probability of a failure decreased as a function of the tank capacity. This tendency can be explained by the fact that the probability of overflow decreased and stemmed from the fact that λ_{b} was greater than λ_{l} meaning that the average time intervals between feeds were smaller than those between drainings. This caused the process to be more prone to malfunction due to overflow.

The times of failures (TF) were investigated as well. Expected failure times are shown in Fig. 4 as a function of the initial buffer and tank capacities. If no failure occurred, then TF was equal to zero, therefore, the expected TF was close to zero as well.

A histogram of the malfunction times is provided in Fig. 5 when $z_0 = 400$ kg and $z_{\max} = 1500$ kg. It demonstrates that no quick failures occurred due to a shortage of material resulting in an increase in the amount of material and the tank overflowing. The distribution of the malfunction time in this case is unimodal and the degree of dispersion is quite large. The dispersion of the malfunction time as a function of the initial buffer and tank capacities can be seen in Fig. 6 which demonstrates that when the tank is half full, large standard deviations with regard to the malfunction times were calculated. In the case of large or small capacities, the malfunction time can be accurately predicted as the degree of dispersion is small.

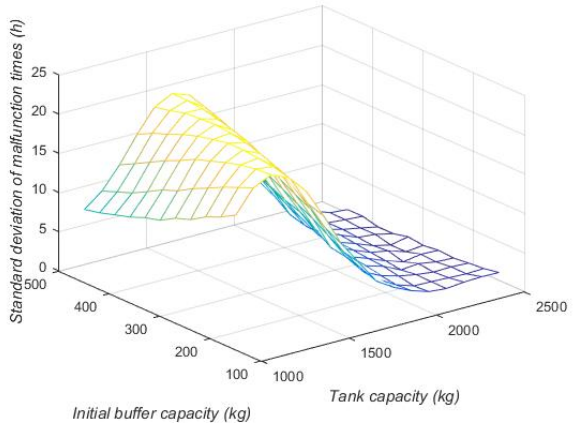

Figure 6: The standard deviation of the malfunction times.

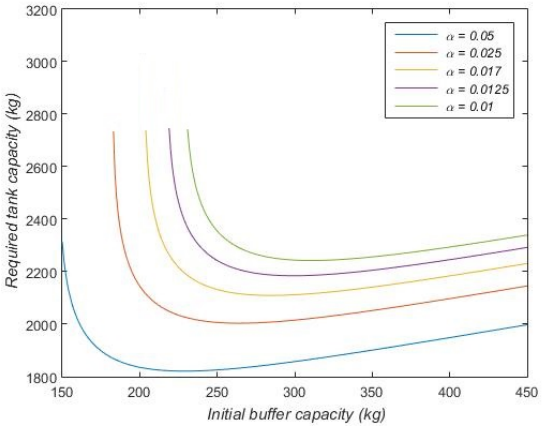

Figure 7: The relationship between the tank and initial buffer capacities that correspond to different levels of reliability $1-\alpha$.

4. Design of the tank and initial buffer capacities for a given reliability level

During previous research, only models that consisted of a batch feed and continuous drainage in the absence of batch drainage [5–7] were studied. In the papers that deal with these models, it has been published that the integral equation for the reliability of the unit could be solved analytically in special cases where the process over an infinite time interval as a function of one variable is observed. In these special cases the solutions to the equation were mainly exponential in form or the linear combination of exponential functions [5, 6]. Consequently, when fitting a function to simulated data, a function was chosen which exhibits similar characteristics.

By fixing $T_{\max}$, seeking Ψ is suggested as a function of the initial buffer capacity x and tank capacity y, in the form of equation

$$H(x,y) = 1 - \left(1 - e^{(-Ax)}\right)^C \left(1 - e^{(-B(y-x))}\right)^D, \tag{9}$$

where $x < y$; A, B, C, and D are positive parameters which have to be optimized. Numerical values of Ψ were computed by a Monte Carlo simulation for some values of z_0 and $z_{\max}$, and the parameters A–D were determined using the least squares method, by minimizing function

$$S(A,B,C,D) = \sum_r \sum_s \left(\Psi(x_r,y_s) - H(x_r,y_s)\right)^2 \tag{10}$$

This function was minimized numerically. The approximated function exhibited a fit to the original function of 95 % on average which was calculated using a Monte Carlo simulation. The error of the fitting was inversely proportional to the number of simulations used to model the system as well as the number of points with regard to the tank and initial buffer capacities investigated. Since the quality of the fit was high (95 % on average), it can be assumed that even if the minimum identified is a local minimum, the approximation is sufficient for use in further computations.

Using the fitted function, equation

$$\begin{aligned} \Psi(x,y) &\sim H(x,y) = \\ &= 1 - \left(1 - e^{-Ax}\right)^C \left(1 - e^{-B(y-x)}\right)^D \\ &= 1 - \alpha. \end{aligned} \tag{11}$$

was solved. Appropriate initial buffer and tank capacities for the process are provided by the solution to the equation above with a reliability of $1-\alpha$ over the time interval $[0, T_{\max}]$.

A link between the values of x and y is provided by the solution to the equation, namely equation

$$y = x - \frac{\ln\left(1 - \left(\frac{1-\alpha}{(1-\exp(-Ax))^C}\right)^{1/D}\right)}{B}. \tag{12}$$

This relationship, using the parameter set presented in the previous section, is given in Fig. 7.

The interval of the initial buffer capacity was $[100, 500]$ kg and the step sizes applied were 100 kg. The interval of the tank capacity was $[1000, 2500]$ kg and the step sizes applied were also 100 kg. To eliminate numerical inaccuracies, the values of the time intervals were transformed into the time intervals $[0, 100]$. By transforming the time intervals into a subset of $[0, 100]$, $A = 0.4966$, $B = 0.12$, $C = 0.9324$, and $D = 86.4875$ were computed. After the computations, the results were transformed into the original time intervals. The required tank capacities as a function of the initial buffer capacity in the intermediate storage corresponding to the reliabilities $1 - \alpha = 0.95, 0.975, \ldots 0.99$ can be seen in Fig. 7.

It can be seen that with some initial values a reliability of 0.99 is infeasible since the likelihood of a shortage itself exceeds level α. The minimum initial amount

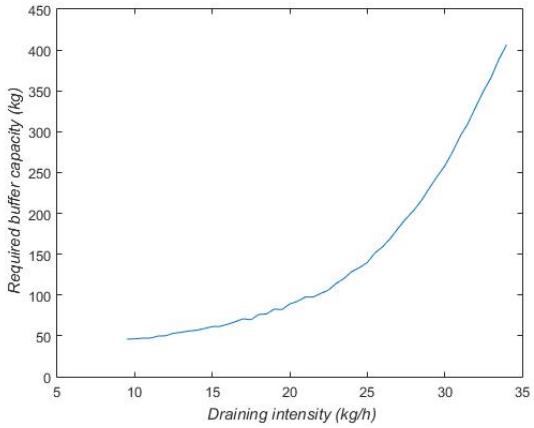

Figure 8: The required initial buffer capacity corresponding to a fixed tank capacity of $1,900$ kg and reliability level of 0.8 as a function of the draining intensity (c) .

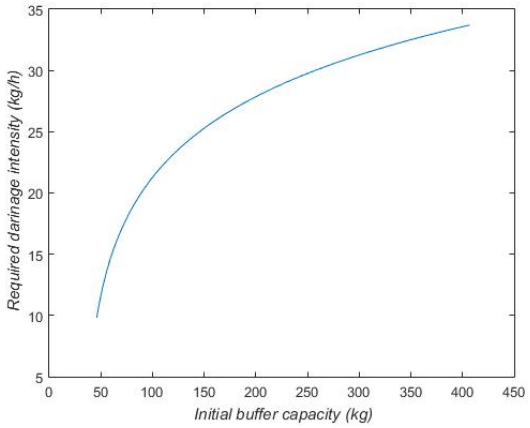

Figure 9: The required drainage intensity corresponding to a fixed tank capacity of $1,900$ kg and a reliability level of 0.8 as a function of the initial buffer capacity.

of material in the intermediate storage with a reliability of $1-\alpha$ can be expressed by

$$\frac{-\ln\left(1-(1-\alpha)^{1/C}\right)}{A} < x_{\min} \tag{13}$$

From Fig. 7 it can be seen that if the lower limit is used as the initial buffer capacity, the corresponding storage capacity is enormous. The reason for this is the fact that the likelihood of a shortage is equal to α and an overflow is undesirable, therefore, the tank capacity must be very large. According to the results shown in Fig. 7, this value is approximately 150 kg. Moreover, if z_0 exceeds a certain level, the function is by and large linear. It is shown by the linear part of the function that when the initial buffer capacity exceeds 250 kg, the likelihood of a failure due to exhaustion of material is almost zero. The likelihood α of an overflow is provided by the difference between the tank and initial buffer capacities. Therefore, to calculate the required tank capacity over this time interval, the volume which can ensure that the likelihood of overflow will remain as α is simply added to the buffer capacity in the intermediate storage.

Finally, the minimum tank capacity that corresponds to a given level of reliability can be determined by numerically minimizing function

$$y = x - \frac{\ln\left(1-\left(\frac{1-\alpha}{(1-\exp(-Ax))^{C}}\right)^{1/D}\right)}{B} \tag{14}$$

For the reliability level $1-\alpha=0.95$, the minimum tank capacity is approximately $1,820$ kg and the required initial buffer capacity approximately 245 kg.

By fixing the tank capacity and reliability level, the dependence of the required initial buffer capacity on the withdrawal rate was investigated. The values of the required initial buffer capacity were determined numerically according to the secant method. The reliability level was $1-\alpha=0.8$ and the tank capacity was $1,900$ kg. The results can be seen in Fig. 8.

According to this result, by increasing the withdrawal rate, the required initial buffer capacity increases sharply which facilitates control of the process.

Finally, the required drainage intensity corresponding to the reliability level of $1-\alpha=0.8$ and fixed tank capacity $z_{\max}=1,900$ kg as a function of the initial buffer capacity was provided (Fig. 9). It can be seen that it is also a monotonically increasing function, but the rate of increase is usually less than in the case of Fig. 8.

5. Economic investigations

According to Fig. 7, if the minimum required amount of initial buffer capacity is supplied then the required level of reliability of the process can be achieved by an infinite number of combinations of tank and initial buffer capacities. To determine the optimal combination, economic evaluations of the design are recommended. It is assumed that following a possible failure, the process is restarted, however, such a restart is time-consuming and expensive. During the calculations both the income and expenditure associated with each parameter are taken into account. These include the costs of raw materials, the buffer tank, malfunctions and repairs as well as the income generated from sales of both the key component and raw product. To determine the income generated by the process at time T, equation

$$\begin{aligned} Q(T) &= G_{\text{key}}(T)+G_{\text{raw}}(T)-K_{\text{mat}}(T)- \\ &- K_{\text{short}}(T)-K_{\text{rep}}(T)-K_{\text{tank}} \end{aligned} \tag{15}$$

was used.

The symbols G and K represent the income and expenditure of the process in USD. The profitability of

the whole process, (Q) stems from the income generated from the sales of the key component (G_{key}) and raw product (G_{raw}). The income is reduced by the various expenses of the process, namely the costs of raw materials (K_{mat}), restoring the buffer capacity of the tank in case of exhaustion (K_{short}), repairs (K_{rep}) and the buffer tank itself (K_{tank}). The method of calculating each source of income and expenditure is shown below.

The main goal of the process is to produce the key component, which is isolated in the continuous subsystem. To calculate the profit that stems from this, equation

$$G_{\mathrm{key}}\left(T\right) = \left(T - \sum_{i=1}^{N_{\mathrm{rep}}(T)} T_{\mathrm{rep}}\right) c\beta_{\mathrm{key}} \qquad (16)$$

was used. In this equation, β_{key} denotes the sale price of the key component (USD kg^{-1}), T represents the duration of the process throughout which the profit (h), the number of malfunctions ($N_{\mathrm{rep}}(T)$), and the random time of repair (T_{rep}) during each malfunction are examined. Additionally, the plant secures an income from the sales of the raw product as well as the remaining raw product at the end of the production process, which can be defined as shown in

$$\begin{aligned} G_{\mathrm{raw}}\left(T\right) \quad = \quad & \beta_{\mathrm{raw}}\left[\delta\left(z_0 - \left(T - \sum_{i=1}^{N_{\mathrm{rep}}(T)} T_{\mathrm{rep}}\right)c + \right.\right. \\ & \left.\left. + \quad \sum_{i=1}^{N_{\mathrm{b}}(T)} y_i^{\mathrm{b}} - \sum_{i=1}^{N_{\mathrm{l}}(T)} y_i^{\mathrm{l}}\right) + \sum_{i=1}^{N_{\mathrm{l}}(T)} y_i^{\mathrm{l}}\right] \end{aligned} \qquad (17)$$

where β_{raw} denotes the sale price of the raw product (USD kg^{-1}) and δ is a factor which defines the price at which the remaining raw product can be sold following production.

Among the expenses, it should be mentioned that the cost of raw materials used for the production of the raw product and the cost of the initial raw product in the tank are calculated according to equation

$$K_{\mathrm{mat}}(T) = \gamma_{\mathrm{mat}} \sum_{i=1}^{N_{\mathrm{b}}(t)} y_i^{\mathrm{b}} + z_0\gamma_{\mathrm{mat}} \qquad (18)$$

where γ_{mat} is the cost of the raw material (USD kg^{-1}). In the event of its exhaustion, additional raw product is required to restore the initial buffer capacity of the tank and the cost of this is shown in

$$K_{\mathrm{short}}(T) = N_{\mathrm{short}}(T) z_0 \gamma_{\mathrm{mat}}, \qquad (19)$$

where $N_{\mathrm{short}}(T)$ denotes the number of malfunctions caused by exhaustion during time T.

Finally, the cost of repairs and installing the intermediate storage itself need to be considered. To determine the installation costs, the installation factor of the tank (f) and the cost of the tank (γ_{tank} in USD) were taken into account. To determine the expense of repairs, the parameter γ_{rep} was used to represent the cost of repairs (USD h^{-1}) which was calculated according to equations

$$K_{\mathrm{rep}}(t) = \sum_{i=1}^{N_{\mathrm{rep}}(t)} T_{\mathrm{rep}}\gamma_{\mathrm{rep}} \qquad (20)$$

and

$$K_{\mathrm{tank}} = f\, z_{\max}^{0.6}\, \gamma_{\mathrm{tank}}. \qquad (21)$$

The cost of installing the buffer tank was calculated according to references found in the literature [12].

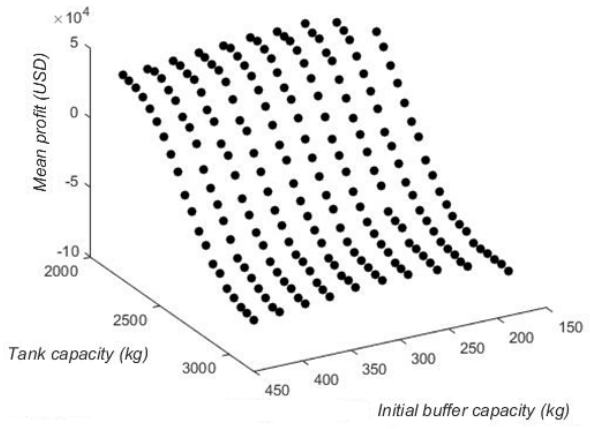

Figure 10: Mean profit as a function of the initial buffer and tank capacities.

The mean of the profit was investigated according to the reliability level of $0.95 \leq 1 - \alpha$ using a Monte Carlo simulation and its optimum was calculated using the grid method. It is shown by the results that if the reliability of the system is high, then the costs of repairs and malfunctions in general are negligible compared to the cost of storage. As a result, the maximum profit was achieved close to the minimum storage capacity which is shown in Fig. 10. This value roughly corresponds to the minimum of the investigated boundary, using a reliability of 0.95. To generate this figure the following parameters were used: $\beta_{\mathrm{key}} = 120$ USD kg^{-1}, $\delta = 0.3$, $\gamma_{\mathrm{mat}} = 80$ USD kg^{-1}, $\beta_{\mathrm{raw}} = 100$ USD kg^{-1}, $f = 100$ USD kg$^{-0.6}$, $\gamma_{\mathrm{tank}} = 12,000$ USD, $m_{t_{\mathrm{rep}}} = 0.5$ h, and $\sigma_{t_{\mathrm{rep}}} = 0.29$ h, where repair times were independent random variables of the uniform distribution during the time interval $[0, 1]$. The maximum profit according to these calculations is $4.76 \cdot 10^4$ USD, which can be achieved by tank and initial buffer capacities of $2,101$ kg and 389 kg, respectively.

6. Conclusion

In this paper, a stochastic storage model was investigated. Random batches as inputs and outputs, as well as continuous withdrawal were allowed. A Monte Carlo simulation was used for the investigation. An analytic function

was fitted to the simulated data, which provided a link between the initial buffer and tank capacities that correspond to a given level of reliability.

The results agree with engineering practice. Although the data for the research did not stem from authentic sources, by utilizing data from the industry, the distribution of the random variables present during the process could be determined using standard statistical methods. Therefore, the method can be a useful supplement during the design phase of a chemical plant and also be utilized to help simplify the overall control of a chemical process.

Symbols

Small letters

c	draining intensity (kg h^{-1})
f	installation factor of a tank (kg$^{-0.6}$)
g	probability density function (h^{-1})
m	expectation
x	fixed initial buffer capacity (kg)
y	fixed tank capacity (kg)
y^{b}	mass of batch fed into the tank (kg)
y^{l}	mass of batch drained from the tank (kg)
z	mass of material (kg)

Capital letters

A, B, C, D	fixed parameters of the approximated failure probability function
G	income (USD)
E	expectation
H	approximated failure probability function
K	expenses (USD)
N	number of events during time interval $[0, T_{\max}]$
P	probability
Q	net income (USD)
T	time (h)
TF	time of failure (h)

Greek letters

α	probability of malfunction
β	sale price (USD kg^{-1})
γ	cost (USD kg^{-1})
δ	ratio of decrease in material value
λ	parameter of exponential distribution (h^{-1})
σ	standard deviation
ψ	function describing the probability of reliable operation during time interval $[0, T_{\max}]$

Indices

0	initial
b	feed
i	index of event ($i = 1, 2, \cdots$)
rep	repair
short	material exhaustion
l	draining
mat	reactant
max	maximum
min	minimum
r	the number of mesh points of the initial buffer capacity
s	the number of mesh points of the tank capacity
t	time
raw	raw material
tank	tank
key	key component

REFERENCES

[1] Towler, G., Sinnott, R. K. Chemical engineering design: principles, practice and economics of plant and process design. (Elsevier, Oxford, UK) 2012, pp. 183. DOI: 10.1016/C2009-0-61216-2

[2] Browning, C., Kumin, H. Stochastic reservoir systems with different assumptions for storage losses, *Am. J. Oper. Res.*, 2016 **6**(5), 414–423 DOI: 10.4236/ajor.2016.65038

[3] Karacan, C. Ö., Olea, R. A. Stochastic reservoir simulation for the modeling of uncertainty in coal seam degasification, *Fuel*, 2015 **148**, 87–97 DOI: 10.1016/j.fuel.2015.01.046

[4] Prabhu, U. U. Stochastic storage processes: queues, insurance risk, dams, and data communication. *Springer Science & Business Media*, 2012. **15**, 63–76 ISBN: 978-1-4612-1742-8

[5] Orbán-Mihálykó, É., Mihálykó, C. Investigation of operation of intermediate storages applying probability density functions satisfying linear differential equation, *Periodica Polytechnica Chemical Engineering*, 2012 **56**(2), 77–82 DOI: 10.3311/pp.ch.2012-2.05.

[6] Orbán-Mihálykó, É., Mihálykó, C. Sizing problem of intermediate storages under stochastic operational conditions, *Periodica Polytechnica Chemical Engineering*, 2015 **59**(3), 236–242 DOI: 10.3311/PPch.7598

[7] Orbán-Mihálykó, É., Mihálykó, C., Lakatos, B. G., Szabó, T., Papp, A. Profit optimization of batch-continuous systems under stochastic processing conditions by simulation, *Hung. J. Ind. Chem.*, 2011 **39**(3), 353–358

[8] Karlin, S., Taylor, H. A first course in stochastic processes. (Academic Press, London, UK) 2014, pp. 113 ISBN: 9780123985521

[9] Zio, E. The Monte Carlo simulation method for system reliability and risk analysis. Vol. 39. (Springer, London, UK) 2013 DOI: 10.1007/978-1-4471-4588-2

[10] Amar, J. G. The Monte Carlo method in science and engineering, *Computing in Science & Engineering*, 2006, **8**(2), 9–19 DOI: 10.1109/MCSE.2006.34

[11] https://www.mathworks.com/products/matlab.html

[12] Stone et al. Plant design and economics for chemical engineers. (McGraw-Hill, New York) 1968 ISBN: 0072392665